

**DEVELOPING METHODS FOR DESIGN AND ANALYSIS
OF CONTINUOUS MIXERS THROUGH
3D NUMERICAL SIMULATION OF FLOW AND MIXING**

by

BHARANI KUMAR ASHOKAN

A Dissertation submitted to the
Graduate School - New Brunswick
Rutgers, The State University of New Jersey
in partial fulfillment of the requirements for the degree of

Doctor of Philosophy

Graduate Program in Food Science

written under the direction of

Dr. Jozef L. Kokini

and approved by

New Brunswick, New Jersey

October, 2008

ABSTRACT OF THE DISSERTATION

Developing Methods for Design and Analysis of Continuous Mixers through 3D Numerical Simulation of Flow and Mixing

by

BHARANI KUMAR ASHOKAN

Dissertation Director:

Dr. Jozef L. Kokini

Design, scale up and selection of alternative geometries for dough mixers in order to achieve a well mixed final product with consistent rheological character is a major challenge in the food industry. The objective of this work is to develop methods to formulate design rules for continuous mixers and identify continuous mixer geometries with similar mixing performance as a model batch mixer using 3D numerical simulations.

FEM simulations were performed with Polyflow (Fluent Inc.) which uses a mixed Galerkin formulation of the isothermal governing equations of motion and continuity. 3D continuous mixer geometries that simulate a 2” Readco Twin Screw mixer with three different paddle configurations were developed and flow profiles and mixing efficiencies were predicted. Accurate predictions of the flow profiles in a continuous mixer were attained by optimizing the FEM mesh, flow geometry and operating conditions through

convergence analysis of velocity and pressure. The predictions were validated with favorable comparisons to experimentally observed velocities that demonstrated the accuracy of the predicted velocities increased with increasing length of mixer geometry, showing the importance of considering the axial flow in a continuous.

Using the calculated flow profiles, trajectories for material points with random initial positions were calculated to predict mixing efficiencies. Segregation scale, mean logarithm of stretching, mean instantaneous efficiency and time averaged efficiency, along with the shear rates and mixing index were used to evaluate mixing. The forward conveying paddle configuration provided the best mixing efficiency when compared to neutral and reverse conveying paddle arrangements and the continuous mixer was also shown to be significantly better than a batch mixer for the same time of operation. Existing numerical techniques that can solve flow problems with moving objects in the flow domain cannot simulate the flow of viscoelastic materials. New techniques were evaluated in this research to simulate the flow and mixing of viscoelastic materials in the twin screw mixing geometry.

ACKNOWLEDGEMENTS

- My advisor, Dr. Jozef L. Kokini, has taught me, provided me with the opportunity to conduct research in his lab, showed me how to develop effective research strategies, write research papers and proposals, analyze data, help develop my creative thinking, supported me through my graduate schooling and patiently encouraged me to complete my dissertation.
- A special thanks is due to Dr. Alberto Cuitino for guiding me through strategies to address the key questions in this research.
- Dr. Muthukumar Dhanasekharan and Dr. Robin Connelly provided me with great insights and valuable guidance in learning the tools. Lindsay Fanning provided data on her experimental validation work. Kiran Vyakaranam was involved in many helpful discussions and assisted me with a few illustrations in this manuscript.
- To all my friends and lab mates at Rutgers, for the fun times we shared and for their encouragement in times of need.
- To my Oral Qualifying Committee: Dr. Jozef L. Kokini, Dr. Alberto Cuitino, Dr. Paul Takhistov and Dr. Sean Liu and to my Final Defense Examination Committee: Dr. Jozef L. Kokini, Dr. Mukund Karwe, Dr. Marianthi Ierapetritou and Dr. Kit Yam.
- Finally, an acknowledgement to all the funding agencies that have supported me at various stages during my research work in Dr. Kokini's lab.

DEDICATION

I dedicate this work to my family:

My wife, Megha, for her love and support and for having stood by me through good times and bad.

My parents, Lalitha and Ashokan, who gave me the educational tools, work ethic and encouragement to follow my dreams.

My brother, Siva, for supporting me and sharing good times through our journey together.

TABLE OF CONTENTS

ABSTRACT OF THE DISSERTATION	ii
ACKNOWLEDGEMENTS	iv
DEDICATION	v
TABLE OF CONTENTS	vi
LIST OF TABLES	x
LIST OF FIGURES	xi
I. Introduction.....	1
II. Literature review.....	5
II.A. Recent Computational Fluid Dynamics (CFD) studies using model classical geometries	8
II.B. Recent CFD studies using model simple mixer geometries	19
II.B.1. Laminar Mixing in Stirred Tank Reactors	19
II.B.2. Mixing in Single and Double Concentric cylindrical mixers	25
II.B.3. Mixing in Double Couette geometry	27
II.C. Simulation of generalized Newtonian and viscoelastic flows in 2D and 3D in complex mixer geometries	29
II.C.1. Continuous mixers	29
II.C.2. Batch Mixers.....	45
II.D. Scale-up and Identification of similar mixer geometries.....	53
II.E. Velocity Characterization in Continuous Mixer.....	55
III. Theoretical Background.....	59
III.A. Governing Equations (Polyflow, 2008).....	59

III.B.	Constitutive equations.....	60
III.B.1.	Generalized Newtonian.....	60
III.B.2.	Shear rate dependent viscosity laws	61
III.B.3.	Temperature dependent viscosity laws	62
III.B.4.	Differential Viscoelastic Constitutive Equations.....	62
III.C.	Discretization Methods	65
III.C.1.	Finite Differences Method	65
III.C.2.	Finite Volumes Method	65
III.C.3.	Finite Elements Method (<i>Reddy, 1993</i>)	66
III.D.	Measures of mixing (Polyflow, 2008)	70
III.D.1.	Distributive Mixing.....	71
III.D.2.	Dispersive Mixing.....	73
III.D.3.	Segregation Scale.....	74
IV.	Materials and Methods.....	76
IV.A.	Numerical simulation.....	76
IV.B.	Initial and Boundary conditions.....	76
IV.C.	Mesh Optimization.....	81
IV.C.1.	Radial Mesh Optimization	81
IV.C.2.	Axial Mesh density	86
IV.D.	Optimum number of paddle pairs	88
IV.E.	Flow through a slit analogy - Pressure comparison	90
IV.F.	Modeling 9 pairs of paddles.....	91
IV.G.	Effect of entrance length.....	93

IV.H.	Calculation of mixing measures.....	94
IV.H.1.	Effect of Paddle Configuration.....	94
IV.H.2.	Effect of Screw Speed.....	96
IV.I.	Numerical simulation of the flow of a viscoelastic fluid in a twin screw mixer	97
IV.I.1.	Pseudo Steady State (PSS) Technique.....	98
IV.I.2.	Application of the PSS technique for the Readco geometry.....	103
IV.I.3.	Verification of PSS technique.....	105
IV.I.4.	Viscoelastic simulation.....	105
IV.I.5.	Evolution.....	106
V.	Results and Discussion	109
V.A.	Mesh Optimization.....	109
V.A.1.	Radial Mesh Optimization	109
V.A.2.	Axial Mesh Density	110
V.B.	Optimum number of paddle pairs	111
V.C.	Flow through a slit analogy – Pressure comparison	115
V.D.	Modeling 9 pairs of paddles.....	117
V.E.	Effect of entrance length.....	119
V.F.	Calculation of mixing measures.....	123
V.F.1.	Effect of configuration.....	123
V.F.2.	Effect of screw speed	132
V.G.	Viscoelastic Simulations.....	140
V.G.1.	Verification of PSS technique with viscous Newtonian solution	140

V.G.2. Simulations with the Oldroyd B model	141
VI. Conclusions.....	145
REFERENCES	147
APPENDIX A.....	153
APPENDIX B.....	154
CURRICULUM VITA	190

LIST OF TABLES

Table II.1 Summary of studies reviewed	7
Table II.2. Influence of fluid rheology on the linear instability of Taylor-couette flow (Al Mubaiyedh <i>et al</i> , 2000)	18
Table II.3. Limits of Deborah number reached by several methods used in viscoelastic simulations during mesh refinement at 1 rpm (Connelly and Kokini, 2003)	30
Table IV.1. Quality of meshes with varying radial gradation.....	85
Table V.1. Comparison of RMS % difference at points P1, P2 and P3 for the four 2D meshes investigated.....	110

LIST OF FIGURES

Figure I.1. Research strategy	4
Figure II.1. The 2:1 Planar Contraction (Owens and Phillips, 2002).	9
Figure II.2. Flow past a cylinder of radius R placed symmetrically in a 2D channel of half width H (Owens and Phillips, 2002).	10
Figure II.3. Geometry of a falling sphere in a cylindrical tube (Owens and Phillips, 2002).	10
Figure II.4. Geometry of the cavity with time-periodic oscillatory lid velocity (Anderson <i>et al</i> , 2000a).....	12
Figure II.5. Effect of increasing amplitude, P on the chaotic advection in the cavity shown as deformation in the material strip (Anderson <i>et al</i> , 2000a)	13
Figure II.6. Generic streamline pattern for Newtonian creeping flow between counter-rotating eccentric cylinders showing stagnation point X_0 and and stagnation streamlines Λ and Γ (Kumar & Homsy, 1996).	14
Figure II.7. Time evolution of Newtonian (N) and shear thinning polyacrylamide fluids dissolved in glycerol to various concentrations (C_1 , C_2 and C_3) in terms of area coverage by a dye (Leong and Ottino, 1990).....	16
Figure II.8. Typical comparison between a computer simulation (finite differences) and an experimental result for a Newtonian fluid (Leong and Ottino, 1990).....	17
Figure II.9. CFD computational grid: (a) cylindrical-polar quadrilateral control volume, (b) angular section of grid, and (c) x/r section of grid (Lamberto <i>et al</i> , 1999).	20

Figure II.10. Probability distribution function of ξ/Re at $Re = 20, 40, 80$ and 160 (Zalc <i>et al</i> , 2001).....	22
Figure II.11. Percentage of the total volume invaded by tracer particles vs. number of impeller revolutions for $Re=20, 40, 80,$ and 160 (Zalc <i>et al</i> , 2002).....	23
Figure II.12. Mixing efficiency as a function of Re (Zalc <i>et al</i> , 2002).....	24
Figure II.13. Finite element mesh of the one-mixing rod geometry (Baloch <i>et al</i> , 2002)	25
Figure II.14. (a) Laser speckle photographs for 1% CMC solution in the one-rod geometry at various Reynolds numbers (b) Stream functions for an inelastic material in the one-rod geometry at various Reynolds numbers (Binding <i>et al</i> , 2003)	26
Figure II.15. Double-couette geometry (Teverovskiy <i>et al</i> , 2000).....	27
Figure II.16. Dye spreading in a double couette geometry in (a) laminar, $Re = 0.1$ and (b) turbulent, $Re = 10^3$ flow regimes (Teverovskiy <i>et al</i> , 2000).....	28
Figure II.17. Shear stress distributions at 1 rpm for relaxation times of (a) 0 s (Newtonian case) and (b) 100 s where the units of stress are gm/cm^2 (Connelly and Kokini, 2003)	31
Figure II.18. Normal stress distributions at 1 rpm for a Newtonian fluid ($\lambda = 0$ s), (a) τ_{11} and (b) τ_{22} where the units of stress are gm/cm^2 (Connelly and Kokini, 2003)	31
Figure II.19. Manas-Zloczower mixing index distributions at 1 rpm of (a) Newtonian, (b) Oldroyd-B with relaxation time of 1.5 s, (c) Bird–Carreau viscous and (d) Phan-Thien Tanner fluid models (Connelly and Kokini, 2004).....	33

Figure II.20. Finite element design of the (A) flow domain and (B) disc dimensions (Ishikawa <i>et al</i> , 2000)	37
Figure II.21. Sequential geometries representing a quarter of rotation cycle (Ishikawa <i>et al</i> , 2000)	38
Figure II.22. Flow diagram of a 3D non-isothermal flow analysis (Ishikawa <i>et al</i> , 2000)	39
Figure II.23. Screw dimensions used in numerical analysis (F: forward, N: neutral B: backward, W: L/D 1.0, WW: L/D 1.5) (Ishikawa, <i>et al</i> , 2001).	40
Figure II.24. Pressure distributions in the axial direction with different stagger angles (Ishikawa <i>et al</i> , 2001)	41
Figure II.25. Temperature distributions in the axial direction with different stagger angles (Ishikawa <i>et al</i> , 2001)	42
Figure II.26. Distributions of area stretch with different stagger angles (Ishikawa <i>et</i> <i>al</i> , 2001)	43
Figure II.27. Distributions of stress magnitudes with different stagger angles (Ishikawa <i>et al</i> , 2001)	43
Figure II.28. Power curves for 0.35% PIB solution in the helical mixer (Bertrand <i>et</i> <i>al</i> , 1999)	45
Figure II.29. Calculated length stretch values (de la Villeon <i>et al</i> , 1998)	47
Figure II.30. The Brabender Farinograph (Connelly, 2004)	49
Figure II.31. Simulated mixing index on a plane across the center of the bowl for (a) corn syrup (b) 2% CMC (c) 0.11% carbopol (Connelly and Kokini, 2006a)	50

Figure II.32. Mixing index results from 10,000 points randomly distributed throughout the flow volume (Connelly and Kokini, 2006a).....	51
Figure II.33. 3D positions of 10,000 initially randomly distributed material points with concentrations of 1 (red/light gray) in the back and 0 (blue/dark gray) in the front viewed from the right side (Connelly and Kokini, 2006b)	52
Figure II.34. Mean time-averaged efficiency of the mixing experienced by 10,000 infinitesimal material lines over three cycles of the blades (Connelly, 2004).....	52
Figure II.35. Demonstration of extruder scale-down (Dhanasekharan and Kokini, 2003).	55
Figure II.36. 2” Readco continuous processor with Plexiglas barrel, showing (a) the LDA probe and beams and (b) the paddle arrangement (Fanning, 2008)	56
Figure II.37. Location of measurement points.....	58
Figure III.1. Typical behavior of time averaged mixing efficiency (Ottino, 1989).....	73
Figure IV.1. Inflow volumetric flow rate.....	77
Figure IV.2. Inflow velocity profile.....	78
Figure IV.3. Rotational speed of paddles.....	79
Figure IV.4. Numerical parameters	80
Figure IV.5. 2D meshes with varying radial mesh density.....	82
Figure IV.6. 432 element 2D paddle mesh	83
Figure IV.7. Position of line 1.	86
Figure IV.8. Barrel meshes with 2, 3, 4 and 5 mesh intervals in the region of the paddles.	87
Figure IV.9. Position of line 2.	88

Figure IV.10. Simulation geometries with (a) 2, (b) 3, (c) 4 and (d) 5 pairs of paddles	89
Figure IV.11. Schematic of the analogy to flow between parallel plates	90
Figure IV.12. 9 paddle pair geometry with the first and last 3 pairs fused into one each to accommodate Polyflow's limitation of 10 moving parts	92
Figure IV.13. Fused 3 pairs long simulation geometry with (a) 9 and (b) 5 axial mesh intervals	93
Figure IV.14. 9 pair paddle geometry in the 45F configuration	95
Figure IV.15. 9 pair paddle geometry in the 45R configuration.....	95
Figure IV.16. Step 0 mesh for the flow between parallel plates.....	99
Figure IV.17. Step 1 mesh for the flow between parallel plates.....	100
Figure IV.18. Representation of nodes of Step 0, CSV file and Step 1 mesh.	102
Figure IV.19. 2D meshes used in the PSS technique with the paddles at (a) 0° (b) 3° (c) 6° and (d) 9° positions.....	104
Figure IV.20. 2D meshes used for PSS technique with viscoelastic constitutive models with the paddles at (a) 0° and (b) 1° positions.	106
Figure V.1. Comparison of velocity magnitudes along line 1 for mesh #1 (1920 el, ■), mesh #2 (1632 el, ◆), mesh #3 (1072 el, ▲) and mesh #4 (512 el, □).....	110
Figure V.2. Velocity comparison along Line 2 for meshes with 2 (■), 3 (◆), 4 (□) and 5 (◇) axial mesh intervals	111
Figure V.3. RMS % difference in the V_x velocity component at point P1 between experimental and simulated values as a function of axial location for	

simulation geometries having 1 pair (■), 2 pairs (◆), 3 pairs (▲), 4 pairs (□) and 5 pairs (◇) of paddles.....	113
Figure V.4. RMS % difference in the V_y velocity component at point P1 between experimental and simulated values as a function of axial location for simulation geometries having 1 pair (■), 2 pairs (◆), 3 pairs (▲), 4 pairs (□) and 5 pairs (◇) of paddles.....	114
Figure V.5. RMS % difference in the V_z velocity component at point P1 between experimental and simulated values as a function of axial location for simulation geometries having 1 pair (■), 2 pairs (◆), 3 pairs (▲), 4 pairs (□) and 5 pairs (◇) of paddles.....	115
Figure V.6. Evolution of pressure along Line 2 for 2, 3, 4 and 5 paddle pair geometries.....	116
Figure V.7. Comparison of pressure drops between numerically simulated and analytical computation using slit flow analogy.....	117
Figure V.8. Velocity comparison along Line 2 for 3 paddle pair meshes with gaps (■), fused 3 paddle pair meshes with 9 (▲) and 5 (□) axial intervals.....	118
Figure V.9. RMS % difference in the V_x velocity component at point P1 between experimental and simulated values as a function of axial location for simulation geometries having 5 pairs (■), 5 pairs with increase in entrance length (□) and 9 pairs (▲) of paddles.....	120
Figure V.10. RMS % difference in the V_y velocity component at point P1 between experimental and simulated values as a function of axial location for	

simulation geometries having 5 pairs (■), 5 pairs with increase in entrance length (□) and 9 pairs (▲) of paddles.....	121
Figure V.11. RMS % difference in the V_z velocity component at point P1 between experimental and simulated values as a function of axial location for simulation geometries having 5 pairs (■), 5 pairs with increase in entrance length (□) and 9 pairs (▲) of paddles.....	122
Figure V.12. Mean logarithm of stretching of the different screw configurations (Farinograph data: courtesy Connelly, 2004).	125
Figure V.13. Mean instantaneous efficiencies of the different screw configurations (Farinograph data: courtesy Connelly, 2004).	126
Figure V.14. Time-averaged efficiencies of the different screw configurations (Farinograph data: courtesy Connelly, 2004).	127
Figure V.15. Contours of mixing index and shear rate for (A) Flat (B) 45F and (C) 45R configurations.....	129
Figure V.16. Normalized segregation scale of the different screw configurations (Farinograph data: courtesy Connelly, 2004).	131
Figure V.17. Mean logarithm of the length of stretch of different screw speeds with a residence time of 6s (Farinograph data: courtesy Connelly, 2004).	133
Figure V.18. Mean logarithm of stretching of the different screw speeds after 10 complete rotations (Farinograph data: courtesy Connelly, 2004).....	134
Figure V.19. Mean instantaneous efficiency of the mixer at different screw speeds with a residence time of 6s (Farinograph data: courtesy Connelly, 2004).	135

Figure V.20. Mean instantaneous efficiency of the mixer at different screw speeds after 10 complete rotations (Farinograph data: courtesy Connelly, 2004).	136
Figure V.21. Time averaged efficiency of the different screw speeds with a residence time of 6s (Farinograph data: courtesy Connelly, 2004).	137
Figure V.22. Time averaged efficiency of the different screw speeds after 10 complete rotations (Farinograph data: courtesy Connelly, 2004).	138
Figure V.23. Normalized segregation scale of the mixer at different screw speeds with a residence time of 6s (Farinograph data: courtesy Connelly, 2004).	139
Figure V.24. Normalized segregation scale of the mixer at different screw speeds after 10 complete rotations (Farinograph data: courtesy Connelly, 2004).	140
Figure V.25. Comparison of velocity magnitudes along line 1 obtained with PSS and MST.....	141
Figure V.26. Velocity magnitude (cm/s) at the end of 1° of paddle rotation using a viscoelastic constitutive equation	143
Figure V.27. Shear rates (1/s) at the end of 1° of paddle rotation using a viscoelastic constitutive equation	144

I. Introduction

Design of dough mixers in order to achieve a well mixed final product with consistent rheological character is a major challenge in the food industry. In particular, designing two different mixers which give the same mixing efficiency remains an elusive goal especially when batch mixers are to be replaced with continuous mixers for automation of manufacturing processes.

Most current practices focus on dimensional analysis for scaling of similar type of equipment. These approaches are based on identical geometries with changing dimensions to accommodate the larger scale. While such empirical relationships have been used in the past to make predictions about the suitability of a mixer, improving on performance demands far greater flexibility. Alternative geometries for batch and continuous mixers need to be identified in order to obtain different throughput rates that perform with similar mixing efficiencies and numerical simulations have provided a viable design alternate in the recent past.

Significant studies have been conducted on the flow and mixing in both batch and continuous mixers, while considering complex geometries in 2D or 3D with complicated fluid rheology including non-linear viscoelastic behavior. While these are positive contributions, the numerical simulations that have been used had to utilize several simplifying assumptions.

These assumptions included simplified geometries, complete fill for continuous mixing and lack of viscous dissipation among others. They limit the effectiveness of the

simulation in accurately predicting the observed experimental data. The field is still considerably far from extrapolating mixing criteria obtained using numerical results with model mixers, to mixers which are used industrially because of these simplifying assumptions. Viscoelastic effects play a significant role in mixing of dough and they have not yet been adequately simulated in a complete numerical simulation of a geometrically accurate 3D batch or continuous mixer. More work is needed to understand the operation of mixers of complex geometry and in extending this understanding to practical industrial applications.

To explore the extent to which improvements in numerical simulations will assist in better prediction of mixing efficiencies, the hypothesis of the research is as follows:

“Experimentally validated 3D numerical simulations of the flow of generalized Newtonian or viscoelastic fluids and their mixing in a twin screw mixer will provide a more accurate measure of mixing than 2D or static 3D simulations. These validated 3D numerical simulations will be a good and realistic design tool to design and configure twin screw mixers.”

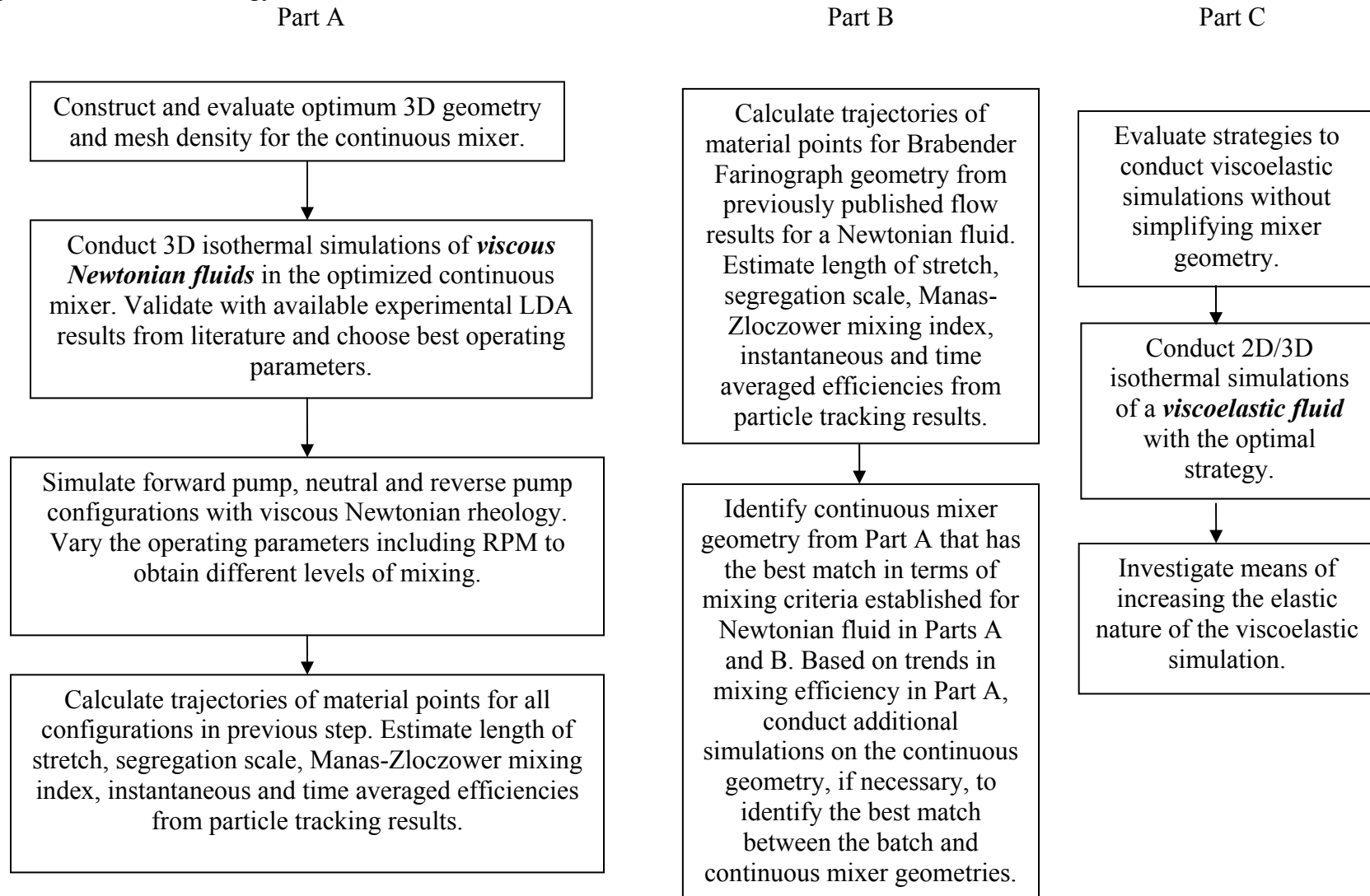
The overall goal of this research is to use 3D numerical simulations to predict the geometrical configuration and processing parameters which result in efficient mixing and to develop the methods that lead to design principles for continuous mixers. Achieving these objectives would result in improved mixer selection and design capabilities in the food industry that give optimum results in a given food processing operation.

The specific objectives of this research are:

1. To simulate and validate the flow and mixing of viscous Newtonian and viscoelastic fluids in a continuous mixer using 3D FEM numerical techniques.
2. To identify continuous mixer geometries which have similar mixing performance as a model batch mixer while mixing Newtonian fluids and to develop the methods that lead to design rules for continuous mixers.

The identification of continuous and batch mixer geometries that produce identical mixing performance through numerical simulation necessitates the prediction of the complete flow profiles in both mixers followed by a study of their mixing effectiveness through the computation of various mixing measures. It is proposed to obtain more accurate predictions of flow and mixing than currently available in literature by removing many of the simplifying assumptions in earlier studies. The steps to be undertaken are illustrated in Figure I.1.

Figure I.1. Research strategy



II. Literature review

Research on the numerical simulation of flow and mixing in batch and continuous mixers can be categorized according to the various geometries of industrially relevant mixers such as the Banbury mixer, Brabender Farinograph, single and twin-screw extruders and helical ribbon mixers that are studied.

Batch or internal mixers such as the Banbury mixer (Ghoreishy and Nassehi, 1997; Yang *et al* 1994; Nassehi and Ghoreishy, 2001) and the Brabender Farinograph (Prakash, 1996; Prakash *et al* 1999; Prakash and Kokini, 1999; Prakash and Kokini, 2000, Connelly and Kokini, 2006a, 2006b) have been studied in the past and in some cases the numerical results were validated with experimental observations (Connelly, 2006a).

Continuous mixers have also been studied with both numerical simulations and experimental observations and include such complex geometries as the single-screw (Dhanasekharan and Kokini, 2000; Connelly and Kokini, 2003; Dhanasekharan and Kokini, 2003; Connelly and Kokini, 2004) or twin screw mixers/extruders (or mixers with kneading elements) (Li and Manas-Zloczower, 1994; Li and Manas-Zloczower, 1995; Kajiwara *et al*, 1996; Cheng and Manas-Zloczower, 1997; Avalosse and Rubin, 2000; Bravo and Hyrmak, 2000; Ishikawa *et al*, 2000; Yoshinaga *et al*, 2000; Ishikawa *et al*, 2001; Ishikawa *et al*, 2002, Connelly and Kokini, 2007) and helical ribbon mixers (Tanguy *et al* 1997; de la Villeon *et al* 1998; Bertrand *et al* 1999).

These research efforts were preceded or complemented by various studies that considered classical benchmark problems such as contraction flows, eccentric cylinder (Kumar and

Homsy, 1996; Ashrafi *et al*, 2001; Rodrigo *et al*, 2003), Taylor-couette flow (Al Mubaiyedh *et al*, 2000, 2002a, b), flow past cylinder and lid-driven cavity mixers (Grillet *et al*, 1999; Anderson *et al*, 2000a, b). The benchmark problems allowed investigators to understand the flow patterns and their rheological influences which were then extended to an understanding for higher geometries. By investigating well defined geometries with clearly identifiable variables, these benchmark studies helped established the fundamental basis of mixing problems and to formulate measures of mixing.

Studies involving simple model mixer geometries including stirred tank reactors (Lamberto *et al*, 1999; Lamberto *et al*, 2001; Zalc *et al*, 2001; Alvarez *et al*, 2002; Zalc *et al*, 2002), couette (Baloch *et al*, 2002; Binding *et al*, 2003; Sujatha *et al*, 2003) and double couette (Teverovskiy *et al*, 2000) geometries have been used to understand mixing phenomena in mixers with geometries closer to industrial mixers. A summary of the various studies reviewed in this manuscript is provided in Table II.1 and detailed descriptions of the individual accomplishments in these studies follow.

Table II.1 Summary of studies reviewed

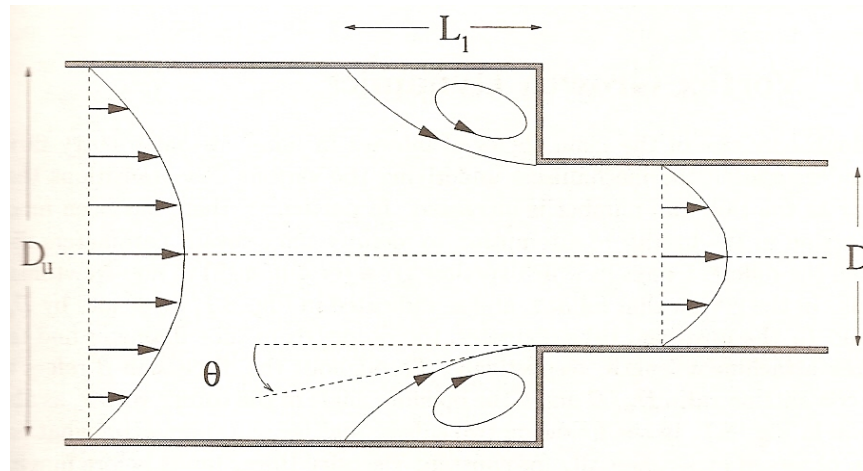
Reference	Geometry	Rheology	Numerical technique
Anderson <i>et al</i> (2000a,b)	Lid-driven cavity	Newtonian	Spectral Methods
Kumar and Homsy (1996)	Eccentric cylinders	Oldroyd B	Finite Differences
Leong and Ottino (1990)	Lid-driven cavity	Newtonian	Finite Differences
Al Mubaiyedh <i>et al</i> (2000, 2002a, 2002b)	Taylor-Couette	Oldroyd B	Spectral Methods
Lamberto <i>et al</i> (2001)	Single impeller unbaffled Stir tank	Newtonian	Finite Volume Method
Zalc <i>et al</i> (2001)	Three impeller unbaffled Stir tank	Newtonian	Finite Volume Method
Couch and coworkers (Baloch <i>et al.</i> , 2002; Binding <i>et al.</i> , 2003; Couch & Binding, 2003; Sujatha <i>et al.</i> , 2003)	Single and double concentric cylindrical mixers	Oldroyd B	Finite Element Method
Teveroskiy <i>et al</i> (2000)	Double Couette	Newtonian	Finite Element Method
Connelly and Kokini (2003)	2D Single screw continuous mixer	Viscoelastic PTT	Finite Element Method
Connelly and Kokini (2007)	2D Twin screw continuous mixer	Generalized Newtonian	Finite Element Method
Connelly (2004)	3D Twin screw mixer – steady state	Generalized Newtonian	Finite Element Method
Avalosee and Rubin (2000)	3D single screw extruder	Generalized Newtonian	Finite Element Method
Kajiwara <i>et al.</i> , 1996; Yoshinaga <i>et al.</i> , 2000; Ishikawa <i>et al.</i> , 2000, 2001, 2002)	3D Twin screw mixer – quasi steady state	Generalized Newtonian	Finite Element Method
Bertrand <i>et al</i> (1999)	Helical ribbon mixer	Generalized Newtonian	Finite Element Method
Jongen <i>et al.</i> , 2000, 2003	2D Plastograph, Do-Corder	Newtonian	Finite Element Method
de la Villeon <i>et al.</i> , 1998	Helical ribbon mixer	Generalized Newtonian	Finite Element Method
Connelly and Kokini (2006a, 2006b)	Brabender Farinograph	Generalized Newtonian	Finite Element Method

II.A. Recent Computational Fluid Dynamics (CFD) studies using model classical geometries

Model flow and mixing studies have concentrated primarily in four basic geometries: 1) contraction flows 2) flow past a cylinder or sphere 3) lid-driven cavity mixers, and 4), eccentric cylinder or journal bearing or Taylor-couette flows for simplicity in mathematical simulation studies and ease of conducting experimental validation experiments.

In contraction flows, fluid passes from one channel to a second smaller (in cross-section) channel (Figure II.1). This type of flow creates strong shearing near the walls and uniaxial extension along the centerline of the flow. As a consequence of the high shear and extensional flows, the rheology of the fluid (changing from Newtonian to a non-Newtonian) exhibits considerable influence in flow patterns, particularly with vortex behavior near the corners where the flow contracts. For this reason, contraction flows have been considered as a benchmark problem in both numerical and experimental works to show differences in flow behavior due to rheology (Owens and Phillips, 2002).

Figure II.1. The 2:1 Planar Contraction (Owens and Phillips, 2002).



Another example of a traditional flow problem that is considered to be a benchmark for numerical solutions is the flow past a cylinder in a channel (Figure II.2) or flow past a sphere in a tube (Figure II.3). In the flow past a cylinder, the region between the cylinder and walls experience shear flow, while the flow near the axis of symmetry and the wake beyond the cylinder exhibit extensional flows. The absence of singularities in the geometry lends itself well to numerical simulations. Flow past a sphere in a tube is similar to that past a cylinder, but is studied more to understand the nature of the drag behind the falling sphere. The steady state drag factor (or wall correction factor) κ , which is the ratio of the drag experienced by the sphere to the drag around the same sphere steadily settling in a unbounded expanse of Newtonian fluid of the same viscosity, μ_0 , is typically used to compare one numerical method against another for accuracy and stability.

$$\kappa = \frac{\text{drag}}{6\pi\eta_0 aU}$$

Equation 1

Figure II.2. Flow past a cylinder of radius R placed symmetrically in a 2D channel of half width H (Owens and Phillips, 2002).

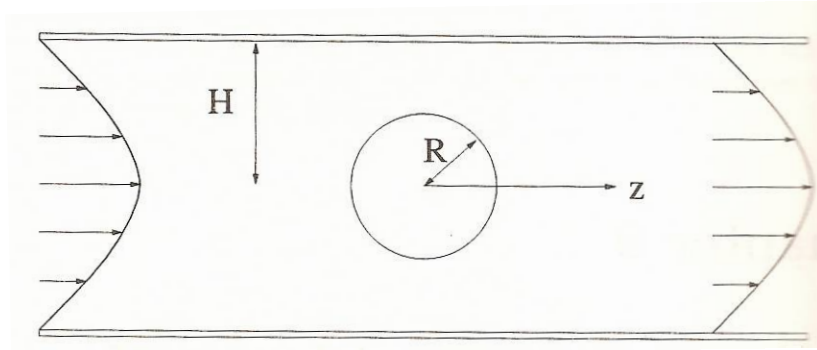
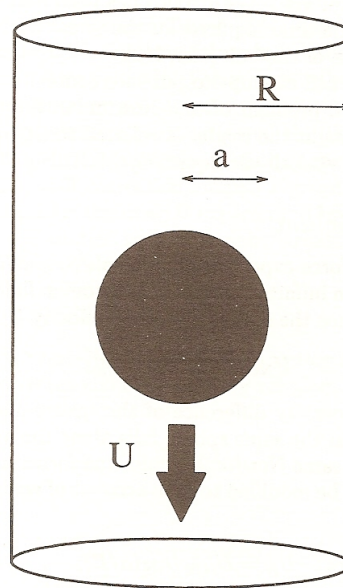


Figure II.3. Geometry of a falling sphere in a cylindrical tube (Owens and Phillips, 2002).

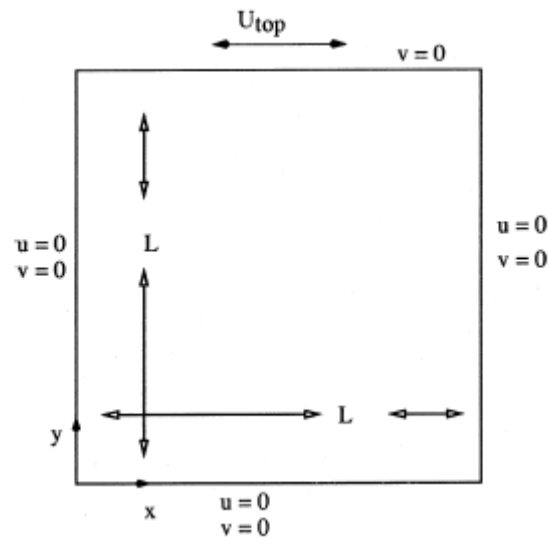


Simulations utilizing precursor geometries such as contraction flows and flows past cylinders and spheres have been traditionally studied to understand and develop new numerical simulation techniques and have been explored in traditional references on the subject. Other benchmark problems such as lid-driven cavities and eccentric cylinders have been used to

explore mixing flows and a few pertinent examples are discussed in more detail in the following section.

The lid-driven cavity mixer geometry has been used effectively to demonstrate the effects of boundary conditions on mixing efficiency. Anderson and co-workers (2000a and 2000b) used spectral element techniques to solve the flow of an incompressible Newtonian fluid in a lid-driven cavity geometries (Figure II.4). They showed that superposition of a pulsating component on the steady lid velocity (Equation 2) can lead to chaotic mixing in the core of the cavity (Figure II.5).

Figure II.4. Geometry of the cavity with time-periodic oscillatory lid velocity (Anderson *et al*, 2000a)

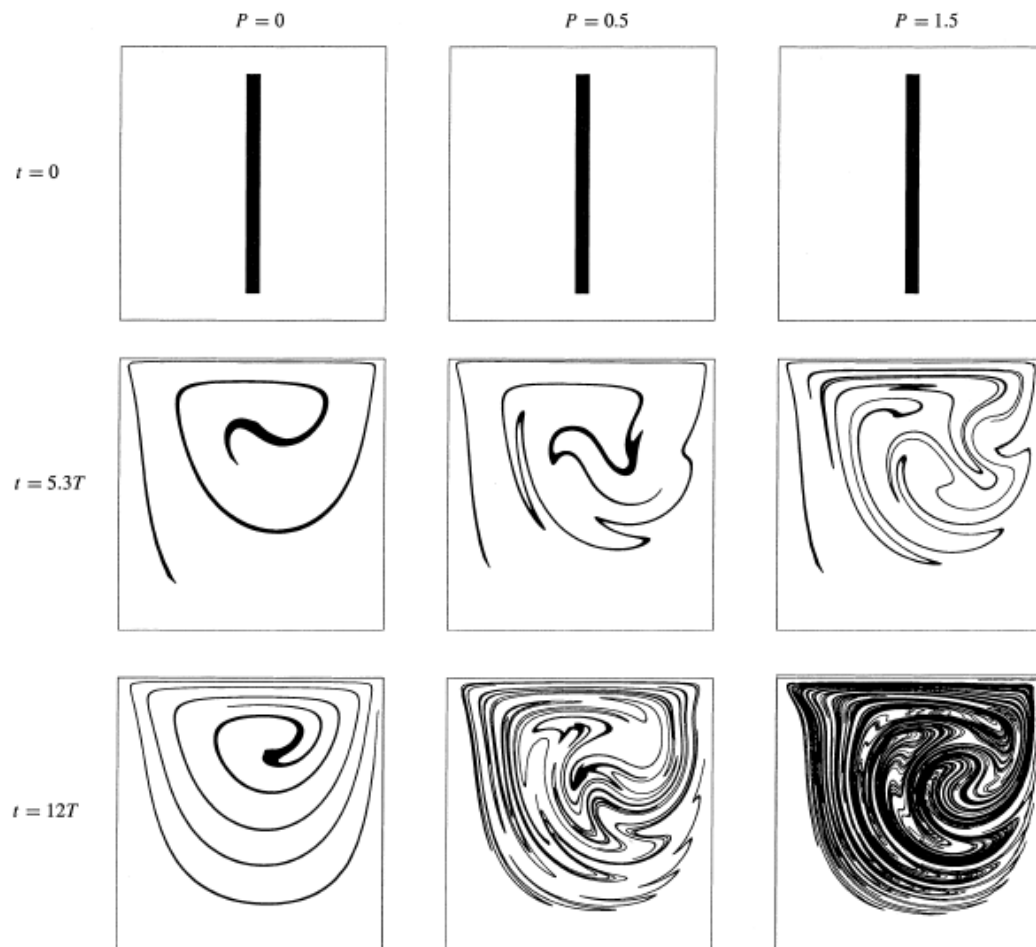


$$\begin{cases} u = U_{top} = 1 + P \sin\left(\frac{2\pi t}{T}\right) & v = 0 \text{ top wall,} \\ u = 0 & v = 0 \text{ side and bottom walls.} \end{cases}$$

Equation 2

P is the amplitude of oscillation over a time period T .

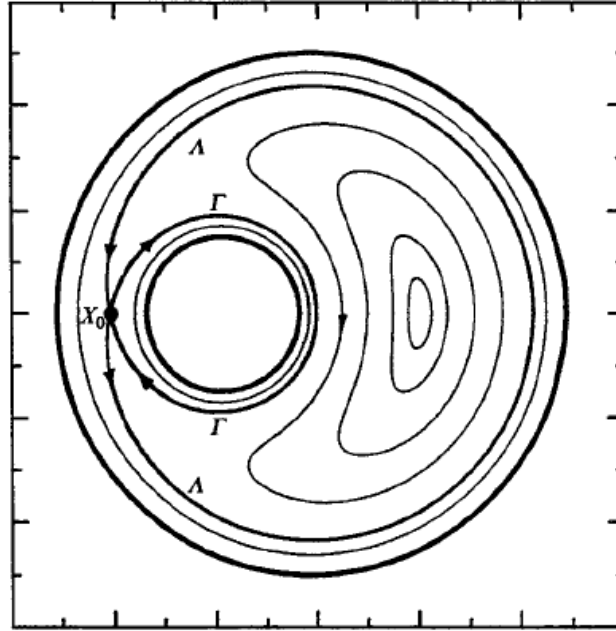
Figure II.5. Effect of increasing amplitude, P on the chaotic advection in the cavity shown as deformation in the material strip (Anderson et al, 2000a)



An extra steady motion of the opposite cavity wall causes the well mixed region to be spread over almost the whole cavity, making mixing more efficient.

This effect of boundary conditions on perturbing the steady motion and improving the mixing efficiency was also noted by Kumar and Homsy (1996). They studied the flow and mixing in counter-rotating eccentric cylinders (Figure II.6) using standard finite differences.

Figure II.6. Generic streamline pattern for Newtonian creeping flow between counter-rotating eccentric cylinders showing stagnation point X_0 and and stagnation streamlines Λ and Γ (Kumar & Homsy, 1996).



The governing equations were reduced to dimensionless forms (Equation 3, Equation 4 and Equation 5) which were then parametrically analyzed with variations in geometry, elasticity, boundary motion type and frequency.

$$\nabla \cdot \mathbf{u} = 0 \quad \text{Equation 3}$$

$$\text{Re} \left(\frac{\partial \mathbf{u}}{\partial t} + \mathbf{u} \cdot \nabla \mathbf{u} \right) = \nabla \cdot \boldsymbol{\sigma} - \nabla p \quad \text{Equation 4}$$

$$\boldsymbol{\sigma} + We \overset{\nabla}{\boldsymbol{\sigma}} = 2(D + WeS \overset{\nabla}{D}) \quad \text{Equation 5}$$

where \mathbf{u} is the velocity, p is the pressure, $\boldsymbol{\sigma}$ is the deviatoric stress, \mathbf{D} is the rate of strain tensor, Re is the Reynolds number, We is the Weissenberg number (a dimensionless measure

of fluid elasticity) and S determines the rheology of the fluid ($S=0$, upper convected Maxwell; $S=1$, Newtonian)

A viscoelastic correction was applied to the Newtonian fluid and a perturbation solution (with a Fourier expansion on the Weissenberg number, Wi) was obtained for this corrected field. They found that the viscoelasticity introduced by the Oldroyd B fluid model increased the rate of chaotic mixing when a different boundary motion was introduced in a perturbation solution by applying a viscoelastic correction to the Newtonian flow field. This led to more efficient mixing and underscored the need to introduce periodic and time-dependent disturbances into the flow to improve mixing efficiency.

Studying a lid-driven cavity flow, Leong and Ottino (1990) showed that shear thinning generally has a detrimental effect on mixing efficiency due to the increase in size and number of isolated islands in the flow. A reduction in the size and intensity of chaotic mixing zones in time-periodic flows lead to a reduction in the stretching. This was shown with an illustration of the reduction in area of coverage by a dye that was allowed to mix in both Newtonian and Boger fluids (fluids exhibiting viscoelastic behavior and having a constant shear viscosity). The Boger fluids were created by dissolving increasing concentrations ($C_1 = 60$ ppm, $C_2 = 125$ ppm and $C_3 = 160$ ppm) of polyacrylamide in glycerine. Image analysis of the fractional coverage of the dye versus the mixing time showed that with increasing shear thinning character, the rate of stretching (slope of the graph) decreased (Figure II.7). The streamlines for Newtonian flow were computed using finite differences and there was good agreement with experimental observations (Figure II.8).

Figure II.7. Time evolution of Newtonian (N) and shear thinning polyacrylamide fluids dissolved in glycerol to various concentrations (C_1 , C_2 and C_3) in terms of area coverage by a dye (Leong and Ottino, 1990)

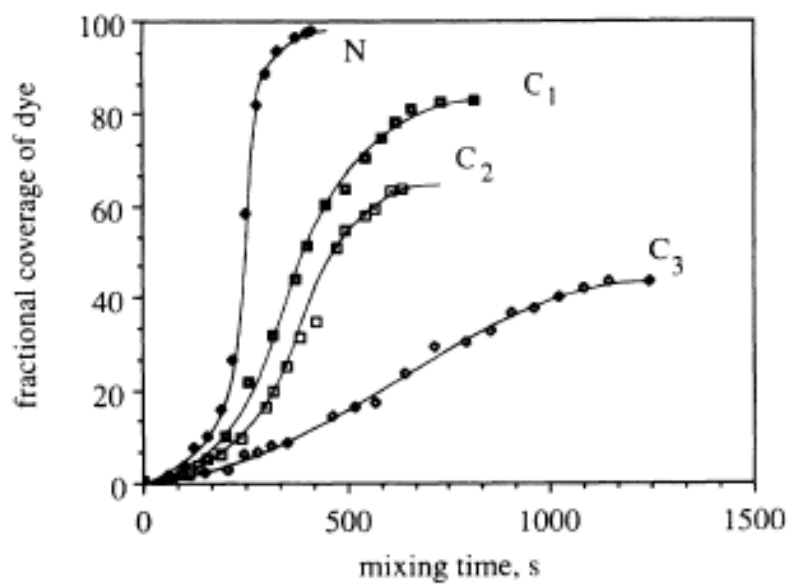
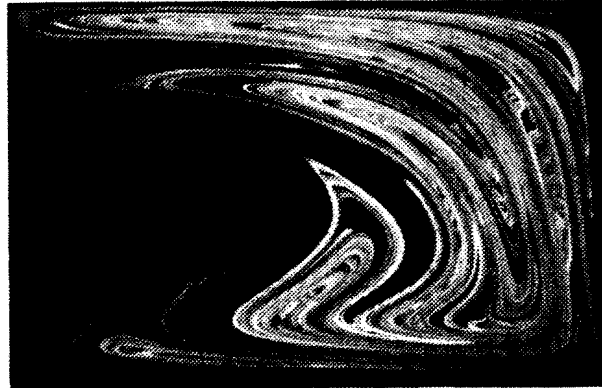
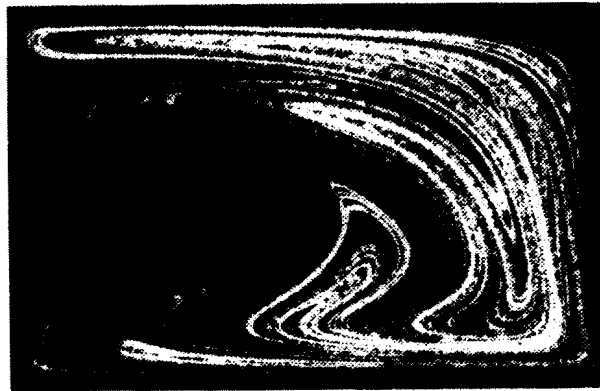


Figure II.8. Typical comparison between a computer simulation (finite differences) and an experimental result for a Newtonian fluid (Leong and Ottino, 1990)



experiment



computation

Al Mubaiyedh and coworkers (Al Mubaiyedh *et al*, 2000, 2002a, 2002b) used the Taylor-couette geometry to demonstrate the linear and non-linear effects of viscoelasticity on the stability of flow of a viscoelastic fluid. They investigated the effects of detailed fluid rheology (spectrum of relaxation times, shear thinning of first normal stresses, finite second normal stresses, and ratio of solvent to total viscosity) on the purely elastic (i.e. $Re \rightarrow 0$) instability of the Taylor-Couette flow (Al Mubaiyedh *et al*, 2000) using a mixed Galerkin

spectral method to solve the non-linear system of equations. They found that the critical Deborah number (De_c , defined as the ratio of fluid relaxation time to a characteristic flow time scale at the onset of instability) decreases as the number of relaxation times describing the rheology of the fluid is increased (Table II.2).

Table II.2. Influence of fluid rheology on the linear instability of Taylor-couette flow (Al Mubaiyedh *et al*, 2000)

Constitutive model	$\delta = 0.912$				$\delta = 0.8$			
	ξ	α_c	De_c	σ_{Ic}	ξ	α_c	De_c	σ_{Ic}
1-mode Oldroyd-B	0	7.7	21.55	0.0480	0	10.5	15.15	0.0755
	1	5.5	16.41	0.0186	1	5.8	11.38	0.0167
	2	5.4	16.09	0.0048	2	6.9	13.41	0.0158
4-mode Oldroyd-B	0	7.8	12.80	0.0216	0	11.9	9.20	0.0331
	1	4.8	8.38	0.0064	1	4.8	5.85	0.0222
	2	4.9	9.38	0.0243	2	5.8	8.16	0.0438
4-mode Phan-Thien and Tanner	0	7.3	68.63	0.0223	0	9.0	32.88	0.0387
	1	4.8	31.44	0.0036	1	4.8	18.81	0.0198
	2	4.9	35.35	0.0238	2	5.7	28.131	0.0446
4-mode Giesekus	0	6.8	90.82	0.0203	0	8.7	37.45	0.0372
	1	4.7	34.16	0.0036	1	4.7	19.63	0.0196
	2	4.8	39.61	0.0230	2	5.8	30.23	0.0421

Discrepancies between the experimentally observed De_c and those from isothermal simulation of purely elastic flows led the researchers to investigate the effects of viscous heating (Al Mubaiyedh *et al*, 2002a, 2002b). This additional complexity in the definition of the problem led to the conclusion that viscous heating caused De_c to be an order of magnitude lower than that predicted by isothermal simulations and closer to the experimental values. The experimentally observed secondary flow patterns were also closely matched by the non-isothermal simulations. The authors attributed the superiority of the non-isothermal

simulations to the temperature sensitivity of the viscosity of the fluid, due to which minor fluctuations in the temperature field due to viscous heating were amplified into observable secondary flow patterns.

The above examples show the usefulness of classical benchmark problems in illustrating the effects of fundamental building blocks of a problem such as the boundary conditions and fluid rheology on understanding flow in a model mixer and estimating mixing efficiency. While these studies demonstrate the importance of understanding the effects of fluid rheology and geometric restrictions on the flow under consideration, they do not contribute substantially to real-life applications due to over simplification of the geometry of the flow problems. Important geometrical features such as complex impellers or convoluted boundary conditions cannot be adequately explored in these geometries leading to inaccuracies in predictions of flow and mixing behavior. Nevertheless, they serve an important function by benchmarking new techniques which can then be applied in more complicated flow geometries.

II.B. Recent CFD studies using model simple mixer geometries

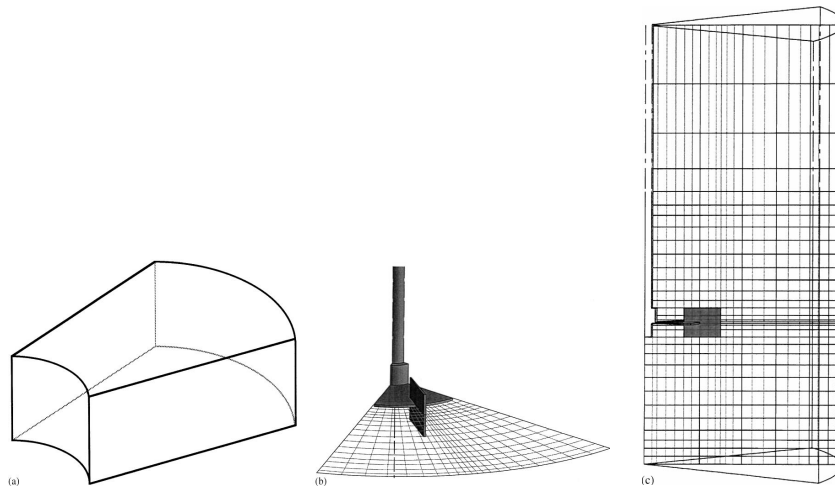
Building on the successes in classical geometries and with improvements in computational power and techniques, several research groups are pursuing mixing studies in model mixers to understand mixing flows.

II.B.1. Laminar Mixing in Stirred Tank Reactors

A group lead by F.J. Muzzio at Rutgers University has been systematically studying stirred tank reactor and static mixer flow and mixing in laminar to turbulent flow regimes using

generalized Newtonian fluids and fluid models with both experimental and CFD techniques. Lamberto *et al* (2001) used a rotating reference frame technique with a finite volume methods solver (Fluent) to explore laminar mixing of a Newtonian fluid in an unbaffled stirred tank with one impeller. One sixth of the 6 paddle impeller-tank geometry was modeled to take advantage of the symmetry in the geometry and a discretized finite volume mesh was constructed (Figure II.9).

Figure II.9. CFD computational grid: (a) cylindrical-polar quadrilateral control volume, (b) angular section of grid, and (c) x/r section of grid (Lamberto *et al*, 1999).

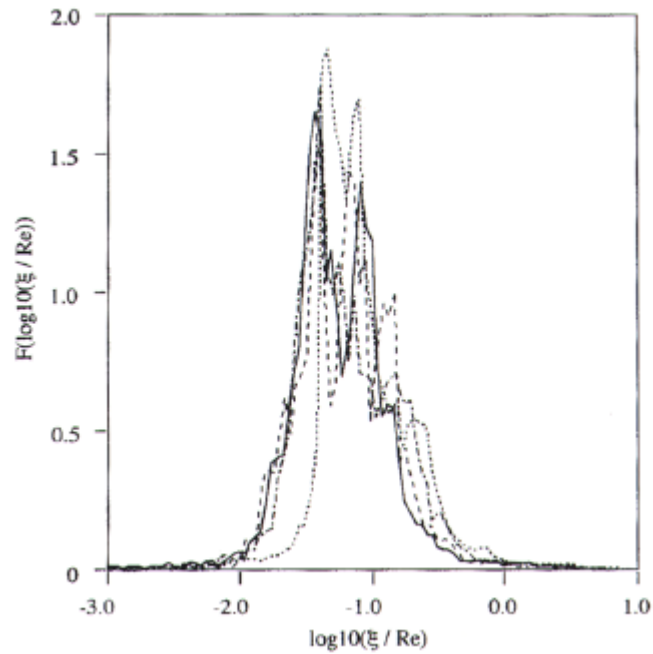


Analogous to the simulations using classical geometries and varying time-periodic boundary conditions, this study explored the effect of time-dependent RPM on mixing performance. They observed that the toroidal structures that are formed when the impeller rotates at a constant RPM are periodically relocated when the RPM oscillates between two set values. This led to an exponential increase in stretching throughout the domain and in general it was observed that higher frequency of speed fluctuations resulted in larger increases in stretching

rate. The numerical results obtained were in good agreement with particle image velocimetry (PIV) experiments on seeded glycerin solutions.

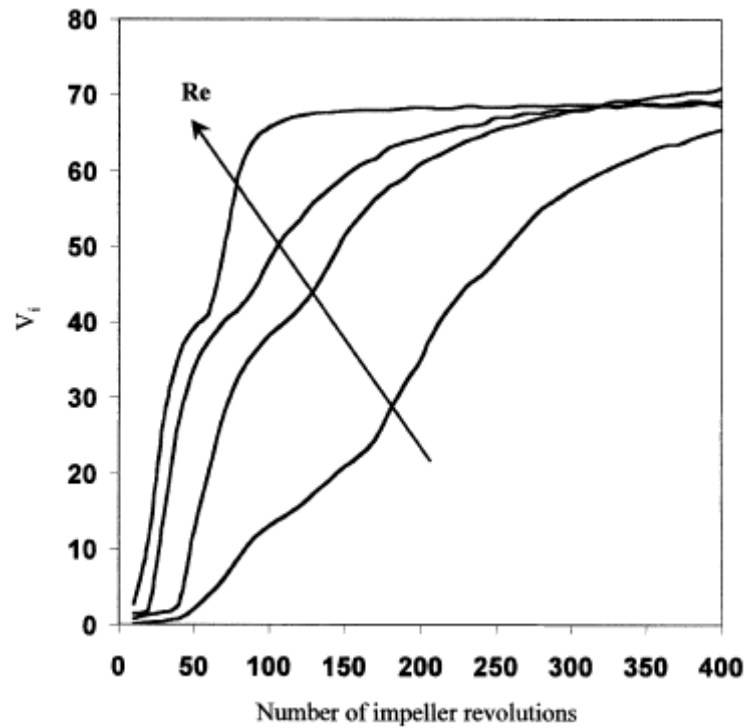
Zalc *et al* (2001) studied the mixing of Newtonian fluid in a three impeller unbaffled stirred tank with a similar rotating reference frame technique as Lamberto *et al* (2001). These results were also validated using PIV experiments on a water/glycerin solution and included an analysis of the calculated magnitude of the deformation tensor, ξ . They concluded that the magnitude of the deformation tensor increased non-linearly with the Reynolds number and constructed a probability density function of ξ/Re (Figure II.10) that showed the increase in ξ with increasing Re . They suggest that the local spatial derivatives of the velocity field are what determine the stretching, folding, and reorientation of fluid elements as they visit different locations in the flow and that knowledge of the velocity gradients at different locations within the flow allows the determination of the regions that have the greatest potential for mixing.

Figure II.10. Probability distribution function of ξ/Re at $Re = 20, 40, 80$ and 160 (Zalc *et al.*, 2001)

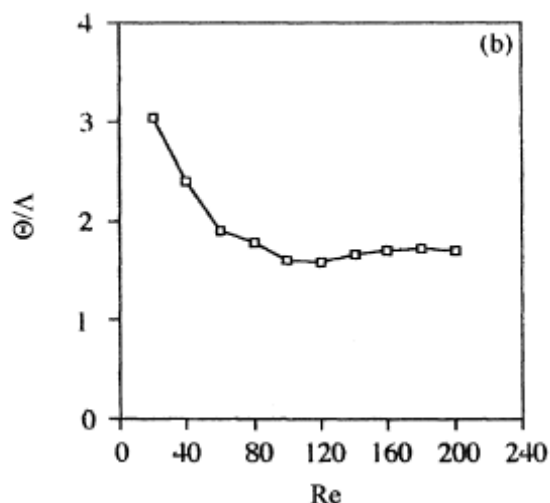


Later results (Alvarez *et al.*, 2002) using computational particle tracking results to create Poincaré sections were able to reveal the segregated regions identified in the experiments and follow their change in shape with changing impeller velocity. Analysis of the percentage of the flow domain that is invaded by tracer particles, V_i , was used as a measure of the homogeneity at any given time during the mixing process and it was observed that V_i increased with increasing Re (Figure II.11).

Figure II.11. Percentage of the total volume invaded by tracer particles vs. number of impeller revolutions for $Re=20, 40, 80,$ and 160 (Zalc *et al.*, 2002)



Analysis of the arithmetic (Θ) and volume averages (Λ) of the length of stretch and the distribution over time of clusters and lines lead to the observation that the mixing does not necessarily improve with increasing Reynolds number and achieves a plateau at high Re (Figure II.12) (Lamberto *et al.*, 2001; Zalc *et al.*, 2002).

Figure II.12. Mixing efficiency as a function of Re (Zalc *et al*, 2002)

Such studies have enabled detailed descriptions of the effect of impeller geometry, number and placement along with the impact of operating parameters such as the RPM and have proven to be very useful in explaining flow and mixing phenomena in simple mixing tanks utilizing Rushton (and other such) impellers in the industry. The insights gained in the understanding of chaotic mixing and segregated regions in such mixers are also very valuable. However, these insights into the effect of impeller geometry, number, or placement and the effect of operating parameters such as RPM on chaotic mixing are not directly applicable to more complicated geometries such as twin-screw mixers with intermeshing regions due to many simplifying assumptions in the geometry, fluid rheology and flow patterns in the mixer. These simplifying assumptions do not account for flow irregularities that are caused due to disturbances by complex impeller geometries or instabilities in chaotic mixing structures due to complicated fluid rheology.

II.B.2. Mixing in Single and Double Concentric cylindrical mixers

Another series of studies in model simple mixer geometries focused on the wetting and peeling of dough and other liquids on solid surfaces through a combination of numerical modeling and experimental validation (Baloch *et al.*, 2002; Binding *et al.*, 2003; Couch & Binding, 2003; Sujatha *et al.*, 2003). The researchers used single and double concentric cylindrical mixers (Figure II.13) for analysis of the flow and mixing in filled and partially filled conditions and the solved the numerical problems using finite element techniques (Baloch *et al.*, 2002). They found the asymmetrical positioning of a single stirrer to provide the best mixing of viscoelastic fluids. Such asymmetries introduce disturbances in the flow and increase chaotic mixing leading to increased mixing efficiency. Close agreement was found between numerical and experimental flow fields and free surface profiles (Figure II.14). The flow in a single concentric cylindrical mixer closely resembles the benchmark problem of the flow in a journal bearing and serves as bridge between this ideal flow problem and the commonly found industrial mixers such as the DoCorder.

Figure II.13. Finite element mesh of the one-mixing rod geometry (Baloch *et al.*, 2002)

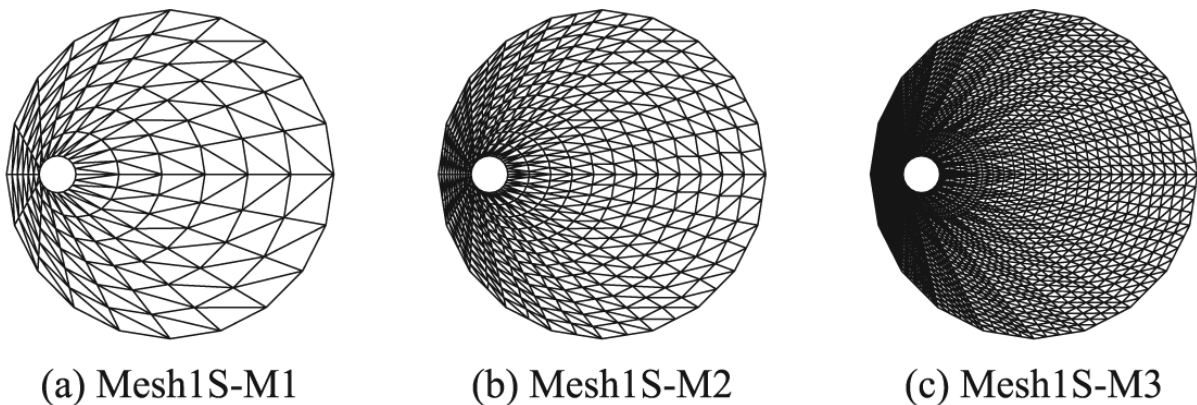
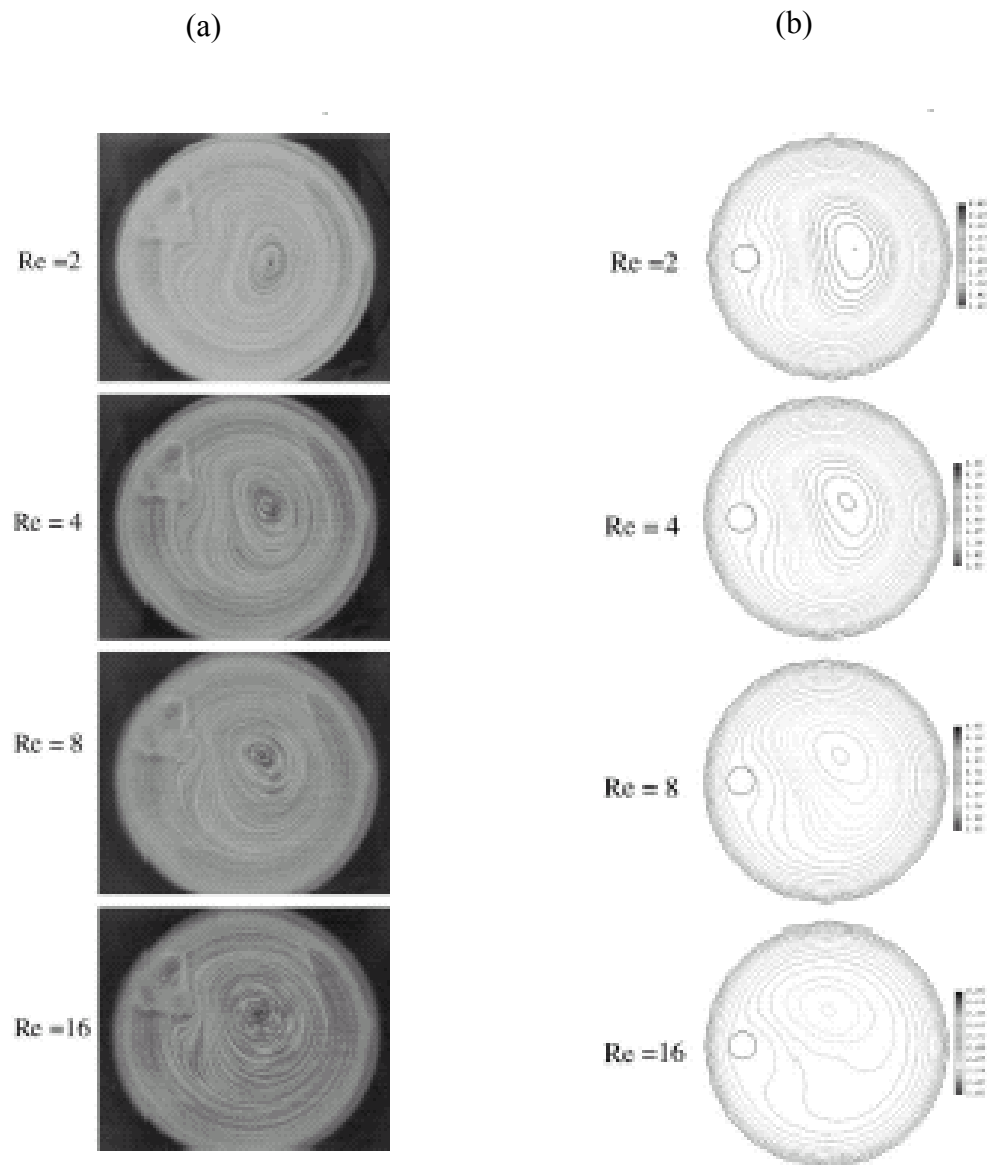


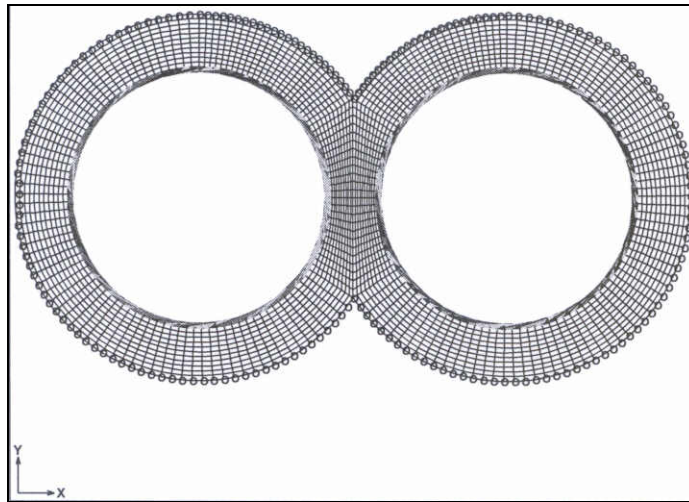
Figure II.14. (a) Laser speckle photographs for 1% CMC solution in the one-rod geometry at various Reynolds numbers (b) Stream functions for an inelastic material in the one-rod geometry at various Reynolds numbers (Binding *et al.*, 2003)



II.B.3. Mixing in Double Couette geometry

An interesting extension of the Taylor-couette geometry detailed in the previous section is a double-couette geometry that was studied by Teverovskiy and coworkers (Teveroskiy *et al*, 2000). In this study, an ‘eight’ shaped barrel similar to the one found in twin-screw extruders and continuous mixers was modeled with two rotating shafts (or couettes) to substitute for the impellers (Figure II.15).

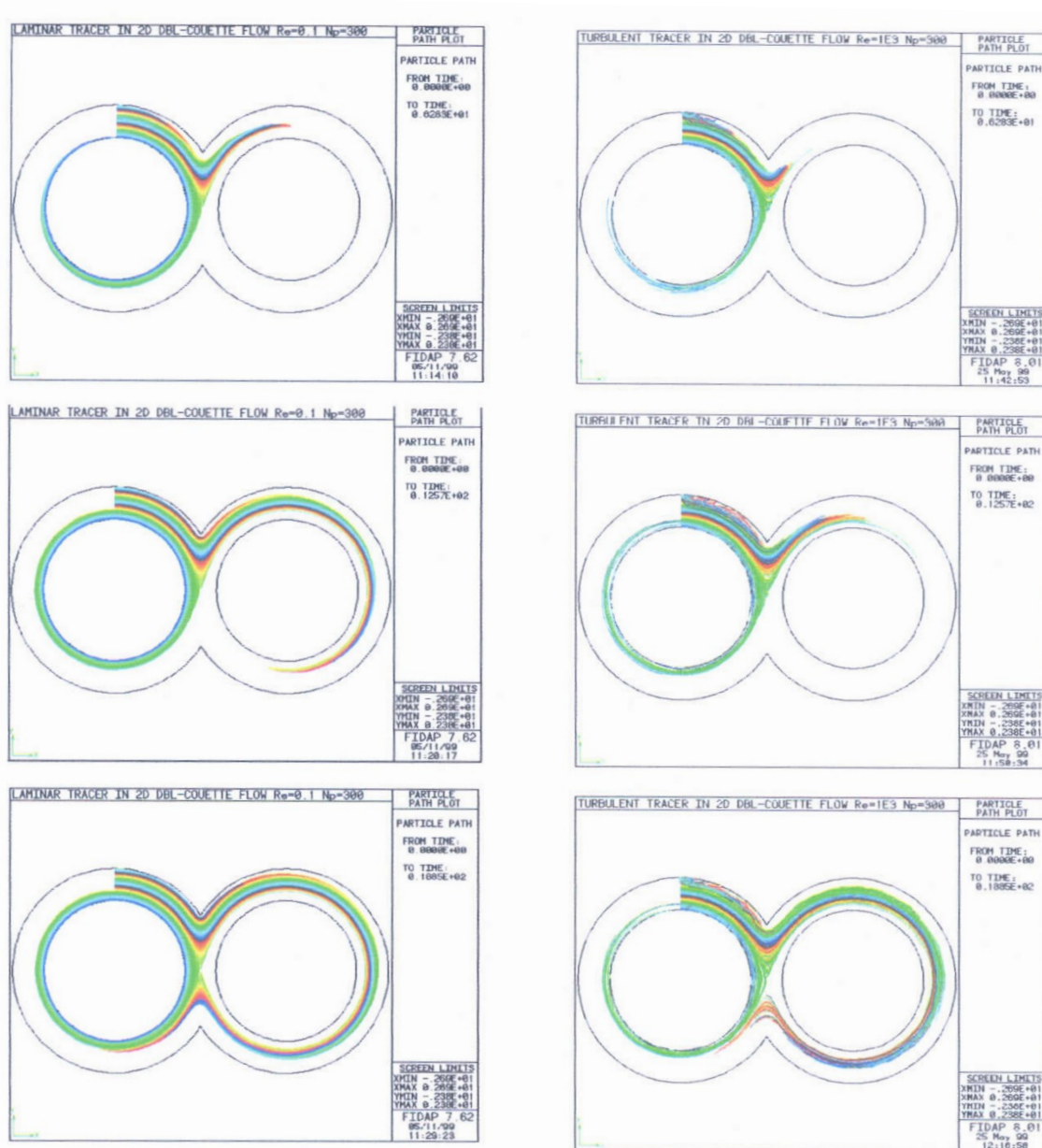
Figure II.15. Double-couette geometry (Teverovskiy *et al*, 2000)



This simplification of the continuous mixer geometry allowed the researchers to investigate the mechanics of flow and mixing of a Newtonian fluid in laminar and turbulent regimes without the need for any time-dependent mesh changes using a finite element method solver. They conducted a qualitative comparison of distributive mixing efficiency in laminar and turbulent flow regimes by considering the spreading of a tracer dye in the matrix and showed

qualitative differences in the manner in which the tracer spreads under different flow regimes (Figure II.16).

Figure II.16. Dye spreading in a double couette geometry in (a) laminar, $Re = 0.1$ and (b) turbulent, $Re = 10^3$ flow regimes (Teverovskiy *et al*, 2000).



While this study allowed the study of a twin-screw geometry by simplification of the geometry, further strides have been made in modeling the complex continuous mixer geometry in accurate detail and these efforts are described in the following section.

II.C. Simulation of generalized Newtonian and viscoelastic flows in 2D and 3D in complex mixer geometries

Mixing in complex geometries such as the twin-screw continuous mixers and batch Farinograph mixers has recently been addressed utilizing new advances in numerical simulation techniques and computational capabilities.

II.C.1. Continuous mixers

Complex mixing geometries, such as twin-screw extruders/mixers, have only recently been simulated in 2D and 3D with more complicated fluid rheology, including viscoelastic flows. 2D finite element method techniques were successfully utilized to explore the effects of viscoelasticity in mixing flows of kneading paddles in a single screw continuous mixer (Connelly & Kokini, 2003). The single-mode, non-linear Phan-Thien Tanner differential viscoelastic model with dough-like parameters (Dhanasekharan and Kokini, 1999; Wang and Kokini, 1995a; b) was chosen and several numerical simulation techniques such as elastic viscous stress splitting, 4X4 sub elements for stresses, streamline upwind and streamline upwind Petrov-Galerkin method were tested and compared for their ability to simulate viscoelastic flows and mixing. The limits of the Deborah number reached by these methods were also identified (Table II.3).

Table II.3. Limits of Deborah number reached by several methods used in viscoelastic simulations during mesh refinement at 1 rpm (Connelly and Kokini, 2003)

Mesh Size	<u>EVSS SUPG</u>		<u>4x4 SUPG</u>		<u>EVSS SU</u>		<u>4x4 SU</u>	
	$\lambda(1 \text{ rpm})$	De						
360 elements	0.327	0.034	0.23	0.024	651.04	68.2	1000	104.7
600 elements	0.178	0.019	1.04	0.109	14.12	1.47	23.4	2.45
1480 elements	0.089	0.009	0.089	0.009	0.73	0.076	131.78	13.8
2080 elements	-	-	0.066	0.007	0.79	0.082	543.58	56.9
3360 elements	-	-	-	-	0.58	0.061	110.32	11.6

Upon comparison with predictions for viscous flows, it was observed that viscoelastic flow predictions differ significantly in shear (Figure II.17) and normal stress (Figure II.18) predictions resulting in a loss of symmetry in velocity and pressure profiles in the flow region.

Figure II.17. Shear stress distributions at 1 rpm for relaxation times of (a) 0 s (Newtonian case) and (b) 100 s where the units of stress are gm/cm^2 (Connelly and Kokini, 2003)

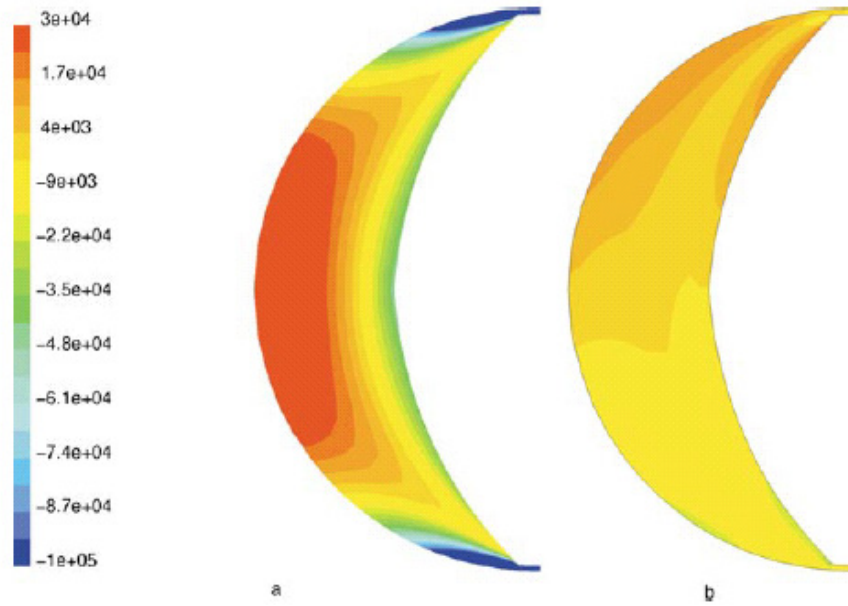
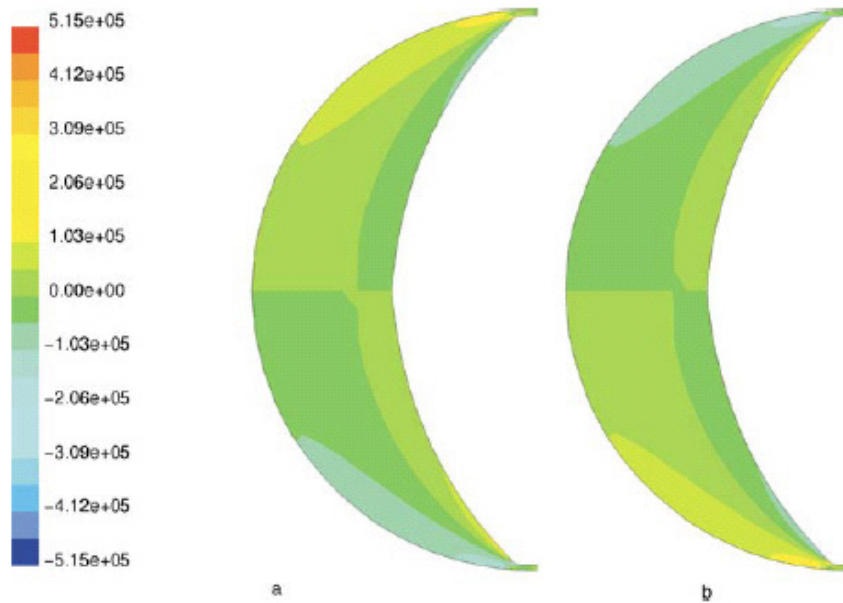
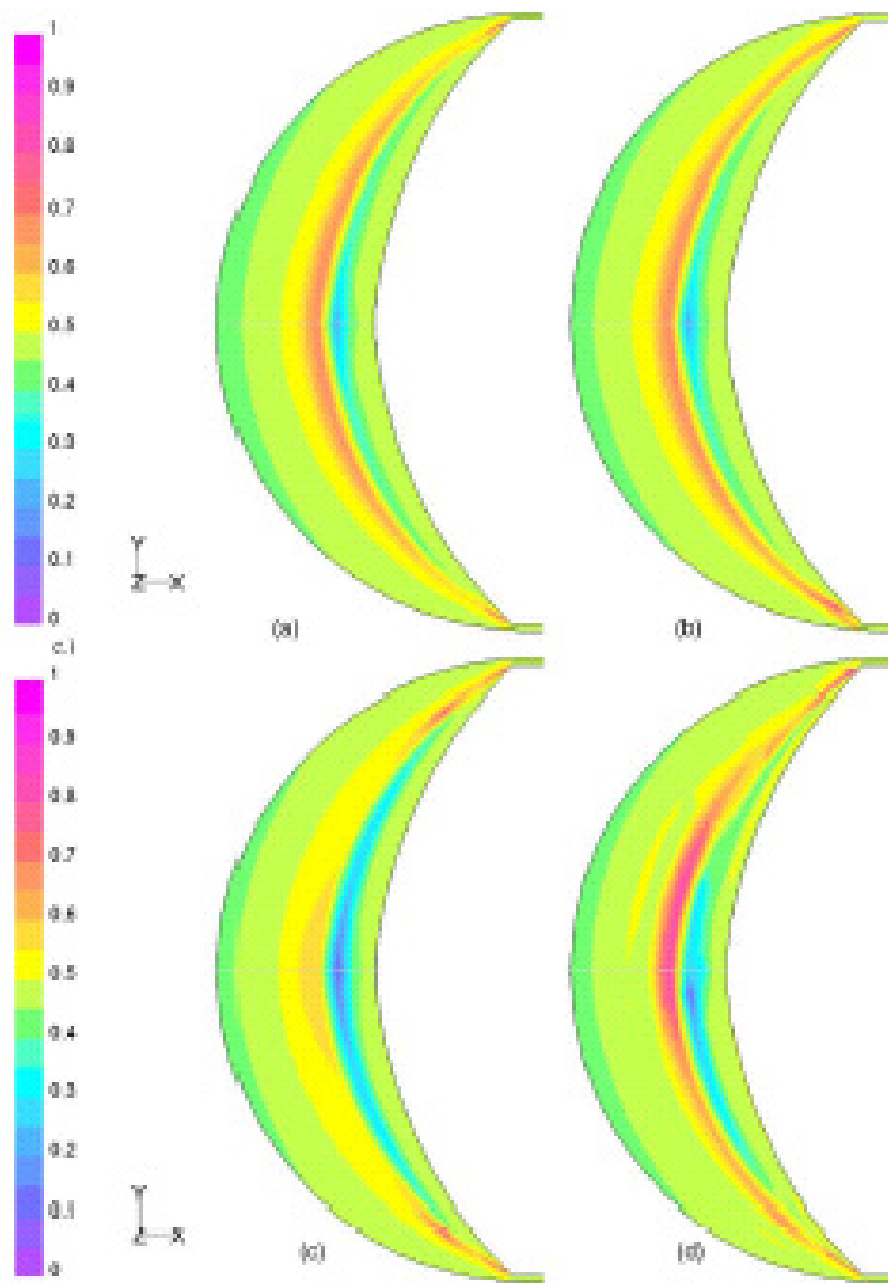


Figure II.18. Normal stress distributions at 1 rpm for a Newtonian fluid ($\lambda = 0$ s), (a) τ_{11} and (b) τ_{22} where the units of stress are gm/cm^2 (Connelly and Kokini, 2003)



The mechanism of mixing and its effectiveness in this 2D single-screw mixer was determined for purely viscous, shear thinning inelastic and viscoelastic fluids using flow profiles to find trajectories for material points with random initial positions (Connelly & Kokini, 2004). The mixing mode was identified as laminar shear and it was observed that the circulating pattern seen in the secondary flow profile dominated the mixing effectiveness. Mixing parameters such as the Manas-Zloczower mixing index (Figure II.19) segregation scale, cluster distribution index, length of stretch and efficiency of mixing were used to characterize the nature of mixing. Both the scale of segregation and the cluster distribution index showed an effect of rheology on the period of circulation. The length of stretch and efficiency of mixing showed some stretching near the walls but overall the efficiency decayed as t^{-1} , with the effect of the rheology evident in the speed of the decay and the negative values in the viscoelastic model results.

Figure II.19. Manas-Zloczower mixing index distributions at 1 rpm of (a) Newtonian, (b) Oldroyd-B with relaxation time of 1.5 s, (c) Bird–Carreau viscous and (d) Phan-Thien Tanner fluid models (Connelly and Kokini, 2004)



To increase the complexity of the mixing domain and to bring the geometric design of the mixer closer to a continuous twin-screw mixer, the 2D single screw mixer was compared in its mixing efficiency to a 2D twin-screw mixer (Connelly and Kokini, 2007). In order to successfully simulate the mutually moving parts in a 2D twin-screw mixer a technique known as ‘mesh superposition’ was utilized.

The mesh superposition technique is a modification of the fictitious domain method (Bertrand *et al.*, 1997) that allows the use of a periodically changing geometry without re-meshing the twin screw simulations. This mathematical simulation technique eliminates much of the challenges involved in simulation at the boundaries between fluid and solid parts. In this technique both the fluid chamber and the rotating parts are meshed even though the rotating parts are solid and do not deform. The technique uses a modification of the Navier-Stokes equation with a penalty term H , to accommodate for the moving parts internal to the flow geometry (Equation 6, Polyflow, 2008).

$$H(\mathbf{v} - \bar{\mathbf{v}}) + (1 - H)(-\nabla p + \nabla \cdot \mathbf{T} + \rho \mathbf{g} - \rho \mathbf{a}) = 0 \quad \text{Equation 6}$$

where H is a step function, \mathbf{v} is the velocity, $\bar{\mathbf{v}}$ is the local part velocity, p is the pressure, \mathbf{T} is the extra stress tensor, $\rho \mathbf{g}$ is the volume force, and $\rho \mathbf{a}$ is the acceleration term.

Each node in the problem is defined as either belonging to the moving part ($H = 1$) or as a part of the fluid ($H = 0$) thus setting the modified Navier-Stokes equation (equation 2) accordingly. To conserve mass in such a numerical scheme, the mass conservation equation is modified with a relative compression factor, β (Equation 7).

$$\nabla \cdot v + \frac{\beta}{\eta} \Delta p = 0 \quad \text{Equation 7}$$

where η is the local viscosity. The limitation of such a technique is its inability to conserve mass at the boundaries of the moving parts and leakage flows into the moving parts will be observed. The resolution of the velocity predictions in the vicinity of a relatively coarse mesh on the moving part will not be very detailed. However, such a technique is very valuable in solving problems with moving internal parts (such as twin-screw extruders and continuous mixers) and easily accounts for their constantly changing time-dependent boundaries.

The length of stretch was calculated for both 2D single-screw and twin-screw mixers and it was observed that it increased exponentially in the case of the twin-screw while only linearly in the single-screw (Connelly and Kokini, 2007). The length of stretch is an important parameter that quantifies the distributive mixing and leads to calculation of local mixing efficiency, with higher values of stretch giving higher values of mixing efficiency. An exponentially increasing length of stretch shows that the mixing is chaotic in nature. It was also qualitatively observed that the 2D single screw mixer had limited mixing capability while the results from the 2D twin screw simulation also showed the presence of dead zones in the twin-screw mixer.

3D numerical simulation studies would have shed more light on the important axial flow and mixing behavior in this twin-screw geometry. The axial component of velocity in a continuous mixer is significant and is responsible for the flow of the material through the barrel. This axial flow is perturbed periodically by the moving impellers which cause a periodic ‘folding’ of the material lines increasing the stretching and thus the mixing

efficiency. The axial component can only be realized in a full 3D simulation and is essential for better prediction of the mixing efficiency.

A 3D steady-state problem at one fixed position of the paddles was solved using finite element methods and Newtonian rheology (Connelly, 2004). The predicted velocity field showed strong evidence of a back flow in the intermeshing region between the two paddles. However, this steady-state approach does not reveal much information about the time-dependent variation of the velocity field which would be critical in predicting the particle positions in a particle tracking simulation that would be used in calculating mixing measures such as segregation scale, length of stretch, efficiency of mixing, etc.

Using finite element techniques, Avalosse & Rubin (2000) modeled the flow and mixing in a 3D single screw extruder. They were able to reproduce the pressure and velocity profiles in the single screw extruder using the rotating reference frame technique with a Bird-Carreau viscous fluid model for HDPE when using mini-element velocity/constant pressure elements for the interpolation.

Similar efforts to understand the mixing ability of a variety of twin-screw elements has been led by K. Funatsu's group using finite element methods and a coordinate system that moves in the axial direction parallel to the flights in order to fix the geometry of the analysis domain (Kajiwara *et al.*, 1996; Yoshinaga *et al.*, 2000) or a quasi steady state analysis at given increments (Ishikawa *et al.*, 2000, 2001, 2002). The finite element design of the twin screw geometry considered in their studies is show in Figure II.20. To represent the dynamic motion of the screws within the barrel, the geometry was broken into 6 sequential geometries (Figure II.21) with 15° increments due to the symmetry of the geometry. The problem was

solved as a steady state solution at the first (0°) step and the solution was used as the initial conditions of the second step. This process was repeated till a complete solution for the required number of rotations was obtained.

Figure II.20. Finite element design of the (A) flow domain and (B) disc dimensions (Ishikawa *et al*, 2000)

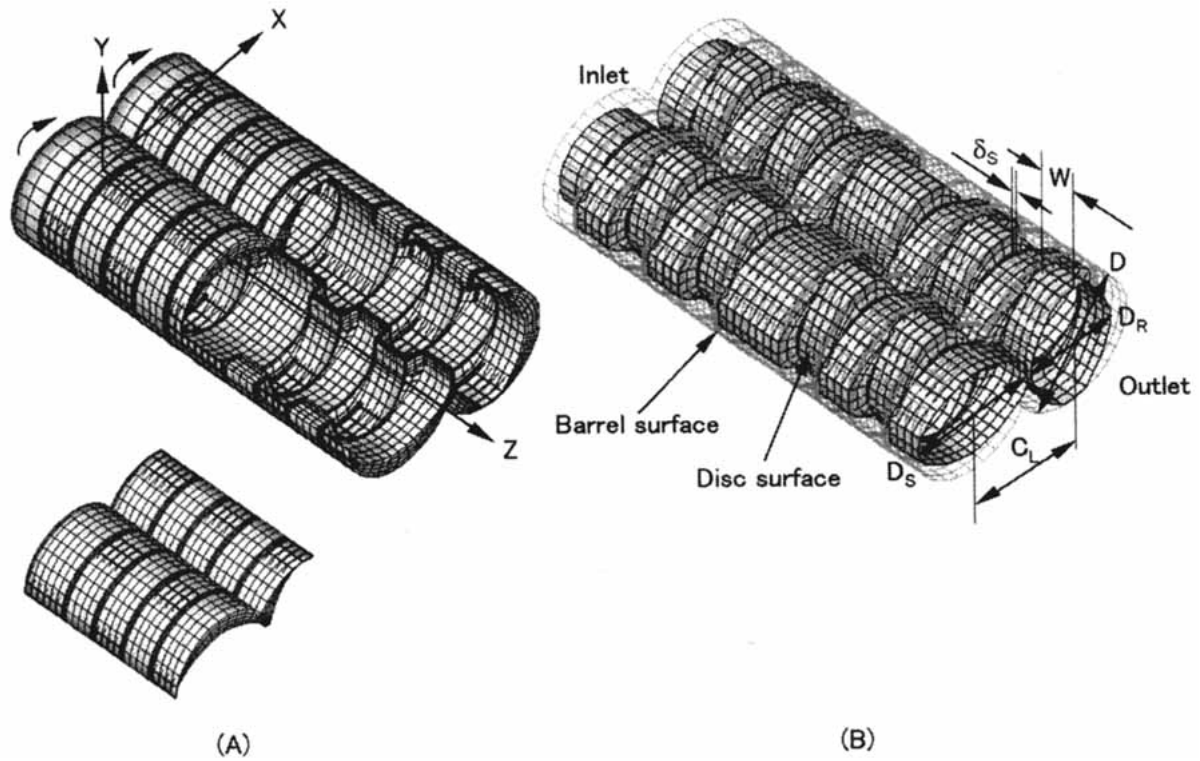
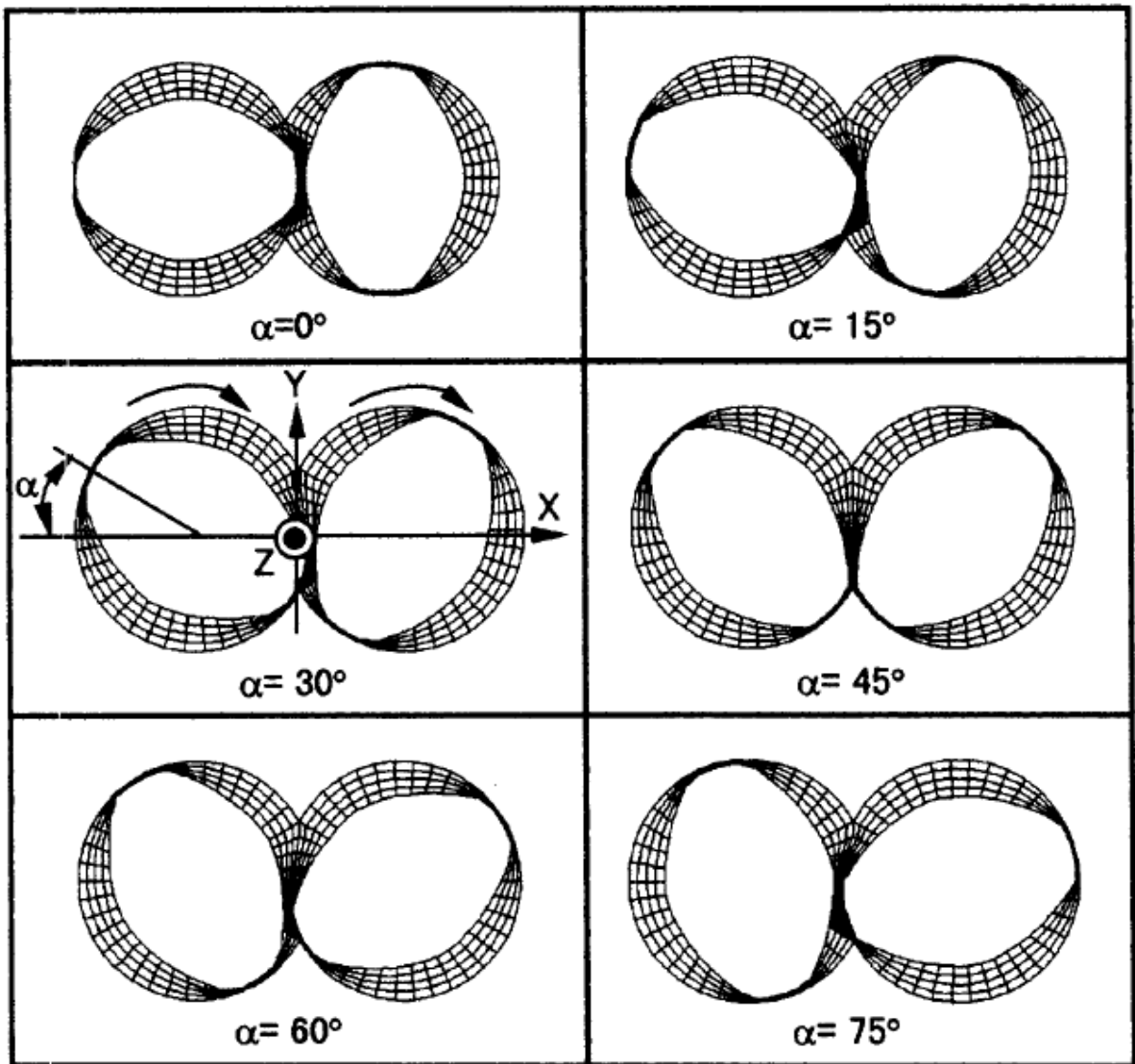
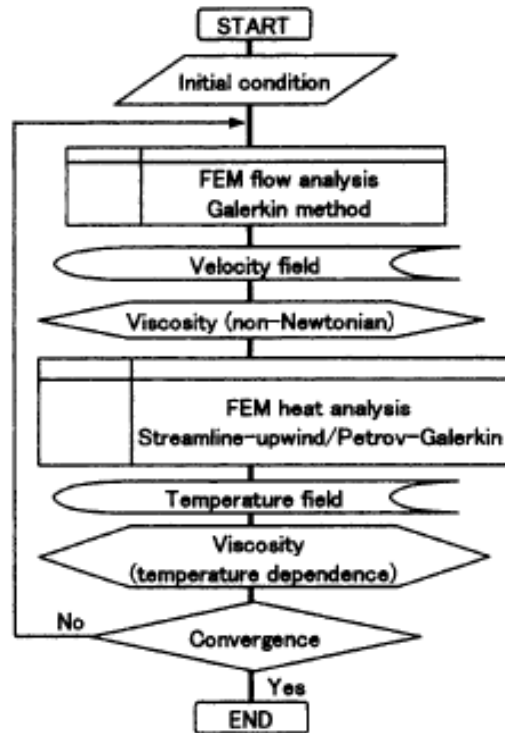


Figure II.21. Sequential geometries representing a quarter of rotation cycle (Ishikawa *et al*, 2000)



Bird-Carreau and Cross generalized Newtonian constitutive models that fit polypropylene steady shear experimental data were used to solve the 3D numerical simulation problem under non-isothermal conditions. The flow and temperature fields were solved separately (Figure II.22) and convergence was assumed when the difference between successive iterations was less than 0.1%.

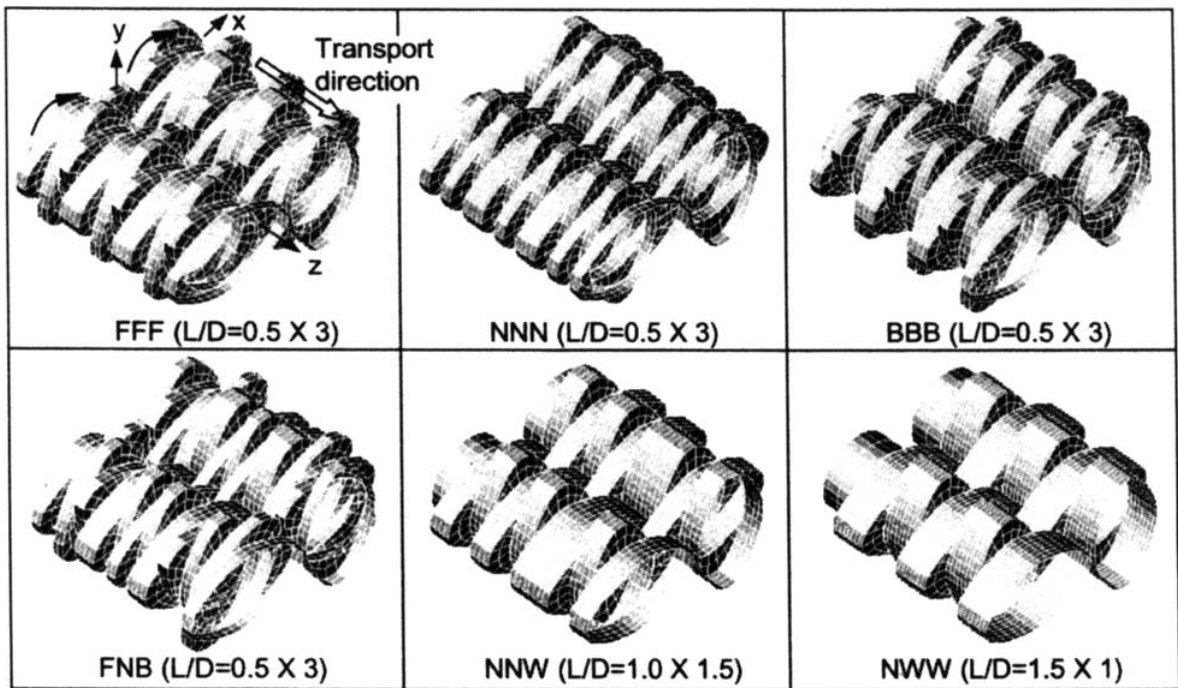
Figure II.22. Flow diagram of a 3D non-isothermal flow analysis (Ishikawa *et al.*, 2000)



Particle marker tracking was used to solve for mixing performance indices that included RTD, stress distribution, mean nearest distance between markers, backward flow mixing index, area stretch, strain history and SME. The pressures and temperatures predicted by the simulation results in Ishikawa *et al.* (2000, 2002) were experimentally validated with measurements taken away from the nip at the top of the barrel using polypropylene melts in several fully filled twin screw extruder configurations with a range of operating conditions and showed acceptable agreement.

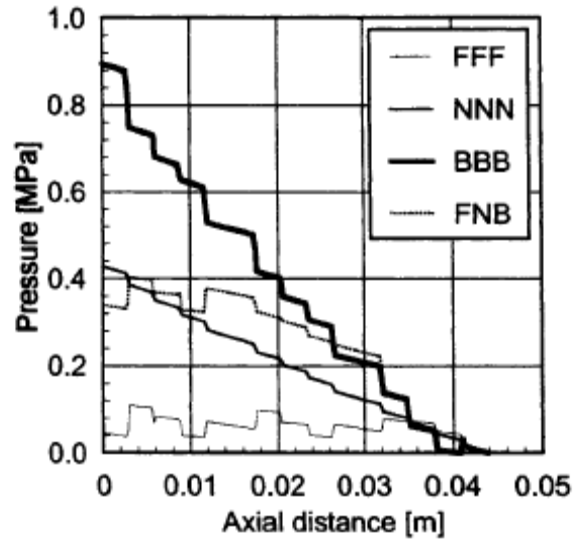
Kneading discs with different thicknesses and stagger angles (Figure II.23) were studied (Ishikawa *et al.*, 2001) and the effect of this geometric variation on temperature and pressure distributions were studied.

Figure II.23. Screw dimensions used in numerical analysis (F: forward, N: neutral B: backward, W: L/D 1.0, WW: L/D 1.5) (Ishikawa, *et al*, 2001).



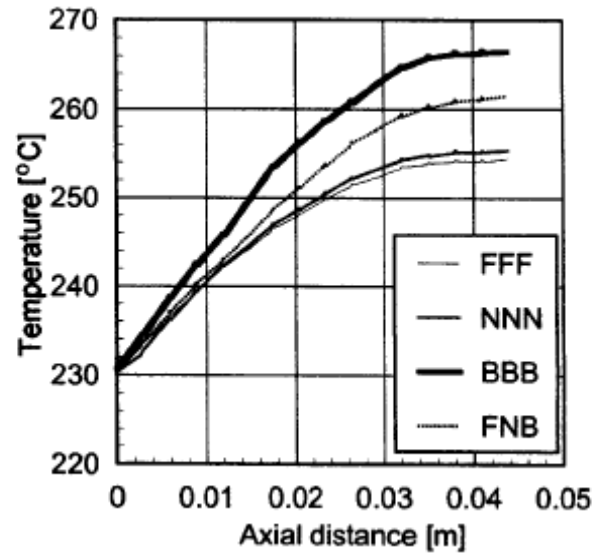
The disk width was shown not to have any effect in pressure or temperature distribution in the axial direction. They showed that the pressure gradient was small when the kneading blocks were arranged in a forward (pumping) stagger (FFF) and larger for the backward (reverse flow) stagger (BBB) (Figure II.24). The small pressure gradient in the FFF configuration is expected due to the strong conveying action of this configuration.

Figure II.24. Pressure distributions in the axial direction with different stagger angles (Ishikawa *et al.*, 2001)



When the influence of stagger angle on the axial temperature distribution was observed, it was once again seen that the backward flow caused by the BBB configuration increased the temperature higher than the FFF configuration (Figure II.25).

Figure II.25. Temperature distributions in the axial direction with different stagger angles (Ishikawa *et al.*, 2001)



The differences in distributive and dispersive mixing performance of these configurations was studied by analyzing the probability density function of area stretch (Figure II.26) and stress magnitudes (Figure II.27) respectively. They concluded that the FNB configuration provided the highest dispersive and distributive mixing as the number of particles passing through the highest stress regions and those experiencing high area stretches is highest in this configuration.

Figure II.26. Distributions of area stretch with different stagger angles (Ishikawa *et al*, 2001)

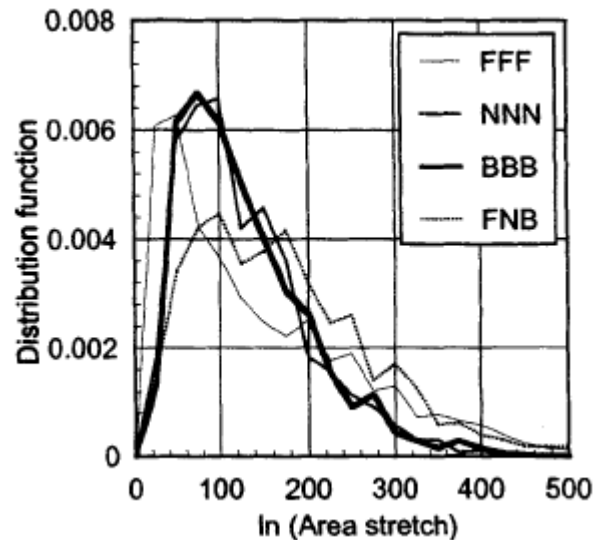
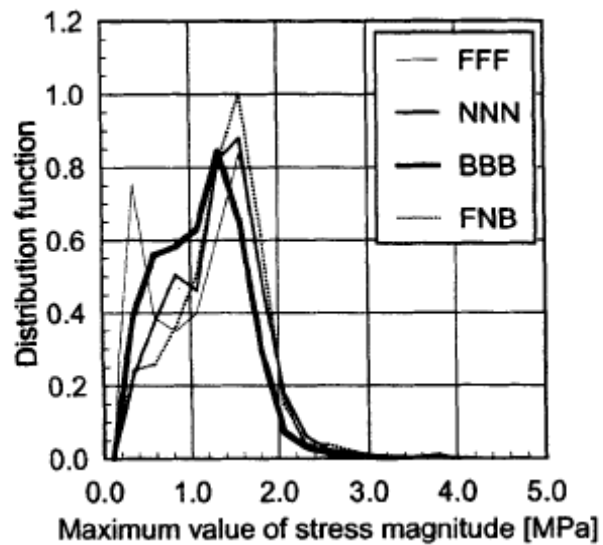


Figure II.27. Distributions of stress magnitudes with different stagger angles (Ishikawa *et al*, 2001)



The studies by this group are an incremental step in the understanding of the flow and mixing in a twin-screw continuous mixer. However, the use of a quasi steady state problem that

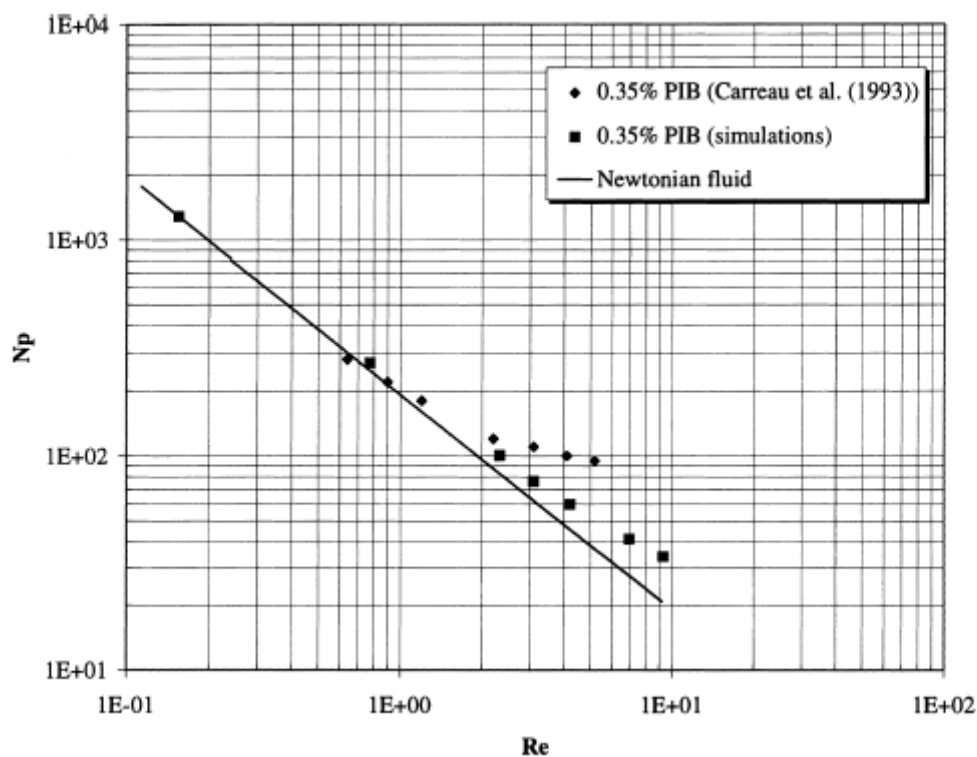
solves for the motion of the paddles in a piecewise fashion could lead to large errors in calculation due to the large time increments utilized. Such problems in accuracy can be overcome by solving the problem in a time-dependent manner with small increments that increase the accuracy of the predictions. While Ishikawa and co-workers used increments of 15° (Ishikawa *et al*, 2000, 2001) and 3° (Ishikawa *et al*, 2002), Bravo and co-workers (Bravo *et al*, 2000, 2004) used a similar quasi-steady state technique with angular increments of 12.86° to study flow and mixing in a five-block kneading paddle. However, both sets of studies did not delve into the effects of changing the angular displacement between sequential geometries on the accuracy of the overall prediction.

Limited new work has been done in simulating the 3D flow of viscoelastic fluids in complex mixers with multiple moving parts. The simulation of viscoelastic fluids in geometries with moving time-dependent boundaries using mesh superposition or custom FEM code is currently not possible due to the exceedingly large size of the numerical problem and the computational difficulties in reaching a converged solution for such fluids with complex rheology due to the presence of many singularities in geometries such as the twin-screw extruder/mixer. A few researchers have tried to address this problem by utilizing reduced forms of viscoelastic equations that do not fully describe the fluid rheology but show some aspects of elasticity.

In one such example, Bertrand *et al.* (1999) modeled a helical ribbon mixer using finite element methods and a second order Criminale-Erikson-Filbey (CEF) rheological model, which allows for a limited form of elastic memory but does not describe relaxation or contain a hyperbolic equation in the extra stress tensor, τ . They were able to predict using the

simulations a rise in power consumed with the addition of elasticity that was similar but smaller than that measured experimentally (Figure II.28).

Figure II.28. Power curves for 0.35% PIB solution in the helical mixer (Bertrand *et al.*, 1999)



A rigorous understanding of the effect of viscoelasticity on mixing in complex mixer geometries such as continuous twin screw mixers remains elusive due to the mathematical challenges in using viscoelastic fluid models in realistic geometries and the present state-of-the-art allows for the use of viscoelastic models only in simplified geometries.

II.C.2. Batch Mixers

Jongen (2000; Jongen *et al.*, 2003) used finite element methods with a modification of the mesh superposition technique to characterize the flow and mixing of Newtonian fluids in

simpler 2D representations of batch mixers such as the Plastograph, Do-Corder and other mixers commonly used to mix viscous pastes such as dough. They utilized a flow deformation parameter, D , to classify the flows in different mixers as lying between the extremes of pure rotational ($D=-1$), pure shear ($D=0$) and pure extensional ($D=1$). This flow deformation parameter D was defined as

$$D = \frac{1 - \mathcal{R}^2}{1 + \mathcal{R}^2} \quad \text{Equation 8}$$

where

$$\mathcal{R}^2 = \frac{\omega^2}{s^2} \quad \text{Equation 9}$$

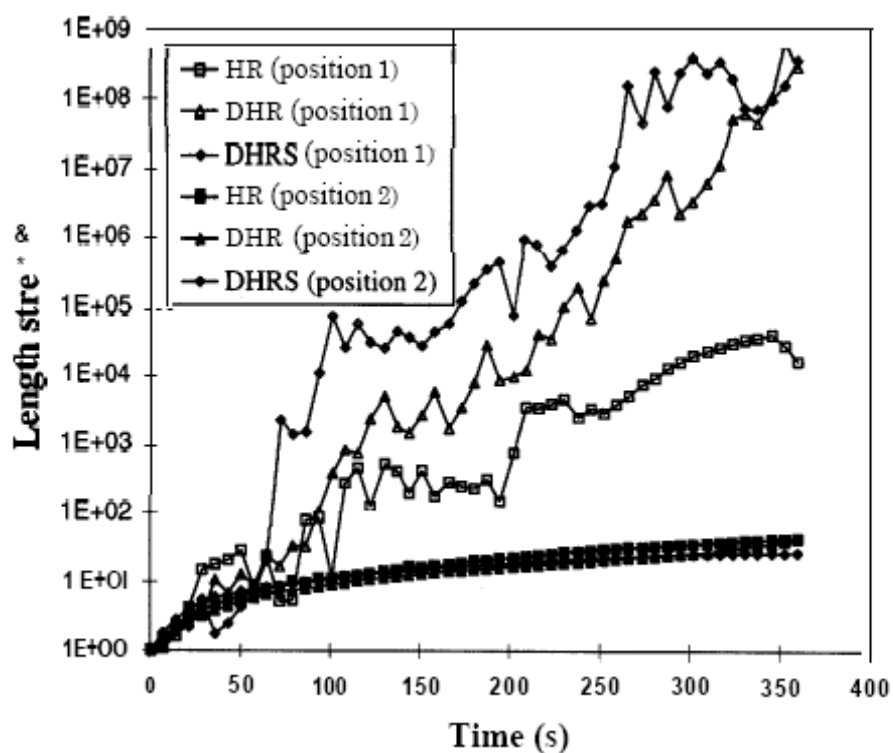
and s^2 and ω^2 are the second invariants of the strain rate and vorticity.

The author(s) suggest that this flow deformation parameter, D , can be used as an objective measure to distinguish the different types of flows in various batch mixers and as aid in designing mixing equipment in a more rigorous manner. They also caution the extension of the usage of this parameter in 3D as it is not entirely accurate and non-trivial

Moving beyond 2D representations of mixing geometries, significant progress has also been made in simulating complex batch mixers in 3D using simple rheological models. The mesh superposition technique was used to study the mixing efficiency of helical ribbon mixers (de la Villeon *et al.*, 1998) and the motion of the impeller was modeled with a Lagrangian reference frame. Velocity flow fields were computed for the flow of shear thinning Carreau-A fluid using a 3D FEM code and tracer tracking was conducted to study mixing measures. The study concluded that a double helical ribbon (DHR) mixer was more efficient in mixing

than a single helical ribbon (HR) mixer. Also, the addition of an axial conveying screw (DHRS), while increasing the power drawn, did not aid in improving the mixing efficiency. They drew conclusions based on the calculation of two measures of mixing efficiencies - the length of stretch and the Manas-Zloczower dispersive mixing index. They showed that the length of stretch increased exponentially in the top half of the mixer (figure 19, position 1), where the impellers agitate the fluid most. In this position, there was a 60% gain in length of stretch due to the addition of a second helical ribbon impeller, and only an additional 20% rise due to the addition of the conveying screw. At the bottom half of the mixer (Figure II.29, position 2), there was no exponential increase in length of stretch, which suggests that the mixing is not chaotic and inefficient in that location.

Figure II.29. Calculated length stretch values (de la Villeon *et al*, 1998)



The authors note that while this study offered a good estimate of the mixing characteristics of helical ribbon mixers, it did not offer enough detail on the power drawn and the energy needed for mixing which are key factors in successful scaling and design of mixers.

The mixing performance of the Brabender Farinograph (Figure II.30) was studied with finite element methods using mesh superposition followed by particle tracking. Flow simulations were predicted for Newtonian, and shear thinning fluids and velocity, pressure, shear rates and mixing indices were evaluated (Connelly and Kokini, 2006a) and compared to those obtained using Laser Doppler Anemometry (LDA) by Prakash and co-workers (Prakash, 1996; Prakash and Kokini, 1999, 2000; Prakash *et al.*, 1999). The batch mixer utilizes two non-intermeshing asymmetrical sigma blades that rotate in a 3:2 speed ratio, with the fast (right) blade turning 93 rpm counterclockwise and the slow (left) blade turning 62 rpm clockwise. A viscosity of 54 poise was used for the Newtonian simulations. Particle tracking simulations were then performed using the flow simulations with Newtonian and the mixing effectiveness of the mixer was evaluated using cluster distribution index, scale of segregation, mean length of stretch and time-averaged efficiency as mixing measures rheology (Connelly and Kokini, 2006b).

Figure II.30. The Brabender Farinograph (Connelly, 2004)



The complex blade geometry and movement was accurately modeled in 3D and the results portray a revealing picture of the mixing processes involved. It was shown that the zone in the center of the mixer between the two blades had excellent distributive and dispersive mixing ability and in contrast, the area that is away from the region swept by the blades demonstrates very slow mixing (Figure II.31). Positions of the blades that provided high and low mixing efficiencies were also identified (Connelly and Kokini, 2006a). The mixing index in the center of the mixer between the two blades for a Newtonian fluid was around 0.7 (Figure II.32) and this is considerable higher than the average value of 0.4 reported in the study on helical ribbon mixers (de la Villeon *et al*, 1998). This could be very well due to the higher shear rates produced in the Farinograph as compared to the helical ribbon mixer with lower clearances between the two blades.

Figure II.31. Simulated mixing index on a plane across the center of the bowl for (a) corn syrup (b) 2% CMC (c) 0.11% carbopol (Connelly and Kokini, 2006a)

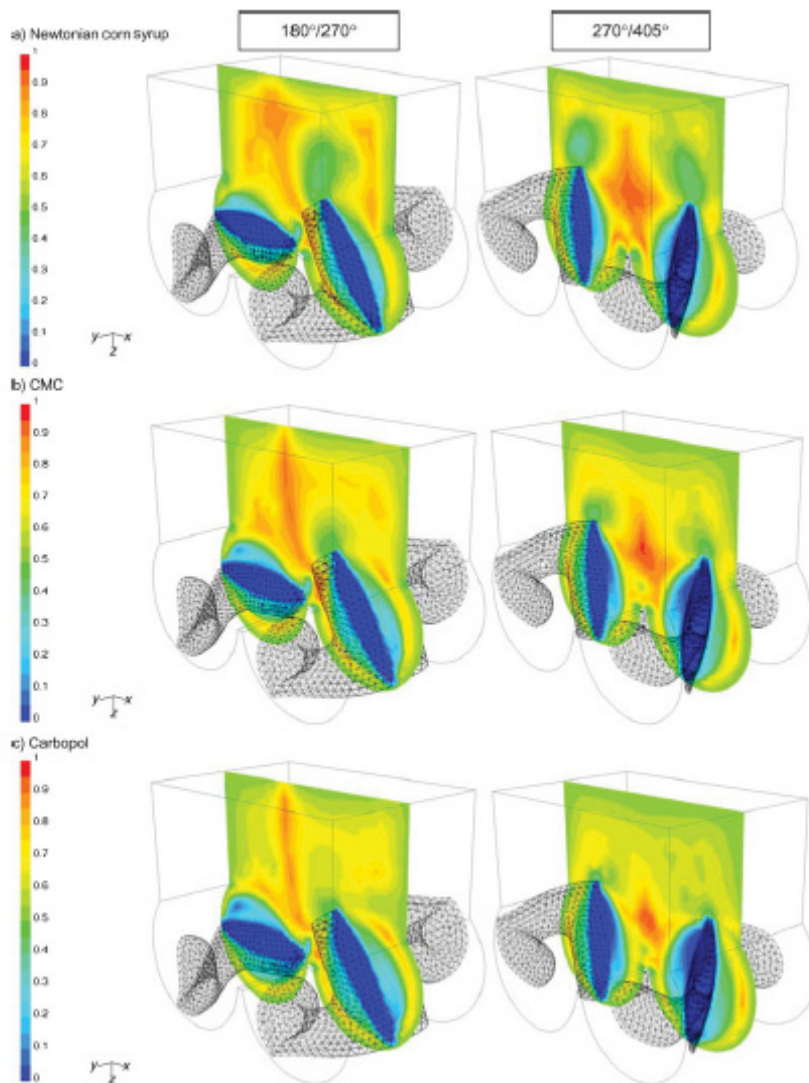


Figure II.32. Mixing index results from 10,000 points randomly distributed throughout the flow volume (Connelly and Kokini, 2006a)

	Mixing Index	Corn Syrup	2% CMC	0.11% Carbopol
180°/270° blade position				
	>0.5	79.9%	90.8%	77.6%
	>0.7	21.5%	18.1%	10.9%
270°/405° blade position				
	>0.5	90.3%	81.7%	78.6%
	>0.7	21.7%	14.1%	8.0%

The results are from the 270°/405° blade position and show the percentage of values in the shear (>0.5) and elongational (>0.7) flow ranges.

Particle tracking results showed the batch Farinograph mixer to have excellent distributive mixing in the center between the two blades and towards the sides of the mixer in the clearance regions as seen from the distribution of clusters of points between the two halves of the mixer (Figure II.33). The mixer was also very efficient with the time-averaged efficiency staying above zero at all times (Figure II.34).

Figure II.33. 3D positions of 10,000 initially randomly distributed material points with concentrations of 1 (red/light gray) in the back and 0 (blue/dark gray) in the front viewed from the right side (Connelly and Kokini, 2006b)

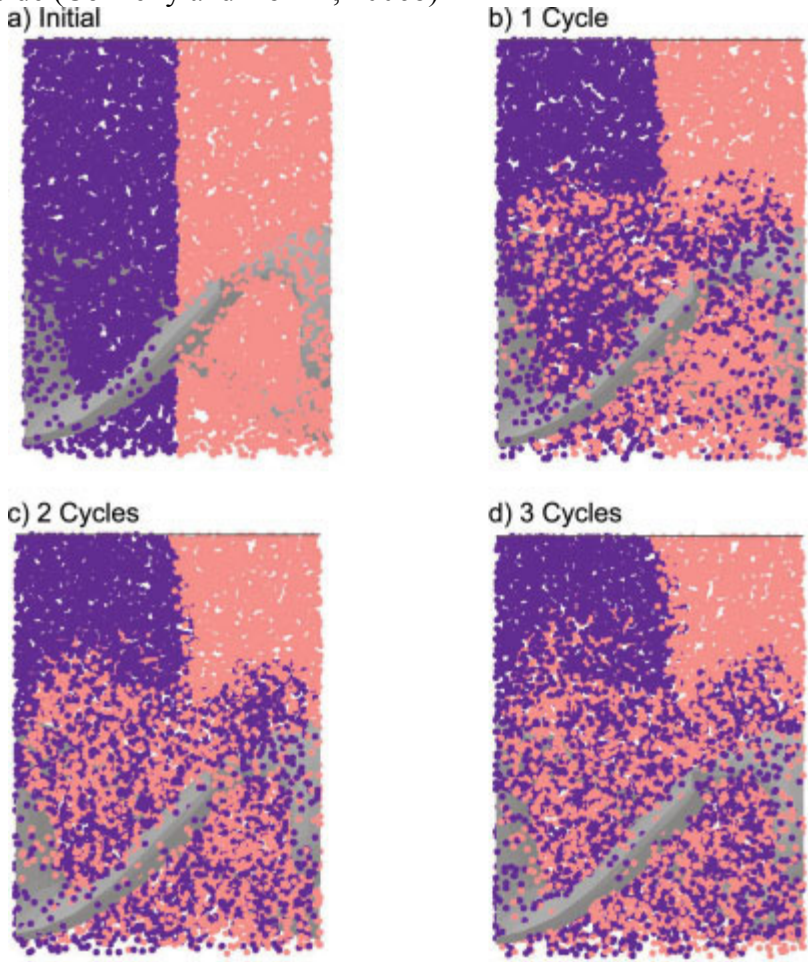
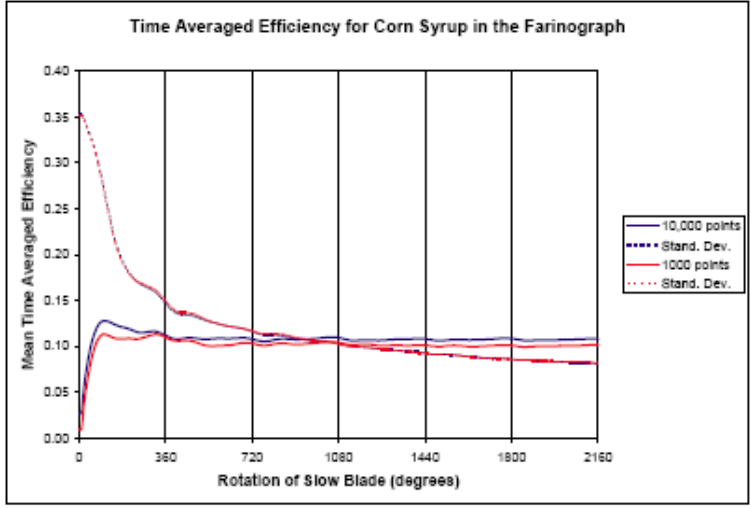


Figure II.34. Mean time-averaged efficiency of the mixing experienced by 10,000 infinitesimal material lines over three cycles of the blades (Connelly, 2004)



While the above studies on batch mixers are encouraging additions to the state-of-the-art, the estimation of energy requirements that can lead to better design and scaling has not been accomplished and further work is required to understand the effects of mixer geometry, operating parameters and fluid rheology on mixing efficiency across differing designs.

II.D. Scale-up and Identification of similar mixer geometries

Scaling laws are usually based on dimensional analysis, where the dimensions of the geometry to be scaled or the operating parameters are related to heat transfer capabilities or power requirements of the equipment.

As an illustration of this concept, a correlation (Equation 10) suggested by Metzner and Otto (Metzner and Otto, 1957) based on their studies on flat-bladed turbines impellers has been widely used to estimate the power consumption in such mixers.

$$\dot{\gamma} = K_s N \quad \text{Equation 10}$$

where $\dot{\gamma}$ is the effective shear rate, N is the rotation speed of the impeller and K_s is a proportionality constant (set to 13 in their experiments). After $\dot{\gamma}$ is determined, it is used to estimate apparent viscosity using the power-law equation. This apparent viscosity is used in the determination of Reynolds number (Re) from

$$\text{Re} = d^2 N \rho / \mu_a \quad \text{Equation 11}$$

This analysis has the advantage of using a Po vs. Re correlation developed for Newtonian fluids to be used for non-Newtonian fluids. Thus the power consumed by a particular fluid in

a flat-turbine mixer can be estimated from only the rotational speed of the impellers and allows for scaling by identification of operating conditions that consume the same amount of power.

While dimensional analysis is a powerful tool, it fails to provide universal scaling laws due to mixed dependencies of surface and volume characteristics (Dhanasekharan and Kokini, 2003). For instance, when a dimension is scaled by ϕ , the flow and power requirements are scaled by ϕ^3 , while heat transfer characteristics will be scaled only by a factor of ϕ^2 . Such unequal scaling laws have been circumvented in the past by considering the geometric constraints of the extruder or mixer such as screw diameter, flight height, etc., as primary variables, whose scaling will affect the secondary variables such as residence time, shear rates, power consumption, heat transfer, etc. (Rauwendaal, 1987). Such an approach has led to successes in scaling of single-screw extruders (Rauwendaal, 1987; Dhanasekharan and Kokini, 2003) where similarity in specific mechanical energy input and residence time distribution have been utilized successfully to scale-down extruders (Dhanasekharan and Kokini, 2003) while varying screw geometry parameters such as L/D, screw diameter, channel depth or screw speed (Figure II.35).

Figure II.35. Demonstration of extruder scale-down (Dhanasekharan and Kokini, 2003).

Geometry 1 (big)

$D = 3.5\text{cm}$, $H = 1\text{cm}$, $D/H = 3.5$, helix angle = 17.66° , $\varepsilon = 0.03\text{ cm}$, $L/D = 6$

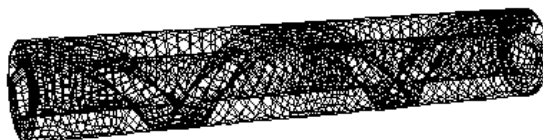


SME = 164.42 KJ/Kg

Average Residence time = 31.16 s

Geometry 2 (small)

$D = 1.6\text{ cm}$; $H = 0.381\text{ cm}$; helix angle = 40° ; $\varepsilon = 0.03\text{ cm}$; $L/D = 6$.



SME = 152.57 KJ/Kg

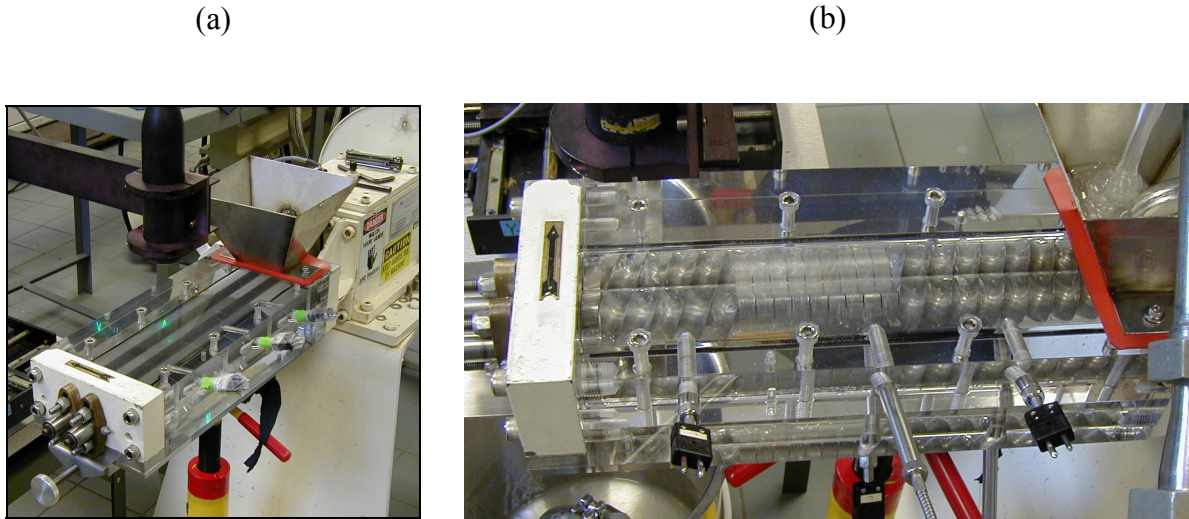
Average Residence time = 31.81 s

When scale-up of internal or batch mixers were considered, requirements of energetic similarity and similar mixing time, temperature regime and Weber number (shearing forces vs. interfacial forces) lead to successful applications in the industry (Sunder, 1994). While such applications have been found in literature, there are no specific examples of scaling or identification of designs in batch and continuous mixers that offer similarity in mixer performance.

II.E. Velocity Characterization in Continuous Mixer

Velocity distributions were determined at various locations in the Readco Continuous mixer (Figure II.36) by Lindsay Fanning (Fanning, 2008). These velocities were utilized in this research to compare and validate the simulated velocity values.

Figure II.36. 2” Readco continuous processor with Plexiglas barrel, showing (a) the LDA probe and beams and (b) the paddle arrangement (Fanning, 2008)

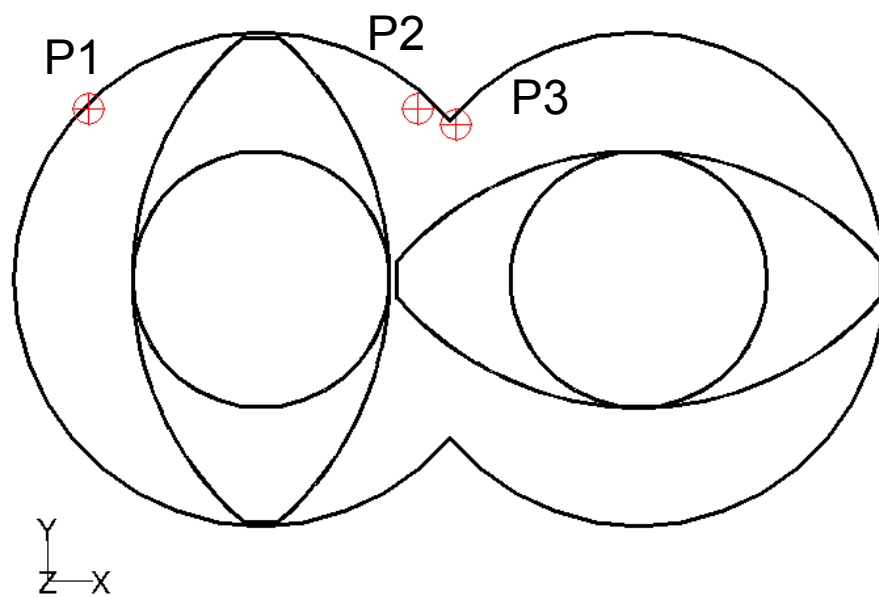


The Readco Products Continuous Processor is a Teledyne Specialty Equipment and is a 2” co-rotating, twin screw, high-intensity mixer that can serve as a model laboratory-scale continuous mixer for scale-up operations. It has a clear Plexiglas barrel that has been modified to incorporate pressure transducers by drilling a pair of pressure ports in the Plexiglas barrel at different angles in the cross-sectional plane so that a pressure profile can be constructed at that position. The self-wiping elements include flat mixing paddles, helical mixing and conveying paddles, reverse helix paddles used to direct the flow into the outlet and conveying screw elements usually used at the feed point.

Using LDA, velocity measurements were obtained inside the barrel of the continuous processor for Globe corn syrup 1142 (Corn Products) with a viscosity of 54 poise at 50°C (Fanning, 2008). This high viscosity corn syrup has good clarity to allow for the LDA

measurements to be taken. The mixer was configured with two pairs of 4" screw elements at the inlet followed by nine aligned pairs of flat paddles and then another pair of 4" screw elements with a pair of reverse helical paddles at the discharge as shown in figure 22b. The mixer was fully filled and operated at 100 rpm. Measurements were taken in the plane of the 4th pair of flat paddles from the inlet. Velocity was measured at points between the paddles and barrel wall as well as in the intermeshing region of the paddles. An encoder was used to keep track of the paddle position in relation to each data point. To allow for calculation of velocity gradients for each point, measurements were also taken 0.5 mm away from the original point in each of the x, y and z directions in the manner of Prakash *et al.* (1999). Three points in the co-ordinate system of the LDA - P1 (-3.74, 1.75, mid-z of the paddle), P2 (-0.34, 1.75, mid-z of the paddle) and P3 (0.05, 1.59, mid-z of the paddle) (Figure II.37) were identified as representative of various locations in the mixer (Point P1 is in the clearance region between the barrel wall and paddle while points P2 and P3 are in the intermeshing region, with P2 closer to the barrel wall) and the velocity components at these locations was reported (Appendix A). These velocity components were used in this research for comparison and validation.

Figure II.37. Location of measurement points



III.Theoretical Background

Numerical simulation of fluid flow in a mixer is conducted by solving the equation of the conservation of momentum, with a rheological equation of state (constitutive models) of the food material to be mixed, along with initial and boundary conditions.

III.A. Governing Equations (Polyflow, 2008)

If an incompressible fluid is assumed, then conservation of mass gives us the equation of continuity

$$\nabla \cdot \mathbf{v} = 0$$

Equation 12

The conservation of momentum gives us the equation of motion and is an account of the momentum transport by convection, diffusion and other sources. Let ρ be the fluid density and \mathbf{f} be the external body force per unit mass. The conservation of linear momentum is then given by:

$$\nabla \cdot \boldsymbol{\sigma} + \rho \mathbf{f} = \rho \left(\frac{\partial \mathbf{v}}{\partial t} + \mathbf{v} \cdot \nabla \mathbf{v} \right)$$

Equation 13

The terms on the right hand side of the equation are called the convection terms and are responsible for momentum transport by convection. The first term on the left hand side is responsible for momentum transport by diffusion. The second term on the left hand side accounts for external forces such as gravitational forces that can impart momentum.

For such an incompressible fluid, the stress tensor $\boldsymbol{\sigma}$ is given as the sum of the isotropic pressure (p) component and an extra stress tensor (\mathbf{T}). The extra stress tensor is described using an appropriate constitutive model.

$$\boldsymbol{\sigma} = -p\mathbf{I} + \mathbf{T}$$

Equation 14

The last equation that is required for cases that are non-isothermal is the equation for conservation of energy which is given as:

$$\rho C(T) \left(\frac{\partial T}{\partial t} + \mathbf{v} \cdot \nabla T \right) = \mathbf{T} : \nabla \mathbf{v} + r - \nabla \cdot \mathbf{q}$$

Equation 15

where $C(T)$ is the heat capacity as a function of temperature, r is the given volumetric heat source and \mathbf{q} is the heat flux. Viscous heating is described through the term $\mathbf{T} : \nabla \mathbf{v}$.

These equations, together with viscous or viscoelastic constitutive models, form a complete set of governing equations whose solutions give velocity and temperature profiles for a particular problem.

III.B. Constitutive equations

III.B.1. Generalized Newtonian

For a generalized Newtonian fluid, the stress tensor \mathbf{T} is given by:

$$\mathbf{T} = 2\eta\mathbf{D}$$

Equation 16

Where \mathbf{D} is the rate-of-deformation tensor and η can be a function of local shear rate $\dot{\gamma}$, temperature T , or both. The local shear rate is defined as

$$\dot{\gamma} = \sqrt{2tr(\mathbf{D}^2)}$$

Equation 17

In simple shear flow $\dot{\gamma}$ reduces to the velocity gradient.

III.B.2. Shear rate dependent viscosity laws

Constant

For Newtonian fluids, a constant viscosity of

$$\eta = \eta_0$$

Equation 18

can be specified. η_0 is referred to as the Newtonian or zero-shear-rate viscosity.

Power Law

The power law for viscosity is

$$\eta = K(\lambda\dot{\gamma})^{n-1}$$

Equation 19

where K is the consistency factor, λ is the natural time, and n is the power-law index, which is a property of a given material.

III.B.3. Temperature dependent viscosity laws

If the flow is non-isothermal, the temperature dependence of the viscosity must be taken into account along with the shear-rate dependence. The viscosity law can be factorized as follows:

$$\eta = H(T)\eta_0(\dot{\gamma})$$

Equation 20

where η_0 is the viscosity law (as computed by one of the shear-rate-dependent laws described above) and $H(T)$ is the Arrhenius law given as

$$H(T) = \exp\left[E_a\left(\frac{1}{T} - \frac{1}{T_a}\right)\right]$$

Equation 21

where E_a is the activation energy and T_a is the reference temperature for which $H(T)=1$.

III.B.4. Differential Viscoelastic Constitutive Equations

For viscoelastic flows, the total extra-stress tensor is decomposed into a viscoelastic component \mathbf{T}_1 and a purely-viscous component \mathbf{T}_2 :

$$\mathbf{T} = \mathbf{T}_1 + \mathbf{T}_2$$

Equation 22

\mathbf{T}_1 is computed differently for each type of viscoelastic model. \mathbf{T}_2 is computed from

$$\mathbf{T}_2 = 2\eta_2\mathbf{D}$$

Equation 23

where η_2 is the viscosity factor for the Newtonian (i.e., purely-viscous) component of the extra-stress tensor.

The viscosity ratio η_r is defined as η_2/η . The relationship of η_1 and η_2 to η is expressed by

$$\eta_1 = (1 - \eta_r)\eta$$

Equation 24

and

$$\eta_2 = \eta_r\eta$$

Equation 25

For a differential viscoelastic flow, the constitutive equations are solved for the extra-stress tensor, the momentum equations, the incompressibility equation, and (for non-isothermal flows) the energy equation.

For the constitutive equations for \mathbf{T} (Equation 22), \mathbf{T}_1 is computed from a differential equation or from an algebraic equation involving a state variable (configuration tensor), which obeys a differential equation. Models of the so-called Oldroyd family (including the Maxwell, Oldroyd-B, White-Metzner, Phan-Thien-Tanner, and Giesekus models) obey a differential equation written in terms of the extra-stress tensor \mathbf{T}_1 .

$$\mathbf{g}(\mathbf{T}_1) \cdot \mathbf{T}_1 + \lambda \frac{\delta \mathbf{T}_1}{\delta t} = 2\eta_1 \mathbf{D}$$

Equation 26

where $\mathbf{g}(\mathbf{T}_1)$ is a model-specific function, λ is a model-specific relaxation time, and η_1 is a model-specific viscosity factor for the viscoelastic component of \mathbf{T} .

Oldroyd-B Model

The Oldroyd-B model is one of the simplest viscoelastic constitutive equations. It allows for the inclusion of the purely-viscous component of the extra stress, which can lead to better

behavior of the numerical scheme. Oldroyd-B is a good choice for fluids that exhibit a very high extensional viscosity. For the Oldroyd-B model, $\mathbf{g}(\mathbf{T}_1)$ is set as 1 and \mathbf{T}_1 is computed as

$$\mathbf{T}_1 + \lambda \overset{\nabla}{\mathbf{T}}_1 = 2\eta_1 \mathbf{D} \quad \text{Equation 27}$$

where $\overset{\nabla}{\mathbf{T}}_1$ is given as

$$\overset{\nabla}{\mathbf{T}}_1 = \frac{D\mathbf{T}_1}{Dt} - \mathbf{T}_1 \cdot \nabla \mathbf{v} - \nabla \mathbf{v}^T \cdot \mathbf{T}_1 \quad \text{Equation 28}$$

The purely-viscous component \mathbf{T}_2 is computed from Equation 23.

Phan-Thien-Tanner (PTT) Model

The Phan-Thien-Tanner (PTT) model exhibits shear thinning and a non-quadratic first normal-stress difference at high shear rates.. Unlike the Oldroyd-B, it is able to account for the effect of viscoelasticity on extensional flows that are an important feature of most dough mixers.

\mathbf{T}_1 is computed as

$$\exp\left[\frac{\epsilon \lambda}{\eta_1} \text{tr}(T_1)\right] T_1 + \lambda \left[\left(1 - \frac{\xi}{2}\right) T_1 + \frac{\xi}{2} \overset{\nabla}{T}_1 \right] = 2\eta_1 D \quad \text{Equation 29}$$

ξ and ϵ are material parameters that control, respectively, the shear viscosity and elongational behavior. In particular, a non-zero value for ξ leads to a bounded steady extensional viscosity. The purely-viscous component \mathbf{T}_2 is computed from Equation 23.

The conservation of mass and momentum along with the energy equation (for non-isothermal problems) and an appropriate constitutive equation are all required to solve for the flow of a fluid in a particular geometry. These equations can seldom be solved analytically and computational techniques such as finite differences, finite elements, finite volumes and spectral methods have been used to discretize and solve these problems numerically.

III.C. Discretization Methods

III.C.1. Finite Differences Method

Finite difference methods approximate the solutions to differential equations using difference quotients to approximate derivatives. The finite difference approximation is usually derived by approximating derivatives with Taylor series expansions of solutions. An ordinary differential equation being solved in 1D across an interval I is discretized into n intervals of interval size h , such that $nh=I$ and the equation is solved by approximating the exact analytical solution to the function by its numerical approximation. In more than one dimension and for irregular geometries, finite differences are difficult to generate and it is preferred to use finite element methods (FEM) due to their greater flexibility (Owens and Phillips, 2002) (FEM is treated in greater depth in the next section).

III.C.2. Finite Volumes Method

Finite volume methods are similar to finite differences, in that values are calculated at discrete nodes in a mesh. However, the 'finite volume' refers to a small volume surrounding each node point on a mesh. In the finite volume method, volume integrals in a partial differential equation that contain a divergence term are converted to surface integrals, using the divergence theorem. These terms are then evaluated as fluxes at the surfaces of each

finite volume. Because the flux entering a given volume is identical to that leaving the adjacent volume, these methods are conservative. FVM also allows for simpler formulation of unstructured meshes which is useful in meshing unbounded fluids and is hence used commonly in CFD techniques that involve simulating the turbulent flow of fluids around surfaces (Owens and Phillips, 2002).

III.C.3. Finite Elements Method (Reddy, 1993)

The Finite Element Method is characterized by three features:

1. The domain of the problem is represented by a collection of simple sub domains called finite elements. The collection of finite elements is called the finite element mesh.
2. Over each finite element, polynomial functions and algebraic equations relating physical quantities at corners of elements, called nodes, approximate the physical process.
3. The element equations are assembled using continuity and/or “balance” of physical quantities.

We can consider the model geometry of interest as a domain Ω over which the velocity, pressure and the stress tensor values are required. The equations of motion can be further simplified by assuming the inertia terms to be negligible. If V and P are the function spaces of the velocity and pressure fields respectively, then the finite element formulations are given by:

$$\int_{\Omega} (-\nabla p + \nabla \cdot \mathbf{T} + \mathbf{f}) \cdot \mathbf{u} d\Omega = 0, \forall \mathbf{u} \in V$$

Equation 30

$$\int_{\Omega} (\nabla \cdot \mathbf{v}) q d\Omega = 0, \forall q \in P$$

Equation 31

where \mathbf{u} and q are weighting functions. The weighted integrals of the error in the governing equations are set to zero to ensure that there are required numbers of independent linear algebraic equations. In order to transfer some of the differentiability requirements from the approximate solutions to the weight functions, integration by parts is performed to obtain the ‘weak’ form of the governing equations.

Integrating Equation 30 using integration by parts:

$$\int_{\Omega} (-p\mathbf{I} + \mathbf{T}) \cdot \nabla \mathbf{u}^T d\Omega = \int_{\Omega} \mathbf{f} \cdot \mathbf{u} d\Omega + \int_{\Omega} t \cdot \mathbf{u} d\Sigma, \forall \mathbf{u} \in V$$

Equation 32

where t denotes the surface traction on the boundary $\partial\Omega$ of Ω . The traction is the natural boundary condition and contains the pressure. The essential boundary condition is the velocity at the boundary. The essential boundary condition is applied by replacing the velocity approximation with the exact value at nodes that fall on the boundary.

The domain Ω , is now discretized using finite elements covering a domain, Ω^h on which the velocity field and pressure fields are approximated using \mathbf{v}^h and p^h . The approximations are obtained using:

$$\mathbf{v}^h = \sum \mathbf{V}^i \psi_i$$

Equation 33

$$p^h = \sum p^i \pi_i$$

Equation 34

where V^i and p^i are nodal variables and ψ_i and π_i are finite element basis functions that are also known as shape functions.

For viscoelastic models, the extra stress tensor, \mathbf{T} , must also be approximated using

$$\mathbf{T}^h = \sum \mathbf{T}^i \phi_i$$

Equation 35

where \mathbf{T}^i are nodal stresses while ϕ_i are the shape functions.

After approximating the velocity, pressure and viscoelastic extra-stress fields by means of the finite element expansions as described by Equation 33 to Equation 35, they are substituted into the isothermal governing equations using Galerkin's method to obtain the following set of equations:

$$\int_{\Omega} \pi_k [\nabla \cdot \mathbf{v}^a] d\Omega = 0$$

Equation 36

$$\int_{\Omega} \left\{ \psi_j \rho \left[\frac{D\mathbf{v}^a}{Dt} - \mathbf{f} \right] + \nabla \psi_j^T \cdot [-p^a \mathbf{I} + 2\eta^2 \mathbf{D}^a + \mathbf{T}_1^a] \right\} d\Omega = \int_{\Omega} \psi_j \boldsymbol{\sigma} \cdot \mathbf{n} ds$$

Equation 37

$$\int_{\Omega} \phi_i [g(\mathbf{T}_1) \cdot \mathbf{T}_1^a + \lambda \frac{\delta \mathbf{T}_1}{\delta t} - 2\eta_1 \mathbf{D}^a] d\Omega = 0 \quad \text{Equation 38}$$

where Equation 36 and Equation 37 represent the discretized forms of conservation of mass and momentum respectively. Equation 38 is the discretized form of the viscoelastic constitutive equation (Equation 26).

Two basic approaches are used to solve the system of Equation 36 to Equation 38. In the first approach, referred to as the coupled method, the extra stress tensor becomes a primary unknown along with the velocity and pressure fields. This procedure is normally used with differential models. The advantage of this method is the possibility of utilizing Newton-Raphson's technique to solve for the primary variables in the nonlinear problem while the accompanying disadvantage is the large number of unknowns and high computational costs for typical flow problems.

The second approach, the decoupled scheme, uses an iterative method. The computation of the viscoelastic extra-stress is performed separately from that of flow kinematics. The kinematics is typically iterated using Picard's iterative algorithm. The number of variables is much smaller than in the coupled method, but the number of iterations is much larger.

A straightforward implementation of these approaches often leads to instability and divergence of the numerical algorithms for viscoelastic problems. Due to the hyperbolic nature of $\lambda \nabla \mathbf{v} \cdot \mathbf{T}_1$ originating from the upper-convected derivative of the extra-stress $\overset{\nabla}{\mathbf{T}}_1$, the accuracy and stability of the mixed Galerkin formulation deteriorates as the elasticity number (the ratio of elastic forces to inertial forces) increases in flows with boundary layers or

singularities. In such cases, the numerical results are stabilized by the use of viscoelastic extra-stress interpolations.

The most robust extra-stress interpolation technique, Streamline Upwinding (SU), consists of applying an artificial diffusivity, $\mathbf{K} = \bar{k} \frac{\mathbf{v}\mathbf{v}}{\mathbf{v}\cdot\mathbf{v}}$ to the hyperbolic term only in the streamwise direction. The discrete constitutive equation then becomes:

$$\int_{\Omega} \phi_i [g(\mathbf{T}_1) \cdot \mathbf{T}_1^a + \lambda \frac{\delta \mathbf{T}_1^a}{\delta t} - 2\eta_1 \mathbf{D}^a] d\Omega + \int_{\Omega} \left[\frac{\lambda \bar{k}}{\mathbf{v}^a \cdot \mathbf{v}^a} (\mathbf{v}^a \cdot \nabla \mathbf{T}_1^a) \mathbf{v}^a \cdot \nabla \phi_i \right] d\Omega = 0 \quad \text{Equation 39}$$

where \bar{k} is a scalar of $O(h)$ and is equal to $\frac{(v_{\eta}^2 + v_{\zeta}^2)^{1/2}}{2}$. A drawback of this technique is that

it gives rise to artificial extra-stress diffusion along the streamlines whose importance decreases when the finite element mesh is refined. In order to eliminate the effects of artificial diffusivity, at least three meshes of decreasing size are used to verify all results.

III.D. Measures of mixing (Polyflow, 2008)

To calculate statistical mixing measures and efficiencies, it is necessary to follow the trajectories of a large number of material points using particle tracking simulations. The initial positions of the material points are generated by randomly distributing a set of material points throughout the flow domain. The trajectories are then calculated by the time integration of the equation

$$\dot{\mathbf{x}} = \mathbf{v}$$

Equation 40

This allows the calculation of the kinematic parameters such as stretching and rate of stretching for each material point along its trajectory.

In general, mixing begins with a ‘distributive’ step (particles are deformed passively), followed by a ‘dispersive’ one (particles break up), and finally by the distribution of the particles in the flow. The first step can be quantitatively explained using length of stretch and stretching efficiencies. Dispersive mixing is given by the Manas-Zloczower mixing index, while the distribution of the particles in the flow can be quantitatively explored by the segregation scale.

III.D.1. Distributive Mixing

Ottino (1989) developed a kinematic approach to model distributive mixing. He used a lamellar model to track the amount of deformation experienced by fluid elements. Let Ω^0 and Ω denote the domain occupied by the homogenous fluid at time 0 and t respectively. The motion of the fluid is described by

$$\mathbf{x} = \chi(\mathbf{X}, t) \tag{Equation 41}$$

where \mathbf{X} denotes the position of a material P in Ω^0 and \mathbf{x} in Ω .

Consider in Ω^0 a material fiber $d\mathbf{X}$ with a unit orientation \mathbf{M} which deforms into a material fiber $d\mathbf{x}$ with a unit orientation \mathbf{m} at a time t. let λ denote the length of stretch dx/dX . Then

$$\lambda(\mathbf{X}, \mathbf{M}, t) = \sqrt{\mathbf{M} \cdot \mathbf{C}\mathbf{M}} \tag{Equation 42}$$

and

$$\mathbf{m} = \frac{\mathbf{F}\mathbf{M}}{\lambda} \quad \text{Equation 43}$$

where \mathbf{F} and \mathbf{C} denote the deformation gradient and the right Cauchy Green strain tensor respectively. A good mixing quality requires high values of λ throughout space and time.

The local efficiency of mixing (e_λ) is defined as:

$$e_\lambda(\mathbf{X}, \mathbf{M}, t) = \frac{\dot{\lambda}/\lambda}{(\mathbf{D}:\mathbf{D})^{1/2}} \quad \text{Equation 44}$$

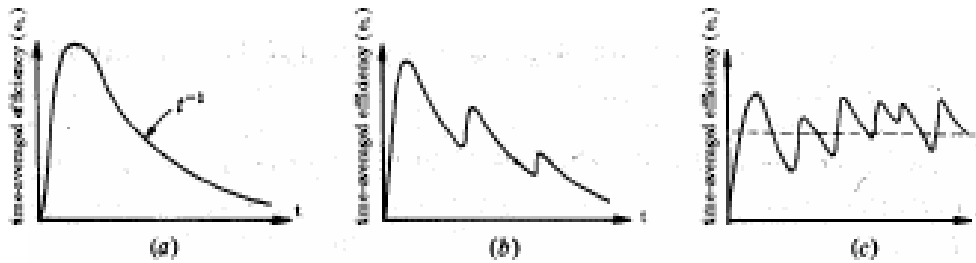
where \mathbf{D} is the rate of strain tensor and $(\mathbf{D}:\mathbf{D})^{1/2}$ is the magnitude of \mathbf{D} . The local efficiency usually falls in the range $[-1,1]$. A value of -1 ($\dot{\lambda} < 0$) would indicate that all the energy dissipated was used to shorten the length of the material line, in effect unmixing it. A value of 1 ($\dot{\lambda} > 0$) indicates that all the energy dissipated was used to stretch the material line.

The time-averaged efficiency ($\langle e_\lambda \rangle$) is defined as:

$$\langle e_\lambda \rangle(\mathbf{X}, \mathbf{M}, t) = \frac{1}{t} \int_0^t e_\lambda(\mathbf{X}, \mathbf{M}, t') dt' \quad \text{Equation 45}$$

Typical behavior of the time averaged mixing efficiency shown in (Figure III.1) ranges from (a) the decay of the efficiency with time as t^{-1} for flows with no reorientation such as the simple shearing flow described earlier, to (b) flows with some periodic reorientation but still decaying on average with time as t^{-1} , and finally (c) flows with strong reorientation with an average constant value of the efficiency (Ottino, 1989).

Figure III.1. Typical behavior of time averaged mixing efficiency (Ottino, 1989).



III.D.2. Dispersive Mixing

Dispersive mixing achieved in a particular configuration can be analyzed by calculating the Manas-Zloczower mixing index which is given as

$$\lambda_{MZ} = \frac{|D|}{|D| + |\Omega|} \quad \text{Equation 46}$$

where $|D|$ and $|\Omega|$ are the magnitudes of the vorticity and strain rate tensors respectively. The Manas-Zloczower mixing index characterizes the importance of elongational and rotational flow components with values from 0 for pure rotation to 0.5 for simple shear to 1 for pure elongation.

A criterion of flow classification similar to the Manas-Zloczower mixing index is used in Jongen (2000) (Equation 8). Pure rotational flow gives a value of -1, pure shear flow gives a value of zero and pure extensional flow gives a value of 1. This flow parameter has the same non-objectivity flaw as the Manas-Zloczower mixing index and is used for a similar purpose in examining the mixing ability of a series of 2-D mixing geometries. Both of these flow

parameters can in turn be related to the local mixing efficiency, e_λ . Specifically, the Manas-Zloczower mixing index is related to the mixing efficiency by the expression

$$\frac{\lambda/\lambda}{[\nabla v : (\nabla v)^T]^{1/2}} = \frac{e_\lambda}{(1 - \mathfrak{R}^2)^{1/2}} \quad \text{Equation 47}$$

III.D.3. Segregation Scale

We assume that two separate fluids A and B are bounded within two halves of a mixer at an initial time, $t=0$. Let $c(\mathbf{X},t)$ denote the concentration of fluid A throughout the mixing process. Since no diffusion occurs between fluids A and B, c equals either 0 or 1 and remains constant along the trajectory of a material point, giving us

$$\dot{c} = 0 \quad \text{Equation 48}$$

At time t , consider a set of M pairs of material points separated by a distance r . For the j^{th} pair and time t , let c_j' and c_j'' denote the concentrations at both points of the pair, \bar{c} denote the average concentration of all points and σ_c the standard deviation. At time t , the correlation coefficient $R(r,t)$ for the concentration is defined as

$$R(r,t) = \frac{\sum_{j=1}^M (c_j' - \bar{c})(c_j'' - \bar{c})}{M\sigma_c^2} \quad \text{Equation 49}$$

The function $R(r,t)$ gives the probability of finding a pair of random points with a relative distance r and with the same concentration.

The segregation scale is then defined as

$$S(t) = \int_0^{\xi} R(r, t) dr$$

Equation 50

where ξ is such that $R(\xi, t) = 0$ when $r = \xi$. The segregation scale $S(t)$ is a measure of the size of the regions of homogenous concentration. $S(t)$ decreases when mixing improves.

IV. Materials and Methods

IV.A. Numerical simulation

The numerical simulations in this research were conducted using the Polyflow suite, a computational fluid dynamics program from the Fluent software group (Fluent, Inc., Lebanon, NH). The software suite includes the mesh generator, Gambit, the Finite Element Method (FEM) solver, Polyflow and the post-processor, FIPost, and is capable of viscoelastic flows. The simulations were run on a Silicon Graphics Octane2 workstation that has dual 600 MHz R14000 64 bit processors and 8.8 GB RAM to conduct 3D FEM simulations with generalized Newtonian and viscoelastic fluids.

Polyflow is a finite-element computational fluid dynamics (CFD) program designed primarily for simulating applications where viscous and viscoelastic flows play an important role. The flows can be isothermal or non-isothermal, two- or three-dimensional, steady-state or time-dependent. It discretizes the flow domain using the finite elements technique and solves for conservation of mass and conservation of momentum as detailed in the numerical methods section. Polyflow has been extensively used in several similar studies that investigated the flow, mixing and scale-up of extruders and mixers (Dhanasekharan *et al.*, 1999, 2001; Dhanasekharan and Kokini, 2000, 2003; Connelly and Kokini, 2003, 2004, 2006a, 2006b and 2007).

IV.B. Initial and Boundary conditions

The rheological properties of the Globe corn syrup used in experimental LDA studies (Fanning, 2008) were modeled using a Newtonian viscosity of 54 poise. Gravitational forces

were neglected and the density was set equal to the fluid density of corn syrup – 1409 kg/m^3 . The inflow volumetric flow rate was set equal to that in the experiments at 53 mL/s (Figure IV.1) and a fully developed velocity profile was imposed on the inlet boundary (Figure IV.2).

Figure IV.1. Inflow volumetric flow rate

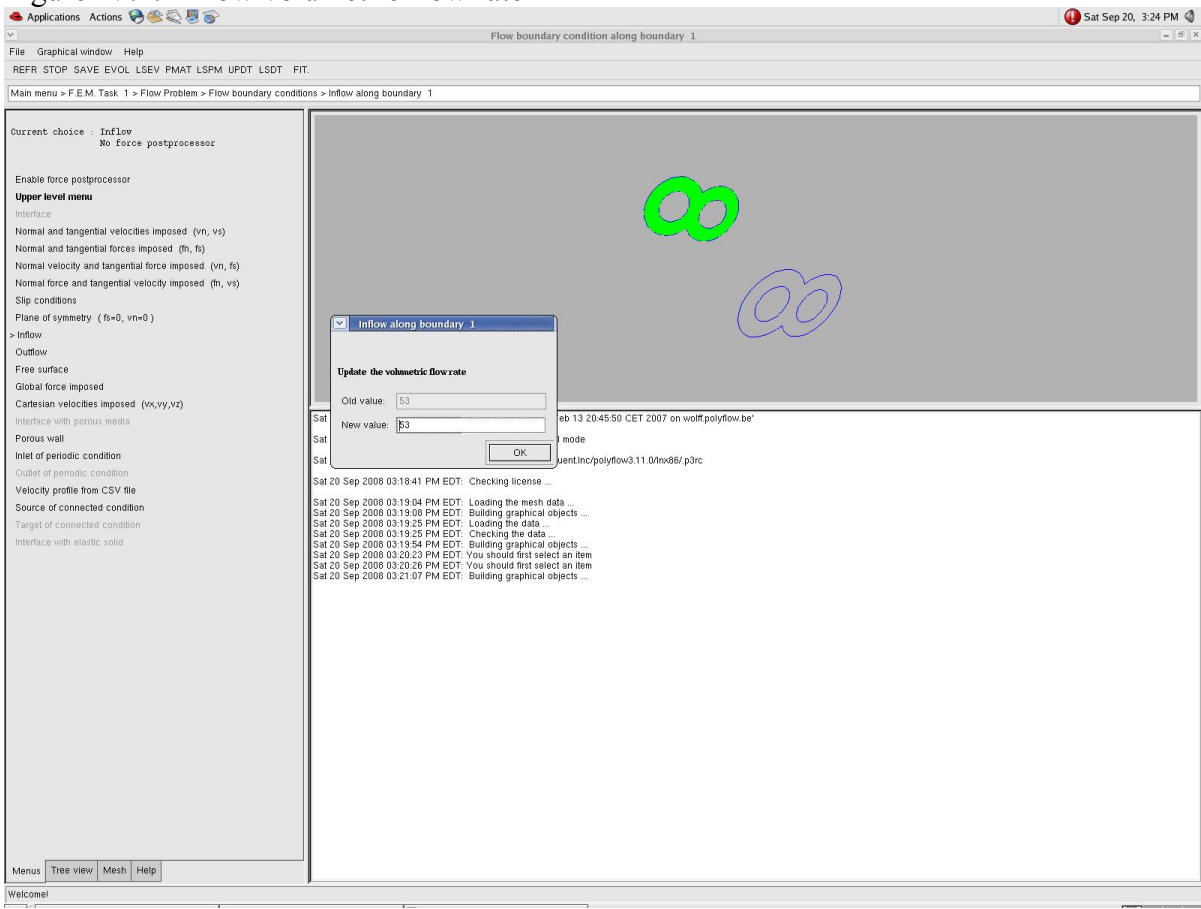
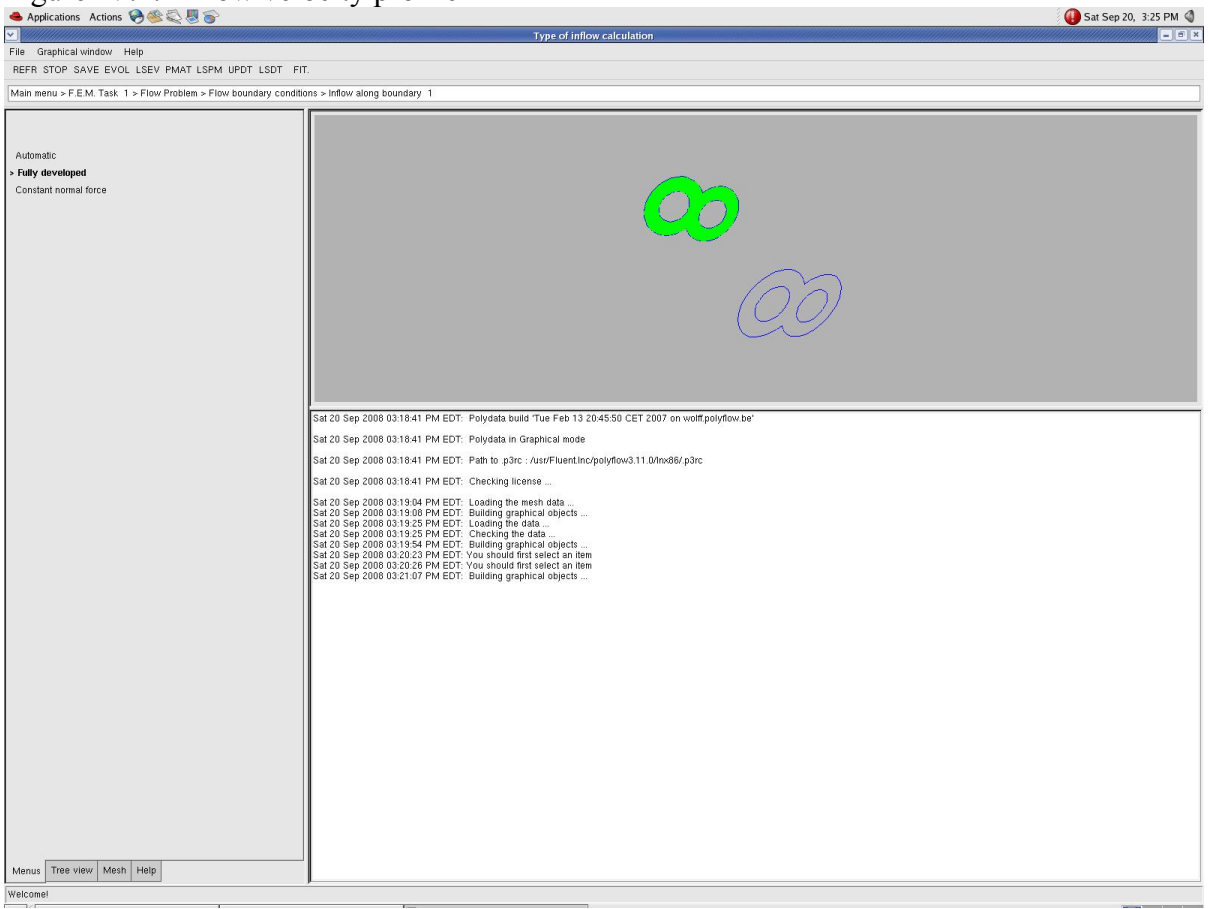
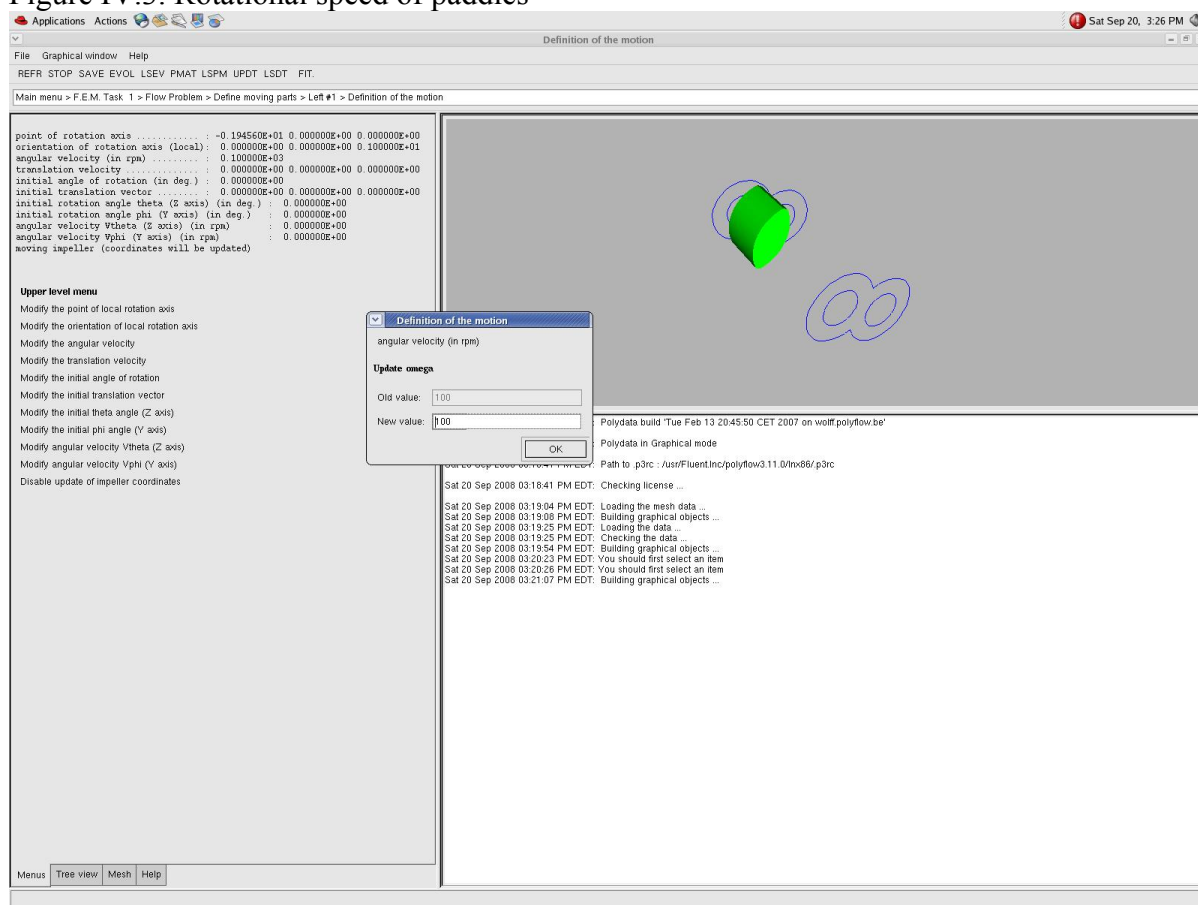


Figure IV.2. Inflow velocity profile



The outflow boundary was set with normal force and tangential velocity equal to zero. The walls of the barrel were impervious and stationary, while the paddles moved within at a rotational speed of 100 rpm (Figure IV.3).

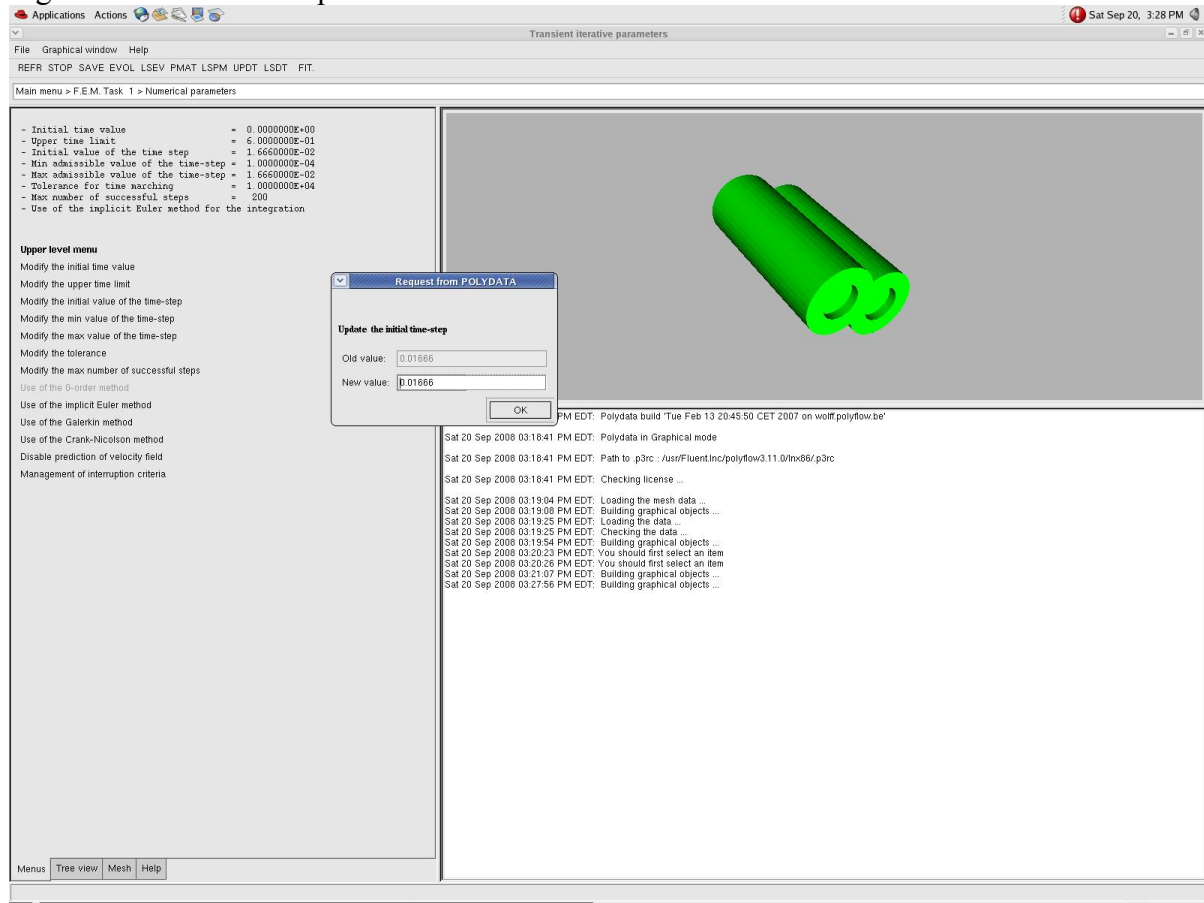
Figure IV.3. Rotational speed of paddles



No slip conditions were assumed on both the barrel and paddle surfaces and the flow domain was assumed to be fully filled. In order to handle the periodically changing twin screw geometry without re-meshing, the mesh superposition technique was used (Avalosse and Rubin, 2000). A mini-element were used for velocity along with a constant pressure element as this has been shown in the past to be the optimal interpolation element for MST problems (Alsteens *et al*, 2004).

The simulations were run for 0.6s to allow the paddles to complete one full turn at 100 rpm, and velocity and pressure results were captured at every 10° of rotation (Figure IV.4).

Figure IV.4. Numerical parameters



The velocity components obtained from the simulation were compared to the experimentally obtained LDA results at three different point locations – P1, P2 and P3 (Figure II.37). Root mean square values for the difference between the simulations to experimental results were calculated (Equation 51) and are expressed as percentage of the range of experimental values (Equation 52).

$$RMS = \frac{\sqrt{(v_s - v_e)^2}}{n}$$

Equation 51

$$RMS\% = \frac{RMS}{(v_{e_{\max}} - v_{e_{\min}})} \times 100$$

Equation 52

The mesh superposition technique is not fully conservative on mass and hence a mesh refinement study is always required to establish the optimum mesh (Alsteens *et al*, 2004).

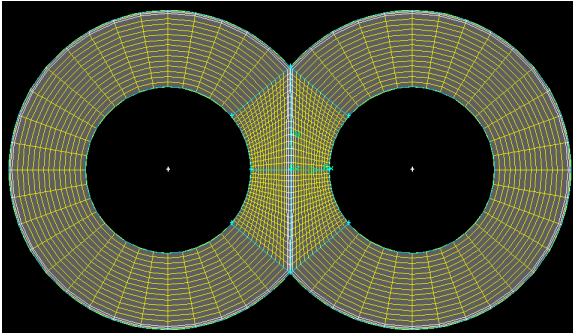
IV.C. Mesh Optimization

IV.C.1. Radial Mesh Optimization

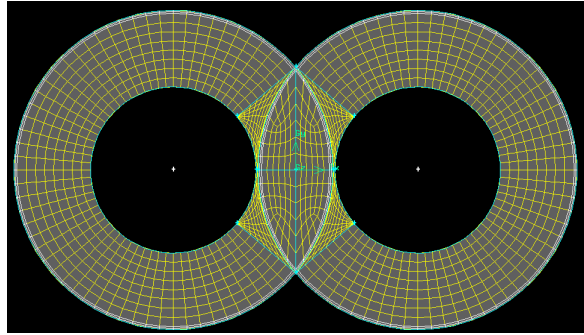
To evaluate the optimal 2D cross-sectional mesh for the Readco geometry, 4 different 2D meshes (Figure IV.5) with varying radial mesh densities were tested. Mesh #1 (Figure IV.5a) has a uniform mesh gradation with 16 intervals in the radial direction (including 2 as a boundary layer) and 28 intervals in the azimuthal direction of the ‘C’-shaped sections of the barrel. The intermeshing region was also meshed with 28 intervals on sides of the shafts to give a total of 1920 elements. The paddles were meshed with a 432 element 2D mesh as shown in Figure IV.6. This mesh configuration was co-developed with Robin Connelly in a previous study (Ashokan *et al*, 2003).

Figure IV.5. 2D meshes with varying radial mesh density

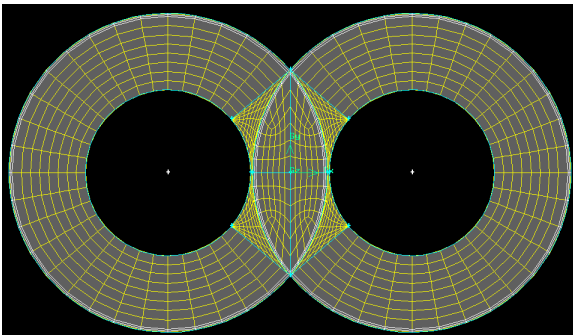
a) Mesh #1



b) Mesh #2



c) Mesh #3



d) Mesh #4

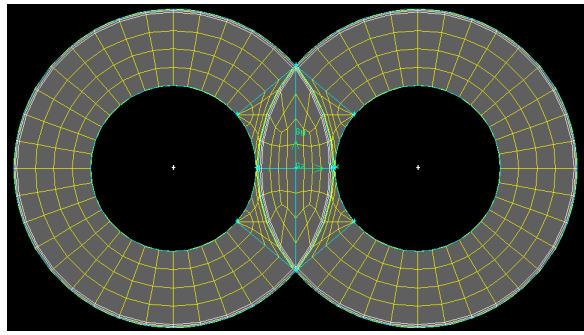
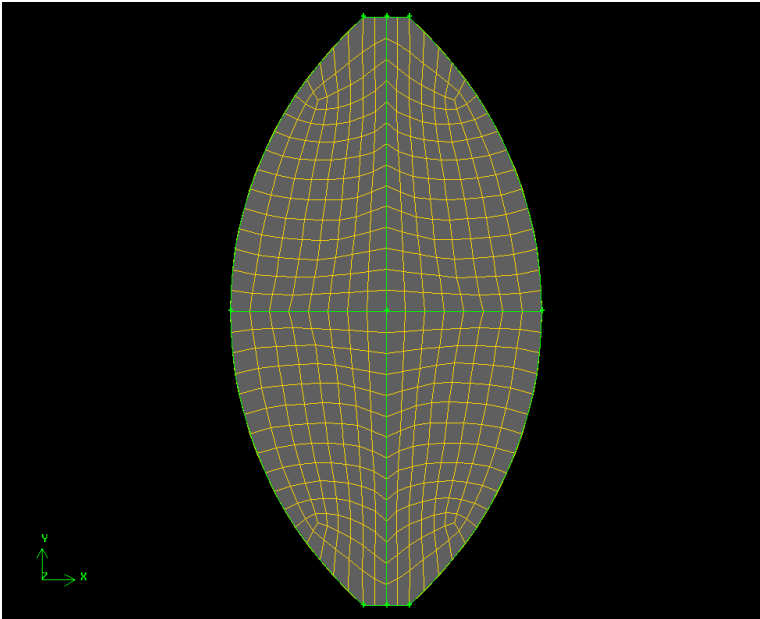


Figure IV.6. 432 element 2D paddle mesh



When Mesh #1 was used in the simulation, some of the elements in the intermeshing region were getting overlapped by both the moving paddles at the same time in the mesh superposition technique, causing errors in the calculations. To correct for this, three other 2D meshes (Figure IV.5b, Figure IV.5c, and Figure IV.5d) were developed with a new mesh scheme in the intermeshing region so that both the paddles do not overlap the same element at any given time. Mesh #2 utilized 10 mesh intervals in the radial direction (2 in the boundary layer) and 56 mesh intervals in the azimuthal direction of the ‘C’-shaped barrel sections. The intermeshing region was split into a lens-shaped region where both the paddles enter and four quadrants in which at a given time only one paddle would be present. Boundary layers were incorporated into the inner sides of the lens-shaped region so that there are always two elements in the gap between the two paddles and no element gets overlapped

by both paddles at the same time. The quadrants were meshed with wedge shaped elements with 8 intervals to give a total of 1632 elements. For mesh #3, the mesh intervals in the azimuthal direction were reduced by half to 28 reducing the total elements to 1072 elements. In mesh #4, the radial mesh intervals were reduced to 6 and the intervals in the quadrants were reduced to 4. This formed the coarsest mesh in the study with only 512 elements.

Polyflow allows the determination of the quality of a mesh with various metrics. One such critical metric is the equiangle skew. Equiangle skew is a normalized measure of skewness of an element and is defined as follows:

$$Q_{EAS} = \max \left\{ \frac{\theta_{\max} - \theta_{eq}}{180 - \theta_{eq}}, \frac{\theta_{eq} - \theta_{\min}}{\theta_{eq}} \right\} \quad \text{Equation 53}$$

where θ_{\max} and θ_{\min} are the maximum and minimum angles in degrees between the edges of the element, and θ_{eq} is the characteristic angle corresponding to an equilateral cell of similar form, which would be 60° for a triangular/ tetrahedral cell and 90° for a quadrilateral/ hexahedral element. By definition, therefore the equiangle skew is between 0 (quadrilateral element) and 1 (degenerate element). In 3D flow problems, an average skewness value of 0.4 is considered excellent. Skewness values up to 0.6 are considered good and fair to poor elements are up to 0.9. Skewness values greater than 0.9 are usually not acceptable.

Another mesh quality metric is the stretch ratio (Q_s) defined as

$$Q_s = 1 - \sqrt{\frac{K \min(s_1, s_2, \dots, s_m)}{\max(d_1, d_2, \dots, d_n)}} \quad \text{Equation 54}$$

where d_i is the length of diagonal i , s_j is the length of the element edge j , and n and m are the total numbers of diagonals and edges, respectively. For quadrilateral elements, $n = 2$, $m = 4$, and $K = 2$; for hexahedral elements, $n = 4$, $m = 12$, and $K = 3$. This metric applies only to quadrilateral and hexahedral elements. By definition $Q_s=0$ describes an equilateral element and $Q_s=1$ a completely degenerate element.

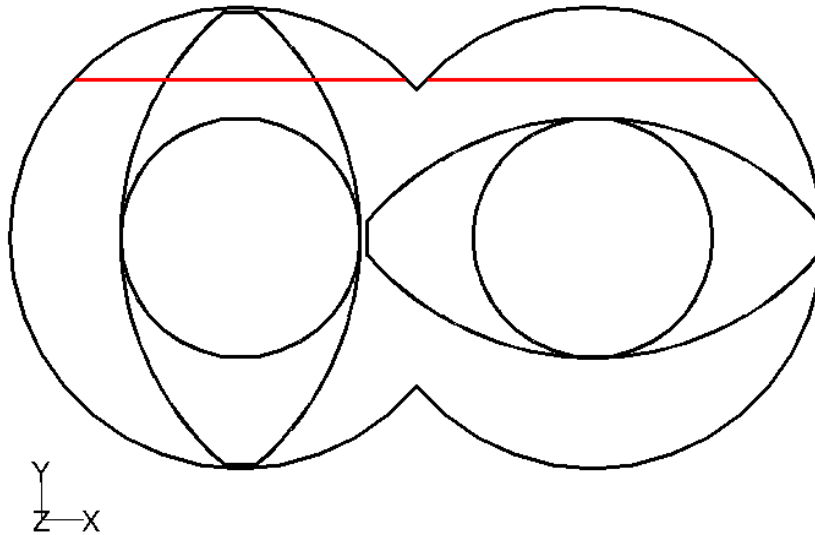
The total number of elements and the quality of the meshes that were used in this study are enumerated in Table IV.1. Quality of meshes with varying radial gradation.

Table IV.1. Quality of meshes with varying radial gradation

Mesh	Number of elements	Equiangle skew > 0.5 (% elements)	Stretch ratio > 0.5 (% elements)
Mesh #1	1920	0	54.27
Mesh #2	1632	14.46	31.86
Mesh #3	1072	22.01	48.51
Mesh #4	512	19.53	46.88

The velocity magnitudes along Line 1 (Figure IV.7) that passes through points P1 and P2 were compared for all the meshes to identify the optimum mesh configuration and density.

Figure IV.7. Position of line 1.

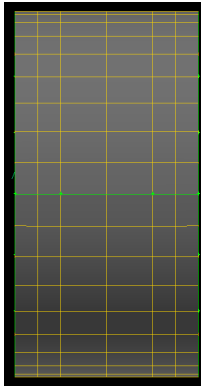


IV.C.2. Axial Mesh density

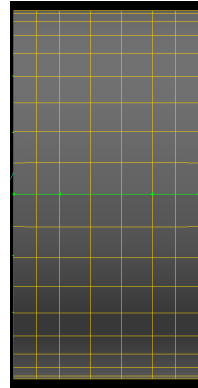
After the evaluation of the optimal 2D cross-sectional mesh, the simulation geometry was extended into 3D with 1 pair of paddles and the optimal axial mesh density and entrance and exit lengths were evaluated. An entrance and exit length of half a paddle's width was initially used to allow the flow to develop before hitting the face of the paddles and two mesh intervals each were used to mesh the entrance and exit regions. The axial mesh density of the section of the barrel that contains the paddle pairs was meshed with 2, 3, 4 or 5 intervals (Figure IV.8) to observe the effect of increasing axial mesh density. Mesh #3 (Figure IV.5c) was used as the radial cross-section mesh in all these and further simulation geometries. The velocity magnitudes along Line 2 in the axial direction were compared for all the meshes to identify the optimum axial mesh density. Line 2 passes through the gap between the paddles when they are at the $0/360^\circ$ position (Figure IV.9).

Figure IV.8. Barrel meshes with 2, 3, 4 and 5 mesh intervals in the region of the paddles.

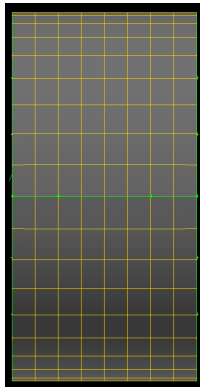
a) 1X-2i



b) 1X-3i



c) 1X-4i



d) 1X-5i

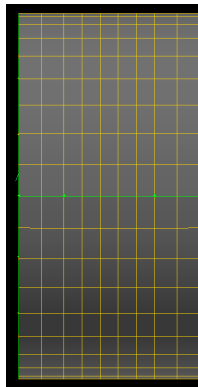
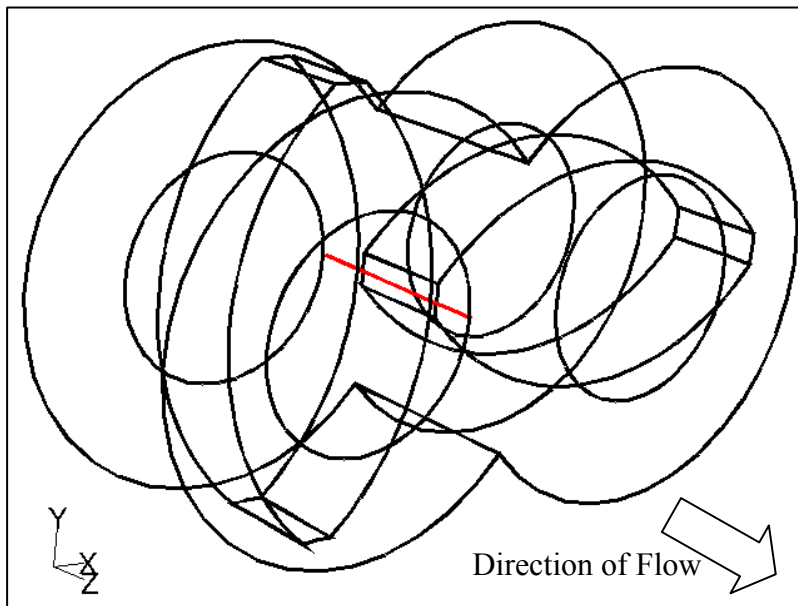


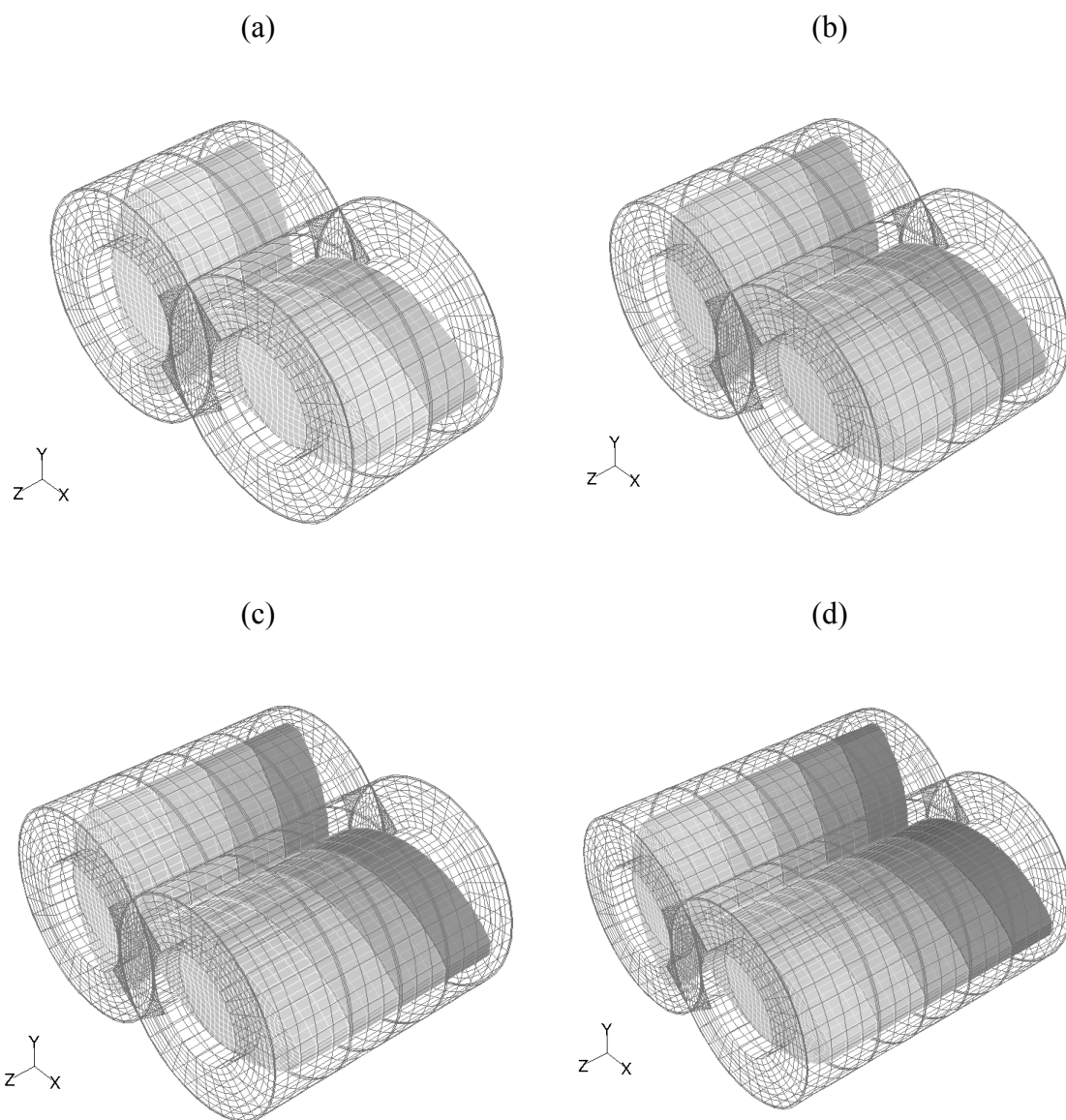
Figure IV.9. Position of line 2.



IV.D. Optimum number of paddle pairs

Once the optimal cross-sectional and axial mesh densities were evaluated the length of the geometry (i.e. the number of paddle pairs) to obtain an accurate velocity profile when compared to experimental LDA velocities were evaluated. Simulation geometries that had 2, 3, 4 and 5 pairs (Figure IV.10) of paddles were tested. Each of these geometries had 3 axial mesh intervals for each paddle pair. Gaps that are present between consecutive paddle pairs in the Readco continuous mixer were also modeled and were meshed with 2 mesh intervals in the axial direction.

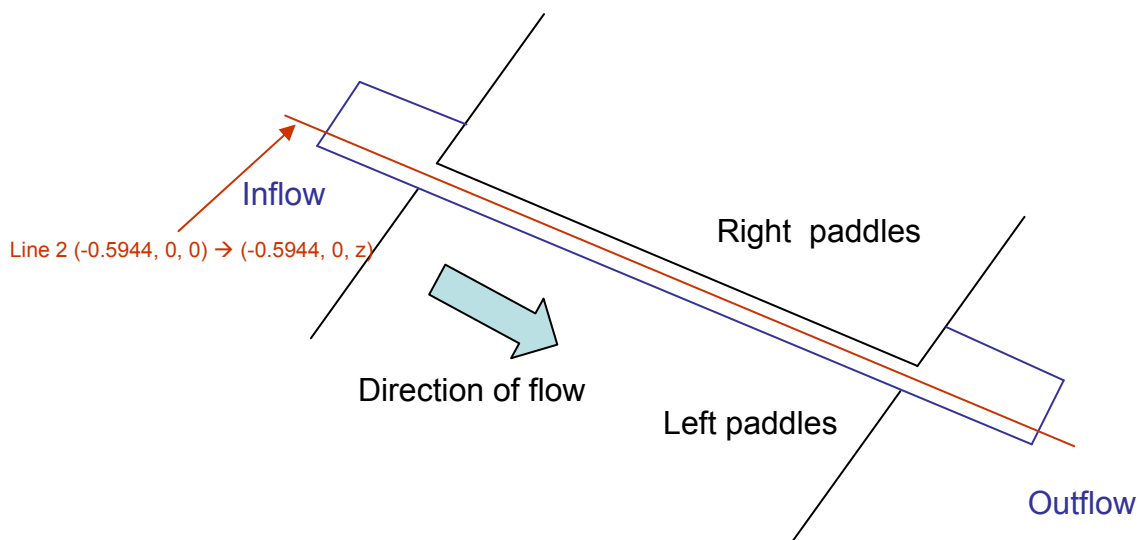
Figure IV.10. Simulation geometries with (a) 2, (b) 3, (c) 4 and (d) 5 pairs of paddles



IV.E. Flow through a slit analogy - Pressure comparison

The flow in the region between the two sets of paddles was likened to the flow between two parallel plates (Figure IV.11). The evolution of pressure along line 2 (Figure IV.9) was observed for the 2, 3, 4 and 5 paddle pairs geometry.

Figure IV.11. Schematic of the analogy to flow between parallel plates



The pressure drop over a given length in the flow between two parallel plates is given by

$$\frac{dp}{dx} = \frac{12\mu Q}{h^4} \quad \text{Equation 55}$$

where μ is the viscosity, Q is the volumetric flow rate and h is the gap between the two infinitely long plates. Using this relationship, the analytically expected pressure drop was calculated for the known paddle length as it increased from the 2 pair to the 5 pair geometry.

The analytical pressure drop was compared to the simulated pressure drop to check for consistency.

IV.F. Modeling 9 pairs of paddles

Polyflow allows only 10 moving parts when used with the mesh superposition technique. To model the complete 9 pairs of paddles in the Readco Processor while overcoming this limitation, the first and last three pairs of paddles were fused as one pair each. These fused pairs had a length that was equal to that of three individual paddle pairs (Figure IV.12). With this arrangement it was necessary to find out if fusing the paddle pairs (i.e. removing the gaps) would adversely affect the simulation accuracy. A simulation geometry (Figure IV.13a) with a paddle pair that was as long as three paddle pairs and without gaps in between was thus modeled and compared to the 3 pairs geometry with gaps (Figure IV.10b). Axial mesh density variation in the fused three pairs geometry was also evaluated with 9 (Figure IV.13a) or 5 (Figure IV.13b) mesh intervals to further optimize the simulation mesh and geometry.

Figure IV.12. 9 paddle pair geometry with the first and last 3 pairs fused into one each to accommodate Polyflow's limitation of 10 moving parts

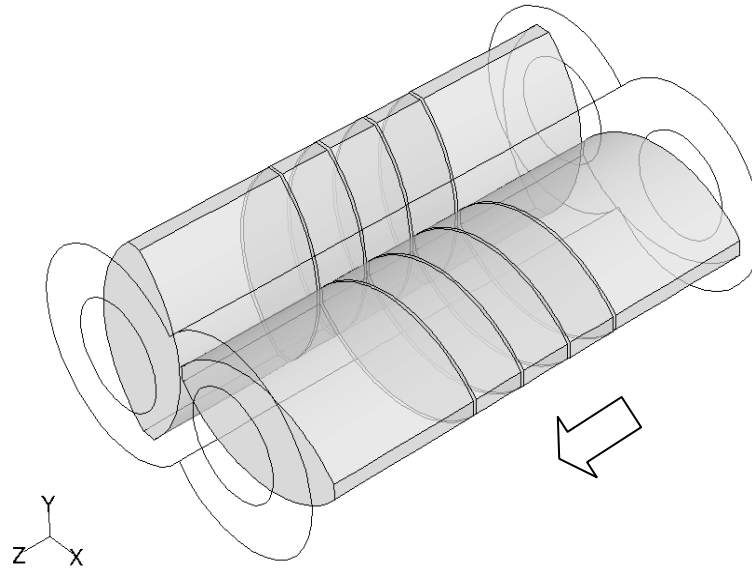
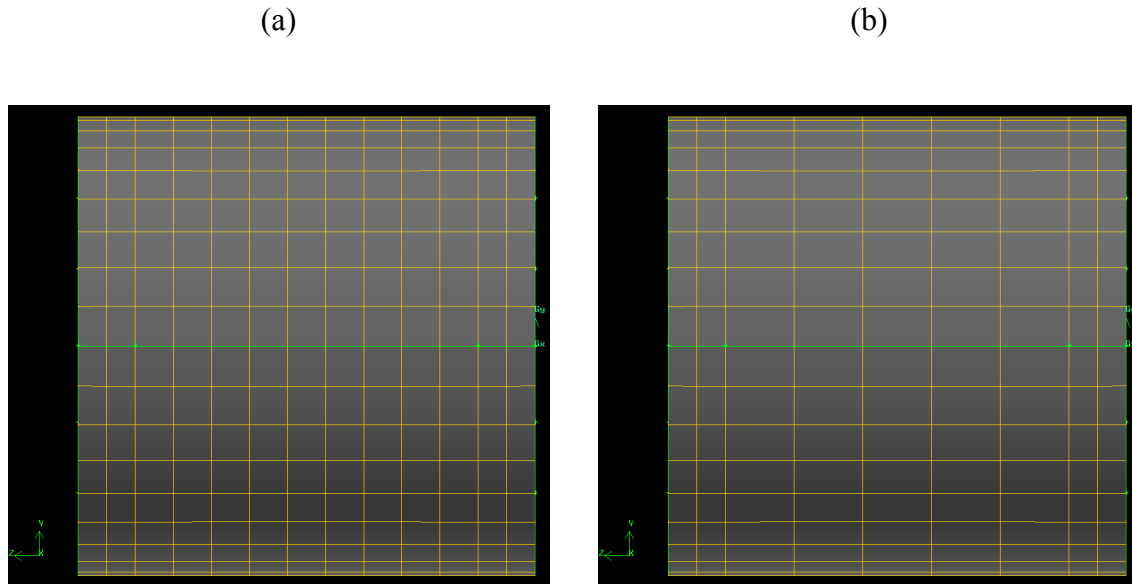


Figure IV.13. Fused 3 pairs long simulation geometry with (a) 9 and (b) 5 axial mesh intervals



IV.G. Effect of entrance length

It has been argued in previous studies that the lack of adequate boundary conditions before the flow hits the face of the first paddle pair in the flow be addressed by either increasing the entrance length (Alsteens *et al*, 2004) or by numerically simulating the conveying elements before the kneading paddles and using their exit conditions as the inlet conditions for the kneading paddles (Jaffer *et al*, 2000). To evaluate the effect of increasing the entrance length, a 5 paddle pair simulation was performed with an entrance length that is equal to the length of 4 paddle pairs and compared to both the 5 paddle pair and 9 paddle pair geometries with half a paddle width's entrance length.

IV.H. Calculation of mixing measures

To improve the ability of the predicted flow profiles to calculate particle trajectories, the flow solutions were extended to a simulation time of 6s (10 complete rotations at 100 rpm). Once these flow solutions were obtained, they were used to predict the mixing efficiencies. The effect of paddle configurations and mixer RPM on trends in mixing performance were studied. The mixing results from the continuous mixer were also compared to those for the batch Farinograph with the Farinograph data taken from Connelly (2004). The results used in the comparison were for simulations that were run with the fast (right) blade turning 93 rpm counterclockwise and the slow (left) blade turning 62 rpm clockwise.

IV.H.1. Effect of Paddle Configuration

Three different paddle configurations were investigated to determine the configurations' effect on the mixing efficiency. The 9 paddle arrangement in Figure IV.12 was labeled 'FLAT' as all the paddles are aligned with each other in the axial direction. In the second configuration, the paddle pairs succeeding the first paddle pair (that is 3 paddle pairs in length) were all successively rotated by 45° in the clockwise direction (when looking in the direction of flow, Figure IV.14). This configuration was labeled as '45F', with the F standing forward a forward pump configuration as this configuration was expected to provide a forward fluid motion in direction of the flow. The third configuration was opposite to the 45F configuration, in that the paddle pairs were rotated 45° in the anti-clockwise direction (when looking in the direction of flow, Figure IV.15) and was labeled as 45R or a reverse pump configuration. The forward, flat and reverse configurations were chosen as it has been shown in literature that using these configurations, differences in overall pressure drop across the screw configurations could be obtained (Alsteens *et al*, 2004).

Figure IV.14. 9 pair paddle geometry in the 45F configuration

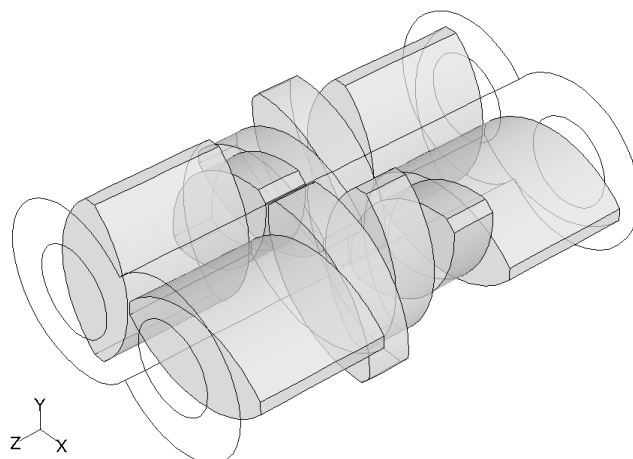
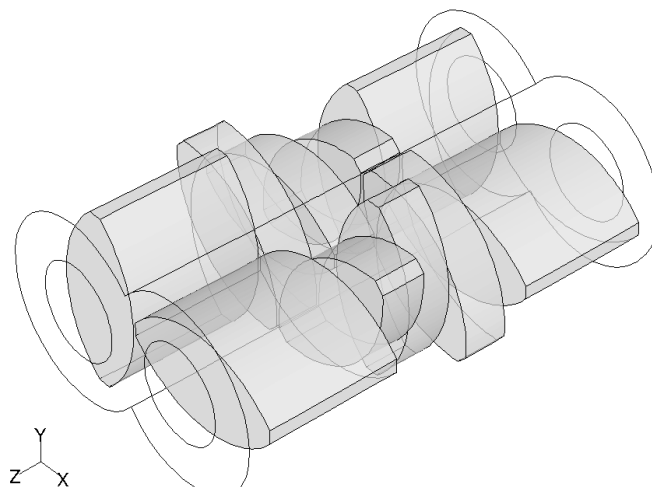


Figure IV.15. 9 pair paddle geometry in the 45R configuration



The flow profiles for the FLAT, 45F and 45R configurations were calculated using the same conditions as detailed above but for a total simulation time of 6s, which resulted in 10 complete rotations of the paddles. After the flow profiles were calculated, the mixing measures for these three different screw configurations were determined as detailed below.

1000 particles were randomly distributed at the beginning of the mixing solution for each of the three screw configurations studied and the particles were allowed to mix for the duration of the flow solution, 6s, i.e., 10 rotations of the screws at 100 rpm. The mean logarithm of the length of stretch, instantaneous mixing efficiency and time averaged mixing efficiency were determined to estimate the distributive mixing. The Manas-Zloczower mixing index, along with the shear rates, was determined to study the dispersive mixing. The concentration of the particles in the right half of the mixer was arbitrarily set at 1 and the left half was assigned a value of 0 and the segregation scale was determined for each configuration. The values were normalized to the initial segregation before the mixer was started. The length of stretch, instantaneous and time averaged efficiencies and the segregation scale were also compared to the values obtained in the Farinograph after operating at the conditions described in Connelly (2004) for 6 s.

IV.H.2. Effect of Screw Speed

To identify operating conditions under which the continuous mixer might approach the batch mixer in mixing efficiency, two additional screw speeds were simulated. The FLAT screw configuration was used to determine the effect of screw speed on the mixing performance. The flow profiles were solved for screw speeds of 50 rpm and 1 rpm and the velocity and pressure results were captured for 10 complete rotations of the screws at both RPMs. The

mean logarithm of the length of stretch, instantaneous mixing efficiency, time averaged mixing efficiency and normalized segregation scale were once again determined at these two RPMs and compared to the values determined for the solution at 100 RPM and also to those obtained in the batch Farinograph by Connelly (2004).

IV.I. Numerical simulation of the flow of a viscoelastic fluid in a twin screw mixer

Polyflow's implementation of the mesh superposition technique does not allow for the use of a viscoelastic constitutive equation. To model the continuously changing geometry in a twin screw mixer and use a viscoelastic constitutive equation, a new methodology had to be devised. This can be done in two approaches – geometry simplification or temporal simplification.

With geometrical simplification, the twin screw mixer can be considered either as two separate halves – the intermeshing and conveying regions - that interact with each other (Chiruvella *et al*, 1996), or as a double couette geometry (Teverovski *et al*, 2000), or a suitable combination of both. While such techniques have proven useful in the past, they are saddled with many simplifying assumptions about the flow (as discussed in prior sections) and are not very suitable to make accurate predictions.

With temporal simplification, the mixer can be modeled with all its geometrical complexity for a given snapshot in time and the flow problem solved at that particular time. The solution can then be used as the initial condition for the next time step and the solution at that time step can then be calculated. This technique, known as the pseudo steady state (PSS) technique, has been used by Funatsu and co-workers (Ishikawa *et al.*, 2000, 2001, 2002) to

model the flow in a twin screw extruder in 3D, albeit using viscous non-Newtonian constitutive models. There has been no work in the literature that has solved the flow problem in twin screw mixer/extruder geometries with a viscoelastic constitutive equation. The time involved in constructing the individual meshes that correspond to each time step is countered by suitably adjusting the time step so that an optimum can be found between efficiency and accuracy.

IV.I.1. Pseudo Steady State (PSS) Technique

The PSS technique was used in this study to develop a solution for the flow of a viscoelastic fluid in the Readco geometry. This technique is illustrated with a simple example of the flow between two parallel plates.

Consider two meshes that correspond to the position of the plates at time $t=0s$ (Step 0, Figure IV.16) and $t=1s$ (Step 1, Figure IV.17). The top and the bottom plates of this geometry are moving towards the right and left respectively at a velocity of 1 cm/s. The initial and boundary conditions imposed on Step 0 are as follows:

1. Edges a and c are stationary
2. Edge b is moving with a velocity of 1 cm/s (to the right) and edge c with a velocity of -1cm/s (to the left).
3. The inertia terms are neglected.
4. Density is 1gm/cc

The computation was conducted for an Oldroyd B viscoelastic constitutive equation with the following parameters:

1. Total viscosity = 54 poise
2. Viscosity ratio = 0.1111
3. Relaxation time = 1s

Figure IV.16. Step 0 mesh for the flow between parallel plates

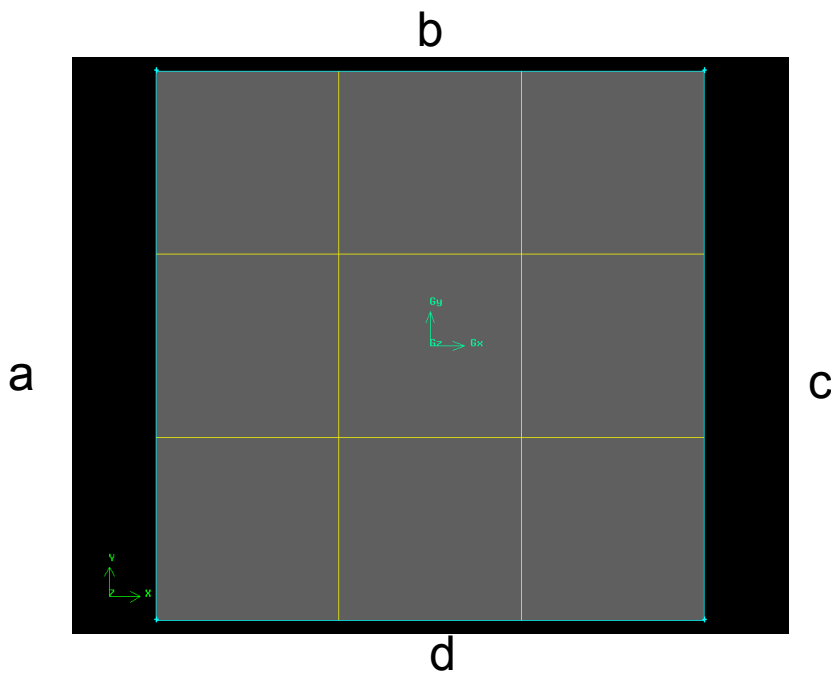
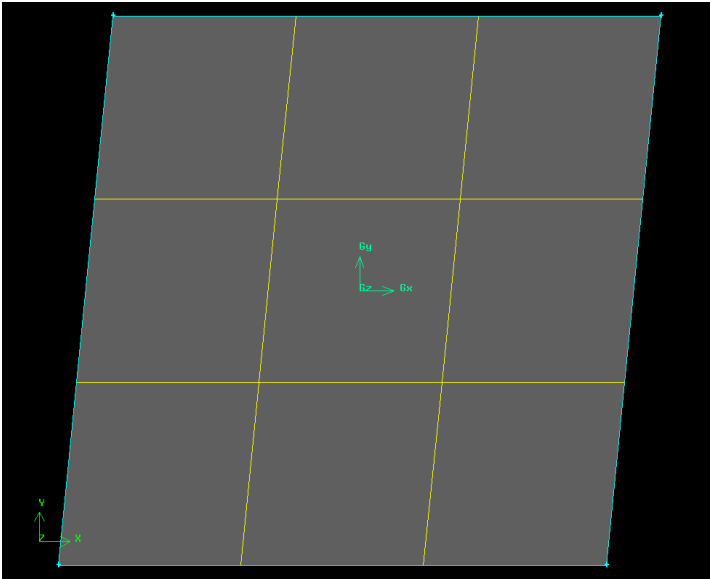


Figure IV.17. Step 1 mesh for the flow between parallel plates



The parameters were chosen such that the viscous part of the equation corresponds to the viscous Newtonian simulation while an elastic relaxation time is added on to the solution. This would enable the effects of elasticity to be isolated.

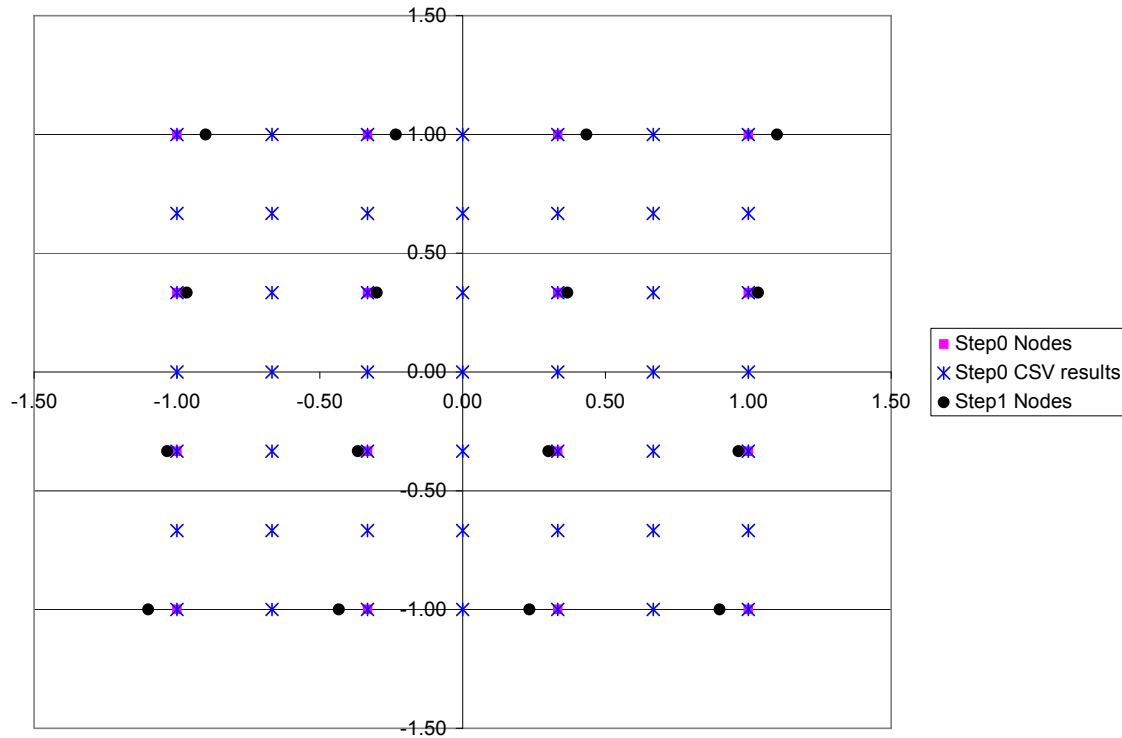
A solution is first computed on the Step 0 mesh and the computed results (including velocity, pressure, stresses) of the solution are stored in a format known as CSV (comma separated variables) file. This result file contains columns with the coordinate information and the corresponding values of the predicted variables at those coordinate values (called nodes in FEM).

The results stored in this CSV file are then used to initialize the nodes of the Step 1 mesh. Mesh-to-mesh interpolation in Polyflow allows for the transfer of results obtained on one

mesh to a second mesh that is unrelated to the first one except through coordinates. There is no assumption that the nodes or element numbering correspond, but, because the transfer process is based on the nodal coordinates in both configurations, a reasonable geometric match is required. If the two geometries do not match exactly, however, the error will be on the order of the geometrical difference. All fields, including velocity and temperature will be transferred from the first mesh to the second.

In cases where the coordinate values across the two meshes are identical, the results get automatically assigned. In other cases, where no one-to-one correspondence between the coordinates exists, a linear interpolation is used to assign values from the nearest neighbors. The relationship between the Step 0 nodes, the coordinate values in the CSV result file for Step 0 and the node values of the Step 1 mesh are shown in (Figure IV.18).

Figure IV.18. Representation of nodes of Step 0, CSV file and Step 1 mesh.



The additional nodes in the CSV file are due to the quadratic elements used to predict velocity when a viscoelastic constitutive equation is used. In this manner, all the nodes of the Step 1 mesh get initialized with values for the variables being calculated. The boundary conditions for this step are then used to evaluate the solution of the flow problem at the end of this step. This process is taken forward using successive meshes for increases in time.

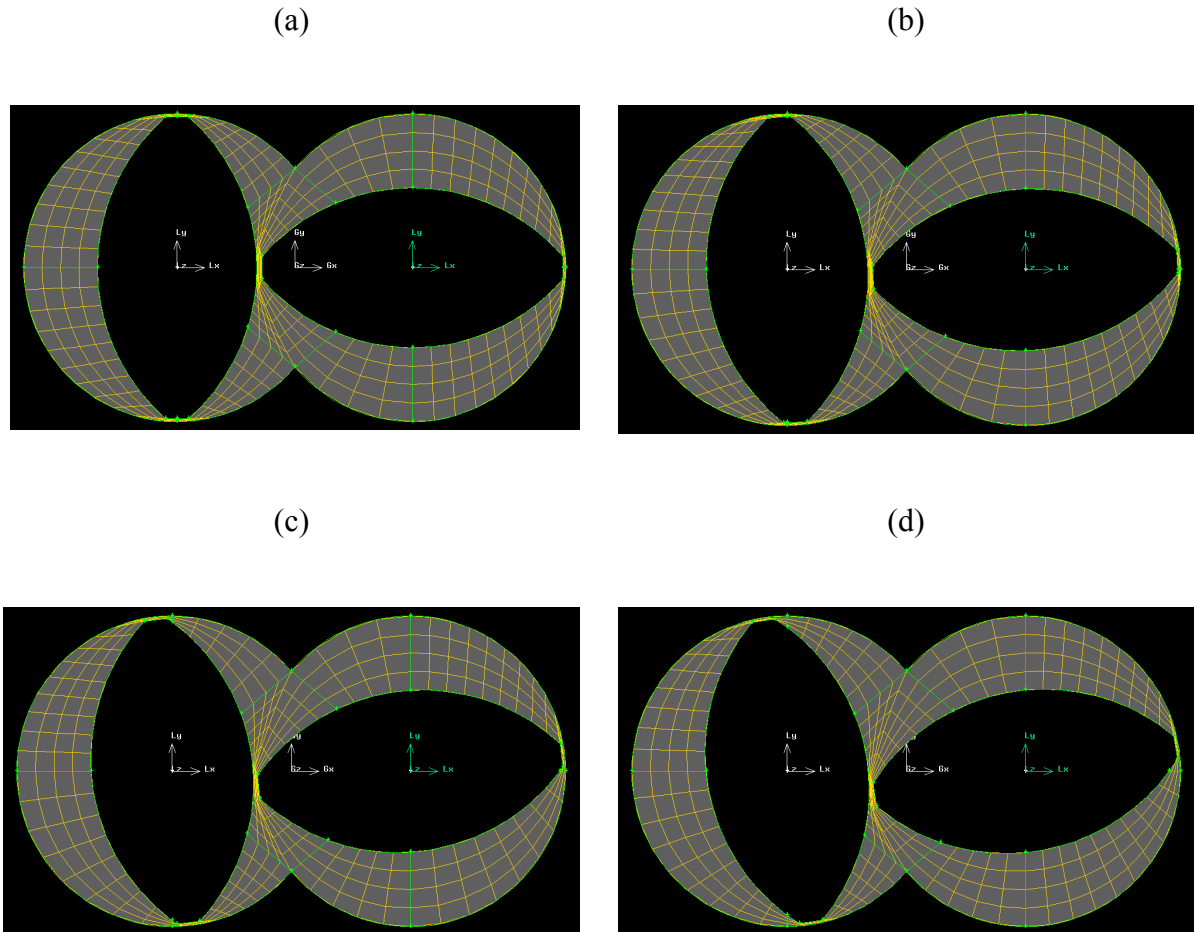
The error in this process comes not only with the calculation of the solution itself, but also from the process of assigning the values from the end of one step to the other. If the time step is too large, imposing a large displacement upon the nodes, then there will be fewer nodes

with a one-to-one correspondence between two successive meshes leading to greater interpolation and compounded error. This can be avoided with a judicious choice of mesh density and time step from one mesh to the next. By creatively designing the meshes such that the parts of the domain where the moving components do not intrude are meshed with a static mesh, the error in translating from one mesh to another can also be minimized.

IV.1.2. Application of the PSS technique for the Readco geometry

To solve the viscoelastic problem in the Readco geometry using the PSS technique, four meshes were constructed with the paddle pairs after 0, 3, 6 and 9 degrees of rotation in the anti-clockwise direction (Figure IV.19). To simplify the problem (i.e. the number of nodes in the CSV file) the meshes were constructed in 2D.

Figure IV.19. 2D meshes used in the PSS technique with the paddles at (a) 0° (b) 3° (c) 6° and (d) 9° positions.



The mesh in the clearance region was constructed with 2 intervals in the radial direction and 18 intervals in the azimuthal direction. This mesh in the clearance region remains the same for all degrees of rotation as the paddles (moving boundaries) do not encroach into this region. This allows for a one-to-one match of the nodes when transferring the results from one mesh to another in this region.

The boundaries of both the paddles were incorporated into the geometry and the mesh for Mesh 0 was appropriately constructed to account for the irregular geometry. When the paddle boundaries moved to the 3° position, the mesh was pivoted around the same points so that the deformation (hence the displacement of the nodes away from the Mesh 0 node positions) was kept to a minimum. This was carried out successively for the Mesh 6 and Mesh 9 meshes also.

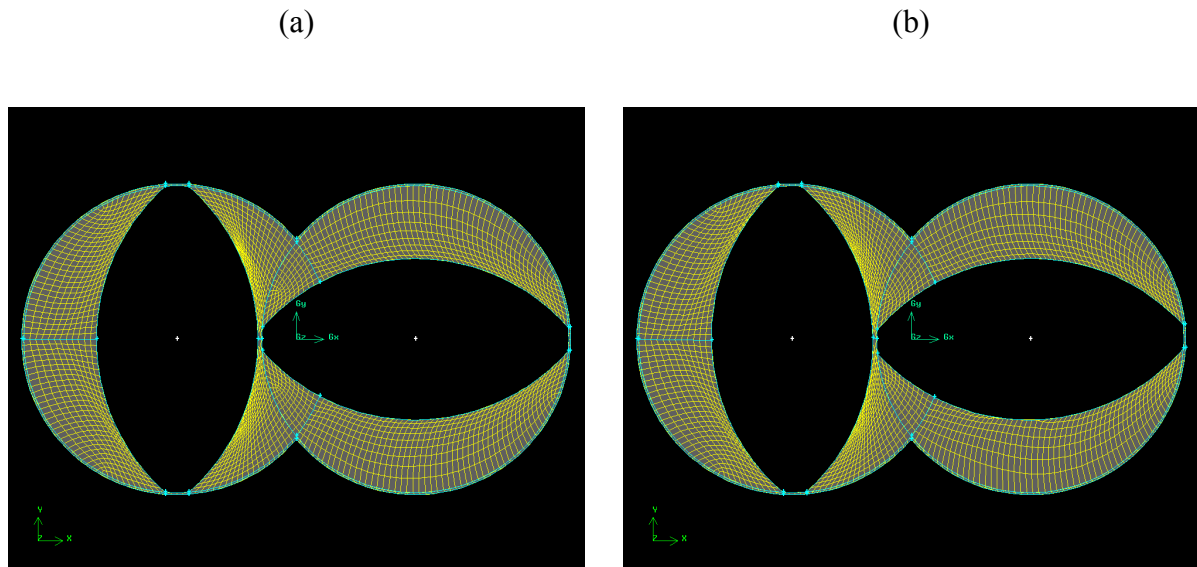
IV.1.3. Verification of PSS technique

A viscous Newtonian solution was first computed using the same parameters as those used with MST. The velocity results along line 1 (Figure IV.7) after 9° of rotation were compared to the velocity results from MST after the first step (i.e. after 10 degrees of rotation).

IV.1.4. Viscoelastic simulation

For the viscoelastic simulations, it was seen that the coarser mesh density and the larger time step developed for the Newtonian test case above did not allow the solution to converge. Hence two new meshes for the were created using the same technique as before.– one for the 0° position and another after 1° rotation of the paddle pairs (Figure IV.20).

Figure IV.20. 2D meshes used for PSS technique with viscoelastic constitutive models with the paddles at (a) 0° and (b) 1° positions.



IV.1.5. Evolution

Polyflow recommends the use of technique called evolution to solve non-linear problems including those that have viscoelastic constitutive equations. The technique involves selecting one or more parameters that cause the non-linearity in the problem and to reduce their values to an extent that the reduced non-linearity does not cause the solution to diverge. The parameters are then increased by a set value that can be dictated by a choice of functions (for example, a linear increase) and the solution is then calculated at this value of the parameter using the predicted solution at the previous value of the parameter as an initial condition. The values of the parameters are thus successively ‘evolved’ till they reach the final set value or till the simulation diverges due to the non-linearity.

In this research, evolution was performed simultaneously on both the angular velocity of the paddle boundaries and also on the relaxation time of the constitutive equation. The evolution function was simply

$$f(S) = S$$

Equation 56

where S is the evolution parameter. The initial value of S was set as 0 and the final value to be attained was set as 1. The initial step size was equal to 10^{-4} . The minimum and maximum step size allowed were 10^{-5} and 0.25 respectively. After successfully solving the problem at $S=0$, Polyflow attempts to solve the problem at $S=10^{-4}$. If the solution is again successful, then it increases the step size by 1.5 times and continues to do so until the maximum step size is reached. On the other hand, if a solution at a particular S value is unsuccessful, the step size is reduced by half and continues to be reduced by half till the minimum step size is reached. If the solution still does not converge, then the problem is said to have diverged and no more attempts will be made.

The Oldroyd B viscoelastic constitutive equation was used with the following parameters:

1. Total viscosity = 54 poise
2. Viscosity ratio = 0.1111
3. Relaxation time = $1 \cdot f(S)$

The angular velocity of both the paddle boundaries were also set to evolve using the function

$$\omega = 10.47692 * f(S)$$

Equation 57

10.47692 is the angular velocity that is equivalent to 100 rpm.

Deborah number (De) is given by

$$De = \lambda \omega$$

Equation 58

The Deborah number is an indication of the amount of viscoelasticity in a particular material. By definition, it is the ratio of the material time (the relaxation time) to the experiment time (in this case, the speed of rotation of the paddles). If the relaxation time is of the same order as the experiment time ($De \sim 1$), then there is a pronounced effect of viscoelasticity in the problem. A $De \sim 0$ is considered to be Newtonian while values much larger than 1 are considered to be highly elastic.

V. Results and Discussion

V.A. Mesh Optimization

V.A.1. Radial Mesh Optimization

The velocity magnitudes along Line 1 (Figure IV.7) for the four different radial meshes tried are shown in Figure V.1. All four meshes capture the velocity trend along this line well. The velocity at the barrel wall is zero and increases rapidly in the gap between the left paddle and the barrel to the highest velocity. It remains zero while inside the paddle face and then drops to zero once again as it comes close to the barrel walls in the middle. The velocity rises as the line moves closer to the right paddle, remains steady as it moves over the paddle face and drops to zero at the barrel. Meshes #1, #2 and #3 follow this profile closely, while the coarsest mesh #4, is unable to capture the highs and lows in velocity in areas with the highest gradients. The RMS % difference of the simulated velocities from the experimental velocities is shown in Table V.1 for all the meshes. Mesh #3 was chosen as the optimum radial mesh configuration as it avoided the overlaps in mesh #1 (see section IV.C.1), while providing better accuracy than mesh #4 and similar accuracy as the more refined mesh #2.

Figure V.1. Comparison of velocity magnitudes along line 1 for mesh #1 (1920 el, ■), mesh #2 (1632 el, ◆), mesh #3 (1072 el, ▲) and mesh #4 (512 el, □).

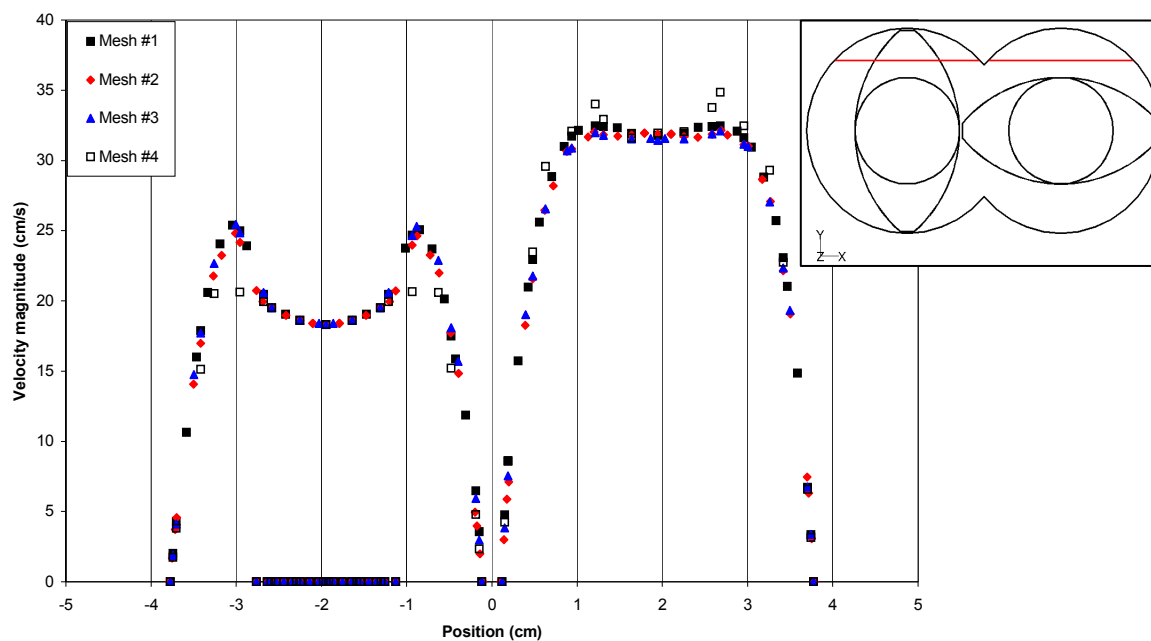


Table V.1. Comparison of RMS % difference at points P1, P2 and P3 for the four 2D meshes investigated

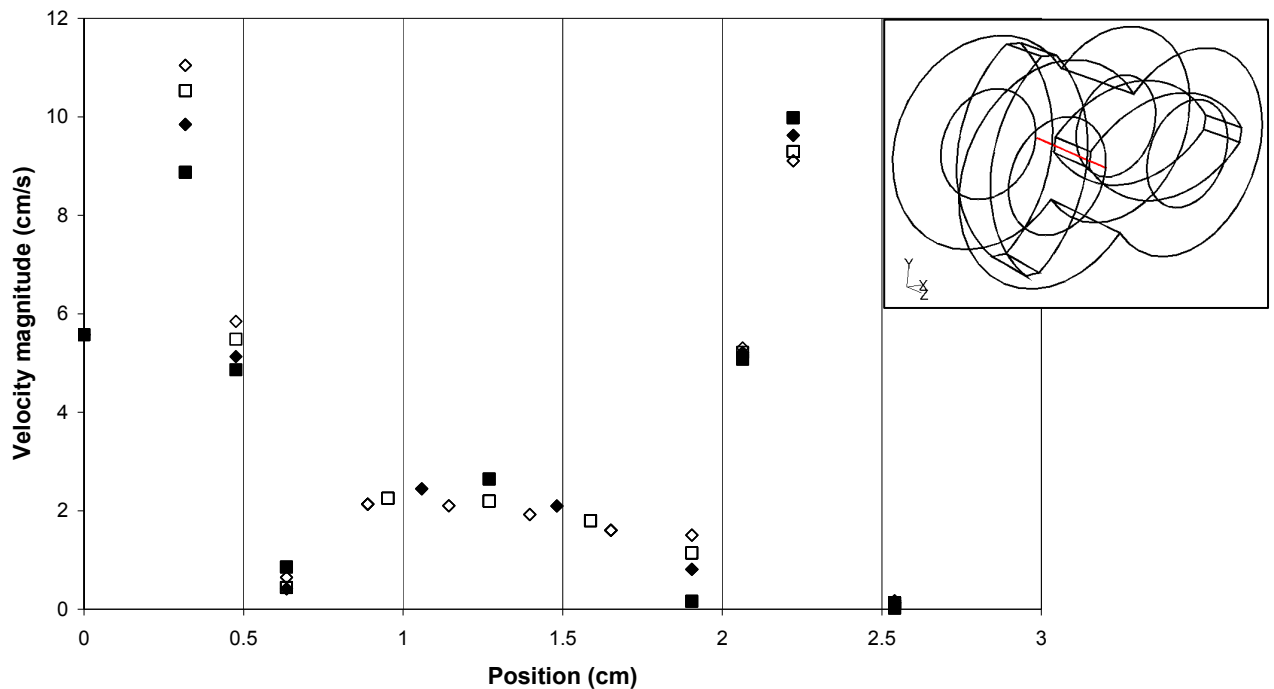
	P1		P2	P3
	V _x	V _y	V _x	V _x
Mesh #1	9.73	2.40	6.92	23.43
Mesh #2	9.66	3.12	7.67	20.57
Mesh #3	9.90	3.22	7.28	20.40
Mesh #4	10.86	4.46	8.59	16.05

V.A.2. Axial Mesh Density

The velocity magnitudes along Line 2 (Figure IV.9) for each of the axial meshes are depicted in Figure V.2. The velocity profile first rises as we approach the paddles from the entrance region and then steadies to an equilibrium value through the narrow gap between the paddles.

Meshes with 3, 4 and 5 axial intervals predict a similar velocity magnitude in the mid-plane of the paddle ($Z = 1.27$ cm) while the predictions from the mesh with 2 intervals deviates slightly from the meshes with the higher refinement. The mesh with an axial mesh density of 3 intervals was chosen as the optimum in terms of computational costs.

Figure V.2. Velocity comparison along Line 2 for meshes with 2 (■), 3 (◆), 4 (□) and 5 (◇) axial mesh intervals



V.B. Optimum number of paddle pairs

The effect of increasing the number of paddle pairs in the simulation geometry on the RMS % difference between the experimental and simulated velocity components in the x, y and z directions is shown in Figure V.3, Figure V.4 and Figure V.5 respectively. Each of the points on the curves represents a RMS % difference with experimental values at point P1 in the

geometry on the axially centered cross-section of each successive paddle. As the length of the geometry increases, the x and y velocity components (Figure V.3 and Figure V.4 respectively) show a slight decrease in the RMS % difference in the axial center of each geometry, with the geometry having 5 paddle pairs showing the least RMS % difference on the center cross-section of its third pair of paddles.

The effect of increasing the axial length of the geometry is more pronounced on the axial z-velocity component (Figure V.5). The RMS % difference with experimental values progressively decreases with the addition of every paddle pair. Once again, the 3rd pair in the 5 pairs geometry shows a marked improvement in reducing the disparity with experimental values when compared to lesser number of paddle pairs. A well developed flow profile is generated in the middle section of the simulation geometry and has greater relevance when compared to experimental results. These results illustrate the importance of additional paddle pairs that insulate the flow profile from entrance and exit effects.

Figure V.3. RMS % difference in the V_x velocity component at point P1 between experimental and simulated values as a function of axial location for simulation geometries having 1 pair (■), 2 pairs (◆), 3 pairs (▲), 4 pairs (□) and 5 pairs (◇) of paddles

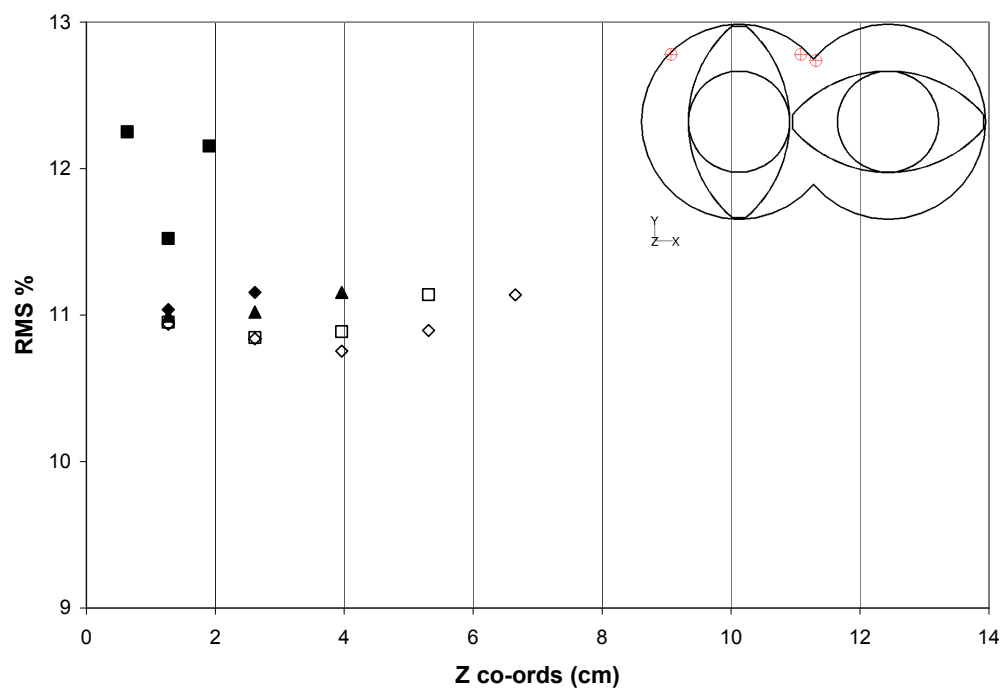


Figure V.4. RMS % difference in the V_y velocity component at point P1 between experimental and simulated values as a function of axial location for simulation geometries having 1 pair (■), 2 pairs (◆), 3 pairs (▲), 4 pairs (□) and 5 pairs (◇) of paddles

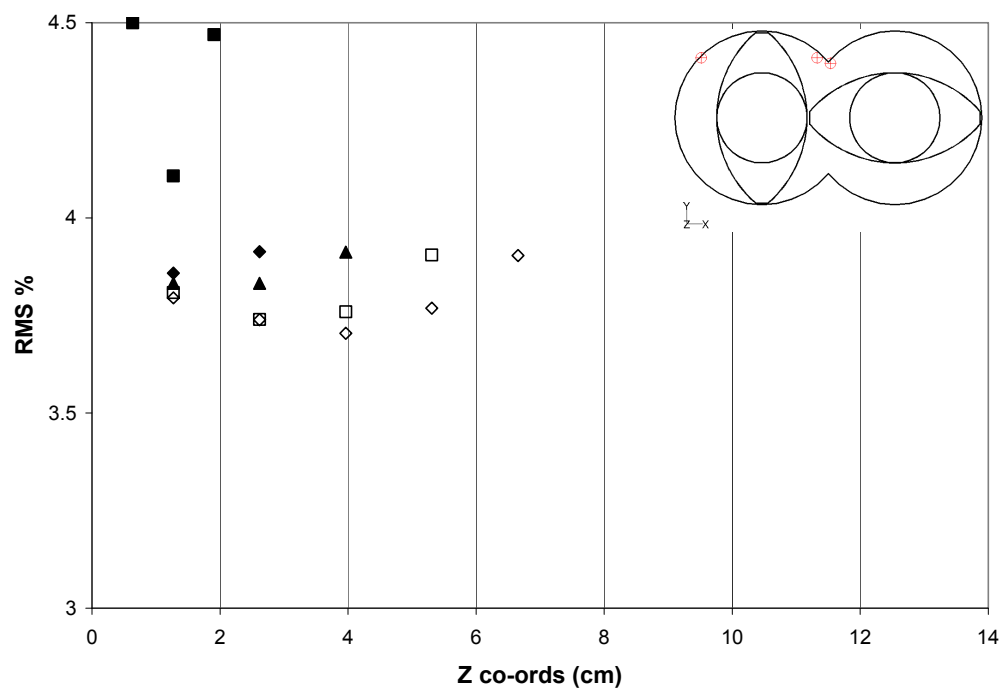
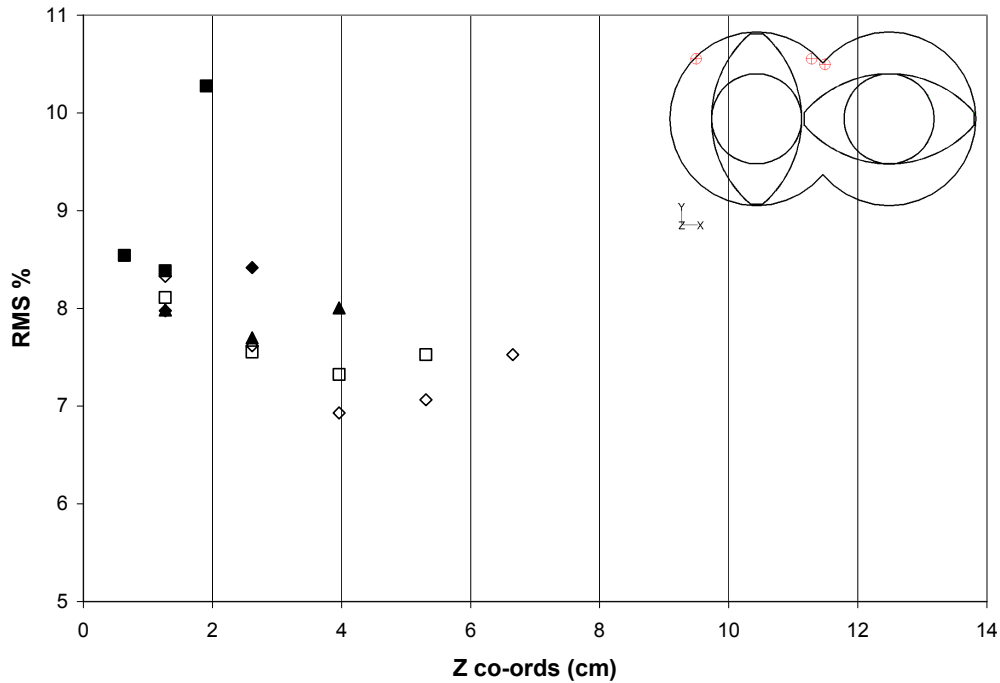


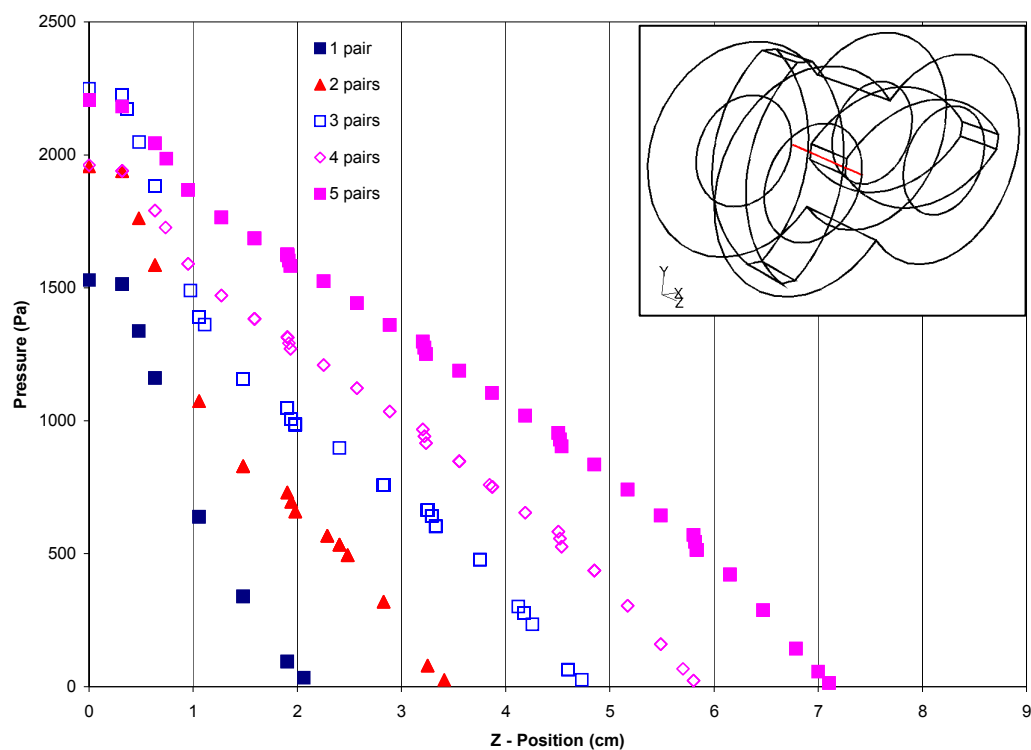
Figure V.5. RMS % difference in the V_z velocity component at point P1 between experimental and simulated values as a function of axial location for simulation geometries having 1 pair (■), 2 pairs (◆), 3 pairs (▲), 4 pairs (□) and 5 pairs (◇) of paddles



V.C. Flow through a slit analogy – Pressure comparison

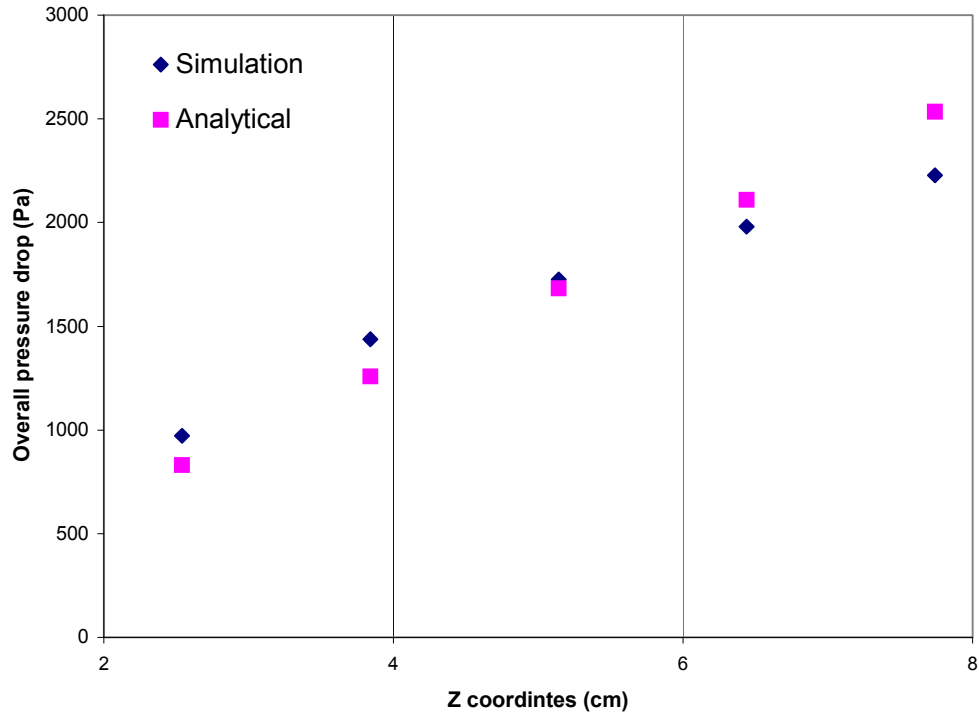
The pressure drop at the end of one rotation across the flow geometry increased as the length of the geometry (and the number of paddle pairs in the geometry) increased (Figure V.6). Line 2 passes through the gap between the two paddles in the intermeshing region and when the paddles are at the $0/360^\circ$ position, the gap resembles a narrow slit. The increase in pressure drop is consistent with an increase in flow geometry length for such a slit flow.

Figure V.6. Evolution of pressure along Line 2 for 2, 3, 4 and 5 paddle pair geometries



When the simulated pressure drops were plotted against the analytically computed pressure drop for the flow through a narrow slit using Equation 55 (Figure V.7), there was a very close correspondence between the two. This shows that the simulations are consistent and accurate. Along with the comparison with actual experimental results, these comparisons (when possible) with analytical solutions offer a means to verify that the simulation is predicting solutions as expected.

Figure V.7. Comparison of pressure drops between numerically simulated and analytical computation using slit flow analogy

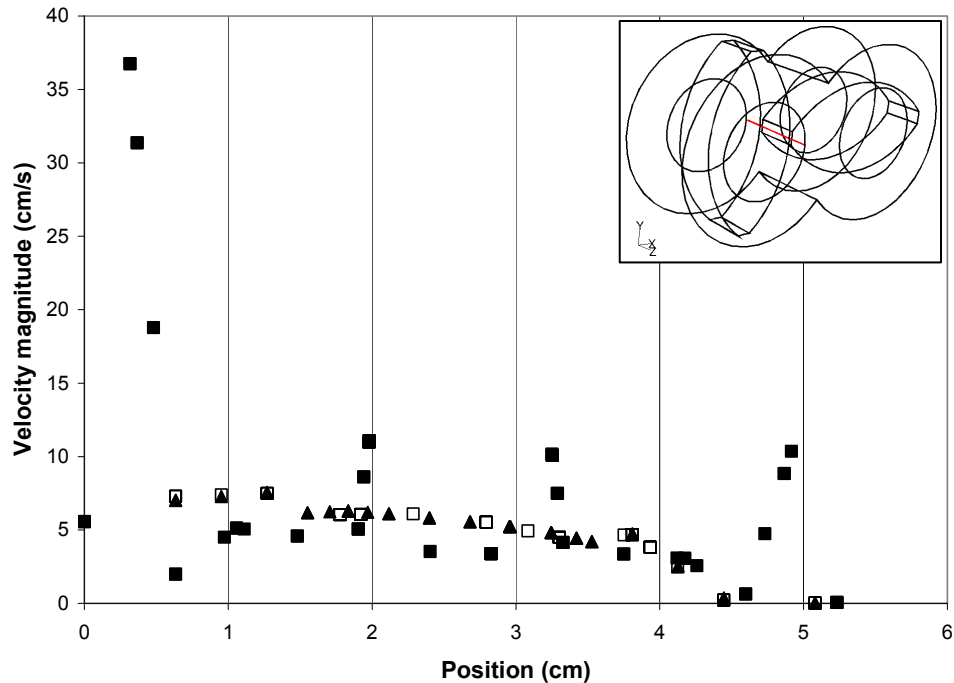


V.D. Modeling 9 pairs of paddles

To increase the length of the simulation geometry to the experimentally accurate 9 pairs of mixing paddles, the first and last three pairs of paddles were fused into one. Figure V.8, provides a comparison of the velocity magnitudes along line 2 for the realistic 3 paddle pair geometry with gaps in between paddles and the fused 3 pair meshes with 9 and 5 axial mesh intervals respectively. The 3 pair simulation geometry with gaps in between captures the variations in the velocity magnitude as the channel first narrows between the first pair of paddles and then widens at each gap, increasing in value during its passage through the gap.

This trend is not captured by the two simulation geometries without the gaps. Even though the variations of the velocity magnitudes in the gaps are not captured by the fused geometry, the magnitude is very close to that of the geometry with gaps. Furthermore, there isn't a significant difference in predictions between the two axial mesh densities of 9 and 5 intervals and the 5 mesh interval fused 3 pair geometry was chosen as the optimal geometry and mesh to be incorporated into the 9 pair geometry.

Figure V.8. Velocity comparison along Line 2 for 3 paddle pair meshes with gaps (■), fused 3 paddle pair meshes with 9 (▲) and 5 (□) axial intervals



The effect of increasing the number of paddle pairs in the simulation geometry from 5 pairs to a 9 pair geometry on the RMS % difference at point P1 between the experimental and simulated velocity components in the x, y and z directions is shown in Figure V.9, Figure V.10 and Figure V.11 respectively. As the length of the geometry increases from 5 pairs to 9,

the x and y velocity components (Figure V.9 and Figure V.10 respectively) show a slight decrease in the RMS % difference in the axial center of both geometries. The error involved in removing the gaps between the paddles and fusing the first and last three pairs of the 9 pair geometry shows up as an increase in the RMS % difference. Once again, the effect of increasing the axial length of the geometry is more pronounced on the axial z-velocity component (Figure V.11). The RMS % difference with experimental values progressively decreases with the addition of every paddle pair reaching a value as low as 5.5% in the center cross-section of the 8th paddle demonstrating the value of additional paddle pairs in describing the problem.

V.E. Effect of entrance length

While there is no improvement in the accuracy of the extended entrance length geometry in the x (Figure V.9) and y (Figure V.10) directions, there is a marked decrease in accuracy in the axial (z) direction (Figure V.11).

Figure V.9. RMS % difference in the V_x velocity component at point P1 between experimental and simulated values as a function of axial location for simulation geometries having 5 pairs (■), 5 pairs with increase in entrance length (□) and 9 pairs (▲) of paddles

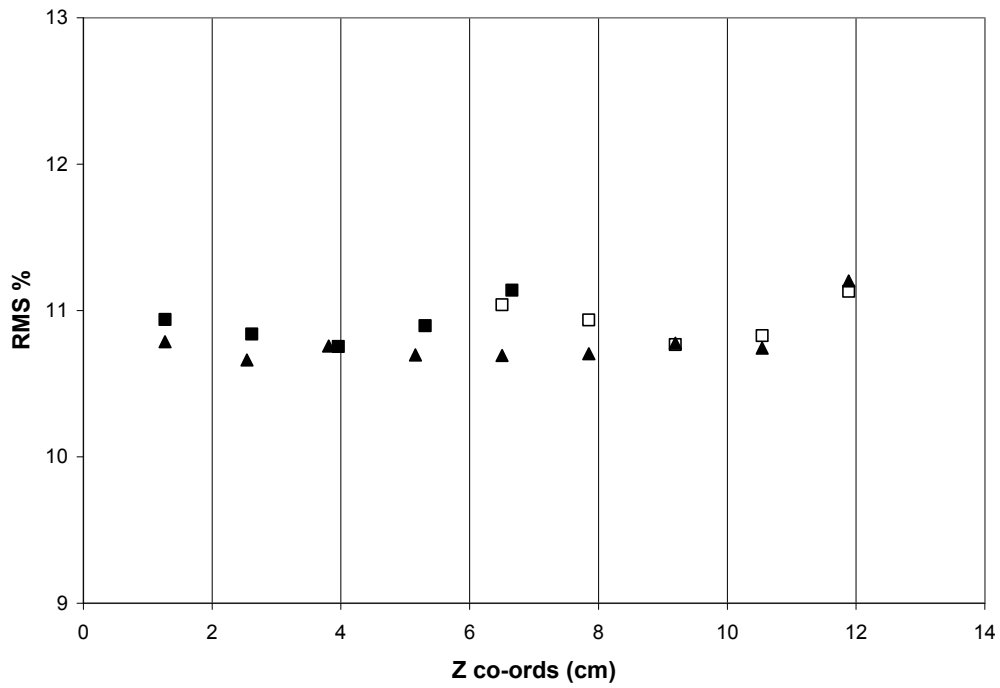


Figure V.10. RMS % difference in the V_y velocity component at point P1 between experimental and simulated values as a function of axial location for simulation geometries having 5 pairs (■), 5 pairs with increase in entrance length (□) and 9 pairs (▲) of paddles

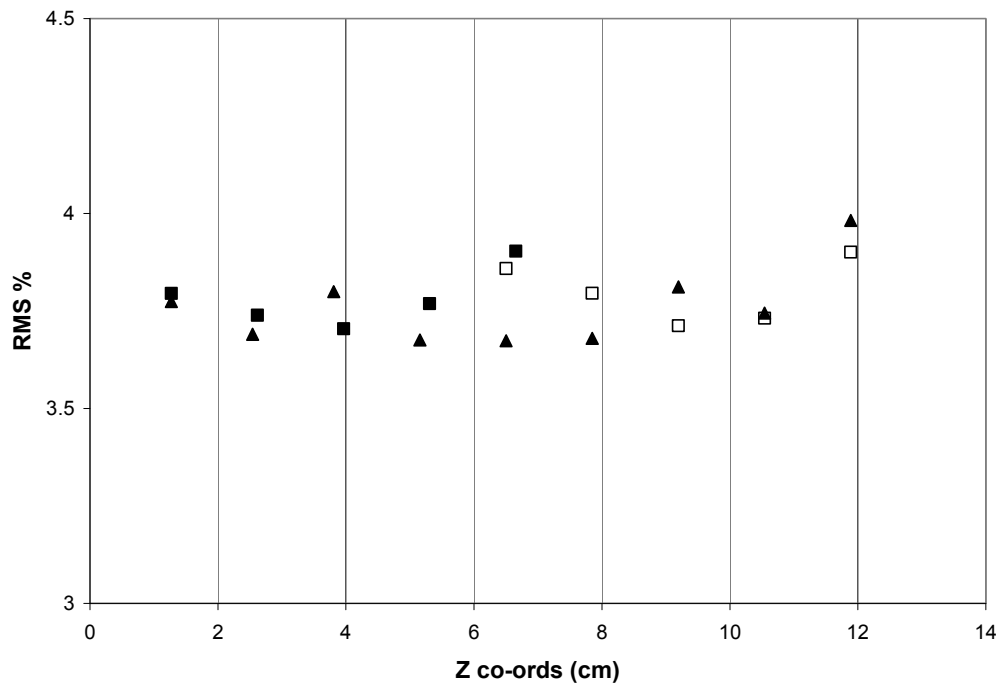
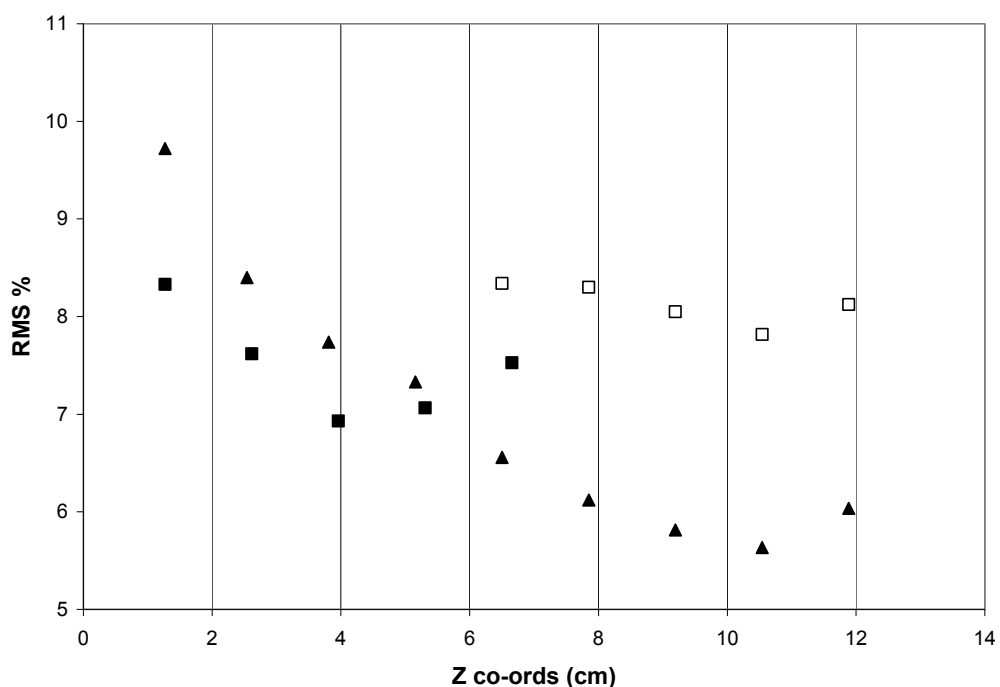


Figure V.11. RMS % difference in the V_z velocity component at point P1 between experimental and simulated values as a function of axial location for simulation geometries having 5 pairs (■), 5 pairs with increase in entrance length (□) and 9 pairs (▲) of paddles



The 9 paddle pair geometry gives us the most accurate values for the experimental 4th pair at the simulated 8th pair. This illustrates that longer simulated paddle geometries are required for obtaining more accurate results. In contrast to the work done by Jaffer and co-workers (Jaffer *et al*, 2000), at high flow rates (53 mL/s in this study as compared to 5 mL/s in their study), the addition of long paddles before and after the kneading blocks increases the accuracy of the predictions. The maximum difference found in this work between the

experimental and simulated values in the x and y directions was around 10% and 4% respectively while in the axial direction the difference was reduced to as little as 5.5%.

Yang and Manas-Zloczower (1992) and Bravo and co-workers (Bravo et al, 2000, 2004) dwelt upon the issue of defining the entrance flow field *a priori* to calculation of the flow field through mixing rotors. The ideal scenario would be to use the exit flow field from the simulation of a conveying screw which would be typical in most applications. However, this would be computationally intensive and the authors chose to assign a nominal value for the normal stress difference in the axial direction between the entrance and exit planes of the geometry as initial boundary conditions. The approach taken in this research has been to isolate the mixing paddles from the entrance effects by lengthening the simulation geometry and comparing the results from paddles farthest away from the entrance to the values recorded through experiments on the 4th (middle) paddle pair of a 9 paddle pair section. From the results, it has been clearly shown that lengthening the geometry has improved the accuracy of the prediction along the axial direction.

V.F. Calculation of mixing measures

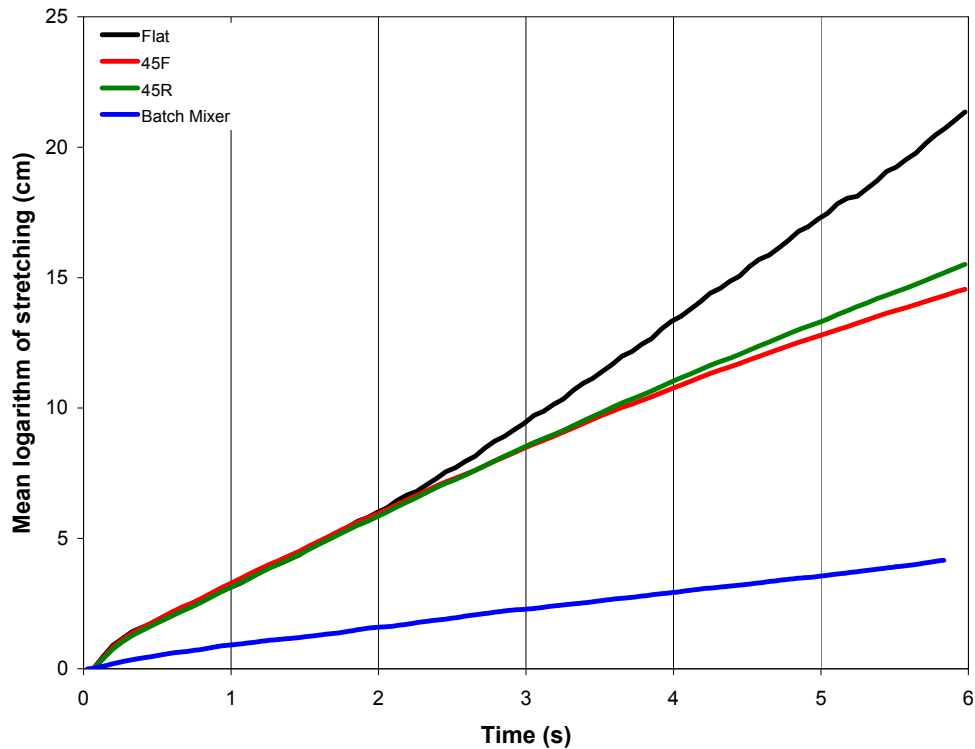
V.F.1. Effect of configuration

Mean logarithm of the length of stretching

Distributive mixing was evaluated by calculating and comparing the mean logarithm of the length of stretch across the different configurations and also with the data for the batch Farinograph mixer (Connelly, 2004). At the end of 10 rotations of the paddles, the length of stretch increased exponentially in all three configurations of the twin screw geometry (Figure

V.12). An exponential increase is expected as the flow in a twin screw mixer has been shown to be chaotic. The 'Flat' configuration showed higher stretching values after 2s when compared to the other two configurations which were close to each other in the amount of stretching. The 45R configuration showed slightly higher stretching than the 45F configuration near the end of 10 rotations. All three configurations showed considerably higher stretching than the batch mixer due to the chaotic nature of mixing in a twin screw mixer which is not present in the batch mixer. The Flat configuration performed better at stretching than the two staggered configurations as the flow path was less tortured than in the other two. This would allow the material to be stretched across longer distances before the material line is broken.

Figure V.12. Mean logarithm of stretching of the different screw configurations (Farinograph data: courtesy Connelly, 2004).



Instantaneous and time averaged efficiencies

The predicted mean instantaneous and time-averaged efficiencies are shown in Figure V.13 and Figure V.14 respectively. The instantaneous efficiency for all configurations rises abruptly from zero as the mixer starts up and then settles to a mean value. The values oscillate periodically about the mean with the changing flow geometry, with the period equal to one rotation (0.6s). The angular position of the left blade being vertical, which is the start of the rotation ($t = 0, 0.6, 1.2, 1.8s, \dots$) shows higher efficiency than the position of the paddles at the mid-point of every rotation ($t = 0.3, 0.9, 1.5s, \dots$) indicating that some

rotational positions of the paddles are more efficient than others. The 45F and 45R geometries equilibrate to an average value of around 0.12 whereas the Flat geometry averages at 0.2 at the end of 10 rotations. Any value of the instantaneous mixing efficiency below zero is unmixing the flow and the maximum value that it can attain is 1 for the best mixing. The batch mixer shows a much greater periodicity but a lower average than all three twin screw configurations, indicating that the mixing in the twin screw geometry is more efficient than in the batch mixer.

Figure V.13. Mean instantaneous efficiencies of the different screw configurations (Farinograph data: courtesy Connelly, 2004).

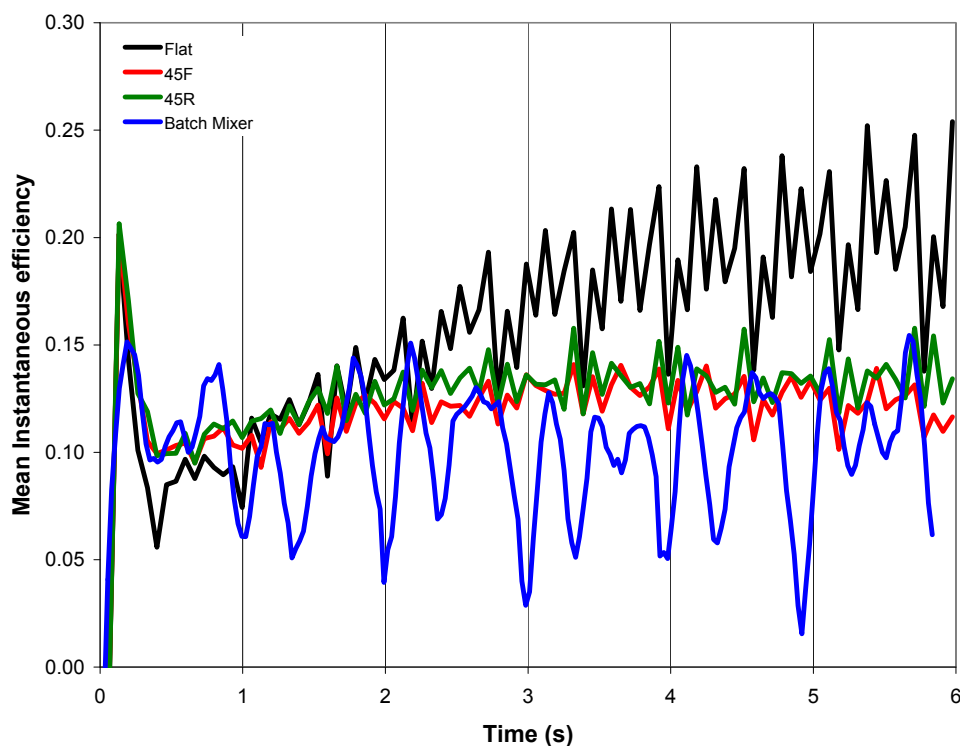
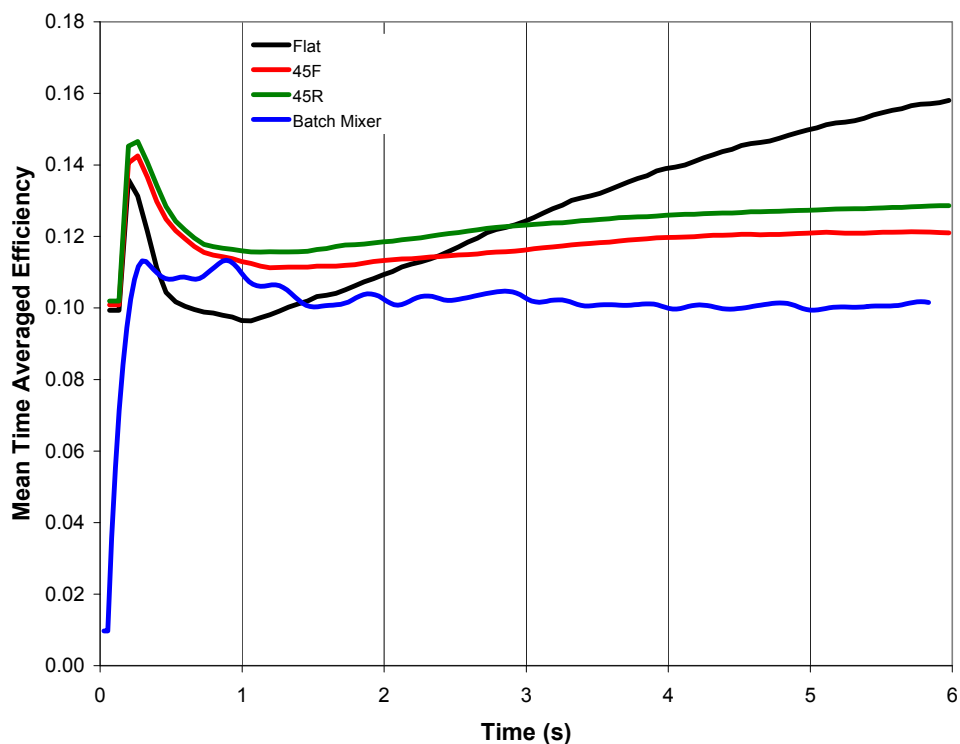


Figure V.14 shows the typical quick rise in the time averaged efficiency as the material initially begins to move followed by a fast drop off as the material points in rotational

patterns or in dead zones fail to maintain a logarithmic increase in the length of stretch. Then the curves levels off at a value above zero that is necessary for an effective mixer. The Flat configuration has a greater initial drop-off, but quickly regains a higher efficiency and eventually mixes more efficiently than the other geometries investigated. The high initial drop-off could be due to the presence of a larger number of dead zones in the intermeshing region that are not broken up due to the lack of staggered paddles as in the 45F and 45R configurations. The twin screw mixer also does not show the pronounced periodicity present in the batch mixer and has a more uniform efficiency curve.

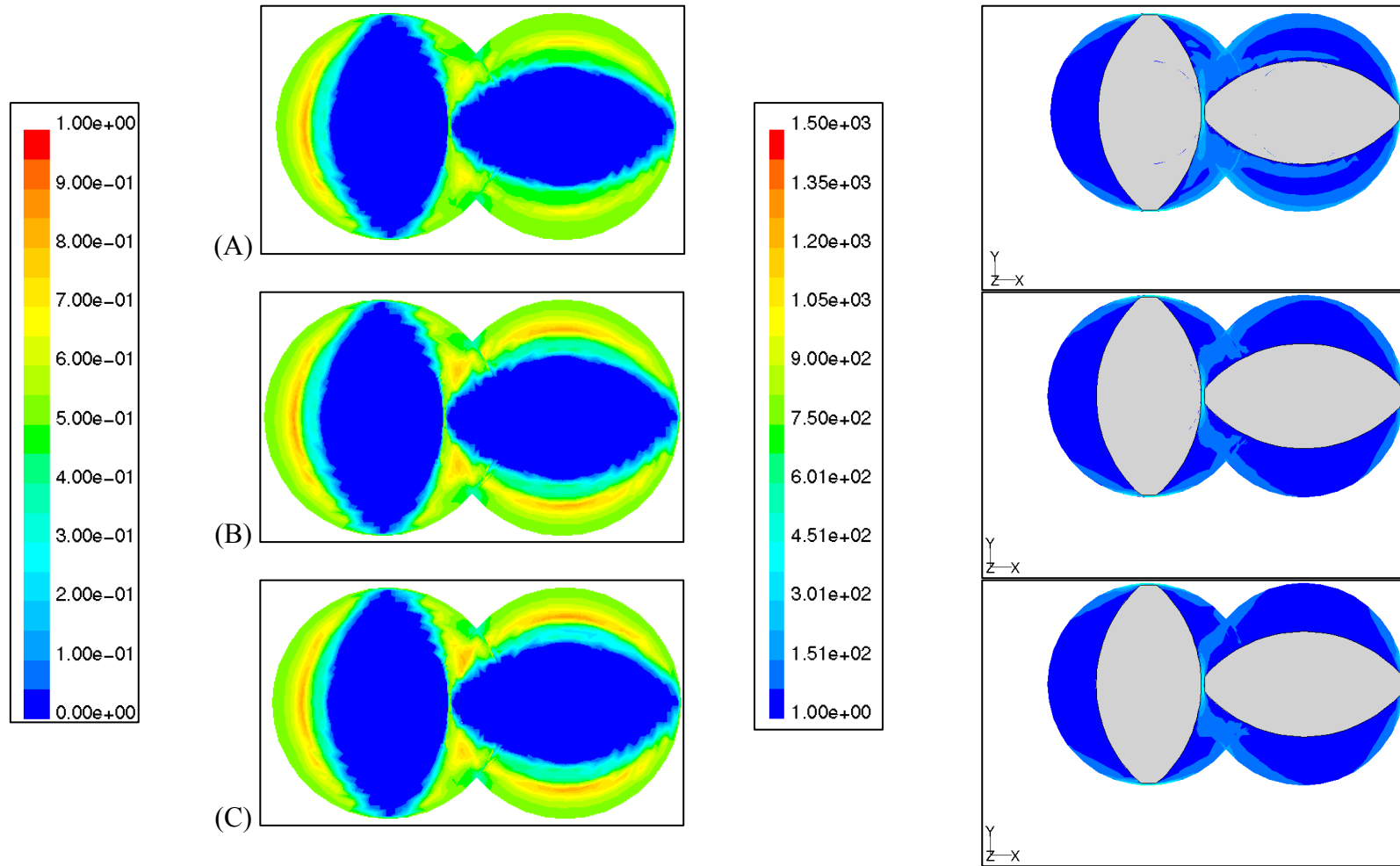
Figure V.14. Time-averaged efficiencies of the different screw configurations (Farinograph data: courtesy Connelly, 2004).



Dispersive mixing – Manas-Zloczower mixing index

The contours of the mixing index and shear rates in a cross-sectional plane through the middle of the 8th paddle for the Flat, 45F and 45R configurations are shown in Figure V.15a, Figure V.15b and Figure V.15c respectively. The cross-section of the 8th paddle was chosen as this cross-section had the least difference when compared to the experimental results. In all three configurations, the mixing index is highest (~0.7) in the intermeshing regions and in the middle of the C-shaped regions between the paddles and the barrel. This corresponds to the areas of the highest shear rates in the mixer and indicates that the dispersive mixing will be good in these regions. In both the 45F and 45R configurations, the regions above and below the right paddle show a marked increase in the mixing index values over the Flat configuration. The presence of the staggered paddles behind the 8th paddle breaks the flow and increases the shear rates in these regions, thus increasing the mixing index. The absence of these staggered paddles in the Flat configuration allows the material to flow without much obstruction over the right side paddles, decreasing the shear rates and also the mixing index. The staggered configurations can thus be considered to be better dispersive mixers than the inline Flat configuration.

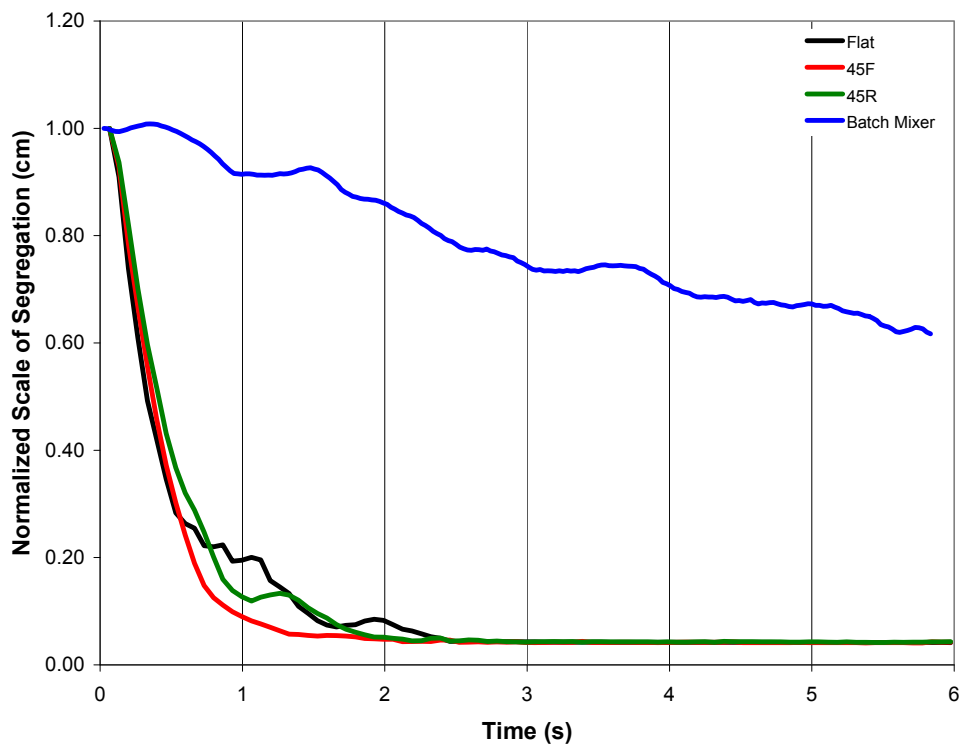
Figure V.15. Contours of mixing index and shear rate for (A) Flat (B) 45F and (C) 45R configurations.



Segregation scale

The normalized segregation scale for all three configurations is shown in Figure V.16. All three configurations show a rapid drop to a segregation of about 0.05 in less than 2s of operation. However, the 45F configuration desegregates the mixer the fastest, followed by the 45R and then the Flat configuration. After 2s of operation (approximately 3 rotations), all three mixer configurations show the same amount of segregation (~0.05) exhibiting the limit of desegregation that can be achieved with this continuous mixer geometry. Both the staggered configurations perform better than the Flat configuration showing that the segregation scale improves with a greater disruption in the flow caused by the staggering of the paddles. When compared to the batch mixer, the decrease in the normalized segregation scale is considerably higher for all three continuous mixer configurations. In 6s, both the continuous mixer paddles and the fast blade of the batch mixer complete 10 rotations. In this time, the continuous mixer does a better job of bringing the material in the two halves of the mixer together.

Figure V.16. Normalized segregation scale of the different screw configurations (Farinograph data: courtesy Connelly, 2004).



The trends in length of stretch, efficiencies and segregation values do not reveal a high degree of separation between the three screw configurations tested. Moreover, changes in configuration alone do not create substantial enough changes in the mixing efficiency to allow the continuous mixer to match the efficiency of the batch mixer. Thus, varying the screw configuration alone is not enough to sufficiently modify the mixing efficiency of the continuous mixer and to identify geometries and operating conditions that are closer in performance to the batch mixer, changes in the screw speed (and a resulting change in residence time) were explored and are discussed below.

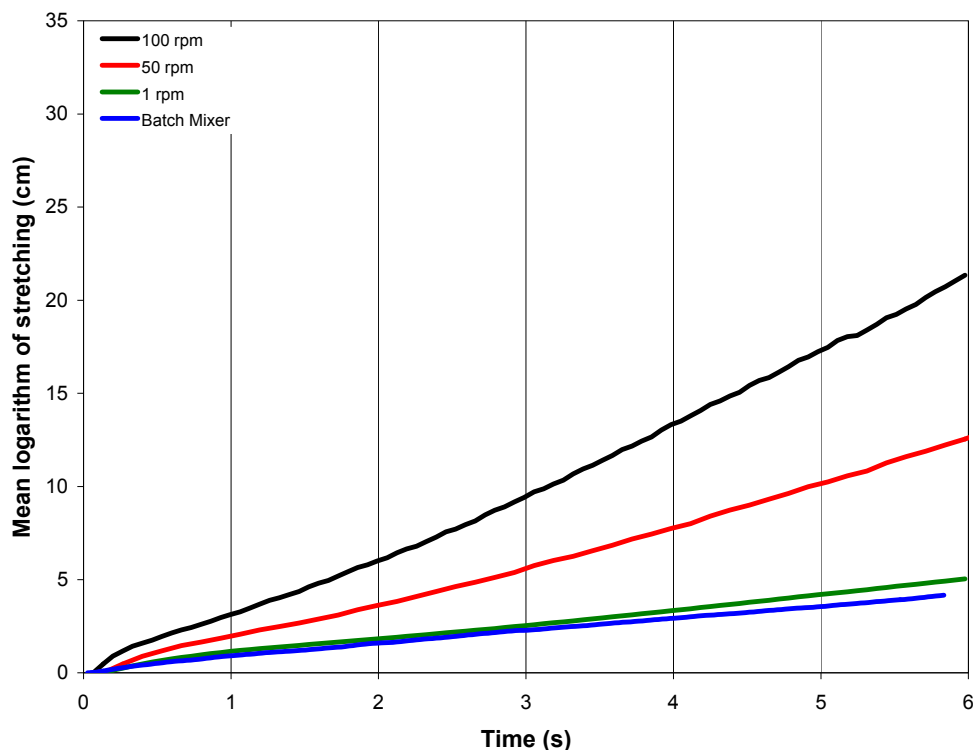
V.F.2. Effect of screw speed

The effect of decreasing the screw speed of the Flat configuration from 100 rpm to 50 and 1 rpm was studied in terms of both the residence time in the mixer and also by the number of rotations completed by the paddles. At 50 rpm, the paddles take 12s to complete 10 rotations and at 1 rpm they take 600s as opposed to the 6s that it takes to complete 10 rotations at 100 rpm. To ascertain if it is the time spent in the mixer or the number of rotations of the paddle that have a more significant impact on the mixing efficiency, it was necessary to conduct the analysis for both time and rotations.

Mean logarithm of the length of stretching

When the mean logarithm of the length of stretching at the three different screw speeds of the Flat configuration were compared at a residence time of 6s, it was seen that the values increased exponentially as is expected for a twin screw mixer (Figure V.17). However, each drop in screw speed brought about a proportional drop in the stretch values, indicating that the amount of stretching is proportional to the screw speed when viewed at a particular residence time. The mixer running at 1 rpm had the lowest amount of stretching as the least amount of work was put in to stretch the material lines, while the mixers running at 50 and 100 rpm had proportionally higher amount of stretching at 6s. When compared to the batch mixer, the length of stretch of the mixer at 1 rpm was quite comparable to the performance of the batch mixer. These results are an illustration on the means to achieve higher or lower distributive mixing in a continuous mixer that is comparable to the distributive mixing in a batch mixer.

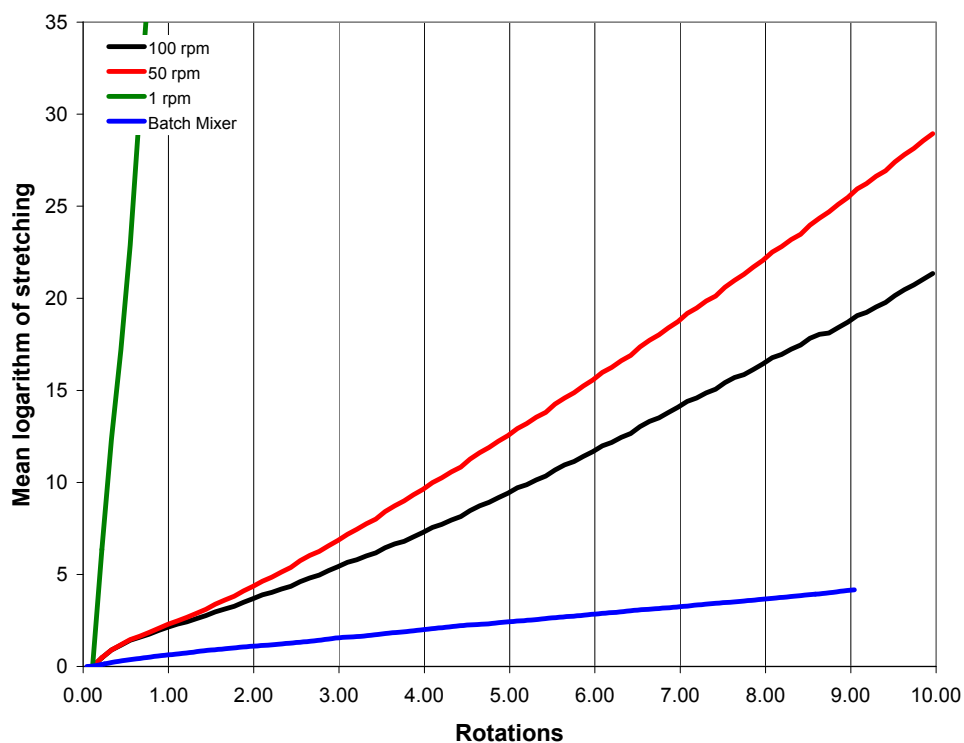
Figure V.17. Mean logarithm of the length of stretch of different screw speeds with a residence time of 6s (Farinograph data: courtesy Connelly, 2004).



Due to the difference in screw speeds, the time taken for the paddles to complete 10 rotations differs. When the results of the mean logarithm of length of stretch are compared at the end of 10 rotations (Figure V.18), it was seen that the large residence time of 600s for the mixer at 1 rpm to complete 10 rotations had a significant impact on the stretch values and they are quite high even after just one complete rotation ($t=60s$). The mixer at 50 rpm completes 10 rotations in only 12 s and this residence time does not allow the length of stretch values to increase as much as the mixer at 1 rpm. Similarly, for the mixer at 100 rpm, 10 rotations are completed in only 6 s further reducing the time for distributive mixing. This indicates that it is the residence time at a particular speed that has a larger impact on the mean logarithm of

stretching than the total number of rotations. When compared to the results of length of stretch values for a batch mixer at the end of 10 rotations of the fast blade, the continuous mixer operating with a very short residence time (in this case through a high RPM for a comparable time) shows the closest match. This analysis of the trends in distributive mixing with changes in operating conditions would allow us to develop a continuous mixer design that could replicate the mixing performance of a batch mixer.

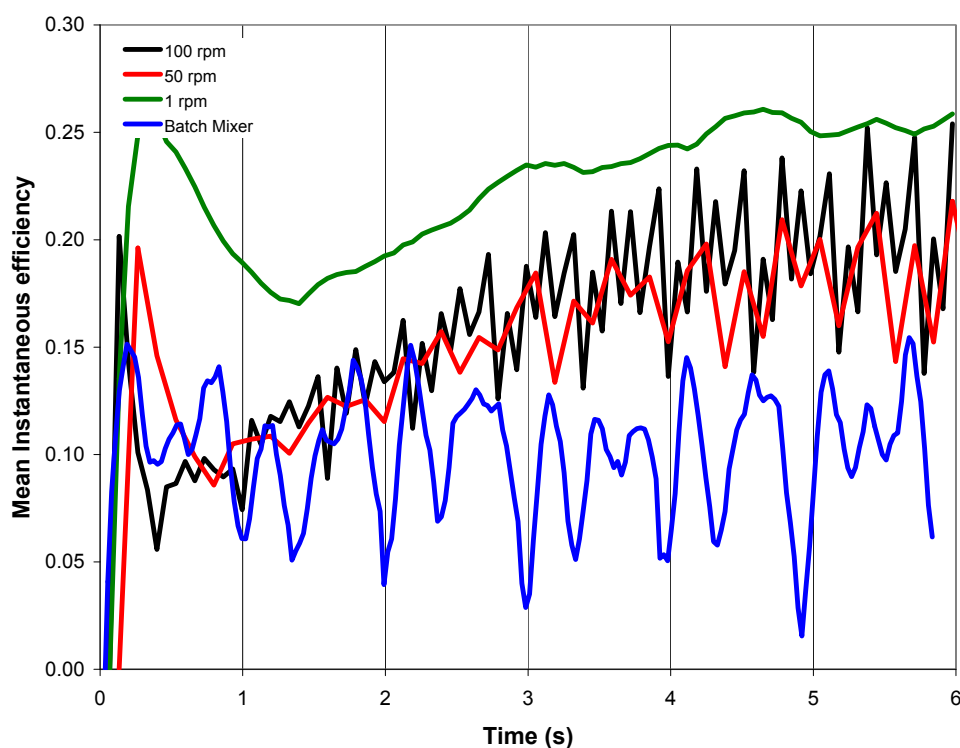
Figure V.18. Mean logarithm of stretching of the different screw speeds after 10 complete rotations (Farinograph data: courtesy Connelly, 2004).



Mean instantaneous and time-averaged efficiency of mixing

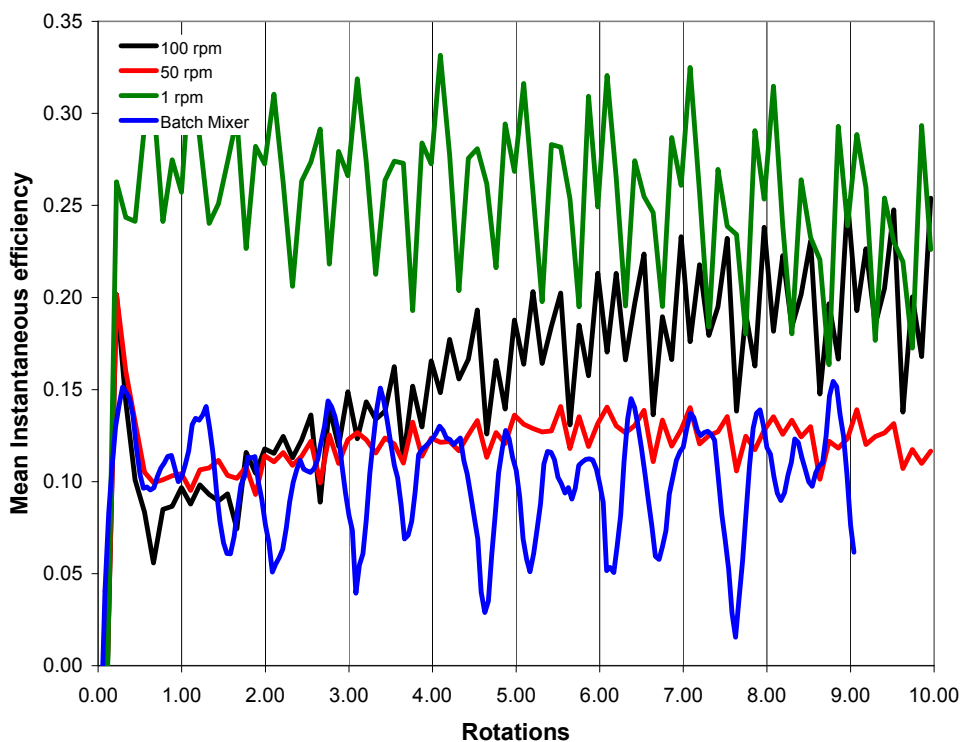
The mean instantaneous efficiency of the mixer at the three speeds after 6s and after 10 rotations is shown in Figure V.19 and Figure V.20 respectively. The instantaneous efficiency peaks initially and then settles to an average value with a set periodicity. A time of 6s is too short for the mixer at 1 rpm to show any periodicity yet and this is reflected in Figure V.19. The time taken to reach the initial peak value of the efficiency also increases with decreasing rotational speed. The mixer at 50 rpm equilibrates to almost the same mean efficiency as the mixer at 100 rpm indicating that the difference in speed does not yet manifest an effect at such short residence times.

Figure V.19. Mean instantaneous efficiency of the mixer at different screw speeds with a residence time of 6s (Farinograph data: courtesy Connelly, 2004).



However, when the results are seen at the end of 10 rotations, the mixer operating at 1 rpm has the highest mean value. The mixer at 1 rpm has also started showing a decrease in the efficiency after about 5 rotations, and a similar decrease in the mean is seen in the mixer at 50 rpm after about 7 rotations. The mixer at 100 rpm however, continues to increase till 10 rotations, and there is a probability that the downturn might happen after 10 rotations (though the simulation was not carried out that far in this research). The comparison with the batch mixing data shows the 50 rpm to be very close in instantaneous efficiency over the time taken to complete 10 rotations in both geometries.

Figure V.20. Mean instantaneous efficiency of the mixer at different screw speeds after 10 complete rotations (Farinograph data: courtesy Connelly, 2004).



The time averaged efficiency of the mixer at 1 rpm is highest when compared to that at 50 rpm and 100 rpm (Figure V.21). This could be an artifact of the short measurement time and a manifestation of the initial rapid increase of efficiency. However, when the corresponding time averaged efficiencies are observed over a longer time scale for 10 complete rotations (Figure V.22), it is clear that the mixer at 1rpm still has the highest efficiency, with the faster speeds for 50 rpm and 100 rpm showing lower efficiencies. Once again, the batch mixer has the lowest efficiency among all the mixing conditions studied.

Figure V.21. Time averaged efficiency of the different screw speeds with a residence time of 6s (Farinograph data: courtesy Connelly, 2004).

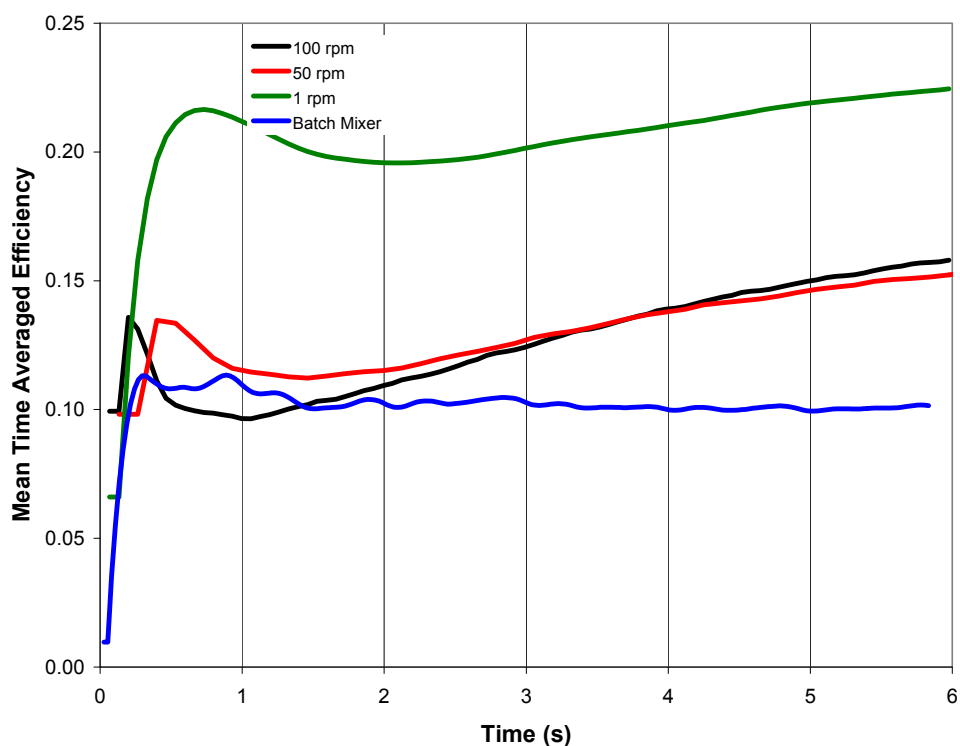
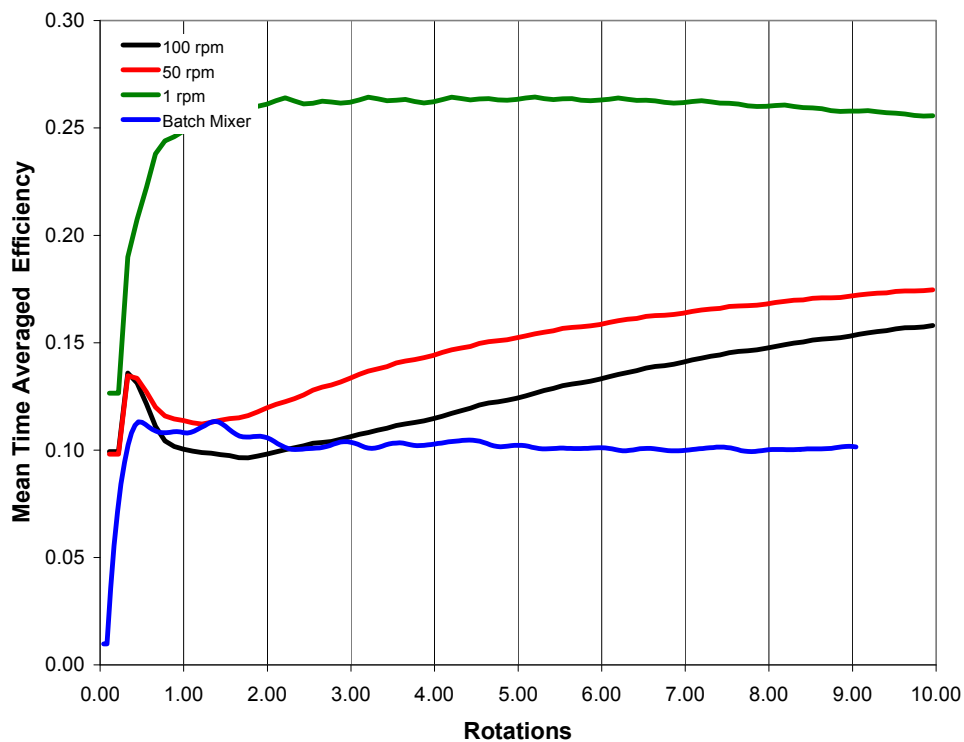


Figure V.22. Time averaged efficiency of the different screw speeds after 10 complete rotations (Farinograph data: courtesy Connelly, 2004).



The continuous mixer running at 100 rpm comes closest to the average efficiency of the batch mixer. However, to match the mixing performance of a continuous mixer to that of a batch mixer it is not imperative to match the efficiency. A higher efficiency is desirable as long as the other mixing indices such as the length of stretch and segregation scale are close to each other across the two mixers.

Segregation scale

While the efficiency of the continuous mixer at 1 rpm is high, it is a poor mixer when desegregating particles in the mixer as seen from the reduction in the normalized segregation scale after either 6s (Figure V.23) or after 10 rotations (Figure V.24). The screw speeds of 50 and 100 rpm perform much better in reducing the segregation scale showing that higher screw speeds are important to distribute material well in the continuous mixer. However, if the objective of the continuous mixer is to match the performance of the batch Farinograph mixer, then the mixer at 1 rpm performs best in comparing well to that batch mixer at both short time scales and over extended periods of mixing.

Figure V.23. Normalized segregation scale of the mixer at different screw speeds with a residence time of 6s (Farinograph data: courtesy Connelly, 2004).

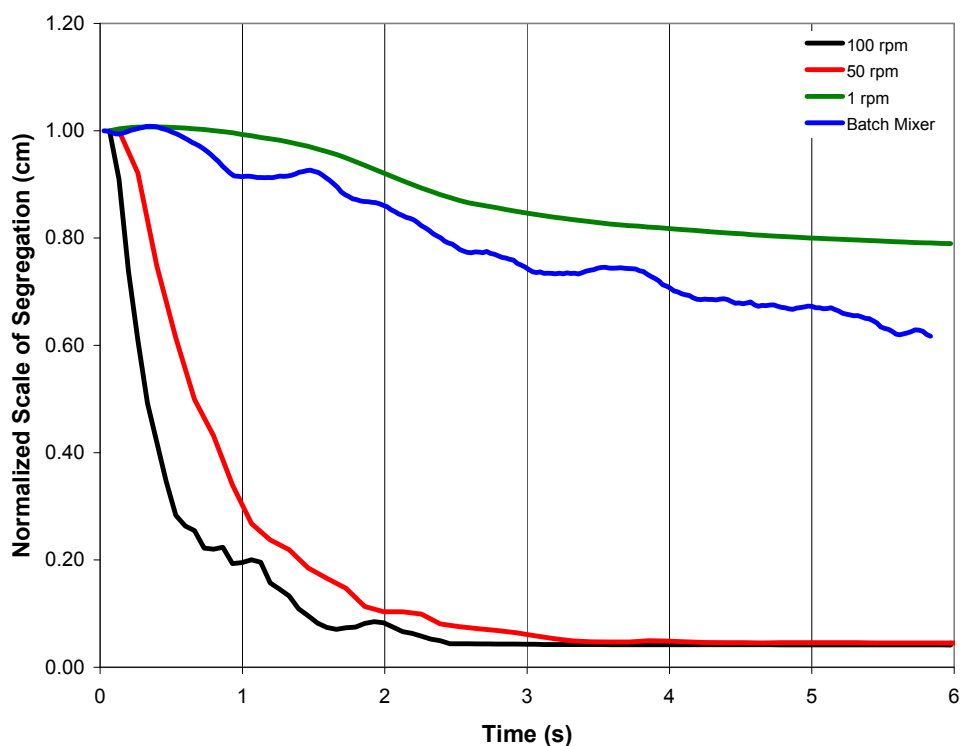
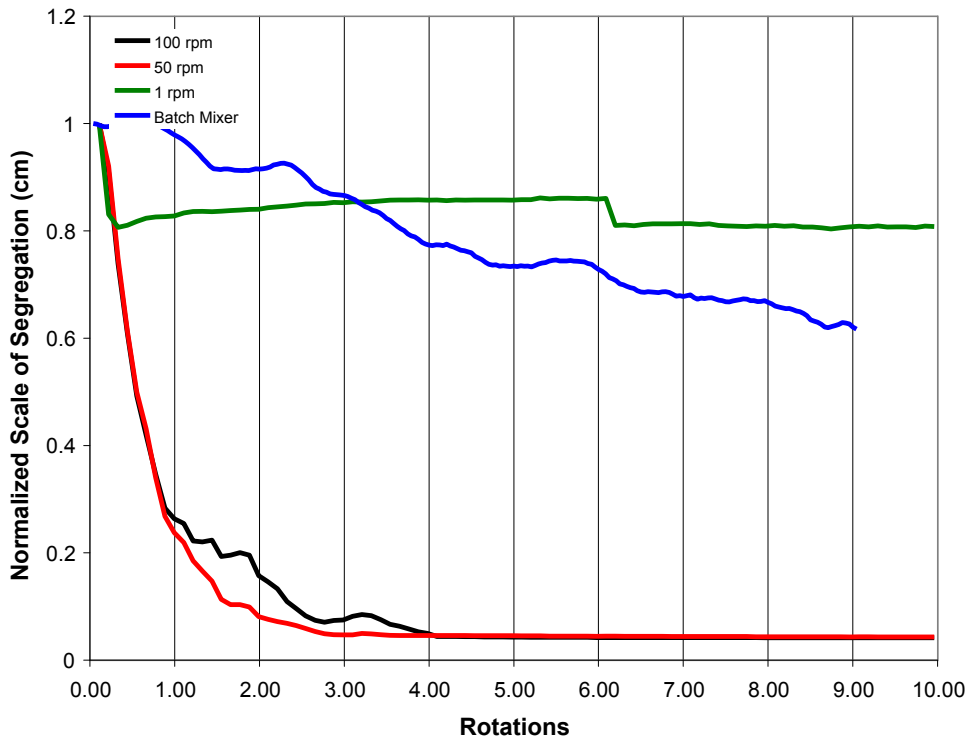


Figure V.24. Normalized segregation scale of the mixer at different screw speeds after 10 complete rotations (Farinograph data: courtesy Connelly, 2004).

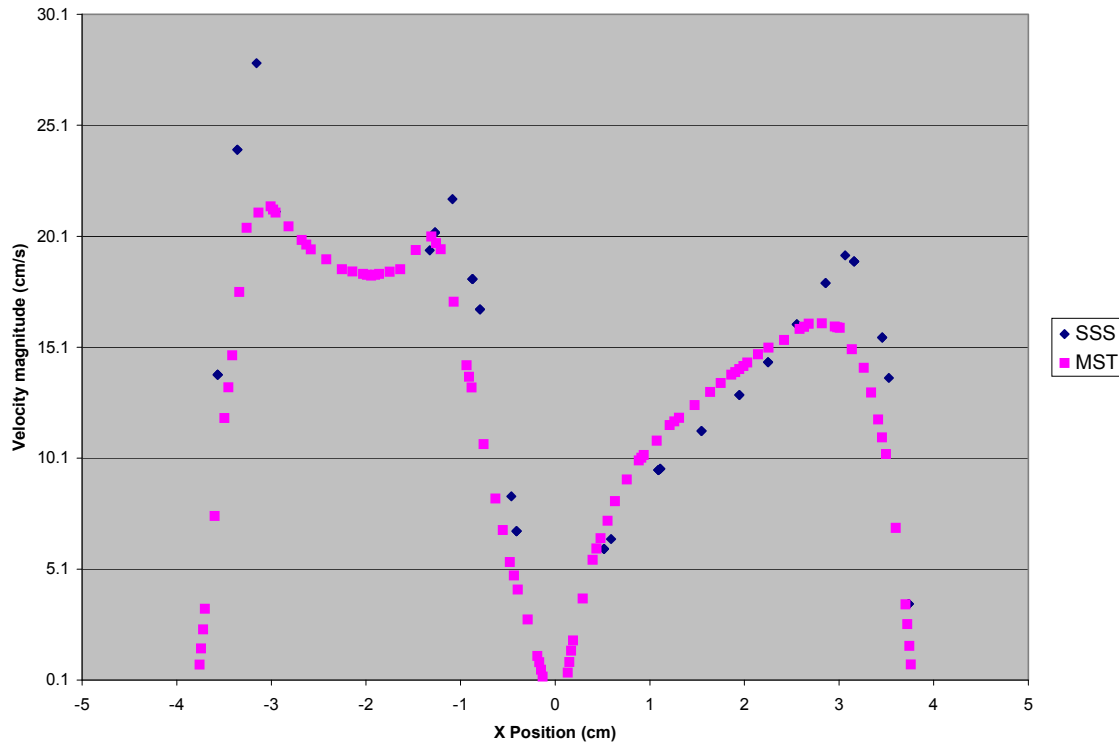


V.G. Viscoelastic Simulations

V.G.1. Verification of PSS technique with viscous Newtonian solution

Figure V.25 shows the comparison of velocity magnitudes along line 1 from the solution of the flow a Newtonian liquid using the PSS technique to those obtained using MST.

Figure V.25. Comparison of velocity magnitudes along line 1 obtained with PSS and MST



The velocity magnitudes compare well between the two techniques. The exceptions are in the clearance areas between the paddles and barrel where the velocity gradients are highest. The coarser mesh of the PSS technique and the inherent error in the technique due to interpolation between the nodes when changing from one mesh to the next, do not allow us to capture these gradients accurately.

V.G.2. Simulations with the Oldroyd B model

Evolution was used to achieve a higher degree of non-linearity while solving the viscoelastic constitutive equation. During the solution of the problem with the paddles at the 0° position,

the value of the evolution parameter started at 0, implying that the solution was for a Newtonian fluid under rest in the mixer. By steadily increasing the evolution parameter, a convergent solution was obtained till a value of $S=1.69 \times 10^{-2}$. This meant that the relaxation time was also 1.69×10^{-2} and the angular velocity of the boundaries that represented the paddles was $10.47692 * 1.69 \times 10^{-2} = 0.177 \text{ rad/s} = 1.69 \text{ rpm}$. The resultant De value was equal to 0.003.

The velocity, pressure, shear rates and stress results obtained from this solution were then used to initialize the nodes of the mesh with the paddles at the 1° position using the procedure outlined before. A relaxation time of 1.69×10^{-2} and an angular velocity of 1.69 rpm were imposed and the steady state solution on this mesh was calculated. An evolution approach could not be utilized to increase the elasticity as the solution did not converge beyond the first step (which is the same as the steady state solution). The steady state solution converged and the values of the velocity magnitude (Figure V.26) and shear rates (Figure V.27) were plotted on contour maps.

Figure V.26. Velocity magnitude (cm/s) at the end of 1° of paddle rotation using a viscoelastic constitutive equation

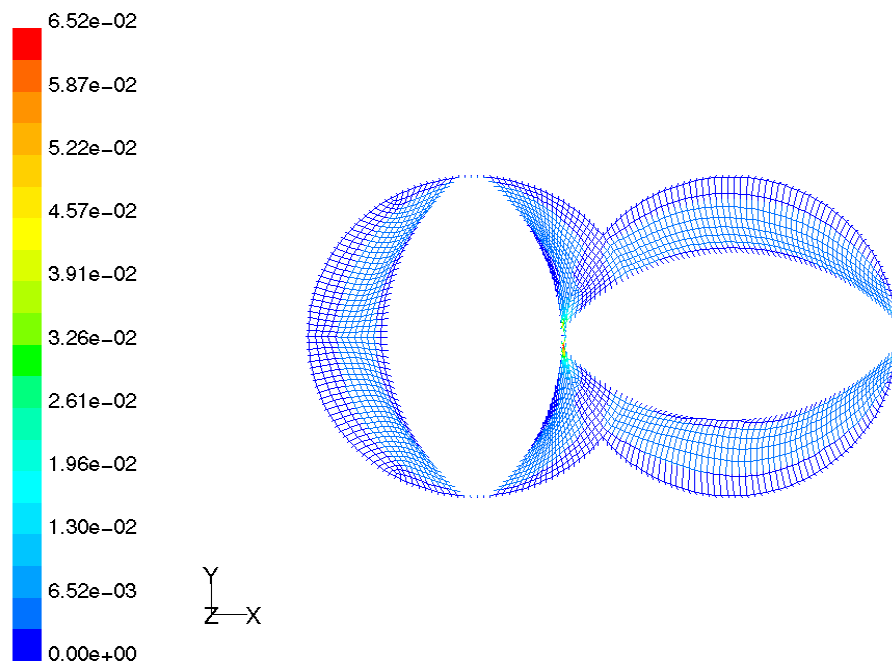
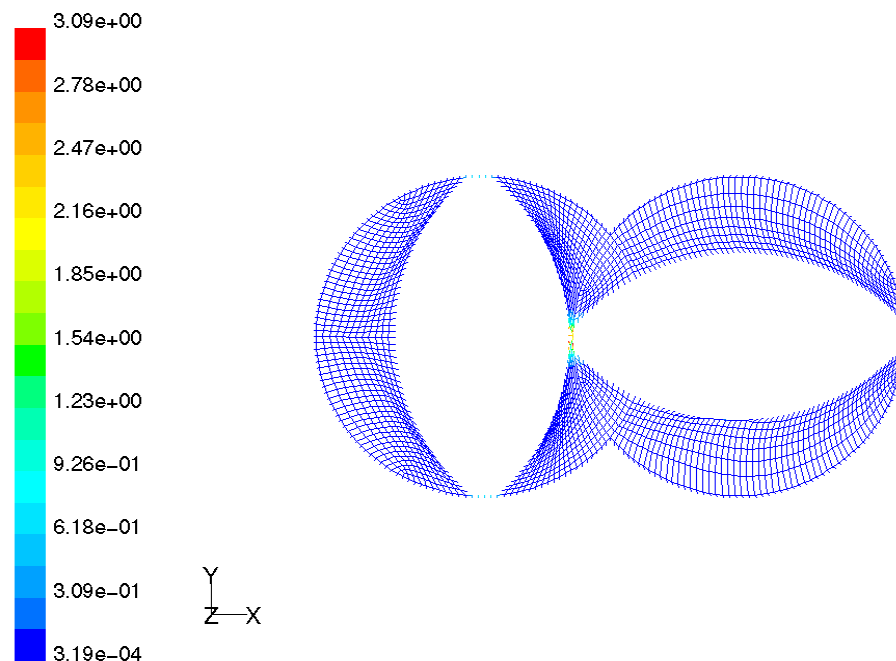


Figure V.27. Shear rates (1/s) at the end of 1° of paddle rotation using a viscoelastic constitutive equation



The velocity magnitudes show the rise in velocity in the intermeshing region and in the clearance region between the paddles and the barrel. A similar increase in shear rates is also observed. These increases in velocity and shear rate indicate that the simulation was indeed successful in translating the results from the initial mesh to a displaced mesh and is the first such demonstration. Viscoelasticity was evident from non-zero values of the stress tensors (appendix B). Values of node #, x and y coordinate values for those node numbers, V_x , V_y , pressure, stress tensors and shear rate at the end of the viscoelastic simulation are given in Appendix B. Further work is required to extend this motion to larger angular rotation of the screws and to greater values of De .

VI. Conclusions

This research addressed important concerns about the accuracy of numerical simulations in depicting experimental observations. An optimum mesh that reduced the errors involved in using the mesh superposition technique and optimum axial mesh densities that reduced the computational costs were developed. A systematic analysis of the number of paddle pairs required to accurately simulate the geometry of the Readco continuous mixer was conducted. An analogy with the flow in a slit was used to verify the simulations. It was found that 9 paddle pair geometry with extended entrance and exit paddle sections provided the best match with experimental observations on the 4th paddle pair of the Readco mixer. It was also observed that these extended paddle geometries could not be simply replaced with a longer entrance length and an accurate description of the boundary conditions requires the simulation of a longer entrance and exit paddle sections. One of the objectives stated in this research was to test the hypotheses that 3D simulations would provide us with a more accurate measure of mixing than 2D or static 3D simulations. The importance of the axial velocity component and the improvement in its accuracy with improvements in axial geometry description proves the importance of considering this third axial dimension.

After establishing the accuracy of the numerical simulations, particle tracking simulations were conducted to discern the influence of paddle configuration and screw speed on distributive and dispersive mixing measures. It was identified that the paddle configurations did not contribute greatly to changes in mixing performance. A reduction in screw speed from 100 rpm to 50 or 1 rpm decreased the amount of desegregation that could be performed by the mixer but increased its efficiency over time. It was observed that the Flat configuration operating at 1 rpm for a short time (~6s) resulted in the best match when

compared to the mixing performance of the batch mixer. These observations also addressed the second objective of this research – to analyze and develop methods for the design of continuous mixers.

This research also showed the first demonstrated simulation of the flow of a viscoelastic fluid in the Readco geometry. Although only low levels of De were achieved, a framework for the solution of the problem was proposed and demonstrated. Further work would be required to improve both the levels of De achieved and also the amount of displacement (or rotation) of the paddles.

REFERENCES

- Al Mubaiyedh, U.A., Sureshkumar, R. and Khomami, B. 2000. Linear stability of viscoelastic Taylor-Couette flow: Influence of fluid rheology and energetics. *Journal of Rheology*, 44(5): 1121-1138.
- Al Mubaiyedh, U.A., Sureshkumar, R. and Khomami, B. 2002a. The effect of viscous heating on the stability of Taylor-Couette flow. *Journal of Fluid Mechanics*, 462: 111-132.
- Al Mubaiyedh, U.A., Sureshkumar, R. and Khomami, B. 2002b. Nonlinear stability analysis of viscoelastic Taylor-Couette flow in the presence of viscous heating. *Physics of Fluids*, 14(3): 1056-1064.
- Alsteens B., Legat, V., Avalosse, T. 2004. Parametric study of the mixing efficiency in a kneading block section of a twin-screw extruder. *International Polymer Processing* 19: 207-217.
- Alvarez, M.M., Zalc, J.M., Shinbrot, T., Arratia, P.E., and Muzzio, F.J., 2002. Mechanisms of mixing and creation of structure in laminar stirred tanks. *AIChE Journal*, 8(10):2135-2148.
- Anderson, P.D., Galaktionov, O.S., Peters, G.W.M., van de Vosse, F.N. and Meijer, H.E.H. 2000a. Chaotic fluid mixing in non-quasi-static time-periodic cavity flows. *International Journal of Heat and Fluid Flow*, 21(2):176-185.
- Anderson, P.D., Galaktionov, O.S., Peters, G.W.M., van de Vosse, F.N. and Meijer, H.E.H. 2000b. Mixing of non-Newtonian fluids in time-periodic cavity flows. *Journal of Non-Newtonian Fluid Mechanics*. 93(2-3):265-286.
- Ashokan, B.K., Fanning, L., Connelly, R.K. and Kokini, J.L. 2003. Determination of the flow and mixing in a continuous mixer using LDA and 3-D numerical simulation. *Proceedings of the Eighth Conference of Food Engineering, A topical conference held in conjunction with the 2003 AIChE Annual Meeting, San Francisco, CA.*
- Ashrafi, N., Binding, D.M. and Walters, K. 2001. Cavitation effects in eccentric-cylinder flows of Newtonian and non-Newtonian fluids. *Chemical Engineering Science*, 56:5565-5574.
- Avalosse, Th. and Rubin, Y. 2000. Analysis of mixing in corotating twin screw extruders through numerical simulation. *Intern. Polymer Process.* XV(2): 117-123.
- Baloch, A., Grant, P.W. and Webster, M.F. 2002. Parallel computation of two-dimensional rotational flows of viscoelastic fluids in cylindrical vessels, *Engineering Computations*. 19(7):820-853.

- Binding, D.M., Couch, M.A., Sujatha, K.S. and Webster, M.F. 2003. Experimental and numerical simulation of dough kneading in filled geometries. *Journal of Food Engineering*. 58(2):111-123.
- Bertrand, F., Tanguy, P.A. and Thibault, F., 1997. A three-dimensional fictitious domain method for incompressible fluid flow problems. *International Journal for Numerical Methods in Fluids*, 25 (6):719-736.
- Bertrand, F., Tanguy, P.A., Brito de la Fuente, E. and Carreau, P. 1999. Numerical modeling of the mixing flow of second-order fluids with helical ribbon impellers. *Computer Methods in Applied Mechanics and Engineering*. 180(3): 267-280.
- Bravo, V.L., Hrymak, A.N., and Wright, J.D. 2000. Numerical simulation of pressure and velocity profiles in kneading elements of a co-rotating twin screw extruder. *Polymer Eng. & Sci.*, 40(2):525-541.
- Bravo, V.L., Hrymak, A.N., and Wright, J.D. 2004. Study of Particle Trajectories, Residence Times and Flow Behavior in Kneading Discs of Intermeshing Co-Rotating Twin-Screw Extruders. *Polymer Eng. & Sci.*, 44(4):779-793.
- Cheng, H. and Manas-Zloczower, I. 1997. Study of mixing efficiency in kneading discs of co-rotating twin-screw extruders. *Polym. Eng. Sci.* 37(6): 1082-1090.
- Chiruvella, R.V., Jaluria, Y. and Karwe, M.V. 1996. Numerical Simulation of the Extrusion Process for Food Materials in a Single-screw Extruder. *Journal of Food Engineering*. 30:449-467.
- Connelly, R.K. & Kokini, J.L., 2003. 2-D numerical simulation of differential viscoelastic fluids in a single-screw continuous mixer: Application of viscoelastic FEM methods, *Advances in Polymer Technology*, 22 (1): 22-41.
- Connelly, R.K., & Kokini, J.L., 2004. Analysis of mixing in a model mixer using 2-D numerical simulation of differential viscoelastic fluids with particle tracking. *Journal of Non-Newtonian Fluid Mechanics*, 123:1-17.
- Connelly, R.K. 2004. *Numerical simulation and validation of the mixing of dough-like materials in model batch and continuous dough mixers*. PhD. Dissertation, Rutgers University, New Brunswick, NJ.
- Connelly, R.K., & Kokini, J.L., 2006a. 3D Numerical Simulation of the Flow of Viscous Newtonian and Shear Thinning Fluids in a Twin Sigma Blade Mixer. *Advances in Polymer Technology*, 25(3):182-194.
- Connelly, R.K., & Kokini, J.L., 2006b. Mixing Simulation of a Viscous Newtonian Liquid in a Twin Sigma Blade Mixer. *AIChE Journal*, 52(10):3383-3393.
- Connelly, R.K., & Kokini, J.L., 2007. Examination of the mixing ability of single and twin screw mixers using 2D finite element method simulation with particle tracking. *Journal of Food Engineering*, 79(3): 956-969.

- Couch, M.A. and Binding, D.M. 2003. An experimental study of the peeling of dough from solid surfaces. *Journal of Food Engineering*. 58(4):299-309.
- de la Villeon, J., Bertrand, F., Tanguy, P.A., Labrie, R., Bousquet, J. and Lebrouvier, D., 1998. Numerical investigation of mixing efficiency of helical ribbons. *AIChE Journal*, 44(4):972-977.
- Dhanasekharan, M., Huang, H. and Kokini, J.L. 1999. Comparison of the observed rheological properties of hard wheat flour dough with the predictions of the Giesekus-Leonov, the White-Metzner, and the Phan-Thien Tanner models. *Journal of Texture Studies*. 30(5):603-623.
- Dhanasekharan, M. and Kokini, J.L. 2000. Viscoelastic flow modeling in the extrusion of a dough-like fluid. *Journal of Food Process Engineering*, 23:237-247.
- Dhanasekharan, K.M. and Kokini, J.L., 2003. Design and scaling of wheat dough extrusion by numerical simulation of flow and heat transfer. *Journal of Food Engineering*, 60:421-430.
- Fanning, L., 2008. *Characterization of Velocity Distribution in a Readco Continuous Mixer Using Laser Doppler Anemometry*. MS Thesis, Rutgers University, New Brunswick, NJ.
- Ghoreishy, M.H.R. and Nassehi, V. 1997. Modeling the transient flow of rubber compounds in the dispersive section of an internal mixer with slip-stick boundary conditions. *Adv. Poly. Tech.* 16(1):45-68.
- Grillet, A.M., Yang, B., Khomami, B., Shaqfeh, E.S.G. 1999. Modeling of viscoelastic lid driven cavity flow using finite element simulations. *J. Non-Newt. Fluid Mech.* 88(1-2):99-131.
- Ishikawa, T., Kihara, S.-I. and Funatsu, K. 2000. 3-D numerical simulations of non-isothermal flow in co-rotating twin screw extruders. *Polymer Engineering & Science*, 40(2): 357-364.
- Ishikawa, T., Kihara, S.-I. and Funatsu, K. 2001. 3-D non-isothermal flow field analysis and mixing performance evaluation of kneading blocks in a co-rotating twin screw extruders. *Polymer Engineering & Science*, 41(5): 840-849.
- Ishikawa, T., Amano, T., Kihara, S.-I. and Funatsu, K. 2002. Flow patterns and mixing mechanisms in the screw mixing element of a co-rotating twin screw extruder. *Polymer Engineering & Science*, 42(5): 925-939.
- Jaffer, S.A., Bravo, V.L., Wood, P.E. and Hrymak, A.N. 2000. Experimental Validation of Numerical Simulations of the Kneading Disc Section in a Twin Screw Extruder. *Polymer Engineering and Science*, 40(4): 892-901.
- Jongen, T., 2000. Characterization of batch mixers using numerical flow simulations. *AIChE Journal*, 46(11):2140-2150.

- Jongen, T.R.G., Brusckke, M.V., and Dekker, J.G. 2003. Analysis of dough kneaders using numerical flow simulations. *Cer. Chem.* 80(4):383-389.
- Kajiwara, T., Nagashima, Y., Nakano, Y. and Funatsu, K. 1996. Numerical study of twin-screw extruders by three-dimensional flow analysis—Development of analysis technique and evaluation of mixing performance for full flight screws. *Polymer Engineering & Science*, 36(16): 2142-2152.
- Kumar, S. and Homsy, G.M. 1996. Chaotic advection in creeping flow of viscoelastic fluids between slowly modulated eccentric cylinders. *Physics of Fluids*, 8(7):1774-1787.
- Lamberto, D.J., Alvarez, M.M. and Muzzio, F.J. 1999. Experimental and computational investigation of the laminar flow structure in a stirred tank. *Chem. Eng. Sci.* 54(7): 919-942.
- Lamberto, D.J., Alvarez, M.M. and Muzzio, F.J. 2001. Computational analysis of regular and chaotic mixing in a stirred tank reactor. *Chemical Engineering Science* 56: 4887-4899.
- Leong, C.W., and Ottino, J.M. 1990. Increase in regularity by polymer addition during chaotic mixing in two-dimensional flows. *Physical Review Letters* 64(8):874-877.
- Li, T. and Manas-Zloczower, I. 1994. Flow field analysis of an intermeshing counter-rotating twin screw extruder. *Polym. Eng. Sci.* 34: 551-558.
- Li, T. and Manas-Zloczower, I. 1995. Evaluation of distributive mixing efficiency in mixing equipment. *Chem. Eng. Commun.* 139: 223-231.
- Metzner, A. B. and Otto, R.E. 1957. Agitation of Non-Newtonian Fluids. *AIChE Journal*, 3(3):3-10.
- Nassehi, V. and Ghoreishy, M.H.R., 2001. Modeling of mixing in internal mixers with long blade tips. *Adv. Poly. Tech.* 20(2): 132-145.
- Owens, R. and Phillips, T. 2002. *Computational Rheology*, Imperial College Press.
- Ottino, J.M. 1989. *The Kinematics of Mixing: Stretching, Chaos and Transport*, Cambridge University Press.
- Polyflow. 2008. User Manual. <http://www.fluent.com>.
- Prakash, S. 1996. *Characterization of Shear Rate Distribution in a Model Mixer Using Laser Doppler Anemometry*. PhD. Thesis, Oct. 1996. Rutgers University, New Brunswick, NJ.
- Prakash, S., Karwe, M., and Kokini, J.L. 1999. Measurement of velocity distribution in the Brabender farinograph as a model mixer, using Laser-doppler anemometry. *J. Food Proc. Eng.* 22:435-454.

- Prakash, S. and Kokini, J.L. 1999. Determination of mixing efficiency in a model food mixer. *Advances in Polymer Technology*. 18(3):208-224.
- Prakash, S. and Kokini, J.L. 2000. Estimation and prediction of shear rate distribution as a model mixer. *J. Food Engr.* 44:135-148.
- Rauwendaal, C. 1987. Scale-up of single screw extruders. *Polym. Eng. Sci.*, 27, 1059-1068.
- Reddy, J.N. 1993. *An Introduction to the Finite Element Method*, 2nd ed. McGraw-Hill.
- Rodrigo, A.J.S., Mota, J.P.B., Lefevre, A. Leprévost, J.C. and Saadtjian, E. 2003. Chaotic advection in a three-dimensional Stokes flow. *AIChE Journal*, 49(11):2749-2758.
- Sunder, J. 1994. Scale-up of internal mixers. In: *Mixing and Compounding of Polymers: Theory and Practice*, Chpt. 8, pp. 225-249, Manas-Zloczower, I. and Tadmor, Z. (eds.), Carl Hanser Verlag, New York.
- Sujatha, K.S., Webster, M.F., Binding, D.M. and Couch, M.A. 2003. Modeling and experimental studies of rotating flows in part-filled vessels: Wetting and peeling. *Journal of Food Engineering*. 57(1):67-79.
- Tanguy, P.A., Thibault, F., Brito-de la Fuente, E., Espinosa-Solares, T. and Tecante, A. 1997. Mixing performance induced by coaxial flat blade-helical ribbon impellers rotating at different speeds. *Chem. Engr. Sci.* 52(11): 1733-1741.
- Teveroskiy, M., Manas-Zloczower, I., Elemans, P, Rekers, G. 2000. Numerical simulations and experiments in a double-Couette flow geometry. *International Polymer Processing*, 15(3):242-254.
- Wang, C. F., and Kokini, J.L. 1995a. Prediction of the nonlinear viscoelastic properties of gluten doughs. *Journal of Food Engineering*, 25: 297-309.
- Wang, C. F., and Kokini, J.L. 1995b. Simulation of the nonlinear rheological properties of gluten dough using the Wagner constitutive model. *Journal of Rheology*, 39(6): 1465-1482.
- Yang, H-H and Manas-Zloczower, I. 1992. Flow Field Analysis of the Kneading Disc Region in a Co-rotating Twin Screw Extruder. *Polymer Engineering and Science*, 32(19): 1411-1417.
- Yang, H.-H., Wong, T.H. and Manas-Zloczower, I. 1994. Flow field analysis of a banbury mixer. In: *Mixing and Compounding of Polymers: Theory and Practice*, Chpt. 7, pp. 187-223, Manas-Zloczower, I. and Tadmor, Z. (eds.), Carl Hanser Verlag, New York.
- Yoshinaga, M., Katsuki, S., Miyazaki, M., Liu, L., Kihara, S.-I., and Funatsu, K. 2000. Mixing Mechanism of three-tip kneading block in twin screw extruders. *Polymer Engineering & Science*, 40(1): 168-178.

Zalc, J.M., Alvarez, M.M., Muzzio, F.J., and Arik, B.E. 2001. Extensive validation of laminar flow in a stirred tank with three Rushton turbines. *AIChE Journal*, 47(10):2144-2154.

Zalc, J.M., Szalai, E.S., Alvarez, M.M., and Muzzio, F.J. 2002. Using CFD to understand chaotic mixing in laminar stirred tanks. *AIChE Journal*, 48(10):2124-2134.

APPENDIX A

Experimental LDA velocities at 10° intervals at points P1, P2 and P3 (Fanning, 2008).

Paddle position (deg)	P1 (-3.74, 1.75, z) cm		P2 (-0.34, 1.75, z) cm		P3 (-0.05, 1.59, z) cm	
	V _x (m/s)	V _z (m/s)	V _x (m/s)	V _z (m/s)	V _x (m/s)	V _z (m/s)
10	-0.11589	0.022833			-0.11174	-0.018478
20	-0.13986	0.014135	-0.10107	-0.02617	-0.07735	-0.055008
30	-0.16759	0.008533			-0.056	0.01002
40			-0.1238	0.059315	-0.05447	0.028449
50			-0.13961	0.06532	-0.05461	0.02547
60	-0.22907	0.02073	-0.15477	0.049283	-0.05699	0.030422
70	-0.17703	0.019974	-0.18409	0.07098	-0.05448	0.034975
80	-0.13747	0.027592	-0.25308	0.051984	-0.07208	0.03456
90	-0.11738	0.040535	-0.32219	0.069959	-0.0669	0.025836
100	-0.0869	0.04551	-0.4027	0.026028	-0.12145	0.019983
110	-0.09576	0.028941	-0.48037	0.00212	-0.15353	-0.002663
120	-0.11227	0.032367	-0.27107	-0.014698	-0.17448	-0.018884
130	-0.07933	0.034375	-0.0472	0.017685		
140	-0.06944	0.03419			-0.16939	0.006059
150	-0.07596	0.022388			-0.17174	-0.01293
160	-0.0813	0.021066			-0.21276	0.00729
170	-0.09366	0.013998			-0.14505	0.01544
180	-0.0902	0.02429			-0.09349	-0.020842
190	-0.11053	0.018157	-0.09514	-0.20711	-0.08327	0.002747
200	-0.13899	0.008363	-0.10107	0.02759	-0.06882	0.002236
210	-0.16768	0.007933	-0.10799	0.044095	-0.05276	0.01822
220			-0.11392	0.049713	-0.04473	0.020608
230	-0.09514	0.00729	-0.13368	0.061	-0.05242	0.032986
240	-0.19546	0.019203	-0.15279	0.077267	-0.04044	0.027197
250	-0.15889	0.024388	-0.16235	0.07428	-0.04967	0.015638
260	-0.1182	0.023187	-0.24735	0.061506	-0.05988	0.026994
270	-0.1092	0.052898	-0.32049	0.079237	-0.07861	0.020754
280	-0.09942	0.06008	-0.41666	0.072106	-0.10423	0.031316
290	-0.08229	0.01438			-0.12659	0.014087
300	-0.09076	0.028731	-0.1517	0.003311	-0.16916	0.030056
310	-0.06944	0.018787	-0.0855	0.00401	-0.19398	-0.01293
320	-0.07587	0.017415			-0.13508	-0.001477
330	-0.07992	0.024916			-0.1667	-0.004464
340	-0.08254	0.019208				
350	-0.11194	0.02798			-0.22116	0.032678
360	-0.08888	0.02319			-0.11392	-0.07358

APPENDIX B

Tabulated results of velocity, pressure, stress and shear rates from viscoelastic simulation

Node #	X co-ord	Y co-ord	Vx (cm/s)	Vy (cm/s)	P (dynes/cm ²)	Txx (dyes/cm ²)	Tyy (dyes/cm ²)	Txy (dyes/cm ²)	λ
1	-2.14E+00	2.49E+00	-6.85E-04	-5.28E-05	2.11E+05	-1.47E+04	1.17E+04	6.94E+03	5.02E-01
2	-3.26E+00	0.00E+00	0.00E+00	-3.63E-04	2.17E+05	8.75E-05	5.27E-04	9.75E+01	8.51E-04
3	-2.36E+00	2.27E+00	-6.25E-04	-1.15E-04	2.20E+05	-5.69E+02	7.94E+02	-1.51E+02	3.82E-03
4	-2.57E+00	2.03E+00	-5.60E-04	-1.71E-04	2.18E+05	-1.98E+01	-2.29E+02	1.49E+02	1.64E-03
5	-2.75E+00	1.78E+00	-4.89E-04	-2.20E-04	2.18E+05	1.06E+02	-7.32E+01	2.53E+01	8.26E-04
6	-2.90E+00	1.51E+00	-4.15E-04	-2.63E-04	2.18E+05	9.26E+01	-9.99E+01	7.35E+01	1.01E-03
7	-3.03E+00	1.22E+00	-3.36E-04	-2.98E-04	2.17E+05	7.67E+01	-7.35E+01	7.74E+01	9.28E-04
8	-3.13E+00	9.26E-01	-2.55E-04	-3.26E-04	2.17E+05	5.66E+01	-5.61E+01	8.79E+01	9.02E-04
9	-3.20E+00	6.22E-01	-1.71E-04	-3.46E-04	2.17E+05	3.78E+01	-3.70E+01	9.31E+01	8.72E-04
10	-3.25E+00	3.12E-01	-8.59E-05	-3.59E-04	2.17E+05	1.88E+01	-1.85E+01	9.64E+01	8.56E-04
11	-2.14E+00	-2.49E+00	6.85E-04	-5.28E-05	2.22E+05	1.48E+04	-1.17E+04	7.03E+03	5.05E-01
12	-2.36E+00	-2.27E+00	6.25E-04	-1.15E-04	2.14E+05	5.82E+02	-7.87E+02	-1.41E+02	3.79E-03
13	-2.57E+00	-2.03E+00	5.60E-04	-1.71E-04	2.16E+05	1.92E+01	2.28E+02	1.48E+02	1.64E-03
14	-2.75E+00	-1.78E+00	4.89E-04	-2.20E-04	2.16E+05	-1.05E+02	7.35E+01	2.56E+01	8.27E-04
15	-2.90E+00	-1.51E+00	4.15E-04	-2.63E-04	2.16E+05	-9.27E+01	9.99E+01	7.34E+01	1.01E-03
16	-3.03E+00	-1.22E+00	3.36E-04	-2.98E-04	2.16E+05	-7.67E+01	7.35E+01	7.74E+01	9.28E-04
17	-3.13E+00	-9.26E-01	2.55E-04	-3.26E-04	2.17E+05	-5.67E+01	5.61E+01	8.79E+01	9.02E-04
18	-3.20E+00	-6.22E-01	1.71E-04	-3.46E-04	2.17E+05	-3.78E+01	3.70E+01	9.31E+01	8.72E-04
19	-3.25E+00	-3.12E-01	8.59E-05	-3.59E-04	2.17E+05	-1.88E+01	1.85E+01	9.64E+01	8.56E-04
20	4.43E+00	1.92E-01	-5.28E-05	6.85E-04	2.69E+04	-1.02E+04	6.22E+03	4.58E+02	2.15E-01
21	1.95E+00	1.32E+00	-3.63E-04	0.00E+00	-5.96E+00	6.10E-01	-5.81E-01	-1.61E+02	1.45E-03
22	4.22E+00	4.17E-01	-1.15E-04	6.25E-04	9.44E+02	-2.04E+03	9.42E+02	-6.09E+02	1.56E-02
23	3.98E+00	6.20E-01	-1.71E-04	5.60E-04	2.69E+03	-2.70E+02	5.89E+02	4.89E+01	3.81E-03
24	3.72E+00	8.00E-01	-2.20E-04	4.89E-04	1.11E+03	-3.60E+02	3.15E+02	-1.79E+02	3.30E-03
25	3.45E+00	9.56E-01	-2.63E-04	4.15E-04	9.39E+02	-1.95E+02	2.16E+02	-1.36E+02	2.22E-03
26	3.17E+00	1.08E+00	-2.98E-04	3.36E-04	6.27E+02	-1.47E+02	1.48E+02	-1.55E+02	1.91E-03
27	2.87E+00	1.19E+00	-3.26E-04	2.55E-04	4.42E+02	-9.92E+01	1.03E+02	-1.55E+02	1.67E-03
28	2.57E+00	1.26E+00	-3.46E-04	1.71E-04	2.76E+02	-6.30E+01	6.46E+01	-1.58E+02	1.54E-03
29	2.26E+00	1.30E+00	-3.59E-04	8.59E-05	1.32E+02	-3.06E+01	3.14E+01	-1.60E+02	1.47E-03
30	1.95E+00	-1.32E+00	3.63E-04	0.00E+00	4.33E+05	-6.07E-01	5.81E-01	-1.61E+02	1.45E-03
31	4.43E+00	-1.92E-01	5.28E-05	6.85E-04	4.06E+05	1.02E+04	-6.18E+03	4.42E+02	2.14E-01
32	2.26E+00	-1.30E+00	3.59E-04	8.59E-05	4.33E+05	3.06E+01	-3.14E+01	-1.60E+02	1.47E-03
33	2.57E+00	-1.26E+00	3.46E-04	1.71E-04	4.33E+05	6.30E+01	-6.46E+01	-1.58E+02	1.54E-03
34	2.87E+00	-1.19E+00	3.26E-04	2.55E-04	4.33E+05	9.92E+01	-1.03E+02	-1.55E+02	1.67E-03
35	3.17E+00	-1.08E+00	2.98E-04	3.36E-04	4.33E+05	1.47E+02	-1.48E+02	-1.55E+02	1.91E-03
36	3.45E+00	-9.56E-01	2.63E-04	4.15E-04	4.32E+05	1.95E+02	-2.16E+02	-1.36E+02	2.22E-03
37	3.72E+00	-8.00E-01	2.20E-04	4.89E-04	4.32E+05	3.60E+02	-3.15E+02	-1.79E+02	3.30E-03
38	3.98E+00	-6.20E-01	1.71E-04	5.60E-04	4.31E+05	2.69E+02	-5.89E+02	4.89E+01	3.81E-03
39	4.22E+00	-4.17E-01	1.15E-04	6.25E-04	4.32E+05	2.04E+03	-9.39E+02	-6.10E+02	1.56E-02
40	-1.75E+00	2.49E+00	-6.85E-04	5.28E-05	1.47E+03	3.32E+03	-5.84E+03	9.59E+02	1.12E-01
41	-7.76E-01	9.82E-01	-2.70E-04	3.22E-04	-1.17E+03	-4.03E+01	5.15E+01	7.02E+01	6.83E-04
42	-1.54E+00	2.28E+00	-6.27E-04	1.13E-04	-3.41E+03	9.21E+01	-2.97E+02	-9.75E+01	4.02E-03

43	-1.34E+00	2.05E+00	-5.64E-04	1.67E-04	-1.89E+03	-6.96E+01	1.62E+02	7.41E+01	1.00E-03
44	-1.16E+00	1.80E+00	-4.96E-04	2.16E-04	-1.79E+03	-1.15E+02	9.64E+01	3.75E+01	9.67E-04
45	-1.01E+00	1.54E+00	-4.24E-04	2.58E-04	-1.49E+03	-1.04E+02	1.04E+02	7.18E+01	1.08E-03
46	-8.79E-01	1.27E+00	-3.48E-04	2.93E-04	-1.30E+03	-8.18E+01	7.51E+01	7.33E+01	9.26E-04
47	-7.76E-01	-9.82E-01	2.70E-04	3.22E-04	4.34E+05	4.03E+01	-5.15E+01	7.02E+01	6.83E-04
48	-1.75E+00	-2.49E+00	6.85E-04	5.28E-05	4.32E+05	-3.31E+03	5.84E+03	9.59E+02	1.12E-01
49	-8.79E-01	-1.27E+00	3.48E-04	2.93E-04	4.35E+05	8.18E+01	-7.51E+01	7.33E+01	9.26E-04
50	-1.01E+00	-1.54E+00	4.24E-04	2.58E-04	4.35E+05	1.04E+02	-1.04E+02	7.18E+01	1.08E-03
51	-1.16E+00	-1.80E+00	4.96E-04	2.16E-04	4.35E+05	1.15E+02	-9.64E+01	3.75E+01	9.67E-04
52	-1.34E+00	-2.05E+00	5.64E-04	1.67E-04	4.35E+05	6.97E+01	-1.62E+02	7.41E+01	1.00E-03
53	-1.54E+00	-2.28E+00	6.27E-04	1.13E-04	4.37E+05	-9.15E+01	2.97E+02	-9.75E+01	4.02E-03
54	6.76E-01	1.07E+00	-2.93E-04	-3.49E-04	-7.39E+02	1.55E+02	-1.66E+02	-1.54E+02	2.05E-03
55	9.83E-01	1.18E+00	-3.23E-04	-2.65E-04	-4.82E+02	1.12E+02	-1.18E+02	-1.65E+02	1.83E-03
56	1.30E+00	1.25E+00	-3.45E-04	-1.78E-04	-3.04E+02	6.79E+01	-7.31E+01	-1.63E+02	1.60E-03
57	1.62E+00	1.30E+00	-3.58E-04	-8.94E-05	-1.50E+02	3.24E+01	-3.47E+01	-1.62E+02	1.49E-03
58	6.76E-01	-1.07E+00	2.93E-04	-3.49E-04	4.34E+05	-1.55E+02	1.66E+02	-1.54E+02	2.05E-03
59	9.83E-01	-1.18E+00	3.23E-04	-2.65E-04	4.34E+05	-1.12E+02	1.18E+02	-1.65E+02	1.83E-03
60	1.30E+00	-1.25E+00	3.45E-04	-1.78E-04	4.34E+05	-6.79E+01	7.31E+01	-1.63E+02	1.60E-03
61	1.62E+00	-1.30E+00	3.58E-04	-8.94E-05	4.33E+05	-3.24E+01	3.47E+01	-1.62E+02	1.49E-03
62	-1.95E+00	2.49E+00	-6.85E-04	0.00E+00	1.64E+05	-1.45E+01	6.05E+02	9.84E+03	1.13E-01
63	-2.04E+00	2.49E+00	-6.85E-04	-2.64E-05	1.74E+05	8.29E+02	-5.73E+04	-3.63E+04	7.23E-02
64	-1.85E+00	2.49E+00	-6.85E-04	2.64E-05	1.02E+05	-2.00E+01	-1.22E+03	1.81E+04	1.59E-01
65	-1.95E+00	-2.49E+00	6.85E-04	0.00E+00	2.69E+05	2.60E+01	-5.86E+02	9.81E+03	1.13E-01
66	-2.04E+00	-2.49E+00	6.85E-04	-2.64E-05	2.59E+05	-8.55E+02	5.77E+04	-3.69E+04	7.23E-02
67	-1.85E+00	-2.49E+00	6.85E-04	2.64E-05	3.32E+05	5.66E+01	1.22E+03	1.81E+04	1.59E-01
68	4.43E+00	0.00E+00	0.00E+00	6.85E-04	2.17E+05	-3.26E+00	1.16E+01	1.41E+04	1.53E-01
69	4.43E+00	9.59E-02	-2.64E-05	6.85E-04	1.41E+05	4.72E+04	-3.89E+02	-5.49E+03	1.50E-01
70	4.43E+00	-9.59E-02	2.64E-05	6.85E-04	2.92E+05	-4.70E+04	3.37E+02	-5.36E+03	1.50E-01
71	-4.49E+00	0.00E+00	0.00E+00	0.00E+00	2.17E+05	5.34E-06	9.98E-04	-1.29E+02	1.46E-03
72	-1.95E+00	2.54E+00	0.00E+00	0.00E+00	1.65E+05	2.37E+02	3.34E+03	-7.49E+03	9.02E-02
73	-4.46E+00	3.61E-01	0.00E+00	0.00E+00	2.17E+05	-3.69E+01	3.68E+01	-1.25E+02	1.47E-03
74	-4.38E+00	7.16E-01	0.00E+00	0.00E+00	2.17E+05	-7.27E+01	7.25E+01	-1.13E+02	1.51E-03
75	-4.26E+00	1.06E+00	0.00E+00	0.00E+00	2.17E+05	-1.07E+02	1.06E+02	-9.20E+01	1.59E-03
76	-4.08E+00	1.37E+00	0.00E+00	0.00E+00	2.17E+05	-1.37E+02	1.37E+02	-6.25E+01	1.72E-03
77	-3.87E+00	1.66E+00	0.00E+00	0.00E+00	2.17E+05	-1.66E+02	1.63E+02	-2.24E+01	1.90E-03
78	-3.61E+00	1.92E+00	0.00E+00	0.00E+00	2.17E+05	-1.76E+02	1.85E+02	2.13E+01	2.15E-03
79	-3.32E+00	2.14E+00	0.00E+00	0.00E+00	2.18E+05	-2.10E+02	1.73E+02	1.07E+02	2.62E-03
80	-3.00E+00	2.31E+00	0.00E+00	0.00E+00	2.18E+05	-1.27E+02	2.45E+02	8.11E+01	3.28E-03
81	-2.66E+00	2.44E+00	0.00E+00	0.00E+00	2.17E+05	-2.89E+01	-1.98E+03	3.44E+02	7.38E-03
82	-2.31E+00	2.51E+00	0.00E+00	0.00E+00	2.25E+05	6.39E+02	1.75E+03	-2.38E+03	3.98E-02
83	-1.95E+00	-2.54E+00	0.00E+00	0.00E+00	2.68E+05	-2.30E+02	-3.33E+03	-7.46E+03	9.01E-02
84	-4.46E+00	-3.61E-01	0.00E+00	0.00E+00	2.17E+05	3.69E+01	-3.68E+01	-1.25E+02	1.47E-03
85	-4.38E+00	-7.16E-01	0.00E+00	0.00E+00	2.17E+05	7.27E+01	-7.25E+01	-1.13E+02	1.51E-03
86	-4.26E+00	-1.06E+00	0.00E+00	0.00E+00	2.17E+05	1.07E+02	-1.06E+02	-9.20E+01	1.59E-03
87	-4.08E+00	-1.37E+00	0.00E+00	0.00E+00	2.17E+05	1.37E+02	-1.37E+02	-6.25E+01	1.72E-03
88	-3.87E+00	-1.66E+00	0.00E+00	0.00E+00	2.17E+05	1.66E+02	-1.63E+02	-2.24E+01	1.90E-03
89	-3.61E+00	-1.92E+00	0.00E+00	0.00E+00	2.16E+05	1.76E+02	-1.85E+02	2.13E+01	2.15E-03
90	-3.32E+00	-2.14E+00	0.00E+00	0.00E+00	2.16E+05	2.10E+02	-1.73E+02	1.07E+02	2.62E-03

91	-3.00E+00	-2.31E+00	0.00E+00	0.00E+00	2.16E+05	1.27E+02	-2.44E+02	8.12E+01	3.28E-03
92	-2.66E+00	-2.44E+00	0.00E+00	0.00E+00	2.17E+05	2.60E+01	1.97E+03	3.38E+02	7.38E-03
93	-2.31E+00	-2.51E+00	0.00E+00	0.00E+00	2.09E+05	-6.38E+02	-1.76E+03	-2.38E+03	3.98E-02
94	4.49E+00	0.00E+00	0.00E+00	0.00E+00	2.17E+05	3.50E+00	1.67E+01	-1.68E+04	1.84E-01
95	1.95E+00	-2.54E+00	0.00E+00	0.00E+00	4.33E+05	1.28E+01	-5.74E+00	1.70E+02	1.95E-03
96	4.46E+00	-3.61E-01	0.00E+00	0.00E+00	4.44E+05	1.28E+03	1.93E+03	-6.91E+03	1.07E-01
97	4.38E+00	-7.16E-01	0.00E+00	0.00E+00	4.28E+05	-4.44E+03	7.65E+01	5.28E+02	1.47E-02
98	4.26E+00	-1.06E+00	0.00E+00	0.00E+00	4.32E+05	-1.75E+02	4.34E+02	-4.32E+02	6.48E-03
99	4.08E+00	-1.37E+00	0.00E+00	0.00E+00	4.32E+05	-3.67E+02	2.63E+02	-8.69E+01	4.20E-03
100	3.87E+00	-1.66E+00	0.00E+00	0.00E+00	4.33E+05	-2.74E+02	2.90E+02	-4.80E+01	3.31E-03
101	3.61E+00	-1.92E+00	0.00E+00	0.00E+00	4.33E+05	-2.36E+02	2.32E+02	3.59E+01	2.74E-03
102	3.32E+00	-2.14E+00	0.00E+00	0.00E+00	4.33E+05	-1.92E+02	1.94E+02	8.71E+01	2.40E-03
103	3.00E+00	-2.31E+00	0.00E+00	0.00E+00	4.33E+05	-1.46E+02	1.46E+02	1.26E+02	2.18E-03
104	2.66E+00	-2.44E+00	0.00E+00	0.00E+00	4.33E+05	-9.83E+01	9.86E+01	1.53E+02	2.04E-03
105	2.31E+00	-2.51E+00	0.00E+00	0.00E+00	4.33E+05	-4.91E+01	4.94E+01	1.68E+02	1.96E-03
106	1.95E+00	2.54E+00	0.00E+00	0.00E+00	0.00E+00	-1.28E+01	5.74E+00	1.70E+02	1.95E-03
107	2.31E+00	2.51E+00	0.00E+00	0.00E+00	9.01E+01	4.91E+01	-4.94E+01	1.68E+02	1.96E-03
108	2.66E+00	2.44E+00	0.00E+00	0.00E+00	1.93E+02	9.83E+01	-9.86E+01	1.53E+02	2.04E-03
109	3.00E+00	2.31E+00	0.00E+00	0.00E+00	3.03E+02	1.46E+02	-1.46E+02	1.26E+02	2.18E-03
110	3.32E+00	2.14E+00	0.00E+00	0.00E+00	4.24E+02	1.92E+02	-1.94E+02	8.71E+01	2.40E-03
111	3.61E+00	1.92E+00	0.00E+00	0.00E+00	5.88E+02	2.36E+02	-2.32E+02	3.59E+01	2.74E-03
112	3.87E+00	1.66E+00	0.00E+00	0.00E+00	7.23E+02	2.74E+02	-2.90E+02	-4.80E+01	3.31E-03
113	4.08E+00	1.37E+00	0.00E+00	0.00E+00	1.20E+03	3.67E+02	-2.63E+02	-8.69E+01	4.20E-03
114	4.26E+00	1.06E+00	0.00E+00	0.00E+00	8.45E+02	1.75E+02	-4.34E+02	-4.32E+02	6.48E-03
115	4.38E+00	7.16E-01	0.00E+00	0.00E+00	5.22E+03	4.44E+03	-7.67E+01	5.28E+02	1.47E-02
116	4.46E+00	3.61E-01	0.00E+00	0.00E+00	-1.12E+04	-1.28E+03	-1.93E+03	-6.91E+03	1.07E-01
117	0.00E+00	1.63E+00	0.00E+00	0.00E+00	-1.04E+03	-1.25E+02	1.17E+02	2.37E+02	2.34E-03
118	-1.67E+00	2.52E+00	0.00E+00	0.00E+00	-9.00E+03	-6.57E+02	-1.94E+03	-3.21E+03	5.82E-02
119	-1.40E+00	2.48E+00	0.00E+00	0.00E+00	-1.50E+03	2.64E+02	1.54E+03	7.54E+02	3.34E-03
120	-1.13E+00	2.41E+00	0.00E+00	0.00E+00	-2.22E+03	1.64E+02	-1.99E+02	2.07E+02	3.80E-03
121	-8.72E-01	2.30E+00	0.00E+00	0.00E+00	-1.73E+03	2.15E+02	-1.70E+02	1.90E+02	3.04E-03
122	-6.28E-01	2.17E+00	0.00E+00	0.00E+00	-1.61E+03	1.99E+02	-2.10E+02	1.00E+02	2.58E-03
123	-3.99E-01	2.02E+00	0.00E+00	0.00E+00	-1.41E+03	1.93E+02	-1.70E+02	5.93E+01	2.16E-03
124	-1.89E-01	1.83E+00	0.00E+00	0.00E+00	-1.55E+03	1.75E+02	-2.19E+02	-1.08E+01	2.05E-03
125	0.00E+00	-1.63E+00	0.00E+00	0.00E+00	4.34E+05	1.25E+02	-1.17E+02	2.37E+02	2.34E-03
126	-1.67E+00	-2.52E+00	0.00E+00	0.00E+00	4.42E+05	6.57E+02	1.94E+03	-3.20E+03	5.82E-02
127	-1.40E+00	-2.48E+00	0.00E+00	0.00E+00	4.35E+05	-2.65E+02	-1.54E+03	7.55E+02	3.34E-03
128	-1.13E+00	-2.41E+00	0.00E+00	0.00E+00	4.36E+05	-1.64E+02	1.98E+02	2.07E+02	3.80E-03
129	-8.72E-01	-2.30E+00	0.00E+00	0.00E+00	4.35E+05	-2.15E+02	1.70E+02	1.90E+02	3.04E-03
130	-6.28E-01	-2.17E+00	0.00E+00	0.00E+00	4.35E+05	-1.99E+02	2.10E+02	1.00E+02	2.58E-03
131	-3.99E-01	-2.02E+00	0.00E+00	0.00E+00	4.35E+05	-1.93E+02	1.70E+02	5.93E+01	2.16E-03
132	-1.89E-01	-1.83E+00	0.00E+00	0.00E+00	4.35E+05	-1.75E+02	2.19E+02	-1.08E+01	2.05E-03
133	1.40E+00	2.48E+00	0.00E+00	0.00E+00	-1.53E+02	-7.35E+01	7.61E+01	1.57E+02	2.03E-03
134	8.72E-01	2.30E+00	0.00E+00	0.00E+00	-3.49E+02	-1.43E+02	1.32E+02	1.23E+02	2.17E-03
135	3.99E-01	2.02E+00	0.00E+00	0.00E+00	-4.31E+02	-2.12E+02	2.46E+02	4.63E+01	2.58E-03
136	1.40E+00	-2.48E+00	0.00E+00	0.00E+00	4.33E+05	7.35E+01	-7.61E+01	1.57E+02	2.03E-03
137	8.72E-01	-2.30E+00	0.00E+00	0.00E+00	4.34E+05	1.43E+02	-1.32E+02	1.23E+02	2.17E-03
138	3.99E-01	-2.02E+00	0.00E+00	0.00E+00	4.34E+05	2.12E+02	-2.46E+02	4.63E+01	2.58E-03

139	-3.57E+00	0.00E+00	1.46E-12	-6.25E-04	2.17E+05	-1.08E-04	-1.10E-04	2.59E+00	1.89E-04
140	-3.87E+00	0.00E+00	1.39E-11	-6.14E-04	2.17E+05	4.23E-05	2.39E-04	-6.40E+01	6.89E-04
141	-4.18E+00	0.00E+00	7.07E-12	-3.87E-04	2.17E+05	3.13E-06	7.12E-04	-1.10E+02	1.19E-03
142	-1.95E+00	2.50E+00	6.26E-04	5.22E-05	1.60E+05	2.37E+03	-3.01E+03	6.75E+03	7.16E-02
143	-1.95E+00	2.51E+00	9.85E-04	-2.78E-04	1.63E+05	2.01E+03	-1.72E+03	-2.42E+02	2.55E-02
144	-1.95E+00	2.53E+00	7.66E-04	-2.26E-04	1.65E+05	1.22E+03	2.77E+03	-3.88E+03	4.28E-02
145	-5.82E-01	1.14E+00	-3.61E-04	4.52E-04	-1.21E+03	-6.61E+00	3.42E+00	-5.33E+01	4.80E-04
146	-3.88E-01	1.31E+00	-4.43E-04	3.68E-04	-1.22E+03	-2.23E+01	2.63E+01	-1.02E+02	1.02E-03
147	-1.94E-01	1.47E+00	-4.68E-04	1.93E-04	-1.30E+03	-1.29E+02	1.75E+01	-4.94E+01	7.00E-04
148	-1.95E+00	-2.53E+00	-7.63E-04	-2.26E-04	2.68E+05	-1.22E+03	-2.78E+03	-3.86E+03	4.28E-02
149	-1.95E+00	-2.51E+00	-9.81E-04	-2.78E-04	2.70E+05	-2.02E+03	1.72E+03	-2.55E+02	2.55E-02
150	-1.95E+00	-2.50E+00	-6.26E-04	5.20E-05	2.74E+05	-2.37E+03	3.01E+03	6.76E+03	7.16E-02
151	-1.94E-01	-1.47E+00	4.68E-04	1.93E-04	4.35E+05	1.29E+02	-1.75E+01	-4.94E+01	7.00E-04
152	-3.88E-01	-1.31E+00	4.43E-04	3.68E-04	4.35E+05	2.22E+01	-2.63E+01	-1.02E+02	1.02E-03
153	-5.82E-01	-1.14E+00	3.61E-04	4.52E-04	4.35E+05	6.61E+00	-3.42E+00	-5.33E+01	4.80E-04
154	1.69E-01	1.49E+00	-5.53E-04	-3.10E-04	-8.30E+02	-4.68E+01	1.08E+02	-9.43E+00	1.16E-03
155	3.38E-01	1.35E+00	-6.87E-04	-4.98E-04	-8.60E+02	-3.97E+01	3.64E+01	-3.28E+01	6.54E-04
156	5.07E-01	1.21E+00	-6.22E-04	-5.10E-04	-8.03E+02	4.05E+01	-3.82E+01	-6.33E+01	9.19E-04
157	5.07E-01	-1.21E+00	6.22E-04	-5.10E-04	4.34E+05	-4.05E+01	3.82E+01	-6.33E+01	9.19E-04
158	3.38E-01	-1.35E+00	6.87E-04	-4.98E-04	4.34E+05	3.97E+01	-3.64E+01	-3.28E+01	6.54E-04
159	1.69E-01	-1.49E+00	5.53E-04	-3.10E-04	4.34E+05	4.68E+01	-1.08E+02	-9.43E+00	1.16E-03
160	1.95E+00	1.62E+00	-7.78E-04	-1.20E-06	-6.11E+00	8.36E-01	-9.26E-01	-2.32E+01	3.14E-04
161	1.95E+00	1.93E+00	-8.00E-04	-2.78E-06	-5.76E+00	7.39E-01	-9.68E-01	7.63E+01	8.08E-04
162	1.95E+00	2.23E+00	-5.12E-04	-3.54E-06	-4.02E+00	-4.07E-01	-6.95E-01	1.46E+02	1.57E-03
163	4.45E+00	0.00E+00	-1.80E-07	2.43E-03	2.17E+05	5.23E+00	2.14E+00	8.57E+03	7.52E-02
164	4.46E+00	0.00E+00	1.28E-07	2.79E-03	2.17E+05	-1.90E+00	-5.08E-01	-3.28E+03	3.98E-02
165	4.47E+00	0.00E+00	-6.56E-08	1.89E-03	2.17E+05	-3.57E+00	4.91E+00	-1.06E+04	1.02E-01
166	1.95E+00	-1.62E+00	7.78E-04	-1.20E-06	4.33E+05	-8.36E-01	9.26E-01	-2.32E+01	3.14E-04
167	1.95E+00	-1.93E+00	8.00E-04	-2.78E-06	4.33E+05	-7.39E-01	9.68E-01	7.63E+01	8.08E-04
168	1.95E+00	-2.23E+00	5.12E-04	-3.54E-06	4.33E+05	4.09E-01	6.95E-01	1.46E+02	1.57E-03
169	-5.44E-01	1.92E-01	-5.28E-05	-6.85E-04	1.14E+04	-2.14E+04	2.21E+04	-9.01E+03	2.69E-01
170	-3.34E-01	4.10E-01	-1.13E-04	-6.27E-04	-2.72E+03	-2.63E+03	2.75E+03	6.47E+01	1.90E-02
171	-1.05E-01	6.08E-01	-1.67E-04	-5.64E-04	-1.01E+03	-2.17E+02	5.00E+02	-5.52E+01	3.07E-03
172	1.41E-01	7.84E-01	-2.16E-04	-4.96E-04	-1.42E+03	-2.40E+01	1.81E+01	1.12E+01	9.04E-04
173	4.02E-01	9.37E-01	-2.58E-04	-4.25E-04	-1.02E+03	1.57E+02	-1.48E+02	-1.10E+02	1.72E-03
174	-5.44E-01	-1.92E-01	5.28E-05	-6.85E-04	4.22E+05	2.15E+04	-2.20E+04	-9.04E+03	2.69E-01
175	4.02E-01	-9.37E-01	2.58E-04	-4.25E-04	4.34E+05	-1.57E+02	1.48E+02	-1.10E+02	1.72E-03
176	1.41E-01	-7.84E-01	2.16E-04	-4.96E-04	4.35E+05	2.40E+01	-1.81E+01	1.11E+01	9.04E-04
177	-1.05E-01	-6.08E-01	1.67E-04	-5.64E-04	4.34E+05	2.17E+02	-5.00E+02	-5.51E+01	3.08E-03
178	-3.34E-01	-4.10E-01	1.13E-04	-6.27E-04	4.36E+05	2.63E+03	-2.74E+03	6.41E+01	1.90E-02
179	-5.44E-01	-9.59E-02	2.64E-05	-6.85E-04	3.04E+05	-7.33E+03	-1.44E+01	-3.74E+04	3.80E-01
180	-5.44E-01	1.11E-16	-3.05E-20	-6.85E-04	2.17E+05	-3.53E+00	8.33E+01	-3.76E+04	4.07E-01
181	-5.44E-01	9.59E-02	-2.64E-05	-6.85E-04	1.30E+05	7.35E+03	1.79E+02	-3.74E+04	3.80E-01
182	-7.37E-01	8.45E-01	-2.32E-04	3.33E-04	-1.14E+03	-2.78E+01	5.96E+01	1.12E+02	1.11E-03
183	-7.03E-01	7.06E-01	-1.94E-04	3.42E-04	-1.16E+03	-6.11E+01	1.28E+02	2.99E+02	3.18E-03
184	-6.76E-01	5.67E-01	-1.56E-04	3.49E-04	-6.22E+02	-1.75E+02	2.98E+02	8.55E+02	8.71E-03
185	-6.55E-01	4.26E-01	-1.17E-04	3.55E-04	4.47E+02	-3.44E+02	4.82E+02	1.86E+03	2.16E-02
186	-6.40E-01	2.84E-01	-7.82E-05	3.59E-04	2.29E+03	-3.71E+03	2.08E+03	1.18E+04	1.14E-01

187	-6.30E-01	1.42E-01	-3.91E-05	3.62E-04	7.12E+04	-1.68E+03	2.63E+03	3.00E+04	3.06E-01
188	-6.27E-01	4.44E-16	-1.22E-19	3.63E-04	2.17E+05	-8.09E-02	7.18E+01	3.49E+04	3.84E-01
189	-6.30E-01	-1.42E-01	3.91E-05	3.62E-04	3.62E+05	1.68E+03	-2.52E+03	3.00E+04	3.06E-01
190	-6.40E-01	-2.84E-01	7.82E-05	3.59E-04	4.31E+05	3.71E+03	-2.06E+03	1.18E+04	1.14E-01
191	-6.55E-01	-4.26E-01	1.17E-04	3.55E-04	4.33E+05	3.44E+02	-4.81E+02	1.86E+03	2.16E-02
192	-6.76E-01	-5.67E-01	1.56E-04	3.49E-04	4.34E+05	1.75E+02	-2.98E+02	8.55E+02	8.71E-03
193	-7.03E-01	-7.06E-01	1.94E-04	3.42E-04	4.34E+05	6.11E+01	-1.28E+02	2.99E+02	3.18E-03
194	-7.37E-01	-8.45E-01	2.32E-04	3.33E-04	4.34E+05	2.78E+01	-5.96E+01	1.12E+02	1.11E-03
195	-2.24E+00	2.51E+00	4.91E-04	1.68E-04	2.23E+05	1.00E+03	-1.70E+03	-2.61E+03	3.23E-02
196	-2.53E+00	2.45E+00	-9.12E-05	-1.87E-06	2.18E+05	-3.66E+02	-3.17E+02	3.24E+02	3.07E-03
197	-2.84E+00	2.30E+00	-1.97E-04	-8.81E-05	2.18E+05	-2.53E+02	3.99E+02	2.28E+02	3.59E-03
198	-3.13E+00	2.11E+00	-2.58E-04	-1.64E-04	2.18E+05	-1.83E+02	1.64E+02	7.43E+01	2.13E-03
199	-3.39E+00	1.88E+00	-2.53E-04	-2.05E-04	2.18E+05	-1.77E+02	1.78E+02	2.24E+01	1.92E-03
200	-3.62E+00	1.62E+00	-2.37E-04	-2.63E-04	2.17E+05	-1.43E+02	1.43E+02	-2.63E+01	1.60E-03
201	-3.82E+00	1.34E+00	-2.04E-04	-3.06E-04	2.17E+05	-1.19E+02	1.18E+02	-5.89E+01	1.44E-03
202	-3.98E+00	1.02E+00	-1.61E-04	-3.41E-04	2.17E+05	-8.94E+01	8.93E+01	-8.17E+01	1.32E-03
203	-4.09E+00	6.92E-01	-1.11E-04	-3.67E-04	2.17E+05	-6.02E+01	6.00E+01	-9.74E+01	1.25E-03
204	-4.16E+00	3.49E-01	-5.67E-05	-3.82E-04	2.17E+05	-3.02E+01	3.01E+01	-1.07E+02	1.21E-03
205	-2.17E+00	2.50E+00	9.62E-04	7.55E-04	2.19E+05	2.06E+02	-4.14E+03	-3.40E+03	2.07E-02
206	-2.40E+00	2.46E+00	-1.39E-04	-4.60E-04	2.19E+05	3.92E+02	-1.09E+02	2.69E+01	6.38E-03
207	-2.68E+00	2.29E+00	-4.62E-04	-1.60E-05	2.18E+05	-3.10E+02	2.79E+02	3.07E+02	3.56E-03
208	-2.94E+00	2.09E+00	-4.37E-04	-2.80E-04	2.18E+05	-1.12E+02	9.87E+01	5.12E+01	1.57E-03
209	-3.18E+00	1.85E+00	-4.55E-04	-3.48E-04	2.18E+05	-1.18E+02	1.16E+02	8.70E+00	1.24E-03
210	-3.38E+00	1.59E+00	-4.10E-04	-4.31E-04	2.17E+05	-9.44E+01	9.46E+01	-2.02E+01	1.04E-03
211	-3.56E+00	1.30E+00	-3.48E-04	-4.97E-04	2.17E+05	-7.19E+01	7.17E+01	-3.85E+01	8.76E-04
212	-3.69E+00	9.91E-01	-2.71E-04	-5.48E-04	2.17E+05	-5.28E+01	5.27E+01	-5.08E+01	7.87E-04
213	-3.79E+00	6.69E-01	-1.86E-04	-5.84E-04	2.17E+05	-3.46E+01	3.46E+01	-5.84E+01	7.29E-04
214	-3.85E+00	3.37E-01	-9.42E-05	-6.06E-04	2.17E+05	-1.71E+01	1.71E+01	-6.27E+01	6.99E-04
215	-2.11E+00	2.50E+00	3.54E-04	4.83E-04	2.12E+05	-4.90E+03	1.35E+04	6.07E+03	6.95E-02
216	-2.27E+00	2.48E+00	3.10E-04	-2.62E-04	2.18E+05	5.89E+03	-5.28E+03	-1.10E+03	2.10E-01
217	-2.52E+00	2.28E+00	-6.05E-04	1.18E-04	2.19E+05	2.93E+02	-4.36E+02	7.85E+01	4.46E-03
218	-2.75E+00	2.06E+00	-5.24E-04	-3.12E-04	2.18E+05	-5.23E+01	1.13E+01	-7.60E+01	1.12E-03
219	-2.96E+00	1.81E+00	-5.48E-04	-3.71E-04	2.18E+05	-2.43E+01	2.96E+01	3.24E+01	4.98E-04
220	-3.14E+00	1.55E+00	-4.82E-04	-4.59E-04	2.17E+05	-1.58E+01	1.52E+01	-4.67E+00	2.52E-04
221	-3.29E+00	1.26E+00	-4.01E-04	-5.17E-04	2.17E+05	-7.51E+00	8.59E+00	2.58E+00	2.37E-04
222	-3.41E+00	9.58E-01	-3.08E-04	-5.65E-04	2.17E+05	-3.08E+00	3.73E+00	8.88E-01	2.10E-04
223	-3.50E+00	6.45E-01	-2.09E-04	-5.98E-04	2.17E+05	-1.20E+00	1.61E+00	1.95E+00	1.98E-04
224	-3.55E+00	3.25E-01	-1.05E-04	-6.18E-04	2.17E+05	-3.13E-01	5.33E-01	2.36E+00	1.91E-04
225	-3.62E-01	1.69E+00	-2.90E-04	2.80E-04	-1.37E+03	1.26E+02	-1.10E+02	2.94E+01	1.31E-03
226	-5.34E-01	1.55E+00	-4.51E-04	4.37E-04	-1.37E+03	4.14E+01	-5.34E+01	-1.68E+01	5.72E-04
227	-7.07E-01	1.41E+00	-4.53E-04	4.62E-04	-1.35E+03	-2.23E+01	1.82E+01	-5.09E+00	2.64E-04
228	-5.52E-01	1.90E+00	-2.88E-04	2.29E-04	-1.51E+03	1.67E+02	-1.78E+02	1.26E+01	1.86E-03
229	-7.04E-01	1.78E+00	-4.68E-04	3.90E-04	-1.52E+03	9.80E+01	-1.02E+02	3.42E+00	1.06E-03
230	-8.56E-01	1.66E+00	-5.15E-04	4.20E-04	-1.52E+03	7.40E+00	-1.07E+01	8.38E+00	2.95E-04
231	-7.61E-01	2.08E+00	-2.92E-04	1.86E-04	-1.64E+03	1.87E+02	-1.76E+02	6.67E+01	2.13E-03
232	-8.94E-01	1.99E+00	-4.93E-04	3.13E-04	-1.68E+03	1.18E+02	-1.05E+02	3.11E+01	1.28E-03
233	-1.03E+00	1.90E+00	-5.65E-04	3.36E-04	-1.74E+03	1.10E+01	-1.63E+01	3.11E+01	4.44E-04
234	-9.88E-01	2.24E+00	-2.73E-04	1.21E-04	-1.89E+03	1.71E+02	-1.87E+02	1.40E+02	2.55E-03

235	-1.10E+00	2.18E+00	-4.67E-04	2.14E-04	-2.00E+03	1.30E+02	-1.62E+02	7.52E+01	1.98E-03
236	-1.22E+00	2.11E+00	-5.73E-04	2.63E-04	-1.97E+03	1.05E+02	-6.60E+01	-9.13E+00	9.38E-04
237	-1.23E+00	2.37E+00	-2.17E-04	5.87E-05	-2.04E+03	2.70E+02	-1.14E+02	2.74E+02	3.59E-03
238	-1.33E+00	2.34E+00	-4.49E-04	3.01E-05	-2.05E+03	1.79E+02	2.87E+02	2.64E+02	3.00E-03
239	-1.43E+00	2.31E+00	-5.43E-04	4.92E-06	-2.67E+03	-3.33E+01	2.09E+02	1.72E+02	4.28E-03
240	-1.49E+00	2.48E+00	-1.26E-05	-2.77E-05	-3.30E+03	-1.85E+02	-5.40E+02	3.25E+01	1.22E-02
241	-1.57E+00	2.48E+00	2.28E-04	-1.59E-04	-4.07E+03	-8.22E+02	1.05E+02	3.92E+01	2.63E-02
242	-1.66E+00	2.49E+00	4.81E-04	-8.24E-04	-1.29E+03	6.71E+02	-6.67E+02	1.04E+03	4.45E-02
243	-1.71E+00	2.52E+00	5.39E-04	2.21E-05	5.43E+03	-1.62E+03	-5.82E+02	-1.71E+03	3.19E-02
244	-1.76E+00	2.51E+00	8.35E-04	8.91E-05	2.79E+04	-1.08E+03	-3.22E+03	2.86E+03	5.38E-02
245	-1.80E+00	2.50E+00	3.71E-04	3.00E-04	6.32E+04	-8.84E+02	4.45E+03	8.11E+03	1.10E-01
246	-3.55E+00	-3.25E-01	1.05E-04	-6.18E-04	2.17E+05	3.14E-01	-5.32E-01	2.36E+00	1.91E-04
247	-3.50E+00	-6.45E-01	2.09E-04	-5.98E-04	2.17E+05	1.20E+00	-1.61E+00	1.95E+00	1.98E-04
248	-3.41E+00	-9.58E-01	3.08E-04	-5.65E-04	2.17E+05	3.09E+00	-3.72E+00	8.92E-01	2.10E-04
249	-3.29E+00	-1.26E+00	4.01E-04	-5.17E-04	2.16E+05	7.50E+00	-8.60E+00	2.56E+00	2.37E-04
250	-3.14E+00	-1.55E+00	4.82E-04	-4.59E-04	2.16E+05	1.58E+01	-1.51E+01	-4.61E+00	2.53E-04
251	-2.96E+00	-1.81E+00	5.48E-04	-3.71E-04	2.16E+05	2.42E+01	-2.98E+01	3.21E+01	4.97E-04
252	-2.75E+00	-2.06E+00	5.24E-04	-3.12E-04	2.16E+05	5.29E+01	-1.06E+01	-7.58E+01	1.12E-03
253	-2.52E+00	-2.28E+00	6.01E-04	1.17E-04	2.15E+05	-2.99E+02	4.31E+02	6.98E+01	4.44E-03
254	-2.27E+00	-2.48E+00	-3.08E-04	-2.65E-04	2.16E+05	-5.96E+03	5.32E+03	-1.13E+03	2.12E-01
255	-2.11E+00	-2.50E+00	-3.60E-04	4.85E-04	2.22E+05	4.95E+03	-1.35E+04	6.07E+03	6.99E-02
256	-3.85E+00	-3.37E-01	9.42E-05	-6.06E-04	2.17E+05	1.71E+01	-1.71E+01	-6.27E+01	6.99E-04
257	-3.79E+00	-6.69E-01	1.86E-04	-5.84E-04	2.17E+05	3.46E+01	-3.45E+01	-5.84E+01	7.29E-04
258	-3.69E+00	-9.91E-01	2.71E-04	-5.48E-04	2.17E+05	5.28E+01	-5.27E+01	-5.08E+01	7.87E-04
259	-3.56E+00	-1.30E+00	3.48E-04	-4.97E-04	2.17E+05	7.19E+01	-7.17E+01	-3.85E+01	8.76E-04
260	-3.38E+00	-1.59E+00	4.10E-04	-4.31E-04	2.16E+05	9.44E+01	-9.46E+01	-2.02E+01	1.04E-03
261	-3.18E+00	-1.85E+00	4.55E-04	-3.48E-04	2.16E+05	1.18E+02	-1.16E+02	8.70E+00	1.24E-03
262	-2.94E+00	-2.09E+00	4.37E-04	-2.80E-04	2.16E+05	1.12E+02	-9.92E+01	5.10E+01	1.57E-03
263	-2.68E+00	-2.29E+00	4.62E-04	-1.62E-05	2.16E+05	3.10E+02	-2.80E+02	3.08E+02	3.56E-03
264	-2.40E+00	-2.46E+00	1.42E-04	-4.61E-04	2.15E+05	-3.83E+02	9.20E+01	3.01E+01	6.44E-03
265	-2.17E+00	-2.50E+00	-9.69E-04	7.57E-04	2.15E+05	-2.16E+02	4.19E+03	-3.46E+03	2.11E-02
266	-4.16E+00	-3.49E-01	5.67E-05	-3.82E-04	2.17E+05	3.02E+01	-3.01E+01	-1.07E+02	1.21E-03
267	-4.09E+00	-6.92E-01	1.11E-04	-3.67E-04	2.17E+05	6.02E+01	-6.00E+01	-9.74E+01	1.25E-03
268	-3.98E+00	-1.02E+00	1.61E-04	-3.41E-04	2.17E+05	8.94E+01	-8.93E+01	-8.17E+01	1.32E-03
269	-3.82E+00	-1.34E+00	2.04E-04	-3.06E-04	2.17E+05	1.19E+02	-1.18E+02	-5.89E+01	1.44E-03
270	-3.62E+00	-1.62E+00	2.37E-04	-2.63E-04	2.16E+05	1.43E+02	-1.43E+02	-2.63E+01	1.60E-03
271	-3.39E+00	-1.88E+00	2.53E-04	-2.05E-04	2.16E+05	1.77E+02	-1.78E+02	2.24E+01	1.92E-03
272	-3.13E+00	-2.11E+00	2.58E-04	-1.64E-04	2.16E+05	1.84E+02	-1.64E+02	7.43E+01	2.13E-03
273	-2.84E+00	-2.30E+00	1.96E-04	-8.81E-05	2.16E+05	2.53E+02	-3.99E+02	2.28E+02	3.58E-03
274	-2.53E+00	-2.45E+00	9.13E-05	-1.62E-06	2.16E+05	3.69E+02	3.21E+02	3.25E+02	3.09E-03
275	-2.24E+00	-2.51E+00	-4.93E-04	1.68E-04	2.11E+05	-1.01E+03	1.70E+03	-2.63E+03	3.24E-02
276	-1.80E+00	-2.50E+00	-3.72E-04	3.00E-04	3.70E+05	8.92E+02	-4.45E+03	8.12E+03	1.10E-01
277	-1.66E+00	-2.49E+00	-4.81E-04	-8.25E-04	4.35E+05	-6.74E+02	6.73E+02	1.04E+03	4.46E-02
278	-1.43E+00	-2.31E+00	5.44E-04	5.00E-06	4.36E+05	3.31E+01	-2.09E+02	1.72E+02	4.28E-03
279	-1.22E+00	-2.11E+00	5.73E-04	2.63E-04	4.35E+05	-1.05E+02	6.61E+01	-9.12E+00	9.38E-04
280	-1.03E+00	-1.90E+00	5.65E-04	3.36E-04	4.35E+05	-1.10E+01	1.63E+01	3.11E+01	4.44E-04
281	-8.56E-01	-1.66E+00	5.15E-04	4.20E-04	4.35E+05	-7.40E+00	1.07E+01	8.38E+00	2.95E-04
282	-7.07E-01	-1.41E+00	4.53E-04	4.62E-04	4.35E+05	2.23E+01	-1.82E+01	-5.09E+00	2.64E-04

283	-1.76E+00	-2.51E+00	-8.36E-04	8.94E-05	4.05E+05	1.08E+03	3.22E+03	2.86E+03	5.38E-02
284	-1.57E+00	-2.48E+00	-2.28E-04	-1.59E-04	4.37E+05	8.22E+02	-1.05E+02	3.93E+01	2.64E-02
285	-1.33E+00	-2.34E+00	4.49E-04	3.01E-05	4.35E+05	-1.79E+02	-2.88E+02	2.64E+02	3.00E-03
286	-1.10E+00	-2.18E+00	4.67E-04	2.14E-04	4.35E+05	-1.30E+02	1.62E+02	7.52E+01	1.98E-03
287	-8.94E-01	-1.99E+00	4.93E-04	3.13E-04	4.35E+05	-1.18E+02	1.05E+02	3.11E+01	1.28E-03
288	-7.04E-01	-1.78E+00	4.68E-04	3.90E-04	4.35E+05	-9.80E+01	1.02E+02	3.42E+00	1.06E-03
289	-5.34E-01	-1.55E+00	4.51E-04	4.37E-04	4.35E+05	-4.14E+01	5.34E+01	-1.68E+01	5.72E-04
290	-1.71E+00	-2.52E+00	-5.39E-04	2.22E-05	4.28E+05	1.62E+03	5.83E+02	-1.70E+03	3.19E-02
291	-1.49E+00	-2.48E+00	1.26E-05	-2.78E-05	4.37E+05	1.85E+02	5.39E+02	3.22E+01	1.22E-02
292	-1.23E+00	-2.37E+00	2.17E-04	5.87E-05	4.35E+05	-2.70E+02	1.14E+02	2.74E+02	3.59E-03
293	-9.88E-01	-2.24E+00	2.73E-04	1.21E-04	4.35E+05	-1.71E+02	1.87E+02	1.40E+02	2.55E-03
294	-7.61E-01	-2.08E+00	2.92E-04	1.86E-04	4.35E+05	-1.87E+02	1.76E+02	6.67E+01	2.13E-03
295	-5.52E-01	-1.90E+00	2.88E-04	2.29E-04	4.35E+05	-1.67E+02	1.78E+02	1.26E+01	1.86E-03
296	-3.62E-01	-1.69E+00	2.90E-04	2.80E-04	4.35E+05	-1.26E+02	1.10E+02	2.94E+01	1.31E-03
297	-5.85E-01	-9.86E-01	2.73E-04	4.70E-04	4.34E+05	-6.13E+01	4.13E+01	-4.00E+01	7.21E-04
298	-5.91E-01	-8.24E-01	1.81E-04	5.55E-04	4.34E+05	-2.45E+02	1.67E+02	-1.78E+01	2.16E-03
299	-6.00E-01	-6.57E-01	1.23E-04	8.24E-04	4.34E+05	-3.87E+02	4.03E+02	2.76E+02	5.43E-03
300	-6.12E-01	-4.86E-01	1.18E-04	1.04E-03	4.32E+05	-7.56E+02	3.39E+02	7.40E+02	1.31E-02
301	-6.27E-01	-3.12E-01	2.18E-04	1.79E-03	4.33E+05	-1.13E+03	1.70E+03	6.91E+03	7.89E-02
302	-6.19E-01	-1.56E-01	4.00E-05	3.64E-03	3.73E+05	-6.97E+02	1.48E+03	2.01E+04	2.27E-01
303	-6.16E-01	5.69E-16	-4.69E-08	4.12E-03	2.17E+05	-1.51E+00	3.76E+01	2.47E+04	2.91E-01
304	-6.19E-01	1.56E-01	-3.99E-05	3.64E-03	6.08E+04	6.98E+02	-1.44E+03	2.01E+04	2.27E-01
305	-6.27E-01	3.12E-01	-2.18E-04	1.79E-03	5.92E+02	1.13E+03	-1.69E+03	6.91E+03	7.89E-02
306	-6.12E-01	4.86E-01	-1.18E-04	1.04E-03	8.41E+02	7.56E+02	-3.38E+02	7.40E+02	1.31E-02
307	-6.00E-01	6.57E-01	-1.23E-04	8.24E-04	-9.00E+02	3.87E+02	-4.03E+02	2.76E+02	5.43E-03
308	-5.91E-01	8.24E-01	-1.81E-04	5.55E-04	-1.01E+03	2.45E+02	-1.67E+02	-1.78E+01	2.17E-03
309	-5.85E-01	9.86E-01	-2.73E-04	4.70E-04	-1.14E+03	6.13E+01	-4.13E+01	-4.00E+01	7.21E-04
310	-4.32E-01	-1.13E+00	3.46E-04	3.89E-04	4.35E+05	1.04E+01	4.00E-01	-1.45E+02	1.52E-03
311	-4.78E-01	-9.38E-01	1.88E-04	4.64E-04	4.34E+05	-1.11E+02	5.07E+01	-1.89E+02	2.11E-03
312	-5.23E-01	-7.42E-01	1.82E-05	7.31E-04	4.34E+05	-3.25E+02	4.18E+02	-1.35E+02	4.38E-03
313	-5.69E-01	-5.40E-01	-1.89E-05	1.19E-03	4.33E+05	-9.32E+02	3.85E+02	1.07E+02	8.66E-03
314	-6.14E-01	-3.32E-01	1.49E-04	2.37E-03	4.33E+05	-2.58E+03	3.09E+03	4.01E+03	5.66E-02
315	-6.07E-01	-1.66E-01	-1.09E-04	5.53E-03	3.80E+05	-1.81E+03	4.03E+03	1.24E+04	1.44E-01
316	-6.05E-01	3.61E-16	-1.22E-07	6.69E-03	2.17E+05	-1.47E+00	1.45E+01	1.50E+04	1.76E-01
317	-6.07E-01	1.66E-01	1.10E-04	5.53E-03	5.35E+04	1.81E+03	-4.01E+03	1.24E+04	1.44E-01
318	-6.14E-01	3.32E-01	-1.49E-04	2.37E-03	-2.39E+00	2.58E+03	-3.08E+03	4.01E+03	5.66E-02
319	-5.69E-01	5.40E-01	1.90E-05	1.19E-03	4.73E+02	9.33E+02	-3.85E+02	1.07E+02	8.66E-03
320	-5.23E-01	7.42E-01	-1.82E-05	7.31E-04	-1.10E+03	3.25E+02	-4.18E+02	-1.35E+02	4.38E-03
321	-4.78E-01	9.38E-01	-1.88E-04	4.64E-04	-1.06E+03	1.11E+02	-5.07E+01	-1.89E+02	2.11E-03
322	-4.32E-01	1.13E+00	-3.46E-04	3.89E-04	-1.20E+03	-1.04E+01	-3.97E-01	-1.45E+02	1.52E-03
323	-2.80E-01	-1.27E+00	4.46E-04	2.51E-04	4.35E+05	2.37E+01	-6.04E+01	-1.60E+02	1.76E-03
324	-3.65E-01	-1.05E+00	2.69E-04	3.18E-04	4.34E+05	-3.03E+00	-2.70E+01	-2.34E+02	2.35E-03
325	-4.47E-01	-8.24E-01	5.27E-05	5.24E-04	4.34E+05	-8.61E+01	1.88E+02	-2.81E+02	3.81E-03
326	-5.26E-01	-5.89E-01	-2.16E-04	1.11E-03	4.33E+05	-1.16E+03	3.18E+02	-2.70E+02	7.58E-03
327	-6.01E-01	-3.46E-01	6.25E-05	2.67E-03	4.34E+05	-2.60E+03	3.46E+03	2.06E+03	4.61E-02
328	-5.96E-01	-1.73E-01	-3.10E-04	6.41E-03	3.85E+05	-2.15E+03	5.22E+03	5.77E+03	7.70E-02
329	-5.94E-01	4.16E-16	-1.81E-07	8.07E-03	2.17E+05	-1.30E+00	2.33E+00	5.49E+03	6.40E-02
330	-5.96E-01	1.73E-01	3.11E-04	6.40E-03	4.88E+04	2.15E+03	-5.22E+03	5.77E+03	7.70E-02

331	-6.01E-01	3.46E-01	-6.28E-05	2.67E-03	-2.47E+02	2.60E+03	-3.46E+03	2.06E+03	4.61E-02
332	-5.26E-01	5.89E-01	2.16E-04	1.11E-03	5.17E+01	1.16E+03	-3.18E+02	-2.70E+02	7.58E-03
333	-4.47E-01	8.24E-01	-5.27E-05	5.24E-04	-1.16E+03	8.61E+01	-1.88E+02	-2.81E+02	3.81E-03
334	-3.65E-01	1.05E+00	-2.69E-04	3.18E-04	-1.13E+03	3.02E+00	2.70E+01	-2.34E+02	2.35E-03
335	-2.80E-01	1.27E+00	-4.46E-04	2.51E-04	-1.18E+03	-2.37E+01	6.04E+01	-1.60E+02	1.76E-03
336	-1.28E-01	-1.40E+00	5.22E-04	8.48E-05	4.35E+05	9.97E+01	-6.06E+01	-1.49E+02	1.61E-03
337	-2.52E-01	-1.16E+00	3.93E-04	1.84E-04	4.34E+05	1.97E+01	-7.31E+01	-2.11E+02	2.44E-03
338	-3.71E-01	-9.01E-01	1.02E-04	3.72E-04	4.34E+05	-1.81E+02	2.61E+01	-2.61E+02	3.39E-03
339	-4.83E-01	-6.32E-01	-4.34E-04	9.43E-04	4.34E+05	-1.38E+03	2.44E+02	-5.47E+02	7.74E-03
340	-5.88E-01	-3.52E-01	-5.41E-05	2.87E-03	4.32E+05	-4.32E+03	3.50E+03	5.09E+02	3.92E-02
341	-5.84E-01	-1.76E-01	-4.56E-04	6.47E-03	3.88E+05	-6.76E+02	5.07E+03	-3.54E+02	5.63E-02
342	-5.83E-01	5.00E-16	-2.08E-07	8.28E-03	2.17E+05	1.49E-01	9.94E-01	-3.89E+03	4.59E-02
343	-5.84E-01	1.76E-01	4.56E-04	6.47E-03	4.58E+04	6.76E+02	-5.07E+03	-3.52E+02	5.64E-02
344	-5.88E-01	3.52E-01	5.36E-05	2.87E-03	8.36E+02	4.32E+03	-3.49E+03	5.09E+02	3.92E-02
345	-4.83E-01	6.32E-01	4.34E-04	9.43E-04	-4.93E+02	1.38E+03	-2.45E+02	-5.47E+02	7.74E-03
346	-3.71E-01	9.01E-01	-1.02E-04	3.72E-04	-1.15E+03	1.81E+02	-2.60E+01	-2.61E+02	3.39E-03
347	-2.52E-01	1.16E+00	-3.93E-04	1.84E-04	-1.14E+03	-1.97E+01	7.31E+01	-2.11E+02	2.44E-03
348	-1.28E-01	1.40E+00	-5.22E-04	8.48E-05	-1.21E+03	-9.97E+01	6.06E+01	-1.49E+02	1.61E-03
349	4.46E-03	-1.28E+00	5.85E-04	-1.74E-04	4.34E+05	9.32E+01	-7.69E+01	-1.83E+02	2.09E-03
350	-1.54E-01	-1.06E+00	3.22E-04	-1.46E-05	4.34E+05	7.19E+01	-7.52E+01	-2.53E+02	2.94E-03
351	-3.04E-01	-8.22E-01	-1.66E-05	2.19E-04	4.34E+05	9.91E+00	-1.22E+02	-3.06E+02	4.28E-03
352	-4.46E-01	-5.69E-01	-7.66E-04	9.00E-04	4.34E+05	-8.61E+02	3.72E+02	-4.40E+02	1.13E-02
353	-5.77E-01	-3.03E-01	-1.33E-03	3.97E-03	4.29E+05	-3.39E+03	3.31E+03	-1.72E+03	4.42E-02
354	-5.74E-01	-1.51E-01	4.63E-05	6.44E-03	3.67E+05	3.27E+02	4.02E+03	-8.02E+03	1.10E-01
355	-5.73E-01	4.44E-16	-1.08E-07	7.46E-03	2.17E+05	2.08E+00	8.63E+00	-1.23E+04	1.42E-01
356	-5.74E-01	1.51E-01	-4.58E-05	6.44E-03	6.60E+04	-3.34E+02	-4.01E+03	-8.03E+03	1.10E-01
357	-5.77E-01	3.03E-01	1.33E-03	3.97E-03	4.62E+03	3.40E+03	-3.31E+03	-1.72E+03	4.41E-02
358	-4.46E-01	5.69E-01	7.66E-04	9.00E-04	-8.18E+02	8.61E+02	-3.72E+02	-4.40E+02	1.13E-02
359	-3.04E-01	8.22E-01	1.66E-05	2.19E-04	-1.05E+03	-9.91E+00	1.22E+02	-3.06E+02	4.28E-03
360	-1.54E-01	1.06E+00	-3.22E-04	-1.46E-05	-1.15E+03	-7.19E+01	7.52E+01	-2.53E+02	2.94E-03
361	4.46E-03	1.28E+00	-5.85E-04	-1.74E-04	-1.10E+03	-9.32E+01	7.69E+01	-1.83E+02	2.09E-03
362	1.37E-01	-1.17E+00	5.69E-04	-3.99E-04	4.34E+05	6.43E+01	-7.20E+01	-1.64E+02	1.93E-03
363	-5.55E-02	-9.66E-01	2.59E-04	-2.30E-04	4.35E+05	1.01E+02	-9.11E+01	-2.58E+02	2.98E-03
364	-2.38E-01	-7.47E-01	-6.34E-05	-2.12E-05	4.34E+05	1.41E+02	-3.41E+02	-2.34E+02	4.63E-03
365	-4.08E-01	-5.11E-01	-8.95E-04	7.57E-04	4.35E+05	-3.87E+02	9.75E+01	-6.25E+02	1.33E-02
366	-5.66E-01	-2.60E-01	-2.31E-03	4.40E-03	4.25E+05	-9.66E+02	1.28E+03	-3.95E+03	6.12E-02
367	-5.64E-01	-1.30E-01	4.63E-04	5.20E-03	3.46E+05	-1.47E+03	2.65E+03	-1.71E+04	1.92E-01
368	-5.63E-01	2.78E-16	6.42E-08	5.67E-03	2.17E+05	3.01E+00	2.52E+01	-2.10E+04	2.38E-01
369	-5.64E-01	1.30E-01	-4.63E-04	5.20E-03	8.77E+04	1.46E+03	-2.61E+03	-1.71E+04	1.91E-01
370	-5.66E-01	2.60E-01	2.31E-03	4.40E-03	8.27E+03	9.69E+02	-1.28E+03	-3.95E+03	6.12E-02
371	-4.08E-01	5.11E-01	8.95E-04	7.57E-04	-1.19E+03	3.88E+02	-9.79E+01	-6.25E+02	1.33E-02
372	-2.38E-01	7.47E-01	6.33E-05	-2.12E-05	-1.01E+03	-1.41E+02	3.41E+02	-2.34E+02	4.63E-03
373	-5.55E-02	9.66E-01	-2.59E-04	-2.30E-04	-1.19E+03	-1.01E+02	9.11E+01	-2.58E+02	2.98E-03
374	1.37E-01	1.17E+00	-5.69E-04	-3.99E-04	-1.04E+03	-6.43E+01	7.21E+01	-1.64E+02	1.93E-03
375	2.70E-01	-1.05E+00	4.86E-04	-5.09E-04	4.34E+05	7.82E+00	-1.14E+01	-1.10E+02	1.35E-03
376	4.28E-02	-8.74E-01	2.21E-04	-4.21E-04	4.35E+05	1.06E+02	-8.72E+01	-1.83E+02	2.17E-03
377	-1.71E-01	-6.76E-01	1.25E-05	-2.95E-04	4.34E+05	2.19E+02	-4.53E+02	-1.58E+01	4.14E-03
378	-3.71E-01	-4.58E-01	-7.30E-04	3.25E-04	4.35E+05	7.97E+02	-8.36E+02	-4.53E+02	1.57E-02

379	-5.55E-01	-2.23E-01	-2.28E-03	3.32E-03	4.22E+05	5.36E+03	-5.52E+03	-6.75E+03	1.30E-01
380	-5.54E-01	-1.11E-01	4.54E-04	2.83E-03	3.24E+05	-7.91E+03	1.77E+03	-2.58E+04	2.97E-01
381	-5.53E-01	1.11E-16	1.68E-07	2.93E-03	2.17E+05	-5.96E-01	4.88E+01	-2.89E+04	3.35E-01
382	-5.54E-01	1.11E-01	-4.54E-04	2.83E-03	1.09E+05	7.90E+03	-1.69E+03	-2.58E+04	2.97E-01
383	-5.55E-01	2.23E-01	2.28E-03	3.32E-03	1.12E+04	-5.36E+03	5.52E+03	-6.75E+03	1.30E-01
384	-3.71E-01	4.58E-01	7.31E-04	3.25E-04	-1.86E+03	-7.96E+02	8.35E+02	-4.53E+02	1.57E-02
385	-1.71E-01	6.76E-01	-1.25E-05	-2.95E-04	-1.02E+03	-2.18E+02	4.53E+02	-1.57E+01	4.14E-03
386	4.28E-02	8.74E-01	-2.21E-04	-4.21E-04	-1.27E+03	-1.06E+02	8.71E+01	-1.83E+02	2.17E-03
387	2.70E-01	1.05E+00	-4.86E-04	-5.09E-04	-1.04E+03	-7.82E+00	1.14E+01	-1.10E+02	1.35E-03
388	8.37E-01	1.39E+00	-7.04E-04	-4.27E-04	-5.38E+02	3.54E+01	-3.79E+01	-2.31E+01	5.54E-04
389	6.91E-01	1.60E+00	-7.26E-04	-4.61E-04	-5.50E+02	-5.54E+01	6.04E+01	5.69E+01	8.09E-04
390	5.45E-01	1.81E+00	-4.52E-04	-3.30E-04	-5.44E+02	-1.52E+02	1.46E+02	9.13E+01	1.88E-03
391	1.19E+00	1.52E+00	-7.45E-04	-2.90E-04	-3.33E+02	1.87E+01	-2.14E+01	-2.18E+01	3.95E-04
392	1.09E+00	1.78E+00	-7.62E-04	-3.11E-04	-3.44E+02	-4.88E+01	4.65E+01	6.97E+01	8.80E-04
393	9.79E-01	2.04E+00	-4.79E-04	-2.08E-04	-3.37E+02	-1.16E+02	1.19E+02	1.17E+02	1.77E-03
394	1.56E+00	1.60E+00	-7.70E-04	-1.46E-04	-1.63E+02	8.43E+00	-1.02E+01	-2.33E+01	3.39E-04
395	1.51E+00	1.89E+00	-7.92E-04	-1.56E-04	-1.67E+02	-2.33E+01	2.27E+01	7.38E+01	8.15E-04
396	1.45E+00	2.19E+00	-5.06E-04	-1.07E-04	-1.65E+02	-5.47E+01	5.40E+01	1.38E+02	1.60E-03
397	4.45E+00	2.95E-01	-3.46E-04	1.27E-03	4.51E+03	2.70E+03	-2.26E+03	-5.99E+03	7.03E-02
398	4.40E+00	5.85E-01	-9.49E-06	1.54E-04	3.73E+03	3.34E+02	-5.36E+02	-1.01E+03	1.94E-02
399	4.25E+00	8.96E-01	-1.86E-04	3.97E-04	1.73E+03	2.01E+02	-3.33E+02	-1.78E+02	4.83E-03
400	4.06E+00	1.18E+00	-2.49E-04	3.90E-04	1.23E+03	3.86E+02	-3.71E+02	-1.05E+02	4.13E-03
401	3.83E+00	1.45E+00	-3.35E-04	3.84E-04	9.04E+02	2.51E+02	-2.46E+02	-4.79E+00	2.73E-03
402	3.57E+00	1.68E+00	-3.83E-04	3.37E-04	6.60E+02	2.06E+02	-2.09E+02	5.05E+01	2.30E-03
403	3.28E+00	1.87E+00	-4.30E-04	2.80E-04	4.89E+02	1.58E+02	-1.58E+02	8.70E+01	1.96E-03
404	2.97E+00	2.03E+00	-4.66E-04	2.16E-04	3.44E+02	1.16E+02	-1.17E+02	1.14E+02	1.77E-03
405	2.64E+00	2.14E+00	-4.93E-04	1.47E-04	2.19E+02	7.65E+01	-7.67E+01	1.30E+02	1.64E-03
406	2.29E+00	2.21E+00	-5.08E-04	7.33E-05	1.05E+02	3.73E+01	-3.74E+01	1.41E+02	1.59E-03
407	4.45E+00	2.29E-01	-7.97E-04	2.09E-03	3.11E+04	-2.62E+03	-6.89E+01	-2.16E+03	5.47E-02
408	4.41E+00	4.54E-01	3.48E-04	9.27E-04	2.97E+03	9.73E+02	-2.13E+03	-1.35E+03	3.44E-02
409	4.24E+00	7.36E-01	-6.22E-04	5.86E-04	2.59E+03	6.50E+02	-1.29E+02	9.67E+01	4.54E-03
410	4.03E+00	9.97E-01	-4.63E-04	7.87E-04	1.40E+03	2.94E+02	-3.02E+02	-1.64E+01	2.62E-03
411	3.79E+00	1.23E+00	-5.67E-04	6.53E-04	1.06E+03	1.75E+02	-1.59E+02	2.48E+01	1.77E-03
412	3.53E+00	1.44E+00	-6.36E-04	5.65E-04	7.53E+02	1.08E+02	-1.11E+02	4.78E+01	1.25E-03
413	3.24E+00	1.61E+00	-6.93E-04	4.59E-04	5.51E+02	8.23E+01	-8.11E+01	6.02E+01	1.07E-03
414	2.94E+00	1.75E+00	-7.39E-04	3.49E-04	3.85E+02	5.67E+01	-5.65E+01	6.74E+01	9.33E-04
415	2.61E+00	1.85E+00	-7.72E-04	2.35E-04	2.44E+02	3.65E+01	-3.62E+01	7.23E+01	8.61E-04
416	2.28E+00	1.91E+00	-7.92E-04	1.17E-04	1.16E+02	1.80E+01	-1.80E+01	7.54E+01	8.26E-04
417	4.44E+00	1.62E-01	-7.55E-05	1.32E-03	8.70E+04	-8.15E+03	2.40E+03	8.18E+03	1.17E-01
418	4.42E+00	3.23E-01	-1.07E-03	2.30E-03	8.46E+03	2.11E+03	-1.61E+03	3.72E+02	5.79E-02
419	4.23E+00	5.76E-01	-8.47E-04	7.54E-04	2.59E+03	1.20E+03	-4.65E+02	4.71E+02	9.90E-03
420	4.01E+00	8.09E-01	-5.21E-04	9.39E-04	1.88E+03	3.63E+01	5.48E+01	-9.59E+01	1.49E-03
421	3.76E+00	1.02E+00	-6.20E-04	7.31E-04	1.16E+03	-1.39E+01	1.78E+01	6.76E+01	8.20E-04
422	3.49E+00	1.20E+00	-6.49E-04	6.09E-04	8.50E+02	-2.33E+01	3.25E+01	-9.39E+00	4.94E-04
423	3.21E+00	1.35E+00	-6.95E-04	4.87E-04	6.04E+02	-2.37E+01	2.71E+01	-5.72E+00	4.08E-04
424	2.90E+00	1.47E+00	-7.28E-04	3.67E-04	4.21E+02	-1.83E+01	2.06E+01	-1.61E+01	3.61E-04
425	2.59E+00	1.55E+00	-7.54E-04	2.45E-04	2.65E+02	-1.25E+01	1.38E+01	-1.98E+01	3.28E-04
426	2.27E+00	1.61E+00	-7.71E-04	1.22E-04	1.26E+02	-5.84E+00	6.34E+00	-2.23E+01	3.12E-04

427	2.29E+00	-2.21E+00	5.08E-04	7.33E-05	4.33E+05	-3.73E+01	3.74E+01	1.41E+02	1.59E-03
428	2.64E+00	-2.14E+00	4.93E-04	1.47E-04	4.33E+05	-7.65E+01	7.67E+01	1.30E+02	1.64E-03
429	2.97E+00	-2.03E+00	4.66E-04	2.16E-04	4.33E+05	-1.16E+02	1.17E+02	1.14E+02	1.77E-03
430	3.28E+00	-1.87E+00	4.30E-04	2.80E-04	4.33E+05	-1.58E+02	1.58E+02	8.70E+01	1.96E-03
431	3.57E+00	-1.68E+00	3.83E-04	3.37E-04	4.33E+05	-2.06E+02	2.09E+02	5.05E+01	2.30E-03
432	3.83E+00	-1.45E+00	3.35E-04	3.84E-04	4.32E+05	-2.51E+02	2.46E+02	-4.79E+00	2.73E-03
433	4.06E+00	-1.18E+00	2.49E-04	3.90E-04	4.32E+05	-3.86E+02	3.71E+02	-1.05E+02	4.13E-03
434	4.25E+00	-8.96E-01	1.86E-04	3.97E-04	4.32E+05	-2.02E+02	3.33E+02	-1.78E+02	4.83E-03
435	4.40E+00	-5.85E-01	9.55E-06	1.54E-04	4.30E+05	-3.33E+02	5.36E+02	-1.01E+03	1.94E-02
436	4.45E+00	-2.95E-01	3.46E-04	1.27E-03	4.29E+05	-2.70E+03	2.27E+03	-5.98E+03	7.03E-02
437	2.28E+00	-1.91E+00	7.92E-04	1.17E-04	4.33E+05	-1.80E+01	1.80E+01	7.54E+01	8.26E-04
438	2.61E+00	-1.85E+00	7.72E-04	2.35E-04	4.33E+05	-3.65E+01	3.62E+01	7.23E+01	8.61E-04
439	2.94E+00	-1.75E+00	7.39E-04	3.49E-04	4.33E+05	-5.67E+01	5.65E+01	6.74E+01	9.33E-04
440	3.24E+00	-1.61E+00	6.93E-04	4.59E-04	4.33E+05	-8.23E+01	8.11E+01	6.02E+01	1.07E-03
441	3.53E+00	-1.44E+00	6.36E-04	5.65E-04	4.33E+05	-1.08E+02	1.11E+02	4.78E+01	1.25E-03
442	3.79E+00	-1.23E+00	5.67E-04	6.53E-04	4.32E+05	-1.75E+02	1.59E+02	2.48E+01	1.77E-03
443	4.03E+00	-9.97E-01	4.63E-04	7.87E-04	4.32E+05	-2.94E+02	3.02E+02	-1.64E+01	2.62E-03
444	4.24E+00	-7.36E-01	6.22E-04	5.86E-04	4.31E+05	-6.51E+02	1.29E+02	9.65E+01	4.54E-03
445	4.41E+00	-4.54E-01	-3.48E-04	9.27E-04	4.30E+05	-9.72E+02	2.13E+03	-1.34E+03	3.44E-02
446	4.45E+00	-2.29E-01	7.96E-04	2.09E-03	4.02E+05	2.62E+03	6.73E+01	-2.15E+03	5.47E-02
447	2.27E+00	-1.61E+00	7.71E-04	1.22E-04	4.33E+05	5.84E+00	-6.34E+00	-2.23E+01	3.12E-04
448	2.59E+00	-1.55E+00	7.54E-04	2.45E-04	4.33E+05	1.25E+01	-1.38E+01	-1.98E+01	3.28E-04
449	2.90E+00	-1.47E+00	7.28E-04	3.67E-04	4.33E+05	1.83E+01	-2.06E+01	-1.61E+01	3.61E-04
450	3.21E+00	-1.35E+00	6.95E-04	4.87E-04	4.33E+05	2.37E+01	-2.71E+01	-5.72E+00	4.08E-04
451	3.49E+00	-1.20E+00	6.49E-04	6.09E-04	4.32E+05	2.33E+01	-3.25E+01	-9.39E+00	4.94E-04
452	3.76E+00	-1.02E+00	6.20E-04	7.31E-04	4.32E+05	1.39E+01	-1.79E+01	6.76E+01	8.20E-04
453	4.01E+00	-8.09E-01	5.21E-04	9.39E-04	4.31E+05	-3.61E+01	-5.48E+01	-9.58E+01	1.49E-03
454	4.23E+00	-5.76E-01	8.47E-04	7.54E-04	4.31E+05	-1.20E+03	4.64E+02	4.72E+02	9.91E-03
455	4.42E+00	-3.23E-01	1.07E-03	2.30E-03	4.25E+05	-2.09E+03	1.60E+03	3.80E+02	5.78E-02
456	4.44E+00	-1.62E-01	7.40E-05	1.32E-03	3.46E+05	8.13E+03	-2.39E+03	8.18E+03	1.17E-01
457	5.45E-01	-1.81E+00	4.52E-04	-3.30E-04	4.34E+05	1.52E+02	-1.46E+02	9.13E+01	1.88E-03
458	9.79E-01	-2.04E+00	4.79E-04	-2.08E-04	4.34E+05	1.16E+02	-1.19E+02	1.17E+02	1.77E-03
459	1.45E+00	-2.19E+00	5.06E-04	-1.07E-04	4.33E+05	5.47E+01	-5.40E+01	1.38E+02	1.60E-03
460	6.91E-01	-1.60E+00	7.26E-04	-4.61E-04	4.34E+05	5.54E+01	-6.04E+01	5.69E+01	8.09E-04
461	1.09E+00	-1.78E+00	7.62E-04	-3.11E-04	4.34E+05	4.88E+01	-4.65E+01	6.97E+01	8.80E-04
462	1.51E+00	-1.89E+00	7.92E-04	-1.56E-04	4.33E+05	2.33E+01	-2.27E+01	7.38E+01	8.15E-04
463	8.37E-01	-1.39E+00	7.04E-04	-4.27E-04	4.34E+05	-3.54E+01	3.79E+01	-2.31E+01	5.54E-04
464	1.19E+00	-1.52E+00	7.45E-04	-2.90E-04	4.34E+05	-1.87E+01	2.14E+01	-2.18E+01	3.95E-04
465	1.56E+00	-1.60E+00	7.70E-04	-1.46E-04	4.33E+05	-8.43E+00	1.02E+01	-2.33E+01	3.39E-04
466	-2.09E+00	2.49E+00	-6.85E-04	-3.96E-05		8.88E+03	-3.41E+05	-2.93E+05	5.13E-01
467	-2.20E+00	2.48E+00	1.94E-03	1.17E-03		-2.42E+03	3.80E+03	3.86E+03	4.38E-01
468	-2.25E+00	2.38E+00	-6.55E-04	-8.37E-05		-1.24E+03	2.57E+02	8.76E+02	2.99E-02
469	-3.26E+00	1.56E-01	-4.30E-05	-3.61E-04		9.10E+00	-8.95E+00	9.43E+01	8.52E-04
470	-3.42E+00	0.00E+00	-7.61E-11	-5.33E-04		-3.56E-05	3.93E-04	4.87E+01	5.52E-04
471	-3.26E+00	-1.56E-01	4.30E-05	-3.61E-04		-9.10E+00	8.95E+00	9.43E+01	8.52E-04
472	-2.44E+00	2.28E+00	-4.64E-04	1.47E-04		-4.27E+01	-1.95E+02	-2.50E+02	4.71E-03
473	-2.46E+00	2.15E+00	-5.92E-04	-1.43E-04		4.48E+02	-6.70E+01	-1.43E+02	2.88E-03
474	-2.66E+00	2.05E+00	-5.44E-04	-3.03E-04		-6.45E+01	-1.52E+02	-6.53E+01	1.39E-03

475	-2.66E+00	1.91E+00	-5.24E-04	-1.95E-04		2.69E+01	-8.53E+01	4.98E+01	1.11E-03
476	-2.85E+00	1.80E+00	-5.42E-04	-3.12E-04		4.25E+01	-2.83E+00	4.15E+01	6.36E-04
477	-2.82E+00	1.64E+00	-4.52E-04	-2.42E-04		1.19E+02	-1.01E+02	5.51E+01	9.68E-04
478	-3.02E+00	1.53E+00	-4.68E-04	-4.00E-04		3.62E+01	-5.14E+01	2.61E+01	5.78E-04
479	-2.97E+00	1.36E+00	-3.75E-04	-2.81E-04		7.89E+01	-8.04E+01	7.06E+01	9.61E-04
480	-3.16E+00	1.24E+00	-3.85E-04	-4.44E-04		3.41E+01	-3.20E+01	3.89E+01	5.81E-04
481	-3.08E+00	1.07E+00	-2.95E-04	-3.12E-04		6.57E+01	-6.34E+01	8.10E+01	9.15E-04
482	-3.27E+00	9.42E-01	-2.93E-04	-4.84E-04		2.64E+01	-2.80E+01	4.22E+01	5.70E-04
483	-3.17E+00	7.74E-01	-2.13E-04	-3.36E-04		4.57E+01	-4.50E+01	8.77E+01	8.85E-04
484	-3.35E+00	6.34E-01	-1.98E-04	-5.11E-04		1.81E+01	-1.83E+01	4.60E+01	5.61E-04
485	-3.23E+00	4.67E-01	-1.29E-04	-3.52E-04		2.75E+01	-2.69E+01	9.22E+01	8.63E-04
486	-3.40E+00	3.19E-01	-9.97E-05	-5.28E-04		9.14E+00	-9.42E+00	4.80E+01	5.54E-04
487	-2.25E+00	-2.38E+00	6.55E-04	-8.37E-05		1.21E+03	-2.63E+02	8.61E+02	3.00E-02
488	-2.20E+00	-2.48E+00	-1.97E-03	1.17E-03		2.43E+03	-3.84E+03	3.95E+03	4.41E-01
489	-2.09E+00	-2.49E+00	6.85E-04	-3.96E-05		-6.86E+03	3.45E+05	-3.00E+05	5.16E-01
490	-2.46E+00	-2.15E+00	5.92E-04	-1.43E-04		-4.45E+02	6.74E+01	-1.42E+02	2.87E-03
491	-2.44E+00	-2.28E+00	4.60E-04	1.45E-04		4.81E+01	1.96E+02	-2.58E+02	4.68E-03
492	-2.66E+00	-1.91E+00	5.24E-04	-1.95E-04		-2.80E+01	8.53E+01	4.95E+01	1.11E-03
493	-2.66E+00	-2.05E+00	5.44E-04	-3.02E-04		6.44E+01	1.52E+02	-6.53E+01	1.38E-03
494	-2.82E+00	-1.64E+00	4.52E-04	-2.42E-04		-1.19E+02	1.01E+02	5.51E+01	9.68E-04
495	-2.85E+00	-1.80E+00	5.41E-04	-3.12E-04		-4.23E+01	3.06E+00	4.12E+01	6.34E-04
496	-2.97E+00	-1.36E+00	3.75E-04	-2.81E-04		-7.90E+01	8.04E+01	7.06E+01	9.61E-04
497	-3.02E+00	-1.53E+00	4.68E-04	-4.00E-04		-3.62E+01	5.13E+01	2.62E+01	5.78E-04
498	-3.08E+00	-1.07E+00	2.95E-04	-3.12E-04		-6.57E+01	6.34E+01	8.10E+01	9.15E-04
499	-3.16E+00	-1.24E+00	3.85E-04	-4.44E-04		-3.41E+01	3.21E+01	3.89E+01	5.81E-04
500	-3.17E+00	-7.74E-01	2.13E-04	-3.36E-04		-4.57E+01	4.50E+01	8.77E+01	8.85E-04
501	-3.27E+00	-9.42E-01	2.93E-04	-4.84E-04		-2.64E+01	2.80E+01	4.22E+01	5.70E-04
502	-3.23E+00	-4.67E-01	1.29E-04	-3.52E-04		-2.75E+01	2.69E+01	9.22E+01	8.63E-04
503	-3.35E+00	-6.34E-01	1.98E-04	-5.11E-04		-1.81E+01	1.83E+01	4.60E+01	5.61E-04
504	-3.40E+00	-3.19E-01	9.97E-05	-5.28E-04		-9.14E+00	9.42E+00	4.80E+01	5.54E-04
505	4.43E+00	1.44E-01	-3.96E-05	6.85E-04		8.75E+04	6.14E+02	-2.17E+04	2.75E-01
506	4.43E+00	2.57E-01	-1.53E-03	2.06E-03		-4.45E+03	2.33E+03	-2.45E+02	1.36E-01
507	4.33E+00	3.04E-01	-8.37E-05	6.55E-04		-2.07E+03	5.01E+03	1.75E+03	3.44E-02
508	1.95E+00	1.47E+00	-6.26E-04	-5.60E-07		5.66E-01	-7.07E-01	-9.06E+01	1.02E-03
509	1.78E+00	1.31E+00	-3.60E-04	-4.47E-05		1.55E+01	-1.63E+01	-1.56E+02	1.47E-03
510	2.10E+00	1.31E+00	-3.61E-04	4.30E-05		-1.47E+01	1.50E+01	-1.55E+02	1.45E-03
511	4.22E+00	4.97E-01	-8.31E-04	8.81E-04		-5.08E+02	6.44E+01	4.35E+02	1.38E-02
512	4.10E+00	5.19E-01	-1.43E-04	5.92E-04		-5.55E+02	9.02E+01	-2.70E+02	7.16E-03
513	3.99E+00	7.14E-01	-3.76E-04	8.30E-04		-6.16E+01	3.47E+02	-1.21E+02	2.95E-03
514	3.85E+00	7.10E-01	-1.95E-04	5.24E-04		-3.91E+02	5.19E+02	-9.52E+01	3.83E-03
515	3.74E+00	9.08E-01	-5.23E-04	6.58E-04		-2.38E+02	1.56E+02	-1.26E+01	2.19E-03
516	3.59E+00	8.78E-01	-2.42E-04	4.52E-04		-2.30E+02	2.16E+02	-1.37E+02	2.63E-03
517	3.47E+00	1.08E+00	-5.16E-04	5.45E-04		-1.06E+02	1.24E+02	-7.46E+01	1.56E-03
518	3.31E+00	1.02E+00	-2.81E-04	3.75E-04		-1.67E+02	1.79E+02	-1.44E+02	2.06E-03
519	3.19E+00	1.22E+00	-5.60E-04	4.35E-04		-9.42E+01	8.67E+01	-7.42E+01	1.32E-03
520	3.02E+00	1.14E+00	-3.12E-04	2.95E-04		-1.16E+02	1.18E+02	-1.48E+02	1.77E-03
521	2.89E+00	1.33E+00	-5.85E-04	3.27E-04		-6.14E+01	6.14E+01	-8.33E+01	1.17E-03
522	2.72E+00	1.22E+00	-3.36E-04	2.13E-04		-7.80E+01	8.05E+01	-1.52E+02	1.59E-03

523	2.58E+00	1.41E+00	-6.07E-04	2.18E-04		-4.03E+01	3.90E+01	-8.68E+01	1.08E-03
524	2.41E+00	1.28E+00	-3.52E-04	1.29E-04		-4.50E+01	4.60E+01	-1.54E+02	1.50E-03
525	2.26E+00	1.45E+00	-6.20E-04	1.09E-04		-1.90E+01	1.88E+01	-8.94E+01	1.03E-03
526	1.95E+00	-1.47E+00	6.26E-04	-5.60E-07		-5.65E-01	7.07E-01	-9.06E+01	1.02E-03
527	2.10E+00	-1.31E+00	3.61E-04	4.30E-05		1.47E+01	-1.50E+01	-1.55E+02	1.45E-03
528	1.78E+00	-1.31E+00	3.60E-04	-4.47E-05		-1.55E+01	1.63E+01	-1.56E+02	1.47E-03
529	4.33E+00	-3.04E-01	8.37E-05	6.55E-04		2.07E+03	-5.01E+03	1.75E+03	3.44E-02
530	4.43E+00	-2.57E-01	1.53E-03	2.05E-03		4.46E+03	-2.33E+03	-2.47E+02	1.36E-01
531	4.43E+00	-1.44E-01	3.96E-05	6.85E-04		-8.63E+04	-8.38E+02	-2.10E+04	2.74E-01
532	2.26E+00	-1.45E+00	6.20E-04	1.09E-04		1.90E+01	-1.88E+01	-8.94E+01	1.03E-03
533	2.41E+00	-1.28E+00	3.52E-04	1.29E-04		4.50E+01	-4.60E+01	-1.54E+02	1.50E-03
534	2.58E+00	-1.41E+00	6.07E-04	2.18E-04		4.03E+01	-3.90E+01	-8.68E+01	1.08E-03
535	2.72E+00	-1.22E+00	3.36E-04	2.13E-04		7.80E+01	-8.05E+01	-1.52E+02	1.59E-03
536	2.89E+00	-1.33E+00	5.85E-04	3.27E-04		6.14E+01	-6.14E+01	-8.33E+01	1.17E-03
537	3.02E+00	-1.14E+00	3.12E-04	2.95E-04		1.16E+02	-1.18E+02	-1.48E+02	1.77E-03
538	3.19E+00	-1.22E+00	5.60E-04	4.35E-04		9.42E+01	-8.67E+01	-7.42E+01	1.32E-03
539	3.31E+00	-1.02E+00	2.81E-04	3.75E-04		1.67E+02	-1.79E+02	-1.44E+02	2.06E-03
540	3.47E+00	-1.08E+00	5.16E-04	5.45E-04		1.06E+02	-1.24E+02	-7.46E+01	1.56E-03
541	3.59E+00	-8.78E-01	2.42E-04	4.52E-04		2.30E+02	-2.16E+02	-1.37E+02	2.63E-03
542	3.74E+00	-9.08E-01	5.23E-04	6.58E-04		2.38E+02	-1.56E+02	-1.26E+01	2.19E-03
543	3.85E+00	-7.10E-01	1.95E-04	5.24E-04		3.91E+02	-5.19E+02	-9.51E+01	3.83E-03
544	3.99E+00	-7.14E-01	3.76E-04	8.30E-04		6.17E+01	-3.47E+02	-1.21E+02	2.95E-03
545	4.10E+00	-5.19E-01	1.43E-04	5.92E-04		5.55E+02	-9.02E+01	-2.70E+02	7.16E-03
546	4.22E+00	-4.97E-01	8.31E-04	8.80E-04		5.09E+02	-6.38E+01	4.37E+02	1.38E-02
547	-1.64E+00	2.38E+00	-6.56E-04	8.28E-05		1.79E+03	-1.06E+03	5.54E+02	1.58E-02
548	-1.71E+00	2.49E+00	1.02E-05	-6.01E-04		2.31E+03	-2.86E+03	4.77E+02	7.71E-02
549	-1.80E+00	2.49E+00	-6.85E-04	3.96E-05		-2.54E+02	3.32E+04	-7.12E+03	1.75E-01
550	-6.79E-01	1.06E+00	-3.18E-04	4.22E-04		-2.03E+01	1.95E+01	1.33E+01	4.60E-04
551	-8.28E-01	1.12E+00	-3.09E-04	3.08E-04		-6.15E+01	5.54E+01	6.49E+01	7.76E-04
552	-7.56E-01	9.13E-01	-2.51E-04	3.27E-04		-3.07E+01	4.97E+01	8.34E+01	8.02E-04
553	-1.44E+00	2.16E+00	-5.95E-04	1.40E-04		-2.37E+02	5.33E+01	-6.81E+01	1.25E-03
554	-1.48E+00	2.29E+00	-5.89E-04	3.44E-05		-9.49E+00	-1.61E+02	1.64E+02	4.30E-03
555	-1.25E+00	1.93E+00	-5.30E-04	1.92E-04		-6.07E+01	9.50E+01	4.42E+01	9.52E-04
556	-1.28E+00	2.08E+00	-5.86E-04	2.47E-04		4.00E+01	6.05E+01	5.79E+00	8.29E-04
557	-1.08E+00	1.67E+00	-4.60E-04	2.37E-04		-1.19E+02	1.05E+02	5.47E+01	1.06E-03
558	-1.09E+00	1.85E+00	-5.51E-04	2.96E-04		-5.37E+01	3.44E+01	3.95E+01	6.85E-04
559	-9.43E-01	1.40E+00	-3.86E-04	2.76E-04		-8.91E+01	8.84E+01	7.30E+01	1.03E-03
560	-9.32E-01	1.60E+00	-4.86E-04	3.69E-04		-4.32E+01	5.11E+01	3.43E+01	6.83E-04
561	-7.93E-01	1.34E+00	-4.11E-04	4.06E-04		-4.74E+01	5.24E+01	2.87E+01	6.50E-04
562	-8.28E-01	-1.12E+00	3.09E-04	3.08E-04		6.15E+01	-5.54E+01	6.49E+01	7.76E-04
563	-6.79E-01	-1.06E+00	3.18E-04	4.22E-04		2.03E+01	-1.95E+01	1.33E+01	4.60E-04
564	-7.56E-01	-9.13E-01	2.51E-04	3.27E-04		3.07E+01	-4.97E+01	8.34E+01	8.02E-04
565	-1.80E+00	-2.49E+00	6.85E-04	3.96E-05		1.89E+02	-3.34E+04	-7.21E+03	1.74E-01
566	-1.71E+00	-2.49E+00	-9.23E-06	-6.01E-04		-2.31E+03	2.86E+03	4.76E+02	7.70E-02
567	-1.64E+00	-2.38E+00	6.56E-04	8.28E-05		-1.79E+03	1.07E+03	5.54E+02	1.58E-02
568	-9.43E-01	-1.40E+00	3.86E-04	2.76E-04		8.91E+01	-8.84E+01	7.30E+01	1.03E-03
569	-7.93E-01	-1.34E+00	4.11E-04	4.06E-04		4.74E+01	-5.24E+01	2.87E+01	6.50E-04
570	-1.08E+00	-1.67E+00	4.60E-04	2.37E-04		1.19E+02	-1.05E+02	5.47E+01	1.06E-03

571	-9.32E-01	-1.60E+00	4.86E-04	3.69E-04		4.32E+01	-5.11E+01	3.43E+01	6.83E-04
572	-1.25E+00	-1.93E+00	5.30E-04	1.92E-04		6.07E+01	-9.50E+01	4.42E+01	9.52E-04
573	-1.09E+00	-1.85E+00	5.51E-04	2.96E-04		5.37E+01	-3.45E+01	3.95E+01	6.85E-04
574	-1.44E+00	-2.16E+00	5.95E-04	1.40E-04		2.37E+02	-5.33E+01	-6.80E+01	1.25E-03
575	-1.28E+00	-2.08E+00	5.86E-04	2.47E-04		-3.99E+01	-6.05E+01	5.82E+00	8.29E-04
576	-1.48E+00	-2.29E+00	5.90E-04	3.45E-05		9.74E+00	1.61E+02	1.64E+02	4.30E-03
577	5.92E-01	1.14E+00	-4.97E-04	-4.51E-04		1.01E+02	-9.34E+01	-1.01E+02	1.59E-03
578	5.39E-01	1.00E+00	-2.75E-04	-3.87E-04		1.60E+02	-1.64E+02	-1.32E+02	1.98E-03
579	8.29E-01	1.12E+00	-3.08E-04	-3.07E-04		1.30E+02	-1.40E+02	-1.57E+02	1.97E-03
580	9.10E-01	1.28E+00	-5.64E-04	-3.58E-04		8.05E+01	-7.44E+01	-8.83E+01	1.35E-03
581	1.14E+00	1.21E+00	-3.34E-04	-2.21E-04		8.50E+01	-8.85E+01	-1.57E+02	1.71E-03
582	1.25E+00	1.39E+00	-5.99E-04	-2.42E-04		4.80E+01	-4.63E+01	-8.98E+01	1.15E-03
583	1.46E+00	1.28E+00	-3.52E-04	-1.34E-04		4.78E+01	-5.02E+01	-1.56E+02	1.54E-03
584	1.59E+00	1.45E+00	-6.20E-04	-1.22E-04		2.28E+01	-2.20E+01	-9.08E+01	1.06E-03
585	5.39E-01	-1.00E+00	2.75E-04	-3.87E-04		-1.60E+02	1.64E+02	-1.32E+02	1.98E-03
586	5.92E-01	-1.14E+00	4.97E-04	-4.51E-04		-1.01E+02	9.34E+01	-1.01E+02	1.59E-03
587	8.29E-01	-1.12E+00	3.08E-04	-3.07E-04		-1.30E+02	1.40E+02	-1.57E+02	1.97E-03
588	9.10E-01	-1.28E+00	5.64E-04	-3.58E-04		-8.05E+01	7.44E+01	-8.83E+01	1.35E-03
589	1.14E+00	-1.21E+00	3.34E-04	-2.21E-04		-8.50E+01	8.85E+01	-1.57E+02	1.71E-03
590	1.25E+00	-1.39E+00	5.99E-04	-2.42E-04		-4.80E+01	4.63E+01	-8.98E+01	1.15E-03
591	1.46E+00	-1.28E+00	3.52E-04	-1.34E-04		-4.78E+01	5.02E+01	-1.56E+02	1.54E-03
592	1.59E+00	-1.45E+00	6.20E-04	-1.22E-04		-2.28E+01	2.20E+01	-9.08E+01	1.06E-03
593	-1.95E+00	2.50E+00	-5.76E-06	2.42E-05		8.66E+02	2.11E+02	8.94E+03	9.74E-02
594	-1.99E+00	2.49E+00	-6.85E-04	-1.32E-05		9.14E+01	-4.61E+03	6.69E+03	8.16E-02
595	-1.90E+00	2.49E+00	-6.85E-04	1.32E-05		3.30E+01	1.12E+03	1.52E+04	1.49E-01
596	-2.07E+00	2.49E+00	-7.01E-04	-2.01E-04		-2.09E+03	-5.98E+03	-1.87E+03	7.62E-02
597	-1.83E+00	2.49E+00	4.52E-05	6.74E-05		-9.41E+02	2.31E+03	1.35E+04	1.39E-01
598	-1.99E+00	-2.49E+00	6.85E-04	-1.32E-05		-8.74E+01	4.59E+03	6.65E+03	8.13E-02
599	-1.95E+00	-2.50E+00	6.95E-06	2.38E-05		-8.60E+02	-2.06E+02	8.93E+03	9.73E-02
600	-1.90E+00	-2.49E+00	6.85E-04	1.32E-05		-6.13E+00	-1.11E+03	1.52E+04	1.49E-01
601	-2.07E+00	-2.49E+00	7.04E-04	-2.02E-04		2.10E+03	6.11E+03	-2.08E+03	7.64E-02
602	-1.83E+00	-2.49E+00	-4.56E-05	6.74E-05		9.63E+02	-2.31E+03	1.35E+04	1.39E-01
603	4.44E+00	0.00E+00	-1.22E-07	1.62E-03		-1.66E+00	7.52E+00	1.15E+04	1.23E-01
604	4.43E+00	4.80E-02	-1.32E-05	6.85E-04		-4.78E+03	-2.25E+01	1.52E+04	1.43E-01
605	4.43E+00	-4.80E-02	1.32E-05	6.85E-04		4.80E+03	4.74E+01	1.52E+04	1.43E-01
606	4.44E+00	1.29E-01	3.02E-04	7.78E-04		4.78E+03	1.18E+02	7.88E+03	1.35E-01
607	4.44E+00	-1.29E-01	-3.02E-04	7.78E-04		-4.72E+03	-1.29E+02	7.91E+03	1.35E-01
608	-4.47E+00	1.81E-01	0.00E+00	0.00E+00		-1.97E+01	1.97E+01	-1.37E+02	1.46E-03
609	-4.33E+00	0.00E+00	4.44E-12	-2.08E-04		7.08E-06	8.48E-04	-1.21E+02	1.37E-03
610	-4.47E+00	-1.81E-01	0.00E+00	0.00E+00		1.97E+01	-1.97E+01	-1.37E+02	1.46E-03
611	-2.13E+00	2.53E+00	0.00E+00	0.00E+00		4.43E+02	-1.05E+04	-2.98E+03	5.74E-02
612	-1.95E+00	2.53E+00	4.56E-04	-1.18E-04		7.70E+02	3.06E+03	-5.73E+03	7.30E-02
613	-1.81E+00	2.53E+00	0.00E+00	0.00E+00		-1.27E+03	9.15E+03	-1.20E+04	1.04E-01
614	-4.42E+00	5.39E-01	0.00E+00	0.00E+00		-5.85E+01	5.85E+01	-1.28E+02	1.49E-03
615	-4.31E+00	3.55E-01	-2.99E-05	-2.05E-04		-3.38E+01	3.38E+01	-1.17E+02	1.38E-03
616	-4.32E+00	8.85E-01	0.00E+00	0.00E+00		-9.62E+01	9.60E+01	-1.11E+02	1.55E-03
617	-4.24E+00	7.04E-01	-5.86E-05	-1.96E-04		-6.69E+01	6.70E+01	-1.06E+02	1.42E-03
618	-4.17E+00	1.21E+00	0.00E+00	0.00E+00		-1.31E+02	1.32E+02	-8.46E+01	1.65E-03

619	-4.12E+00	1.04E+00	-8.46E-05	-1.82E-04		-9.87E+01	9.87E+01	-8.80E+01	1.50E-03
620	-3.97E+00	1.52E+00	0.00E+00	0.00E+00		-1.64E+02	1.62E+02	-4.69E+01	1.80E-03
621	-3.95E+00	1.35E+00	-1.06E-04	-1.62E-04		-1.29E+02	1.29E+02	-6.15E+01	1.62E-03
622	-3.74E+00	1.79E+00	0.00E+00	0.00E+00		-1.90E+02	1.97E+02	-3.30E+00	2.01E-03
623	-3.74E+00	1.64E+00	-1.23E-04	-1.38E-04		-1.56E+02	1.53E+02	-2.55E+01	1.79E-03
624	-3.46E+00	2.03E+00	0.00E+00	0.00E+00		-2.15E+02	1.86E+02	7.42E+01	2.32E-03
625	-3.50E+00	1.90E+00	-1.26E-04	-1.09E-04		-1.78E+02	1.89E+02	2.40E+01	2.08E-03
626	-3.16E+00	2.22E+00	0.00E+00	0.00E+00		-2.38E+02	3.42E+02	1.24E+02	3.01E-03
627	-3.22E+00	2.12E+00	-1.31E-04	-7.66E-05		-2.03E+02	1.63E+02	8.20E+01	2.44E-03
628	-2.83E+00	2.37E+00	0.00E+00	0.00E+00		-2.80E+02	-1.45E+02	3.95E+02	4.67E-03
629	-2.92E+00	2.31E+00	-8.03E-05	-5.01E-05		-1.95E+02	3.28E+02	1.54E+02	3.37E-03
630	-2.48E+00	2.48E+00	0.00E+00	0.00E+00		-3.69E+02	4.74E+03	2.80E+02	1.78E-02
631	-2.60E+00	2.44E+00	-2.28E-05	7.62E-05		-1.86E+02	-1.09E+03	3.20E+02	5.60E-03
632	-2.27E+00	2.51E+00	2.25E-04	3.41E-07		8.21E+02	5.09E+02	-2.26E+03	3.70E-02
633	-1.95E+00	-2.53E+00	-4.54E-04	-1.18E-04		-7.67E+02	-3.06E+03	-5.71E+03	7.29E-02
634	-2.13E+00	-2.53E+00	0.00E+00	0.00E+00		-4.40E+02	1.05E+04	-2.97E+03	5.72E-02
635	-1.81E+00	-2.53E+00	0.00E+00	0.00E+00		1.29E+03	-9.14E+03	-1.20E+04	1.04E-01
636	-4.31E+00	-3.55E-01	2.99E-05	-2.05E-04		3.38E+01	-3.38E+01	-1.17E+02	1.38E-03
637	-4.42E+00	-5.39E-01	0.00E+00	0.00E+00		5.85E+01	-5.85E+01	-1.28E+02	1.49E-03
638	-4.24E+00	-7.04E-01	5.86E-05	-1.96E-04		6.69E+01	-6.70E+01	-1.06E+02	1.42E-03
639	-4.32E+00	-8.85E-01	0.00E+00	0.00E+00		9.62E+01	-9.60E+01	-1.11E+02	1.55E-03
640	-4.12E+00	-1.04E+00	8.46E-05	-1.82E-04		9.87E+01	-9.87E+01	-8.80E+01	1.50E-03
641	-4.17E+00	-1.21E+00	0.00E+00	0.00E+00		1.31E+02	-1.32E+02	-8.46E+01	1.65E-03
642	-3.95E+00	-1.35E+00	1.06E-04	-1.62E-04		1.29E+02	-1.29E+02	-6.15E+01	1.62E-03
643	-3.97E+00	-1.52E+00	0.00E+00	0.00E+00		1.64E+02	-1.62E+02	-4.69E+01	1.80E-03
644	-3.74E+00	-1.64E+00	1.23E-04	-1.38E-04		1.56E+02	-1.53E+02	-2.55E+01	1.79E-03
645	-3.74E+00	-1.79E+00	0.00E+00	0.00E+00		1.90E+02	-1.97E+02	-3.30E+00	2.01E-03
646	-3.50E+00	-1.90E+00	1.26E-04	-1.09E-04		1.78E+02	-1.89E+02	2.40E+01	2.08E-03
647	-3.46E+00	-2.03E+00	0.00E+00	0.00E+00		2.15E+02	-1.86E+02	7.41E+01	2.32E-03
648	-3.22E+00	-2.12E+00	1.31E-04	-7.66E-05		2.03E+02	-1.63E+02	8.20E+01	2.44E-03
649	-3.16E+00	-2.22E+00	0.00E+00	0.00E+00		2.38E+02	-3.41E+02	1.24E+02	3.01E-03
650	-2.92E+00	-2.31E+00	8.03E-05	-5.00E-05		1.95E+02	-3.28E+02	1.54E+02	3.36E-03
651	-2.83E+00	-2.37E+00	0.00E+00	0.00E+00		2.80E+02	1.43E+02	3.94E+02	4.66E-03
652	-2.60E+00	-2.44E+00	2.25E-05	7.61E-05		1.86E+02	1.09E+03	3.18E+02	5.61E-03
653	-2.48E+00	-2.48E+00	0.00E+00	0.00E+00		3.74E+02	-4.73E+03	2.90E+02	1.78E-02
654	-2.27E+00	-2.51E+00	-2.25E-04	2.32E-07		-8.23E+02	-5.06E+02	-2.27E+03	3.70E-02
655	4.47E+00	1.81E-01	0.00E+00	0.00E+00		2.18E+04	-1.89E+03	-1.33E+04	1.66E-01
656	4.48E+00	0.00E+00	-1.10E-07	1.07E-03		1.32E-01	9.92E+00	-1.38E+04	1.53E-01
657	4.47E+00	-1.81E-01	0.00E+00	0.00E+00		-2.18E+04	1.92E+03	-1.33E+04	1.66E-01
658	2.13E+00	-2.53E+00	0.00E+00	0.00E+00		-2.51E+01	2.45E+01	1.81E+02	1.94E-03
659	1.95E+00	-2.39E+00	2.74E-04	-3.33E-06		2.65E+00	-2.15E+00	1.60E+02	1.83E-03
660	1.67E+00	-2.51E+00	0.00E+00	0.00E+00		4.27E+01	-4.49E+01	1.88E+02	1.99E-03
661	4.42E+00	-5.39E-01	0.00E+00	0.00E+00		9.22E+03	8.69E+02	-3.17E+03	4.08E-02
662	4.46E+00	-3.28E-01	5.52E-05	6.18E-04		4.03E+02	2.15E+03	-6.12E+03	9.36E-02
663	4.32E+00	-8.85E-01	0.00E+00	0.00E+00		-1.46E+03	4.52E+02	-3.35E+02	1.03E-02
664	4.39E+00	-6.50E-01	1.71E-04	4.66E-05		-2.55E+03	3.15E+02	-3.71E+02	1.49E-02
665	4.17E+00	-1.21E+00	0.00E+00	0.00E+00		-1.70E+02	4.23E+02	-3.42E+02	5.02E-03
666	4.25E+00	-9.75E-01	6.69E-05	2.08E-04		-1.57E+02	3.92E+02	-3.20E+02	5.92E-03

667	3.97E+00	-1.52E+00	0.00E+00	0.00E+00		-3.82E+02	3.33E+02	-7.99E+01	3.69E-03
668	4.07E+00	-1.28E+00	1.38E-04	1.81E-04		-4.00E+02	3.14E+02	-1.13E+02	4.21E-03
669	3.74E+00	-1.79E+00	0.00E+00	0.00E+00		-2.72E+02	2.87E+02	-7.80E+00	2.97E-03
670	3.85E+00	-1.56E+00	1.69E-04	2.00E-04		-2.56E+02	2.71E+02	-2.15E+01	3.10E-03
671	3.46E+00	-2.03E+00	0.00E+00	0.00E+00		-2.34E+02	2.31E+02	6.96E+01	2.54E-03
672	3.59E+00	-1.80E+00	2.01E-04	1.73E-04		-2.27E+02	2.22E+02	4.31E+01	2.60E-03
673	3.16E+00	-2.22E+00	0.00E+00	0.00E+00		-1.82E+02	1.83E+02	1.16E+02	2.27E-03
674	3.30E+00	-2.01E+00	2.28E-04	1.48E-04		-1.76E+02	1.77E+02	8.86E+01	2.25E-03
675	2.83E+00	-2.37E+00	0.00E+00	0.00E+00		-1.31E+02	1.31E+02	1.51E+02	2.10E-03
676	2.98E+00	-2.17E+00	2.49E-04	1.15E-04		-1.33E+02	1.33E+02	1.22E+02	2.04E-03
677	2.48E+00	-2.48E+00	0.00E+00	0.00E+00		-7.88E+01	7.91E+01	1.73E+02	1.99E-03
678	2.65E+00	-2.29E+00	2.65E-04	7.83E-05		-8.84E+01	8.83E+01	1.43E+02	1.91E-03
679	2.30E+00	-2.36E+00	2.73E-04	3.94E-05		-4.30E+01	4.37E+01	1.56E+02	1.84E-03
680	1.67E+00	2.51E+00	0.00E+00	0.00E+00		-4.26E+01	4.49E+01	1.88E+02	1.99E-03
681	1.95E+00	2.39E+00	-2.74E-04	-3.33E-06		-2.65E+00	2.15E+00	1.60E+02	1.83E-03
682	2.13E+00	2.53E+00	0.00E+00	0.00E+00		2.51E+01	-2.45E+01	1.81E+02	1.94E-03
683	2.48E+00	2.48E+00	0.00E+00	0.00E+00		7.89E+01	-7.91E+01	1.73E+02	1.99E-03
684	2.30E+00	2.36E+00	-2.73E-04	3.94E-05		4.30E+01	-4.37E+01	1.56E+02	1.84E-03
685	2.83E+00	2.37E+00	0.00E+00	0.00E+00		1.31E+02	-1.31E+02	1.51E+02	2.10E-03
686	2.65E+00	2.29E+00	-2.65E-04	7.83E-05		8.84E+01	-8.83E+01	1.43E+02	1.91E-03
687	3.16E+00	2.22E+00	0.00E+00	0.00E+00		1.82E+02	-1.83E+02	1.16E+02	2.27E-03
688	2.98E+00	2.17E+00	-2.49E-04	1.15E-04		1.33E+02	-1.33E+02	1.22E+02	2.04E-03
689	3.46E+00	2.03E+00	0.00E+00	0.00E+00		2.34E+02	-2.31E+02	6.96E+01	2.54E-03
690	3.30E+00	2.01E+00	-2.28E-04	1.48E-04		1.76E+02	-1.77E+02	8.86E+01	2.25E-03
691	3.74E+00	1.79E+00	0.00E+00	0.00E+00		2.72E+02	-2.87E+02	-7.81E+00	2.97E-03
692	3.59E+00	1.80E+00	-2.01E-04	1.73E-04		2.28E+02	-2.22E+02	4.31E+01	2.60E-03
693	3.97E+00	1.52E+00	0.00E+00	0.00E+00		3.82E+02	-3.33E+02	-7.99E+01	3.69E-03
694	3.85E+00	1.56E+00	-1.69E-04	2.00E-04		2.56E+02	-2.71E+02	-2.15E+01	3.10E-03
695	4.17E+00	1.21E+00	0.00E+00	0.00E+00		1.70E+02	-4.23E+02	-3.42E+02	5.02E-03
696	4.07E+00	1.28E+00	-1.38E-04	1.81E-04		4.00E+02	-3.14E+02	-1.13E+02	4.21E-03
697	4.32E+00	8.85E-01	0.00E+00	0.00E+00		1.46E+03	-4.52E+02	-3.35E+02	1.03E-02
698	4.25E+00	9.75E-01	-6.69E-05	2.08E-04		1.57E+02	-3.92E+02	-3.20E+02	5.92E-03
699	4.42E+00	5.39E-01	0.00E+00	0.00E+00		-9.22E+03	-8.68E+02	-3.16E+03	4.08E-02
700	4.39E+00	6.50E-01	-1.71E-04	4.66E-05		2.55E+03	-3.15E+02	-3.71E+02	1.49E-02
701	4.46E+00	3.28E-01	-5.52E-05	6.18E-04		-4.02E+02	-2.15E+03	-6.13E+03	9.36E-02
702	-9.70E-02	1.55E+00	-3.76E-04	8.96E-05		9.03E+01	3.24E+01	8.16E+01	1.30E-03
703	-9.47E-02	1.73E+00	0.00E+00	0.00E+00		2.42E+02	-1.79E+02	3.79E+01	2.29E-03
704	-6.41E-02	1.52E+00	-4.41E-04	3.14E-05		-5.18E+01	8.97E+01	6.67E+01	1.52E-03
705	8.45E-02	1.56E+00	-3.88E-04	-1.73E-04		-1.95E+02	1.28E+02	1.10E+02	1.97E-03
706	2.00E-01	1.82E+00	0.00E+00	0.00E+00		-3.04E+02	2.60E+02	5.49E+01	3.08E-03
707	-1.69E+00	2.52E+00	2.51E-04	4.50E-05		-1.21E+03	-1.65E+03	-2.29E+03	4.72E-02
708	-1.53E+00	2.50E+00	0.00E+00	0.00E+00		-2.18E+02	-3.42E+03	-1.03E+03	1.44E-02
709	-1.44E+00	2.48E+00	-3.18E-05	-4.83E-05		4.82E+01	5.86E+02	3.54E+02	6.00E-03
710	-1.26E+00	2.44E+00	0.00E+00	0.00E+00		2.56E+02	4.72E+00	4.56E+02	4.87E-03
711	-1.18E+00	2.39E+00	-9.86E-05	3.26E-05		2.15E+02	-1.92E+02	2.45E+02	3.78E-03
712	-1.00E+00	2.35E+00	0.00E+00	0.00E+00		2.09E+02	-2.89E+02	2.02E+02	3.28E-03
713	-9.30E-01	2.27E+00	-1.44E-04	5.81E-05		1.96E+02	-1.77E+02	1.60E+02	2.85E-03
714	-7.50E-01	2.24E+00	0.00E+00	0.00E+00		2.22E+02	-2.16E+02	1.50E+02	2.82E-03

715	-6.95E-01	2.13E+00	-1.53E-04	9.72E-05		1.93E+02	-1.96E+02	8.60E+01	2.42E-03
716	-5.14E-01	2.09E+00	0.00E+00	0.00E+00		2.14E+02	-2.10E+02	8.43E+01	2.35E-03
717	-4.76E-01	1.96E+00	-1.55E-04	1.13E-04		1.94E+02	-1.72E+02	2.46E+01	2.09E-03
718	-2.94E-01	1.93E+00	0.00E+00	0.00E+00		1.61E+02	-1.93E+02	1.12E+01	2.07E-03
719	-2.76E-01	1.76E+00	-1.54E-04	1.64E-04		1.45E+02	-1.81E+02	2.29E+01	1.78E-03
720	-9.70E-02	-1.55E+00	3.76E-04	8.96E-05		-9.03E+01	-3.24E+01	8.16E+01	1.30E-03
721	-9.47E-02	-1.73E+00	0.00E+00	0.00E+00		-2.42E+02	1.79E+02	3.79E+01	2.29E-03
722	-6.41E-02	-1.52E+00	4.41E-04	3.14E-05		5.18E+01	-8.97E+01	6.67E+01	1.52E-03
723	8.45E-02	-1.56E+00	3.88E-04	-1.73E-04		1.95E+02	-1.28E+02	1.10E+02	1.97E-03
724	2.00E-01	-1.82E+00	0.00E+00	0.00E+00		3.04E+02	-2.60E+02	5.49E+01	3.08E-03
725	-1.69E+00	-2.52E+00	-2.50E-04	4.50E-05		1.21E+03	1.65E+03	-2.29E+03	4.72E-02
726	-1.53E+00	-2.50E+00	0.00E+00	0.00E+00		2.18E+02	3.42E+03	-1.04E+03	1.44E-02
727	-1.44E+00	-2.48E+00	3.18E-05	-4.83E-05		-4.80E+01	-5.86E+02	3.54E+02	6.00E-03
728	-1.26E+00	-2.44E+00	0.00E+00	0.00E+00		-2.56E+02	-4.25E+00	4.56E+02	4.87E-03
729	-1.18E+00	-2.39E+00	9.86E-05	3.26E-05		-2.15E+02	1.92E+02	2.45E+02	3.78E-03
730	-1.00E+00	-2.35E+00	0.00E+00	0.00E+00		-2.09E+02	2.89E+02	2.02E+02	3.28E-03
731	-9.30E-01	-2.27E+00	1.44E-04	5.81E-05		-1.96E+02	1.77E+02	1.60E+02	2.85E-03
732	-7.50E-01	-2.24E+00	0.00E+00	0.00E+00		-2.22E+02	2.16E+02	1.50E+02	2.82E-03
733	-6.95E-01	-2.13E+00	1.53E-04	9.72E-05		-1.93E+02	1.96E+02	8.60E+01	2.42E-03
734	-5.14E-01	-2.09E+00	0.00E+00	0.00E+00		-2.14E+02	2.10E+02	8.43E+01	2.35E-03
735	-4.76E-01	-1.96E+00	1.55E-04	1.13E-04		-1.94E+02	1.72E+02	2.46E+01	2.09E-03
736	-2.94E-01	-1.93E+00	0.00E+00	0.00E+00		-1.61E+02	1.93E+02	1.12E+01	2.07E-03
737	-2.76E-01	-1.76E+00	1.54E-04	1.64E-04		-1.45E+02	1.81E+02	2.29E+01	1.78E-03
738	1.13E+00	2.39E+00	0.00E+00	0.00E+00		-1.25E+02	1.18E+02	1.64E+02	2.09E-03
739	1.42E+00	2.33E+00	-2.69E-04	-5.95E-05		-6.38E+01	6.60E+01	1.50E+02	1.88E-03
740	6.36E-01	2.16E+00	0.00E+00	0.00E+00		-1.87E+02	2.07E+02	9.06E+01	2.34E-03
741	9.26E-01	2.17E+00	-2.54E-04	-1.10E-04		-1.38E+02	1.29E+02	1.20E+02	2.04E-03
742	4.72E-01	1.91E+00	-2.40E-04	-1.94E-04		-1.84E+02	2.00E+02	6.97E+01	2.33E-03
743	1.13E+00	-2.39E+00	0.00E+00	0.00E+00		1.25E+02	-1.18E+02	1.64E+02	2.09E-03
744	1.42E+00	-2.33E+00	2.69E-04	-5.95E-05		6.38E+01	-6.60E+01	1.50E+02	1.88E-03
745	6.36E-01	-2.16E+00	0.00E+00	0.00E+00		1.87E+02	-2.07E+02	9.06E+01	2.34E-03
746	9.26E-01	-2.17E+00	2.54E-04	-1.10E-04		1.38E+02	-1.29E+02	1.20E+02	2.04E-03
747	4.72E-01	-1.91E+00	2.40E-04	-1.94E-04		1.84E+02	-2.00E+02	6.97E+01	2.33E-03
748	-3.56E+00	1.62E-01	-5.28E-05	-6.22E-04		7.63E-02	4.17E-02	4.43E+00	1.89E-04
749	-3.72E+00	0.00E+00	2.10E-11	-6.50E-04		-1.85E-06	-6.65E-06	-3.14E+01	3.41E-04
750	-3.56E+00	-1.62E-01	5.28E-05	-6.22E-04		-7.61E-02	-4.16E-02	4.43E+00	1.89E-04
751	-3.86E+00	1.68E-01	-4.74E-05	-6.14E-04		-8.36E+00	8.40E+00	-6.21E+01	6.92E-04
752	-4.03E+00	0.00E+00	1.42E-13	-5.24E-04		1.84E-05	4.31E-04	-8.68E+01	9.65E-04
753	-3.86E+00	-1.68E-01	4.74E-05	-6.14E-04		8.36E+00	-8.40E+00	-6.21E+01	6.92E-04
754	-4.17E+00	1.75E-01	-2.89E-05	-3.91E-04		-1.48E+01	1.48E+01	-1.06E+02	1.20E-03
755	-4.17E+00	-1.75E-01	2.89E-05	-3.91E-04		1.48E+01	-1.48E+01	-1.06E+02	1.20E-03
756	-1.95E+00	2.51E+00	9.04E-04	-1.47E-04		2.36E+03	-4.06E+03	2.53E+03	4.87E-02
757	-2.03E+00	2.50E+00	-2.59E-04	-7.86E-05		-8.78E+01	3.49E+03	2.72E+03	7.56E-02
758	-1.88E+00	2.50E+00	8.04E-04	-1.25E-04		2.47E+02	-3.69E+03	8.74E+03	9.93E-02
759	-1.95E+00	2.52E+00	9.43E-04	-2.89E-04		1.63E+03	7.60E+02	-2.04E+03	2.27E-02
760	-2.06E+00	2.51E+00	2.97E-04	4.29E-04		-2.55E+02	4.42E+03	2.95E+03	2.97E-02
761	-1.85E+00	2.51E+00	1.44E-03	-2.78E-04		6.57E+01	-3.20E+03	1.79E+03	4.21E-02
762	-2.09E+00	2.52E+00	3.43E-04	4.64E-04		3.65E+02	-4.55E+03	-9.21E+02	3.70E-02

763	-1.83E+00	2.52E+00	1.19E-03	-3.45E-04		-6.75E+02	1.02E+03	-5.38E+03	4.95E-02
764	-4.85E-01	1.23E+00	-4.07E-04	4.27E-04		-3.93E+00	1.57E+01	-8.69E+01	8.79E-04
765	-6.44E-01	1.28E+00	-4.16E-04	4.59E-04		-2.56E+01	1.89E+01	-2.40E+01	3.80E-04
766	-5.83E-01	1.07E+00	-3.17E-04	4.56E-04		2.06E+01	-2.06E+01	-4.66E+01	5.56E-04
767	-2.91E-01	1.39E+00	-4.68E-04	2.88E-04		-4.58E+01	2.61E+01	-7.98E+01	8.93E-04
768	-4.61E-01	1.43E+00	-4.55E-04	4.24E-04		1.36E+01	-8.76E+00	-4.96E+01	6.28E-04
769	-4.10E-01	1.22E+00	-4.04E-04	3.74E-04		-2.70E+01	1.49E+01	-1.20E+02	1.33E-03
770	-2.78E-01	1.58E+00	-3.65E-04	2.64E-04		3.33E+01	-3.72E+01	1.28E+01	7.08E-04
771	-2.37E-01	1.37E+00	-4.84E-04	2.24E-04		-1.40E+02	4.31E+01	-9.26E+01	1.35E-03
772	-1.95E+00	-2.52E+00	-9.39E-04	-2.89E-04		-1.63E+03	-7.69E+02	-2.04E+03	2.27E-02
773	-2.09E+00	-2.52E+00	-3.42E-04	4.64E-04		-3.63E+02	4.56E+03	-9.21E+02	3.71E-02
774	-1.83E+00	-2.52E+00	-1.19E-03	-3.45E-04		6.77E+02	-1.02E+03	-5.38E+03	4.95E-02
775	-1.95E+00	-2.51E+00	-9.02E-04	-1.47E-04		-2.37E+03	4.06E+03	2.51E+03	4.87E-02
776	-2.06E+00	-2.51E+00	-2.95E-04	4.29E-04		2.64E+02	-4.42E+03	2.97E+03	3.01E-02
777	-1.85E+00	-2.51E+00	-1.44E-03	-2.78E-04		-6.90E+01	3.20E+03	1.80E+03	4.21E-02
778	-2.03E+00	-2.50E+00	2.63E-04	-7.87E-05		9.43E+01	-3.47E+03	2.69E+03	7.56E-02
779	-1.88E+00	-2.50E+00	-8.04E-04	-1.25E-04		-2.41E+02	3.69E+03	8.74E+03	9.93E-02
780	-2.91E-01	-1.39E+00	4.68E-04	2.88E-04		4.58E+01	-2.61E+01	-7.98E+01	8.93E-04
781	-2.78E-01	-1.58E+00	3.65E-04	2.64E-04		-3.33E+01	3.72E+01	1.28E+01	7.08E-04
782	-2.37E-01	-1.37E+00	4.84E-04	2.24E-04		1.40E+02	-4.31E+01	-9.26E+01	1.35E-03
783	-4.85E-01	-1.23E+00	4.07E-04	4.27E-04		3.93E+00	-1.57E+01	-8.69E+01	8.79E-04
784	-4.61E-01	-1.43E+00	4.55E-04	4.24E-04		-1.36E+01	8.76E+00	-4.96E+01	6.28E-04
785	-4.10E-01	-1.22E+00	4.04E-04	3.74E-04		2.70E+01	-1.49E+01	-1.20E+02	1.33E-03
786	-6.44E-01	-1.28E+00	4.16E-04	4.59E-04		2.56E+01	-1.89E+01	-2.40E+01	3.80E-04
787	-5.83E-01	-1.07E+00	3.17E-04	4.56E-04		-2.06E+01	2.06E+01	-4.66E+01	5.56E-04
788	8.67E-02	1.39E+00	-6.19E-04	-2.58E-04		-4.74E+01	8.64E+01	-9.70E+01	1.33E-03
789	2.54E-01	1.42E+00	-6.48E-04	-4.28E-04		-5.93E+01	7.65E+01	-1.99E+01	9.09E-04
790	3.57E-01	1.65E+00	-5.01E-04	-3.57E-04		-1.38E+02	1.35E+02	5.26E+01	1.65E-03
791	2.38E-01	1.26E+00	-6.50E-04	-4.62E-04		-4.32E+01	4.35E+01	-9.77E+01	1.21E-03
792	4.23E-01	1.28E+00	-6.84E-04	-5.25E-04		-3.58E+00	4.67E+00	-4.70E+01	6.30E-04
793	5.15E-01	1.47E+00	-7.19E-04	-5.08E-04		-5.38E+01	3.98E+01	2.00E+01	6.29E-04
794	3.88E-01	1.13E+00	-5.65E-04	-5.18E-04		2.55E+01	-2.63E+01	-8.90E+01	1.12E-03
795	6.72E-01	1.30E+00	-6.69E-04	-4.78E-04		4.23E+01	-4.90E+01	-4.42E+01	7.25E-04
796	3.88E-01	-1.13E+00	5.65E-04	-5.18E-04		-2.55E+01	2.63E+01	-8.90E+01	1.12E-03
797	4.23E-01	-1.28E+00	6.84E-04	-5.25E-04		3.58E+00	-4.67E+00	-4.70E+01	6.30E-04
798	6.72E-01	-1.30E+00	6.69E-04	-4.78E-04		-4.23E+01	4.90E+01	-4.42E+01	7.25E-04
799	2.38E-01	-1.26E+00	6.50E-04	-4.62E-04		4.32E+01	-4.35E+01	-9.77E+01	1.21E-03
800	2.54E-01	-1.42E+00	6.48E-04	-4.28E-04		5.93E+01	-7.65E+01	-1.99E+01	9.09E-04
801	5.15E-01	-1.47E+00	7.19E-04	-5.08E-04		5.38E+01	-3.98E+01	2.00E+01	6.29E-04
802	8.67E-02	-1.39E+00	6.19E-04	-2.58E-04		4.74E+01	-8.64E+01	-9.70E+01	1.33E-03
803	3.57E-01	-1.65E+00	5.01E-04	-3.57E-04		1.38E+02	-1.35E+02	5.26E+01	1.65E-03
804	1.75E+00	1.61E+00	-7.72E-04	-7.32E-05		5.30E+00	-6.05E+00	-2.69E+01	3.26E-04
805	1.95E+00	1.78E+00	-8.33E-04	-2.04E-06		8.98E-01	-9.29E-01	2.74E+01	3.24E-04
806	2.11E+00	1.61E+00	-7.73E-04	6.04E-05		-2.72E+00	2.91E+00	-2.56E+01	3.09E-04
807	1.73E+00	1.91E+00	-8.03E-04	-8.00E-05		-1.04E+01	9.91E+00	7.18E+01	8.05E-04
808	1.95E+00	2.08E+00	-6.90E-04	-3.44E-06		6.96E-01	-5.18E-01	1.11E+02	1.22E-03
809	2.11E+00	1.92E+00	-8.00E-04	5.72E-05		9.29E+00	-9.23E+00	7.39E+01	8.18E-04
810	1.70E+00	2.21E+00	-5.26E-04	-5.72E-05		-2.63E+01	2.58E+01	1.37E+02	1.58E-03

811	2.12E+00	2.22E+00	-5.18E-04	3.52E-05		1.83E+01	-1.79E+01	1.40E+02	1.58E-03
812	4.45E+00	0.00E+00	1.11E-07	2.80E-03		4.07E+00	-9.06E-01	2.20E+03	4.74E-02
813	4.44E+00	8.11E-02	-1.37E-04	1.66E-03		-7.72E+02	-5.55E+02	5.18E+03	1.09E-01
814	4.44E+00	-8.11E-02	1.37E-04	1.66E-03		7.65E+02	5.59E+02	5.19E+03	1.09E-01
815	4.47E+00	0.00E+00	5.06E-08	2.47E-03		-2.45E+00	1.47E+00	-7.08E+03	6.19E-02
816	4.45E+00	1.14E-01	-6.57E-04	2.00E-03		-9.09E+03	-2.89E+02	5.65E+02	4.96E-02
817	4.45E+00	-1.14E-01	6.57E-04	2.00E-03		9.10E+03	2.88E+02	5.71E+02	4.96E-02
818	4.46E+00	1.48E-01	-8.59E-04	1.48E-03		4.95E+03	-1.24E+03	-6.99E+03	9.80E-02
819	4.46E+00	-1.48E-01	8.59E-04	1.48E-03		-4.93E+03	1.25E+03	-6.98E+03	9.80E-02
820	1.95E+00	-1.78E+00	8.33E-04	-2.04E-06		-8.98E-01	9.29E-01	2.74E+01	3.24E-04
821	2.11E+00	-1.61E+00	7.73E-04	6.04E-05		2.72E+00	-2.91E+00	-2.56E+01	3.09E-04
822	1.75E+00	-1.61E+00	7.72E-04	-7.32E-05		-5.30E+00	6.05E+00	-2.69E+01	3.26E-04
823	1.95E+00	-2.08E+00	6.90E-04	-3.44E-06		-6.95E-01	5.18E-01	1.11E+02	1.22E-03
824	2.11E+00	-1.92E+00	8.00E-04	5.72E-05		-9.29E+00	9.23E+00	7.39E+01	8.18E-04
825	1.73E+00	-1.91E+00	8.03E-04	-8.00E-05		1.04E+01	-9.91E+00	7.18E+01	8.05E-04
826	2.12E+00	-2.22E+00	5.18E-04	3.52E-05		-1.83E+01	1.79E+01	1.40E+02	1.58E-03
827	1.70E+00	-2.21E+00	5.26E-04	-5.72E-05		2.63E+01	-2.58E+01	1.37E+02	1.58E-03
828	-5.49E-01	2.07E-01	1.53E-03	1.84E-03		-1.37E+04	1.33E+04	-8.43E+03	2.12E-01
829	-5.44E-01	1.44E-01	-3.96E-05	-6.85E-04		-5.72E+03	1.70E+03	-2.95E+04	3.90E-01
830	-4.39E-01	3.01E-01	-8.27E-05	-6.56E-04		-3.75E+03	4.15E+03	-8.08E+02	6.88E-02
831	-3.52E-01	4.34E-01	4.30E-04	-5.16E-05		-1.77E+03	1.76E+03	-2.23E+02	1.77E-02
832	-2.19E-01	5.09E-01	-1.40E-04	-5.95E-04		-5.61E+02	5.73E+01	2.84E+02	8.57E-03
833	-1.38E-01	6.42E-01	-8.47E-05	-4.14E-04		-1.92E+02	5.14E+02	1.32E+01	3.51E-03
834	1.82E-02	6.96E-01	-1.91E-04	-5.30E-04		-1.51E+02	2.12E+02	2.75E+01	2.11E-03
835	9.20E-02	8.29E-01	-2.15E-04	-4.80E-04		-8.37E+01	4.70E+01	-9.78E+01	1.41E-03
836	2.72E-01	8.60E-01	-2.37E-04	-4.60E-04		1.05E+02	-1.32E+02	-5.25E+01	1.11E-03
837	3.36E-01	9.94E-01	-4.00E-04	-4.93E-04		7.62E+01	-5.53E+01	-1.01E+02	1.49E-03
838	-5.49E-01	-2.07E-01	-1.53E-03	1.84E-03		1.37E+04	-1.33E+04	-8.43E+03	2.12E-01
839	-4.39E-01	-3.01E-01	8.27E-05	-6.56E-04		3.75E+03	-4.15E+03	-8.09E+02	6.88E-02
840	-5.44E-01	-1.44E-01	3.96E-05	-6.85E-04		5.68E+03	-1.59E+03	-2.95E+04	3.90E-01
841	3.36E-01	-9.94E-01	4.00E-04	-4.93E-04		-7.62E+01	5.53E+01	-1.01E+02	1.49E-03
842	2.72E-01	-8.60E-01	2.37E-04	-4.60E-04		-1.05E+02	1.32E+02	-5.25E+01	1.11E-03
843	9.20E-02	-8.29E-01	2.15E-04	-4.80E-04		8.36E+01	-4.70E+01	-9.77E+01	1.41E-03
844	1.82E-02	-6.96E-01	1.91E-04	-5.30E-04		1.51E+02	-2.12E+02	2.75E+01	2.11E-03
845	-1.38E-01	-6.42E-01	8.47E-05	-4.14E-04		1.92E+02	-5.14E+02	1.31E+01	3.52E-03
846	-2.19E-01	-5.09E-01	1.40E-04	-5.95E-04		5.62E+02	-5.79E+01	2.84E+02	8.56E-03
847	-3.52E-01	-4.34E-01	-4.29E-04	-5.18E-05		1.77E+03	-1.76E+03	-2.24E+02	1.77E-02
848	-5.49E-01	-1.04E-01	2.30E-04	1.27E-03		-7.44E+03	1.32E+03	-3.19E+04	3.50E-01
849	-5.44E-01	-4.80E-02	1.32E-05	-6.85E-04		-2.53E+03	7.38E+01	-3.79E+04	4.06E-01
850	-5.48E-01	1.11E-16	9.16E-08	1.25E-03		-2.65E+00	6.48E+01	-3.32E+04	3.81E-01
851	-5.44E-01	4.80E-02	-1.32E-05	-6.85E-04		2.53E+03	9.60E+01	-3.79E+04	4.06E-01
852	-5.49E-01	1.04E-01	-2.30E-04	1.26E-03		7.44E+03	-1.19E+03	-3.19E+04	3.50E-01
853	-7.20E-01	7.76E-01	-2.13E-04	3.37E-04		-3.49E+01	7.98E+01	1.69E+02	1.87E-03
854	-6.61E-01	9.16E-01	-2.60E-04	4.39E-04		9.38E+00	-2.20E+01	5.89E+01	8.39E-04
855	-6.90E-01	6.36E-01	-1.75E-04	3.45E-04		-7.15E+01	1.99E+02	5.18E+02	5.54E-03
856	-6.47E-01	7.65E-01	-2.11E-04	5.21E-04		7.92E+01	-1.31E+02	2.07E+02	2.76E-03
857	-6.65E-01	4.96E-01	-1.37E-04	3.52E-04		-3.67E+02	3.66E+02	1.20E+03	1.30E-02
858	-6.38E-01	6.12E-01	-1.76E-04	6.98E-04		4.48E+01	-1.40E+02	6.46E+02	7.28E-03

859	-6.47E-01	3.55E-01	-9.77E-05	3.57E-04		-3.42E+02	8.50E+02	4.08E+03	5.24E-02
860	-6.33E-01	4.56E-01	-1.46E-04	8.00E-04		2.11E+02	-1.43E+02	1.43E+03	1.81E-02
861	-6.35E-01	2.13E-01	-5.87E-05	3.61E-04		-2.36E+02	2.36E+03	1.86E+04	2.03E-01
862	-6.33E-01	2.98E-01	-1.99E-04	1.24E-03		-1.53E+03	-1.80E+02	9.77E+03	1.00E-01
863	-6.29E-01	7.12E-02	-1.96E-05	3.62E-04		-4.91E+03	1.63E+03	3.64E+04	3.71E-01
864	-6.25E-01	1.49E-01	-6.89E-05	2.21E-03		-4.73E+02	4.22E+02	2.51E+04	2.76E-01
865	-6.29E-01	-7.12E-02	1.96E-05	3.62E-04		4.91E+03	-1.48E+03	3.64E+04	3.71E-01
866	-6.22E-01	5.07E-16	-1.25E-08	2.40E-03		-8.09E-01	5.35E+01	2.97E+04	3.50E-01
867	-6.35E-01	-2.13E-01	5.87E-05	3.61E-04		2.37E+02	-2.32E+03	1.86E+04	2.03E-01
868	-6.25E-01	-1.49E-01	6.89E-05	2.21E-03		4.74E+02	-3.51E+02	2.51E+04	2.76E-01
869	-6.47E-01	-3.55E-01	9.77E-05	3.57E-04		3.42E+02	-8.48E+02	4.08E+03	5.24E-02
870	-6.33E-01	-2.98E-01	1.99E-04	1.24E-03		1.53E+03	1.91E+02	9.77E+03	1.00E-01
871	-6.65E-01	-4.96E-01	1.37E-04	3.52E-04		3.67E+02	-3.66E+02	1.20E+03	1.30E-02
872	-6.33E-01	-4.56E-01	1.46E-04	8.00E-04		-2.11E+02	1.44E+02	1.43E+03	1.81E-02
873	-6.90E-01	-6.36E-01	1.75E-04	3.45E-04		7.15E+01	-1.99E+02	5.18E+02	5.54E-03
874	-6.38E-01	-6.12E-01	1.76E-04	6.98E-04		-4.48E+01	1.40E+02	6.46E+02	7.28E-03
875	-7.20E-01	-7.76E-01	2.13E-04	3.37E-04		3.49E+01	-7.98E+01	1.69E+02	1.87E-03
876	-6.47E-01	-7.65E-01	2.11E-04	5.21E-04		-7.91E+01	1.31E+02	2.07E+02	2.76E-03
877	-6.61E-01	-9.16E-01	2.60E-04	4.39E-04		-9.38E+00	2.20E+01	5.89E+01	8.39E-04
878	-2.21E+00	2.50E+00	7.72E-04	4.62E-04		6.68E+02	-1.58E+03	-2.36E+03	2.74E-02
879	-2.39E+00	2.48E+00	2.29E-06	-3.57E-04		2.78E+02	3.58E+03	-3.28E+02	9.67E-03
880	-2.46E+00	2.46E+00	-1.53E-04	-2.28E-04		-1.29E+02	-4.79E+02	1.63E+02	3.46E-03
881	-2.69E+00	2.38E+00	-1.88E-04	8.27E-05		-2.21E+02	-2.67E+02	3.65E+02	4.02E-03
882	-2.76E+00	2.30E+00	-3.23E-04	-6.32E-05		-2.71E+02	3.90E+02	2.71E+02	3.77E-03
883	-2.99E+00	2.21E+00	-2.30E-04	-1.59E-04		-1.64E+02	2.25E+02	1.07E+02	2.65E-03
884	-3.04E+00	2.10E+00	-3.59E-04	-2.29E-04		-1.39E+02	1.17E+02	6.63E+01	1.83E-03
885	-3.26E+00	2.00E+00	-2.67E-04	-1.79E-04		-1.83E+02	1.77E+02	4.16E+01	2.04E-03
886	-3.29E+00	1.87E+00	-3.64E-04	-2.86E-04		-1.48E+02	1.46E+02	1.22E+01	1.63E-03
887	-3.51E+00	1.75E+00	-2.51E-04	-2.43E-04		-1.54E+02	1.54E+02	-1.30E+00	1.74E-03
888	-3.50E+00	1.60E+00	-3.33E-04	-3.62E-04		-1.18E+02	1.18E+02	-2.28E+01	1.35E-03
889	-3.72E+00	1.48E+00	-2.26E-04	-2.91E-04		-1.28E+02	1.28E+02	-4.23E+01	1.51E-03
890	-3.69E+00	1.32E+00	-2.86E-04	-4.19E-04		-9.47E+01	9.42E+01	-4.90E+01	1.18E-03
891	-3.90E+00	1.18E+00	-1.87E-04	-3.30E-04		-1.01E+02	1.01E+02	-6.85E+01	1.37E-03
892	-3.83E+00	1.01E+00	-2.24E-04	-4.64E-04		-7.08E+01	7.07E+01	-6.63E+01	1.08E-03
893	-4.03E+00	8.58E-01	-1.39E-04	-3.60E-04		-7.30E+01	7.31E+01	-8.77E+01	1.28E-03
894	-3.94E+00	6.81E-01	-1.54E-04	-4.97E-04		-4.72E+01	4.71E+01	-7.80E+01	1.01E-03
895	-4.12E+00	5.21E-01	-8.55E-05	-3.81E-04		-4.42E+01	4.41E+01	-9.98E+01	1.22E-03
896	-4.01E+00	3.43E-01	-7.84E-05	-5.17E-04		-2.36E+01	2.35E+01	-8.47E+01	9.77E-04
897	-2.14E+00	2.50E+00	9.26E-04	8.67E-04		-1.80E+03	2.61E+03	-5.82E+02	3.79E-02
898	-2.29E+00	2.48E+00	4.62E-04	-1.72E-04		1.45E+03	-2.38E+03	-1.60E+03	9.87E-03
899	-2.33E+00	2.47E+00	1.01E-04	-4.69E-04		8.47E+02	-5.12E+02	6.68E+02	2.68E-02
900	-2.54E+00	2.38E+00	-3.37E-04	-2.43E-05		-2.23E+00	9.86E+00	5.04E+01	3.56E-03
901	-2.60E+00	2.29E+00	-5.78E-04	3.67E-05		-1.24E+02	6.36E+01	2.48E+02	3.32E-03
902	-2.81E+00	2.19E+00	-4.36E-04	-2.17E-04		-2.04E+02	2.15E+02	1.29E+02	2.69E-03
903	-2.85E+00	2.07E+00	-4.96E-04	-3.08E-04		-7.68E+01	4.91E+01	1.09E+01	1.29E-03
904	-3.06E+00	1.97E+00	-4.61E-04	-3.15E-04		-1.06E+02	1.12E+02	2.80E+01	1.28E-03
905	-3.07E+00	1.83E+00	-5.18E-04	-3.79E-04		-6.98E+01	7.08E+01	1.74E+01	8.02E-04
906	-3.28E+00	1.72E+00	-4.39E-04	-3.94E-04		-1.07E+02	1.05E+02	-5.45E+00	1.17E-03

907	-3.26E+00	1.57E+00	-4.61E-04	-4.67E-04		-5.55E+01	5.41E+01	-1.26E+01	6.26E-04
908	-3.47E+00	1.44E+00	-3.83E-04	-4.68E-04		-8.00E+01	8.06E+01	-2.85E+01	9.40E-04
909	-3.42E+00	1.28E+00	-3.87E-04	-5.32E-04		-3.98E+01	3.96E+01	-1.90E+01	4.84E-04
910	-3.63E+00	1.14E+00	-3.12E-04	-5.26E-04		-6.08E+01	6.11E+01	-4.38E+01	8.28E-04
911	-3.55E+00	9.75E-01	-3.00E-04	-5.84E-04		-2.81E+01	2.77E+01	-2.56E+01	4.15E-04
912	-3.74E+00	8.30E-01	-2.30E-04	-5.70E-04		-4.25E+01	4.28E+01	-5.34E+01	7.54E-04
913	-3.65E+00	6.57E-01	-2.04E-04	-6.21E-04		-1.80E+01	1.78E+01	-2.89E+01	3.71E-04
914	-3.82E+00	5.03E-01	-1.41E-04	-5.99E-04		-2.52E+01	2.53E+01	-5.93E+01	7.11E-04
915	-3.70E+00	3.31E-01	-1.03E-04	-6.43E-04		-8.77E+00	8.67E+00	-3.08E+01	3.48E-04
916	-2.19E+00	2.49E+00	1.35E-03	8.69E-04		2.04E+03	-1.65E+04	-7.85E+03	2.25E-01
917	-2.40E+00	2.38E+00	-3.04E-04	-3.09E-04		1.32E+02	-1.97E+02	3.23E+02	9.90E-03
918	-2.64E+00	2.17E+00	-6.65E-04	-2.22E-04		-2.62E+02	2.41E+02	1.34E+02	2.97E-03
919	-2.86E+00	1.94E+00	-5.45E-04	-3.29E-04		-1.04E+01	-5.38E+00	3.30E+01	5.49E-04
920	-3.05E+00	1.68E+00	-5.24E-04	-4.21E-04		-2.54E+01	2.94E+01	8.51E+00	3.47E-04
921	-3.22E+00	1.40E+00	-4.42E-04	-4.88E-04		-6.84E+00	7.38E+00	3.42E+00	2.51E-04
922	-3.35E+00	1.11E+00	-3.55E-04	-5.42E-04		-3.76E+00	4.70E+00	2.97E+00	2.20E-04
923	-3.46E+00	8.02E-01	-2.59E-04	-5.82E-04		-7.92E-01	1.39E+00	3.47E+00	2.04E-04
924	-3.53E+00	4.85E-01	-1.57E-04	-6.09E-04		-7.62E-02	4.16E-01	4.05E+00	1.94E-04
925	-4.57E-01	1.79E+00	-2.83E-04	2.62E-04		1.64E+02	-1.56E+02	1.82E+01	1.73E-03
926	-4.48E-01	1.62E+00	-3.95E-04	3.70E-04		8.61E+01	-8.18E+01	2.40E+00	9.01E-04
927	-6.19E-01	1.66E+00	-4.58E-04	4.24E-04		7.31E+01	-7.65E+01	-6.03E+00	8.39E-04
928	-6.20E-01	1.48E+00	-4.69E-04	4.70E-04		1.23E+01	-1.35E+01	-1.39E+01	2.99E-04
929	-7.81E-01	1.53E+00	-4.84E-04	4.47E-04		-9.30E+00	7.05E+00	5.53E+00	2.42E-04
930	-6.56E-01	1.99E+00	-2.96E-04	2.11E-04		1.64E+02	-1.67E+02	3.76E+01	1.92E-03
931	-6.28E-01	1.84E+00	-3.93E-04	3.23E-04		1.32E+02	-1.37E+02	8.78E+00	1.48E-03
932	-7.99E-01	1.88E+00	-4.85E-04	3.53E-04		1.08E+02	-1.04E+02	1.73E+01	1.19E-03
933	-7.80E-01	1.72E+00	-5.09E-04	4.25E-04		5.51E+01	-5.48E+01	4.23E+00	5.86E-04
934	-9.42E-01	1.78E+00	-5.47E-04	3.80E-04		1.11E+01	-1.60E+01	1.78E+01	3.61E-04
935	-8.75E-01	2.16E+00	-2.95E-04	1.60E-04		1.84E+02	-1.96E+02	9.89E+01	2.39E-03
936	-8.28E-01	2.03E+00	-4.07E-04	2.59E-04		1.55E+02	-1.39E+02	4.54E+01	1.74E-03
937	-1.00E+00	2.08E+00	-4.92E-04	2.75E-04		1.06E+02	-1.29E+02	5.38E+01	1.49E-03
938	-9.61E-01	1.94E+00	-5.47E-04	3.40E-04		6.37E+01	-5.79E+01	2.85E+01	7.72E-04
939	-1.12E+00	2.00E+00	-5.68E-04	2.97E-04		1.64E+01	-7.16E+00	3.07E+01	5.14E-04
940	-1.11E+00	2.31E+00	-2.41E-04	1.03E-04		1.87E+02	-1.56E+02	1.83E+02	2.97E-03
941	-1.05E+00	2.21E+00	-3.80E-04	1.70E-04		1.45E+02	-1.66E+02	1.14E+02	2.27E-03
942	-1.22E+00	2.26E+00	-4.65E-04	1.50E-04		2.27E+02	-1.30E+02	1.84E+02	2.77E-03
943	-1.16E+00	2.14E+00	-5.32E-04	2.49E-04		1.21E+02	-1.14E+02	3.19E+01	1.54E-03
944	-1.33E+00	2.21E+00	-6.38E-04	1.69E-04		1.14E+02	-1.45E+02	1.03E+02	1.96E-03
945	-1.36E+00	2.43E+00	-1.73E-04	3.40E-05		1.42E+02	-3.99E+02	2.75E+02	4.24E-03
946	-1.28E+00	2.36E+00	-3.38E-04	5.31E-05		2.46E+02	7.11E+01	2.67E+02	3.12E-03
947	-1.45E+00	2.41E+00	-1.87E-04	1.73E-04		-3.00E+02	-5.76E+02	5.43E+01	4.59E-03
948	-1.38E+00	2.33E+00	-5.15E-04	4.52E-06		3.06E+01	3.05E+02	2.05E+02	3.57E-03
949	-1.55E+00	2.40E+00	-1.26E-04	7.11E-05		-1.42E+02	1.97E+02	7.83E+02	1.05E-02
950	-1.60E+00	2.50E+00	1.93E-04	4.61E-05		-7.25E+02	3.13E+03	-6.63E+02	2.17E-02
951	-1.53E+00	2.48E+00	7.54E-05	-4.07E-05		-4.79E+02	-1.44E+02	5.45E+01	1.90E-02
952	-1.67E+00	2.50E+00	4.37E-04	-3.25E-04		-4.51E+02	8.54E+03	1.43E+03	4.60E-02
953	-1.62E+00	2.49E+00	4.03E-04	-4.67E-04		-4.37E+02	-1.35E+01	5.51E+02	3.89E-02
954	-1.73E+00	2.49E+00	8.03E-05	-4.02E-04		1.89E+03	-4.95E+03	1.08E+04	9.06E-02

955	-1.74E+00	2.51E+00	7.59E-04	2.25E-05		-1.41E+03	-1.93E+03	6.44E+02	3.50E-02
956	-1.78E+00	2.50E+00	7.01E-04	2.28E-04		-6.99E+02	-1.20E+03	6.03E+03	8.26E-02
957	-3.70E+00	-3.31E-01	1.03E-04	-6.43E-04		8.77E+00	-8.67E+00	-3.08E+01	3.48E-04
958	-3.53E+00	-4.85E-01	1.57E-04	-6.09E-04		7.54E-02	-4.16E-01	4.05E+00	1.94E-04
959	-3.65E+00	-6.57E-01	2.04E-04	-6.21E-04		1.80E+01	-1.78E+01	-2.89E+01	3.71E-04
960	-3.46E+00	-8.02E-01	2.59E-04	-5.82E-04		7.96E-01	-1.39E+00	3.47E+00	2.04E-04
961	-3.55E+00	-9.75E-01	3.00E-04	-5.84E-04		2.81E+01	-2.77E+01	-2.56E+01	4.15E-04
962	-3.35E+00	-1.11E+00	3.55E-04	-5.42E-04		3.75E+00	-4.69E+00	2.97E+00	2.20E-04
963	-3.42E+00	-1.28E+00	3.87E-04	-5.32E-04		3.98E+01	-3.96E+01	-1.90E+01	4.84E-04
964	-3.22E+00	-1.40E+00	4.42E-04	-4.88E-04		6.89E+00	-7.39E+00	3.42E+00	2.51E-04
965	-3.26E+00	-1.57E+00	4.61E-04	-4.67E-04		5.55E+01	-5.40E+01	-1.26E+01	6.26E-04
966	-3.05E+00	-1.68E+00	5.24E-04	-4.21E-04		2.52E+01	-2.94E+01	8.51E+00	3.46E-04
967	-3.07E+00	-1.83E+00	5.18E-04	-3.79E-04		6.98E+01	-7.08E+01	1.74E+01	8.02E-04
968	-2.86E+00	-1.94E+00	5.46E-04	-3.29E-04		1.10E+01	5.23E+00	3.32E+01	5.49E-04
969	-2.85E+00	-2.07E+00	4.96E-04	-3.08E-04		7.71E+01	-4.93E+01	1.08E+01	1.29E-03
970	-2.64E+00	-2.17E+00	6.65E-04	-2.22E-04		2.60E+02	-2.41E+02	1.34E+02	2.96E-03
971	-2.60E+00	-2.29E+00	5.76E-04	3.63E-05		1.20E+02	-6.63E+01	2.46E+02	3.31E-03
972	-2.40E+00	-2.38E+00	3.09E-04	-3.09E-04		-1.17E+02	2.01E+02	3.32E+02	9.96E-03
973	-2.33E+00	-2.47E+00	-9.61E-05	-4.73E-04		-8.51E+02	5.17E+02	6.71E+02	2.70E-02
974	-2.19E+00	-2.49E+00	-1.36E-03	8.72E-04		-2.11E+03	1.67E+04	-8.16E+03	2.27E-01
975	-2.14E+00	-2.50E+00	-9.36E-04	8.71E-04		1.81E+03	-2.62E+03	-6.18E+02	3.84E-02
976	-4.01E+00	-3.43E-01	7.84E-05	-5.17E-04		2.36E+01	-2.35E+01	-8.47E+01	9.77E-04
977	-3.82E+00	-5.03E-01	1.41E-04	-5.99E-04		2.52E+01	-2.53E+01	-5.93E+01	7.11E-04
978	-3.94E+00	-6.81E-01	1.54E-04	-4.97E-04		4.72E+01	-4.71E+01	-7.80E+01	1.01E-03
979	-3.74E+00	-8.30E-01	2.30E-04	-5.70E-04		4.25E+01	-4.28E+01	-5.34E+01	7.54E-04
980	-3.83E+00	-1.01E+00	2.24E-04	-4.64E-04		7.08E+01	-7.07E+01	-6.63E+01	1.08E-03
981	-3.63E+00	-1.14E+00	3.12E-04	-5.26E-04		6.08E+01	-6.11E+01	-4.38E+01	8.28E-04
982	-3.69E+00	-1.32E+00	2.86E-04	-4.19E-04		9.47E+01	-9.42E+01	-4.90E+01	1.18E-03
983	-3.47E+00	-1.44E+00	3.83E-04	-4.68E-04		8.00E+01	-8.06E+01	-2.85E+01	9.40E-04
984	-3.50E+00	-1.60E+00	3.33E-04	-3.62E-04		1.18E+02	-1.18E+02	-2.28E+01	1.35E-03
985	-3.28E+00	-1.72E+00	4.39E-04	-3.94E-04		1.07E+02	-1.05E+02	-5.44E+00	1.17E-03
986	-3.29E+00	-1.87E+00	3.64E-04	-2.86E-04		1.48E+02	-1.46E+02	1.22E+01	1.63E-03
987	-3.06E+00	-1.97E+00	4.61E-04	-3.15E-04		1.06E+02	-1.12E+02	2.79E+01	1.28E-03
988	-3.04E+00	-2.10E+00	3.59E-04	-2.29E-04		1.39E+02	-1.18E+02	6.62E+01	1.83E-03
989	-2.81E+00	-2.19E+00	4.37E-04	-2.17E-04		2.05E+02	-2.15E+02	1.30E+02	2.69E-03
990	-2.76E+00	-2.30E+00	3.23E-04	-6.33E-05		2.70E+02	-3.91E+02	2.71E+02	3.77E-03
991	-2.54E+00	-2.38E+00	3.37E-04	-2.39E-05		1.87E+00	-9.78E+00	4.82E+01	3.56E-03
992	-2.46E+00	-2.46E+00	1.54E-04	-2.28E-04		1.33E+02	4.77E+02	1.63E+02	3.50E-03
993	-2.29E+00	-2.48E+00	-4.62E-04	-1.74E-04		-1.46E+03	2.36E+03	-1.62E+03	1.00E-02
994	-2.21E+00	-2.50E+00	-7.76E-04	4.63E-04		-6.76E+02	1.60E+03	-2.40E+03	2.77E-02
995	-4.12E+00	-5.21E-01	8.55E-05	-3.81E-04		4.42E+01	-4.41E+01	-9.99E+01	1.22E-03
996	-4.03E+00	-8.58E-01	1.39E-04	-3.60E-04		7.30E+01	-7.31E+01	-8.77E+01	1.28E-03
997	-3.90E+00	-1.18E+00	1.87E-04	-3.30E-04		1.01E+02	-1.01E+02	-6.85E+01	1.37E-03
998	-3.72E+00	-1.48E+00	2.26E-04	-2.91E-04		1.28E+02	-1.28E+02	-4.23E+01	1.51E-03
999	-3.51E+00	-1.75E+00	2.51E-04	-2.43E-04		1.54E+02	-1.54E+02	-1.31E+00	1.74E-03
1000	-3.26E+00	-2.00E+00	2.67E-04	-1.79E-04		1.83E+02	-1.77E+02	4.16E+01	2.04E-03
1001	-2.99E+00	-2.21E+00	2.30E-04	-1.59E-04		1.64E+02	-2.25E+02	1.07E+02	2.65E-03
1002	-2.69E+00	-2.38E+00	1.87E-04	8.27E-05		2.20E+02	2.69E+02	3.65E+02	4.02E-03

1003	-2.39E+00	-2.48E+00	-6.79E-07	-3.57E-04		-2.74E+02	-3.60E+03	-3.19E+02	9.70E-03
1004	-1.78E+00	-2.50E+00	-7.02E-04	2.28E-04		7.05E+02	1.20E+03	6.03E+03	8.27E-02
1005	-1.73E+00	-2.49E+00	-7.99E-05	-4.02E-04		-1.88E+03	4.96E+03	1.08E+04	9.07E-02
1006	-1.62E+00	-2.49E+00	-4.03E-04	-4.67E-04		4.37E+02	1.36E+01	5.51E+02	3.89E-02
1007	-1.55E+00	-2.40E+00	1.26E-04	7.11E-05		1.42E+02	-1.97E+02	7.84E+02	1.05E-02
1008	-1.38E+00	-2.33E+00	5.15E-04	4.59E-06		-3.06E+01	-3.05E+02	2.05E+02	3.57E-03
1009	-1.33E+00	-2.21E+00	6.38E-04	1.69E-04		-1.14E+02	1.45E+02	1.03E+02	1.96E-03
1010	-1.16E+00	-2.14E+00	5.32E-04	2.49E-04		-1.21E+02	1.14E+02	3.19E+01	1.54E-03
1011	-1.12E+00	-2.00E+00	5.68E-04	2.97E-04		-1.64E+01	7.17E+00	3.07E+01	5.14E-04
1012	-9.61E-01	-1.94E+00	5.47E-04	3.40E-04		-6.37E+01	5.79E+01	2.85E+01	7.72E-04
1013	-9.42E-01	-1.78E+00	5.47E-04	3.80E-04		-1.11E+01	1.60E+01	1.78E+01	3.61E-04
1014	-7.80E-01	-1.72E+00	5.09E-04	4.25E-04		-5.51E+01	5.49E+01	4.24E+00	5.86E-04
1015	-7.81E-01	-1.53E+00	4.84E-04	4.47E-04		9.30E+00	-7.05E+00	5.53E+00	2.42E-04
1016	-6.20E-01	-1.48E+00	4.69E-04	4.70E-04		-1.23E+01	1.35E+01	-1.39E+01	2.99E-04
1017	-1.74E+00	-2.51E+00	-7.59E-04	2.27E-05		1.41E+03	1.93E+03	6.45E+02	3.50E-02
1018	-1.67E+00	-2.50E+00	-4.37E-04	-3.25E-04		4.51E+02	-8.54E+03	1.43E+03	4.60E-02
1019	-1.53E+00	-2.48E+00	-7.55E-05	-4.08E-05		4.79E+02	1.44E+02	5.43E+01	1.90E-02
1020	-1.45E+00	-2.41E+00	1.87E-04	1.73E-04		3.00E+02	5.76E+02	5.42E+01	4.59E-03
1021	-1.28E+00	-2.36E+00	3.38E-04	5.31E-05		-2.46E+02	-7.13E+01	2.67E+02	3.12E-03
1022	-1.22E+00	-2.26E+00	4.65E-04	1.50E-04		-2.27E+02	1.30E+02	1.84E+02	2.77E-03
1023	-1.05E+00	-2.21E+00	3.80E-04	1.70E-04		-1.45E+02	1.66E+02	1.14E+02	2.27E-03
1024	-1.00E+00	-2.08E+00	4.92E-04	2.75E-04		-1.06E+02	1.29E+02	5.38E+01	1.49E-03
1025	-8.28E-01	-2.03E+00	4.07E-04	2.59E-04		-1.55E+02	1.39E+02	4.54E+01	1.74E-03
1026	-7.99E-01	-1.88E+00	4.85E-04	3.53E-04		-1.08E+02	1.04E+02	1.73E+01	1.19E-03
1027	-6.28E-01	-1.84E+00	3.93E-04	3.23E-04		-1.32E+02	1.37E+02	8.78E+00	1.48E-03
1028	-6.19E-01	-1.66E+00	4.58E-04	4.24E-04		-7.31E+01	7.65E+01	-6.03E+00	8.39E-04
1029	-4.48E-01	-1.62E+00	3.95E-04	3.70E-04		-8.61E+01	8.18E+01	2.40E+00	9.01E-04
1030	-1.60E+00	-2.50E+00	-1.93E-04	4.60E-05		7.25E+02	-3.13E+03	-6.62E+02	2.18E-02
1031	-1.36E+00	-2.43E+00	1.73E-04	3.41E-05		-1.42E+02	3.99E+02	2.75E+02	4.24E-03
1032	-1.11E+00	-2.31E+00	2.41E-04	1.03E-04		-1.87E+02	1.56E+02	1.83E+02	2.97E-03
1033	-8.75E-01	-2.16E+00	2.95E-04	1.60E-04		-1.84E+02	1.96E+02	9.89E+01	2.39E-03
1034	-6.56E-01	-1.99E+00	2.96E-04	2.11E-04		-1.64E+02	1.67E+02	3.76E+01	1.92E-03
1035	-4.57E-01	-1.79E+00	2.83E-04	2.62E-04		-1.64E+02	1.56E+02	1.82E+01	1.73E-03
1036	-5.09E-01	-1.06E+00	3.02E-04	4.46E-04		-3.37E+01	3.28E+01	-9.59E+01	1.16E-03
1037	-5.88E-01	-9.05E-01	2.27E-04	5.00E-04		-1.26E+02	9.74E+01	-2.11E+01	1.24E-03
1038	-5.34E-01	-8.81E-01	1.72E-04	5.26E-04		-1.73E+02	1.24E+02	-9.94E+01	2.04E-03
1039	-5.95E-01	-7.40E-01	1.36E-04	6.63E-04		-3.20E+02	3.00E+02	7.99E+01	3.70E-03
1040	-5.62E-01	-7.00E-01	5.76E-05	8.12E-04		-3.49E+02	4.86E+02	1.16E+02	4.79E-03
1041	-6.06E-01	-5.71E-01	1.34E-04	9.57E-04		-5.68E+02	3.08E+02	4.71E+02	7.71E-03
1042	-5.90E-01	-5.13E-01	5.58E-05	1.16E-03		-8.18E+02	4.30E+02	4.81E+02	1.03E-02
1043	-6.19E-01	-3.99E-01	8.16E-05	1.30E-03		-5.32E+02	1.09E+03	2.10E+03	3.63E-02
1044	-6.20E-01	-3.22E-01	1.90E-04	2.15E-03		-1.73E+03	2.63E+03	5.70E+03	6.59E-02
1045	-6.23E-01	-2.34E-01	-4.21E-05	2.58E-03		-3.47E+03	9.90E+02	1.23E+04	1.45E-01
1046	-6.13E-01	-1.61E-01	-1.88E-05	4.74E-03		-1.23E+03	2.91E+03	1.64E+04	1.83E-01
1047	-6.17E-01	-7.80E-02	2.53E-04	4.38E-03		2.44E+03	-1.56E+02	2.58E+04	2.78E-01
1048	-6.11E-01	4.65E-16	-8.56E-08	5.56E-03		-1.45E+00	2.47E+01	1.98E+04	2.33E-01
1049	-6.17E-01	7.80E-02	-2.53E-04	4.38E-03		-2.44E+03	2.35E+02	2.58E+04	2.78E-01
1050	-6.13E-01	1.61E-01	1.89E-05	4.74E-03		1.23E+03	-2.88E+03	1.64E+04	1.83E-01

1051	-6.23E-01	2.34E-01	4.22E-05	2.58E-03		3.47E+03	-9.71E+02	1.23E+04	1.45E-01
1052	-6.20E-01	3.22E-01	-1.90E-04	2.15E-03		1.73E+03	-2.63E+03	5.70E+03	6.59E-02
1053	-6.19E-01	3.99E-01	-8.17E-05	1.30E-03		5.31E+02	-1.08E+03	2.10E+03	3.63E-02
1054	-5.90E-01	5.13E-01	-5.58E-05	1.16E-03		8.19E+02	-4.30E+02	4.82E+02	1.03E-02
1055	-6.06E-01	5.71E-01	-1.34E-04	9.57E-04		5.68E+02	-3.08E+02	4.71E+02	7.71E-03
1056	-5.62E-01	7.00E-01	-5.76E-05	8.12E-04		3.50E+02	-4.86E+02	1.16E+02	4.79E-03
1057	-5.95E-01	7.40E-01	-1.36E-04	6.63E-04		3.20E+02	-3.00E+02	7.99E+01	3.70E-03
1058	-5.34E-01	8.81E-01	-1.72E-04	5.26E-04		1.73E+02	-1.24E+02	-9.95E+01	2.04E-03
1059	-5.88E-01	9.05E-01	-2.27E-04	5.00E-04		1.26E+02	-9.74E+01	-2.11E+01	1.24E-03
1060	-5.09E-01	1.06E+00	-3.02E-04	4.46E-04		3.37E+01	-3.27E+01	-9.59E+01	1.16E-03
1061	-3.56E-01	-1.20E+00	4.01E-04	3.23E-04		8.03E+00	-3.20E+01	-1.56E+02	1.67E-03
1062	-4.55E-01	-1.03E+00	2.71E-04	4.18E-04		-3.48E+01	3.13E+01	-1.59E+02	1.79E-03
1063	-4.21E-01	-9.94E-01	2.21E-04	3.93E-04		-6.99E+01	1.37E+01	-2.09E+02	2.23E-03
1064	-5.01E-01	-8.40E-01	9.74E-05	5.54E-04		-1.38E+02	2.20E+02	-1.48E+02	2.82E-03
1065	-4.85E-01	-7.83E-01	2.13E-05	6.28E-04		-2.40E+02	3.29E+02	-2.14E+02	4.10E-03
1066	-5.46E-01	-6.41E-01	-3.43E-05	9.76E-04		-7.32E+02	3.98E+02	-1.10E+02	6.41E-03
1067	-5.48E-01	-5.65E-01	-1.14E-04	1.17E-03		-9.97E+02	3.89E+02	-3.57E+01	7.98E-03
1068	-5.91E-01	-4.36E-01	1.46E-05	1.56E-03		-2.99E+02	1.48E+03	1.18E+03	2.46E-02
1069	-6.07E-01	-3.39E-01	9.89E-05	2.55E-03		-2.52E+03	3.40E+03	3.11E+03	5.06E-02
1070	-6.11E-01	-2.49E-01	-3.72E-04	3.77E-03		-6.16E+03	2.90E+03	7.48E+03	9.83E-02
1071	-6.01E-01	-1.70E-01	-2.03E-04	6.09E-03		-1.98E+03	4.79E+03	9.15E+03	1.08E-01
1072	-6.06E-01	-8.31E-02	3.40E-04	7.00E-03		3.88E+02	1.00E+03	1.56E+04	1.70E-01
1073	-5.99E-01	3.89E-16	-1.53E-07	7.53E-03		-1.36E+00	7.05E+00	1.02E+04	1.20E-01
1074	-6.06E-01	8.31E-02	-3.40E-04	7.01E-03		-3.87E+02	-9.70E+02	1.56E+04	1.70E-01
1075	-6.01E-01	1.70E-01	2.03E-04	6.09E-03		1.98E+03	-4.78E+03	9.16E+03	1.08E-01
1076	-6.11E-01	2.49E-01	3.73E-04	3.76E-03		6.16E+03	-2.89E+03	7.49E+03	9.83E-02
1077	-6.07E-01	3.39E-01	-9.91E-05	2.55E-03		2.52E+03	-3.40E+03	3.11E+03	5.06E-02
1078	-5.91E-01	4.36E-01	-1.47E-05	1.56E-03		2.98E+02	-1.48E+03	1.18E+03	2.46E-02
1079	-5.48E-01	5.65E-01	1.15E-04	1.17E-03		9.98E+02	-3.89E+02	-3.56E+01	7.98E-03
1080	-5.46E-01	6.41E-01	3.43E-05	9.76E-04		7.32E+02	-3.98E+02	-1.11E+02	6.41E-03
1081	-4.85E-01	7.83E-01	-2.13E-05	6.28E-04		2.40E+02	-3.29E+02	-2.14E+02	4.10E-03
1082	-5.01E-01	8.40E-01	-9.74E-05	5.54E-04		1.38E+02	-2.20E+02	-1.48E+02	2.82E-03
1083	-4.21E-01	9.94E-01	-2.21E-04	3.93E-04		6.99E+01	-1.37E+01	-2.09E+02	2.23E-03
1084	-4.55E-01	1.03E+00	-2.71E-04	4.18E-04		3.48E+01	-3.13E+01	-1.59E+02	1.79E-03
1085	-3.56E-01	1.20E+00	-4.01E-04	3.23E-04		-8.03E+00	3.20E+01	-1.56E+02	1.67E-03
1086	-2.04E-01	-1.33E+00	4.87E-04	1.69E-04		-5.86E-01	-5.71E+01	-1.76E+02	1.69E-03
1087	-3.23E-01	-1.16E+00	3.79E-04	2.76E-04		4.20E+01	-3.12E+01	-1.75E+02	2.08E-03
1088	-3.09E-01	-1.10E+00	3.33E-04	2.46E-04		-7.64E+00	-4.93E+01	-2.34E+02	2.40E-03
1089	-4.06E-01	-9.37E-01	1.58E-04	3.90E-04		-5.75E+01	9.17E+01	-2.00E+02	2.44E-03
1090	-4.09E-01	-8.63E-01	8.88E-05	4.38E-04		-1.78E+02	1.01E+02	-2.78E+02	3.47E-03
1091	-4.87E-01	-7.07E-01	-1.34E-04	7.73E-04		-4.33E+02	2.80E+02	-3.94E+02	6.91E-03
1092	-5.05E-01	-6.11E-01	-3.29E-04	1.03E-03		-1.20E+03	3.05E+02	-3.69E+02	7.36E-03
1093	-5.64E-01	-4.67E-01	-3.47E-05	1.58E-03		-1.48E+02	1.52E+03	6.76E+02	1.79E-02
1094	-5.95E-01	-3.49E-01	3.35E-07	2.80E-03		-2.78E+03	3.49E+03	1.25E+03	4.33E-02
1095	-5.98E-01	-2.59E-01	-8.34E-04	4.36E-03		-7.59E+03	3.71E+03	3.86E+03	7.07E-02
1096	-5.90E-01	-1.74E-01	-3.90E-04	6.55E-03		-1.56E+03	5.31E+03	2.66E+03	5.59E-02
1097	-5.95E-01	-8.65E-02	3.18E-04	8.33E-03		-8.92E+02	1.74E+03	5.76E+03	6.97E-02
1098	-5.88E-01	4.58E-16	-2.02E-07	8.32E-03		-7.25E-01	3.30E-01	8.35E+02	3.28E-02

1099	-5.95E-01	8.65E-02	-3.18E-04	8.33E-03		8.92E+02	-1.74E+03	5.75E+03	6.97E-02
1100	-5.90E-01	1.74E-01	3.91E-04	6.55E-03		1.56E+03	-5.32E+03	2.66E+03	5.59E-02
1101	-5.98E-01	2.59E-01	8.35E-04	4.36E-03		7.60E+03	-3.70E+03	3.87E+03	7.07E-02
1102	-5.95E-01	3.49E-01	-7.07E-07	2.80E-03		2.78E+03	-3.48E+03	1.25E+03	4.33E-02
1103	-5.64E-01	4.67E-01	3.47E-05	1.58E-03		1.48E+02	-1.52E+03	6.77E+02	1.79E-02
1104	-5.05E-01	6.11E-01	3.29E-04	1.03E-03		1.20E+03	-3.05E+02	-3.69E+02	7.37E-03
1105	-4.87E-01	7.07E-01	1.34E-04	7.73E-04		4.33E+02	-2.80E+02	-3.94E+02	6.91E-03
1106	-4.09E-01	8.63E-01	-8.89E-05	4.38E-04		1.78E+02	-1.01E+02	-2.78E+02	3.47E-03
1107	-4.06E-01	9.37E-01	-1.58E-04	3.90E-04		5.75E+01	-9.17E+01	-2.00E+02	2.44E-03
1108	-3.09E-01	1.10E+00	-3.33E-04	2.46E-04		7.65E+00	4.93E+01	-2.34E+02	2.40E-03
1109	-3.23E-01	1.16E+00	-3.79E-04	2.76E-04		-4.20E+01	3.12E+01	-1.75E+02	2.08E-03
1110	-2.04E-01	1.33E+00	-4.87E-04	1.69E-04		5.89E-01	5.71E+01	-1.76E+02	1.69E-03
1111	-6.18E-02	-1.34E+00	5.63E-04	-4.13E-05		1.03E+02	-6.97E+01	-1.57E+02	1.84E-03
1112	-1.90E-01	-1.28E+00	4.84E-04	1.31E-04		7.39E+01	-6.36E+01	-1.64E+02	2.07E-03
1113	-2.03E-01	-1.11E+00	3.54E-04	8.82E-05		4.80E+01	-7.20E+01	-2.33E+02	2.66E-03
1114	-3.11E-01	-1.03E+00	2.54E-04	2.38E-04		4.99E+01	-3.78E-01	-2.24E+02	2.74E-03
1115	-3.38E-01	-8.62E-01	3.23E-05	3.07E-04		-6.18E+01	-3.82E+01	-2.90E+02	3.79E-03
1116	-4.27E-01	-7.67E-01	-7.75E-05	5.34E-04		-3.28E+01	1.65E+02	-4.13E+02	6.43E-03
1117	-4.65E-01	-6.01E-01	-6.44E-04	9.26E-04		-1.15E+03	3.00E+02	-4.76E+02	9.47E-03
1118	-5.36E-01	-4.92E-01	-9.09E-05	1.51E-03		2.20E+02	1.39E+03	3.11E+02	1.54E-02
1119	-5.83E-01	-3.27E-01	-6.81E-04	3.47E-03		-3.72E+03	3.45E+03	-7.85E+02	3.90E-02
1120	-5.86E-01	-2.64E-01	-1.37E-03	4.59E-03		-9.31E+03	3.68E+03	9.35E+02	5.89E-02
1121	-5.79E-01	-1.64E-01	-2.16E-04	6.59E-03		-3.48E+02	4.65E+03	-4.11E+03	8.12E-02
1122	-5.83E-01	-8.80E-02	2.51E-04	8.41E-03		-1.36E+03	1.99E+03	-3.80E+03	4.75E-02
1123	-5.78E-01	4.72E-16	-1.64E-07	7.99E-03		1.29E+00	3.83E+00	-8.14E+03	9.44E-02
1124	-5.83E-01	8.80E-02	-2.51E-04	8.41E-03		1.36E+03	-1.99E+03	-3.80E+03	4.75E-02
1125	-5.79E-01	1.64E-01	2.17E-04	6.59E-03		3.43E+02	-4.65E+03	-4.12E+03	8.12E-02
1126	-5.86E-01	2.64E-01	1.37E-03	4.59E-03		9.31E+03	-3.68E+03	9.38E+02	5.89E-02
1127	-5.83E-01	3.27E-01	6.80E-04	3.47E-03		3.72E+03	-3.45E+03	-7.85E+02	3.90E-02
1128	-5.36E-01	4.92E-01	9.09E-05	1.51E-03		-2.20E+02	-1.39E+03	3.12E+02	1.54E-02
1129	-4.65E-01	6.01E-01	6.44E-04	9.27E-04		1.15E+03	-3.01E+02	-4.77E+02	9.47E-03
1130	-4.27E-01	7.67E-01	7.75E-05	5.34E-04		3.26E+01	-1.65E+02	-4.13E+02	6.43E-03
1131	-3.38E-01	8.62E-01	-3.23E-05	3.07E-04		6.18E+01	3.83E+01	-2.90E+02	3.79E-03
1132	-3.11E-01	1.03E+00	-2.54E-04	2.38E-04		-4.99E+01	3.85E-01	-2.24E+02	2.74E-03
1133	-2.03E-01	1.11E+00	-3.54E-04	8.82E-05		-4.80E+01	7.20E+01	-2.33E+02	2.66E-03
1134	-1.90E-01	1.28E+00	-4.84E-04	1.31E-04		-7.39E+01	6.36E+01	-1.64E+02	2.07E-03
1135	-6.18E-02	1.34E+00	-5.63E-04	-4.13E-05		-1.03E+02	6.97E+01	-1.57E+02	1.84E-03
1136	7.08E-02	-1.23E+00	5.85E-04	-2.96E-04		7.59E+01	-6.88E+01	-1.76E+02	2.08E-03
1137	-7.47E-02	-1.17E+00	4.73E-04	-9.87E-05		8.64E+01	-8.54E+01	-2.24E+02	2.64E-03
1138	-1.05E-01	-1.01E+00	2.88E-04	-1.22E-04		8.71E+01	-7.89E+01	-2.61E+02	3.04E-03
1139	-2.29E-01	-9.42E-01	1.64E-04	8.56E-05		3.21E+01	-5.31E+01	-2.90E+02	3.33E-03
1140	-2.71E-01	-7.85E-01	-5.33E-05	1.09E-04		7.71E+01	-2.23E+02	-2.84E+02	4.53E-03
1141	-3.75E-01	-6.96E-01	-2.63E-04	3.91E-04		2.06E+01	1.99E+01	-6.28E+02	7.09E-03
1142	-4.27E-01	-5.40E-01	-8.52E-04	8.54E-04		-6.59E+02	2.84E+02	-5.54E+02	1.24E-02
1143	-5.11E-01	-4.36E-01	-2.28E-04	1.93E-03		-8.85E+02	1.50E+03	-1.01E+03	2.10E-02
1144	-5.72E-01	-2.81E-01	-1.88E-03	4.30E-03		-1.73E+03	2.37E+03	-3.05E+03	5.09E-02
1145	-5.75E-01	-2.27E-01	-1.76E-03	5.16E-03		-8.05E+03	3.12E+03	-2.53E+03	7.34E-02
1146	-5.69E-01	-1.41E-01	2.79E-04	5.97E-03		-8.76E+02	3.32E+03	-1.25E+04	1.47E-01

1147	-5.73E-01	-7.57E-02	2.26E-04	7.61E-03		-6.46E+02	1.47E+03	-1.23E+04	1.37E-01
1148	-5.68E-01	3.61E-16	-2.89E-08	6.69E-03		2.72E+00	1.58E+01	-1.67E+04	1.90E-01
1149	-5.73E-01	7.57E-02	-2.26E-04	7.61E-03		6.47E+02	-1.45E+03	-1.23E+04	1.37E-01
1150	-5.69E-01	1.41E-01	-2.78E-04	5.96E-03		8.68E+02	-3.29E+03	-1.25E+04	1.47E-01
1151	-5.75E-01	2.27E-01	1.76E-03	5.16E-03		8.05E+03	-3.12E+03	-2.52E+03	7.34E-02
1152	-5.72E-01	2.81E-01	1.88E-03	4.30E-03		1.73E+03	-2.36E+03	-3.05E+03	5.09E-02
1153	-5.11E-01	4.36E-01	2.28E-04	1.93E-03		8.85E+02	-1.50E+03	-1.01E+03	2.10E-02
1154	-4.27E-01	5.40E-01	8.53E-04	8.54E-04		6.59E+02	-2.84E+02	-5.54E+02	1.24E-02
1155	-3.75E-01	6.96E-01	2.63E-04	3.90E-04		-2.07E+01	-1.99E+01	-6.28E+02	7.09E-03
1156	-2.71E-01	7.85E-01	5.33E-05	1.09E-04		-7.70E+01	2.23E+02	-2.84E+02	4.53E-03
1157	-2.29E-01	9.42E-01	-1.64E-04	8.56E-05		-3.20E+01	5.31E+01	-2.90E+02	3.33E-03
1158	-1.05E-01	1.01E+00	-2.88E-04	-1.22E-04		-8.71E+01	7.89E+01	-2.61E+02	3.04E-03
1159	-7.47E-02	1.17E+00	-4.73E-04	-9.87E-05		-8.64E+01	8.54E+01	-2.24E+02	2.64E-03
1160	7.08E-02	1.23E+00	-5.85E-04	-2.96E-04		-7.59E+01	6.88E+01	-1.76E+02	2.08E-03
1161	2.03E-01	-1.11E+00	5.38E-04	-4.74E-04		3.96E+01	-4.63E+01	-1.39E+02	1.65E-03
1162	4.08E-02	-1.07E+00	4.32E-04	-3.29E-04		9.00E+01	-8.94E+01	-2.18E+02	2.59E-03
1163	-6.32E-03	-9.20E-01	2.36E-04	-3.33E-04		1.10E+02	-8.48E+01	-2.27E+02	2.67E-03
1164	-1.47E-01	-8.57E-01	9.90E-05	-1.26E-04		9.81E+01	-1.39E+02	-2.67E+02	3.33E-03
1165	-2.05E-01	-7.11E-01	-4.09E-05	-1.58E-04		1.90E+02	-4.21E+02	-1.32E+02	4.48E-03
1166	-3.23E-01	-6.29E-01	-3.28E-04	8.20E-05		3.85E+02	-2.11E+02	-6.76E+02	8.66E-03
1167	-3.90E-01	-4.85E-01	-8.74E-04	5.89E-04		2.37E+02	-3.36E+02	-5.95E+02	1.42E-02
1168	-4.87E-01	-3.85E-01	-6.30E-04	1.85E-03		-3.63E+02	1.89E+02	-2.56E+03	2.87E-02
1169	-5.60E-01	-2.41E-01	-2.48E-03	4.14E-03		2.56E+03	-1.90E+03	-5.69E+03	8.60E-02
1170	-5.65E-01	-1.95E-01	-1.59E-03	4.72E-03		-6.01E+02	1.56E+03	-9.99E+03	1.16E-01
1171	-5.59E-01	-1.21E-01	5.22E-04	4.15E-03		-4.43E+03	2.17E+03	-2.17E+04	2.43E-01
1172	-5.63E-01	-6.49E-02	1.92E-04	5.84E-03		-1.15E+03	9.64E+02	-2.08E+04	2.34E-01
1173	-5.58E-01	1.94E-16	1.35E-07	4.42E-03		1.69E+00	3.63E+01	-2.51E+04	2.86E-01
1174	-5.63E-01	6.49E-02	-1.92E-04	5.84E-03		1.16E+03	-9.12E+02	-2.08E+04	2.34E-01
1175	-5.59E-01	1.21E-01	-5.21E-04	4.15E-03		4.42E+03	-2.11E+03	-2.17E+04	2.43E-01
1176	-5.65E-01	1.95E-01	1.59E-03	4.72E-03		6.05E+02	-1.55E+03	-9.98E+03	1.16E-01
1177	-5.60E-01	2.41E-01	2.48E-03	4.13E-03		-2.55E+03	1.90E+03	-5.69E+03	8.60E-02
1178	-4.87E-01	3.85E-01	6.30E-04	1.85E-03		3.64E+02	-1.88E+02	-2.56E+03	2.87E-02
1179	-3.90E-01	4.85E-01	8.74E-04	5.89E-04		-2.36E+02	3.36E+02	-5.95E+02	1.42E-02
1180	-3.23E-01	6.29E-01	3.28E-04	8.19E-05		-3.85E+02	2.11E+02	-6.76E+02	8.66E-03
1181	-2.05E-01	7.11E-01	4.09E-05	-1.58E-04		-1.90E+02	4.21E+02	-1.32E+02	4.48E-03
1182	-1.47E-01	8.57E-01	-9.90E-05	-1.26E-04		-9.81E+01	1.39E+02	-2.67E+02	3.33E-03
1183	-6.32E-03	9.20E-01	-2.36E-04	-3.33E-04		-1.10E+02	8.47E+01	-2.27E+02	2.67E-03
1184	4.08E-02	1.07E+00	-4.32E-04	-3.29E-04		-9.00E+01	8.94E+01	-2.18E+02	2.59E-03
1185	2.03E-01	1.11E+00	-5.38E-04	-4.74E-04		-3.96E+01	4.63E+01	-1.39E+02	1.65E-03
1186	1.56E-01	-9.63E-01	3.68E-04	-4.85E-04		5.80E+01	-4.99E+01	-1.49E+02	1.76E-03
1187	-6.42E-02	-7.75E-01	1.02E-04	-3.48E-04		1.29E+02	-2.01E+02	-1.59E+02	2.61E-03
1188	-2.71E-01	-5.67E-01	-1.88E-04	-3.31E-04		7.36E+02	-4.45E+02	-4.30E+02	9.25E-03
1189	-4.63E-01	-3.40E-01	-6.94E-04	8.96E-04		1.59E+03	-2.37E+03	-3.06E+03	4.54E-02
1190	-5.54E-01	-1.67E-01	-8.05E-04	2.74E-03		9.55E+03	-5.30E+02	-2.13E+04	2.28E-01
1191	-5.54E-01	-5.57E-02	1.12E-04	3.09E-03		-1.06E+03	4.82E+02	-2.99E+04	3.29E-01
1192	-5.54E-01	5.57E-02	-1.12E-04	3.09E-03		1.07E+03	-3.78E+02	-2.99E+04	3.29E-01
1193	-5.54E-01	1.67E-01	8.05E-04	2.75E-03		-9.55E+03	5.91E+02	-2.12E+04	2.28E-01
1194	-4.63E-01	3.40E-01	6.94E-04	8.96E-04		-1.59E+03	2.37E+03	-3.06E+03	4.54E-02

1195	-2.71E-01	5.67E-01	1.88E-04	-3.31E-04		-7.36E+02	4.45E+02	-4.30E+02	9.25E-03
1196	-6.42E-02	7.75E-01	-1.02E-04	-3.48E-04		-1.29E+02	2.01E+02	-1.59E+02	2.61E-03
1197	1.56E-01	9.63E-01	-3.68E-04	-4.85E-04		-5.80E+01	4.99E+01	-1.49E+02	1.76E-03
1198	1.01E+00	1.45E+00	-7.22E-04	-3.58E-04		2.89E+01	-3.34E+01	-2.55E+01	4.58E-04
1199	7.64E-01	1.49E+00	-7.56E-04	-4.63E-04		-5.75E+00	1.33E+01	1.94E+01	3.95E-04
1200	8.88E-01	1.69E+00	-7.47E-04	-3.91E-04		-5.23E+01	5.02E+01	6.19E+01	8.87E-04
1201	6.18E-01	1.70E+00	-6.22E-04	-4.17E-04		-1.02E+02	1.06E+02	7.75E+01	1.37E-03
1202	7.62E-01	1.92E+00	-4.75E-04	-2.78E-04		-1.36E+02	1.31E+02	1.05E+02	1.88E-03
1203	1.38E+00	1.56E+00	-7.55E-04	-2.17E-04		1.50E+01	-1.69E+01	-2.63E+01	3.60E-04
1204	1.14E+00	1.65E+00	-7.97E-04	-3.14E-04		-1.19E+01	1.36E+01	2.61E+01	3.73E-04
1205	1.30E+00	1.83E+00	-7.84E-04	-2.34E-04		-3.40E+01	3.23E+01	6.83E+01	8.42E-04
1206	1.03E+00	1.91E+00	-6.52E-04	-2.76E-04		-8.08E+01	8.22E+01	9.45E+01	1.36E-03
1207	1.22E+00	2.11E+00	-5.11E-04	-1.60E-04		-8.04E+01	8.01E+01	1.21E+02	1.65E-03
1208	1.54E+00	1.74E+00	-8.25E-04	-1.58E-04		-5.88E+00	6.57E+00	2.64E+01	3.34E-04
1209	1.48E+00	2.04E+00	-6.82E-04	-1.39E-04		-3.83E+01	3.86E+01	1.06E+02	1.24E-03
1210	4.45E+00	2.62E-01	-6.67E-04	1.81E-03		-7.98E+02	-1.30E+03	-4.00E+03	5.31E-02
1211	4.42E+00	4.40E-01	4.46E-04	6.85E-04		-1.90E+02	-2.07E+03	-3.69E+03	3.69E-02
1212	4.40E+00	5.19E-01	2.65E-04	4.35E-04		1.22E+03	-1.26E+03	-1.20E+03	2.56E-02
1213	4.32E+00	7.40E-01	-3.68E-04	3.32E-04		8.97E+02	-3.52E+02	-3.51E+02	8.29E-03
1214	4.24E+00	8.16E-01	-4.10E-04	5.25E-04		3.01E+02	-1.86E+02	-3.61E+01	4.03E-03
1215	4.15E+00	1.04E+00	-1.73E-04	4.74E-04		3.46E+02	-4.17E+02	-2.15E+02	4.73E-03
1216	4.04E+00	1.09E+00	-3.67E-04	6.01E-04		3.63E+02	-3.41E+02	-4.55E+01	3.61E-03
1217	3.94E+00	1.32E+00	-3.12E-04	4.00E-04		2.69E+02	-2.72E+02	-6.64E+01	3.21E-03
1218	3.81E+00	1.34E+00	-4.70E-04	5.36E-04		2.12E+02	-1.98E+02	5.62E+00	2.29E-03
1219	3.70E+00	1.56E+00	-3.65E-04	3.73E-04		2.26E+02	-2.22E+02	2.61E+01	2.51E-03
1220	3.55E+00	1.56E+00	-5.32E-04	4.70E-04		1.55E+02	-1.59E+02	5.15E+01	1.84E-03
1221	3.43E+00	1.78E+00	-4.15E-04	3.14E-04		1.75E+02	-1.76E+02	6.61E+01	2.10E-03
1222	3.26E+00	1.74E+00	-5.87E-04	3.85E-04		1.20E+02	-1.19E+02	7.40E+01	1.56E-03
1223	3.12E+00	1.95E+00	-4.57E-04	2.53E-04		1.34E+02	-1.33E+02	9.86E+01	1.85E-03
1224	2.95E+00	1.89E+00	-6.32E-04	2.95E-04		8.56E+01	-8.63E+01	9.10E+01	1.39E-03
1225	2.80E+00	2.09E+00	-4.87E-04	1.84E-04		9.40E+01	-9.40E+01	1.19E+02	1.70E-03
1226	2.63E+00	2.00E+00	-6.64E-04	1.99E-04		5.61E+01	-5.63E+01	1.02E+02	1.29E-03
1227	2.47E+00	2.18E+00	-5.08E-04	1.12E-04		5.56E+01	-5.54E+01	1.33E+02	1.61E-03
1228	2.29E+00	2.06E+00	-6.83E-04	9.93E-05		2.75E+01	-2.77E+01	1.09E+02	1.24E-03
1229	4.44E+00	1.95E-01	-5.59E-04	1.91E-03		-4.03E+03	1.54E+03	1.96E+03	8.82E-02
1230	4.43E+00	3.41E-01	-3.46E-04	1.80E-03		1.37E+04	-2.43E+03	-3.00E+03	4.94E-02
1231	4.42E+00	3.88E-01	-1.65E-04	1.64E-03		1.16E+03	-2.10E+03	-4.23E+02	4.97E-02
1232	4.32E+00	5.95E-01	-1.85E-04	8.41E-04		4.62E+01	-1.08E+03	-9.83E+02	1.36E-02
1233	4.23E+00	6.56E-01	-7.78E-04	6.78E-04		8.38E+02	-2.13E+02	2.33E+02	6.58E-03
1234	4.13E+00	8.66E-01	-4.40E-04	8.10E-04		2.35E+02	-1.42E+02	-2.66E+01	2.24E-03
1235	4.02E+00	9.03E-01	-5.29E-04	9.11E-04		1.64E+02	-1.29E+02	-2.60E+01	1.47E-03
1236	3.91E+00	1.11E+00	-5.14E-04	7.23E-04		2.02E+02	-2.25E+02	-5.19E-01	2.27E-03
1237	3.78E+00	1.12E+00	-6.27E-04	7.26E-04		7.79E+01	-7.38E+01	4.58E+01	1.05E-03
1238	3.66E+00	1.33E+00	-6.09E-04	6.14E-04		1.28E+02	-1.19E+02	3.54E+01	1.40E-03
1239	3.51E+00	1.32E+00	-6.82E-04	6.14E-04		3.89E+01	-3.92E+01	2.27E+01	5.32E-04
1240	3.39E+00	1.52E+00	-6.68E-04	5.15E-04		9.28E+01	-9.28E+01	5.32E+01	1.16E-03
1241	3.22E+00	1.48E+00	-7.34E-04	4.95E-04		2.68E+01	-2.77E+01	2.90E+01	4.63E-04
1242	3.09E+00	1.68E+00	-7.20E-04	4.06E-04		6.69E+01	-6.56E+01	6.20E+01	9.91E-04

1243	2.92E+00	1.61E+00	-7.75E-04	3.74E-04		1.75E+01	-1.82E+01	2.72E+01	3.85E-04
1244	2.78E+00	1.80E+00	-7.59E-04	2.93E-04		4.52E+01	-4.46E+01	6.80E+01	8.93E-04
1245	2.60E+00	1.70E+00	-8.06E-04	2.50E-04		1.10E+01	-1.14E+01	2.74E+01	3.48E-04
1246	2.45E+00	1.88E+00	-7.86E-04	1.77E-04		2.65E+01	-2.61E+01	7.18E+01	8.39E-04
1247	2.28E+00	1.76E+00	-8.25E-04	1.25E-04		5.67E+00	-5.90E+00	2.75E+01	3.28E-04
1248	4.43E+00	2.43E-01	-1.41E-03	2.04E-03		5.02E+03	3.18E+03	8.26E+03	9.73E-02
1249	4.32E+00	4.50E-01	-1.50E-04	1.82E-03		1.00E+03	-1.64E+03	7.53E+01	1.37E-02
1250	4.12E+00	6.92E-01	-5.26E-04	7.95E-04		-2.09E+02	2.36E+02	7.21E+01	3.34E-03
1251	3.88E+00	9.12E-01	-5.85E-04	8.49E-04		4.40E+01	-9.23E+00	4.59E+01	8.74E-04
1252	3.63E+00	1.11E+00	-6.23E-04	6.59E-04		-4.75E+01	4.81E+01	9.11E+00	6.48E-04
1253	3.35E+00	1.27E+00	-6.71E-04	5.48E-04		-2.62E+01	3.10E+01	-6.20E+00	4.30E-04
1254	3.05E+00	1.41E+00	-7.09E-04	4.25E-04		-2.49E+01	2.71E+01	-1.50E+01	3.88E-04
1255	2.75E+00	1.51E+00	-7.40E-04	3.05E-04		-1.72E+01	1.87E+01	-2.06E+01	3.41E-04
1256	2.43E+00	1.58E+00	-7.61E-04	1.83E-04		-1.02E+01	1.10E+01	-2.41E+01	3.19E-04
1257	2.29E+00	-2.06E+00	6.83E-04	9.93E-05		-2.75E+01	2.77E+01	1.09E+02	1.24E-03
1258	2.47E+00	-2.18E+00	5.08E-04	1.12E-04		-5.56E+01	5.54E+01	1.33E+02	1.61E-03
1259	2.63E+00	-2.00E+00	6.64E-04	1.99E-04		-5.61E+01	5.63E+01	1.02E+02	1.29E-03
1260	2.80E+00	-2.09E+00	4.87E-04	1.84E-04		-9.40E+01	9.40E+01	1.19E+02	1.70E-03
1261	2.95E+00	-1.89E+00	6.32E-04	2.95E-04		-8.56E+01	8.63E+01	9.10E+01	1.39E-03
1262	3.12E+00	-1.95E+00	4.57E-04	2.53E-04		-1.34E+02	1.33E+02	9.86E+01	1.85E-03
1263	3.26E+00	-1.74E+00	5.87E-04	3.85E-04		-1.20E+02	1.19E+02	7.40E+01	1.56E-03
1264	3.43E+00	-1.78E+00	4.15E-04	3.14E-04		-1.75E+02	1.76E+02	6.61E+01	2.10E-03
1265	3.55E+00	-1.56E+00	5.32E-04	4.70E-04		-1.55E+02	1.59E+02	5.15E+01	1.84E-03
1266	3.70E+00	-1.56E+00	3.65E-04	3.73E-04		-2.26E+02	2.22E+02	2.61E+01	2.51E-03
1267	3.81E+00	-1.34E+00	4.70E-04	5.36E-04		-2.13E+02	1.98E+02	5.62E+00	2.29E-03
1268	3.94E+00	-1.32E+00	3.12E-04	4.00E-04		-2.69E+02	2.72E+02	-6.64E+01	3.21E-03
1269	4.04E+00	-1.09E+00	3.67E-04	6.01E-04		-3.63E+02	3.41E+02	-4.55E+01	3.61E-03
1270	4.15E+00	-1.04E+00	1.73E-04	4.74E-04		-3.46E+02	4.17E+02	-2.15E+02	4.73E-03
1271	4.24E+00	-8.16E-01	4.10E-04	5.25E-04		-3.01E+02	1.85E+02	-3.62E+01	4.03E-03
1272	4.32E+00	-7.40E-01	3.68E-04	3.32E-04		-8.96E+02	3.52E+02	-3.51E+02	8.29E-03
1273	4.40E+00	-5.19E-01	-2.65E-04	4.35E-04		-1.22E+03	1.26E+03	-1.20E+03	2.57E-02
1274	4.42E+00	-4.40E-01	-4.46E-04	6.85E-04		1.88E+02	2.08E+03	-3.69E+03	3.69E-02
1275	4.45E+00	-2.62E-01	6.67E-04	1.81E-03		8.02E+02	1.30E+03	-3.99E+03	5.30E-02
1276	2.28E+00	-1.76E+00	8.25E-04	1.25E-04		-5.67E+00	5.90E+00	2.75E+01	3.28E-04
1277	2.45E+00	-1.88E+00	7.86E-04	1.77E-04		-2.65E+01	2.61E+01	7.18E+01	8.39E-04
1278	2.60E+00	-1.70E+00	8.06E-04	2.50E-04		-1.10E+01	1.14E+01	2.74E+01	3.48E-04
1279	2.78E+00	-1.80E+00	7.59E-04	2.93E-04		-4.52E+01	4.46E+01	6.80E+01	8.93E-04
1280	2.92E+00	-1.61E+00	7.75E-04	3.74E-04		-1.75E+01	1.82E+01	2.72E+01	3.85E-04
1281	3.09E+00	-1.68E+00	7.20E-04	4.06E-04		-6.69E+01	6.56E+01	6.20E+01	9.91E-04
1282	3.22E+00	-1.48E+00	7.34E-04	4.95E-04		-2.68E+01	2.77E+01	2.90E+01	4.63E-04
1283	3.39E+00	-1.52E+00	6.68E-04	5.15E-04		-9.28E+01	9.28E+01	5.32E+01	1.16E-03
1284	3.51E+00	-1.32E+00	6.82E-04	6.14E-04		-3.89E+01	3.92E+01	2.27E+01	5.32E-04
1285	3.66E+00	-1.33E+00	6.09E-04	6.14E-04		-1.28E+02	1.19E+02	3.54E+01	1.40E-03
1286	3.78E+00	-1.12E+00	6.27E-04	7.26E-04		-7.79E+01	7.38E+01	4.58E+01	1.05E-03
1287	3.91E+00	-1.11E+00	5.14E-04	7.23E-04		-2.02E+02	2.25E+02	-4.98E-01	2.27E-03
1288	4.02E+00	-9.03E-01	5.29E-04	9.11E-04		-1.64E+02	1.29E+02	-2.60E+01	1.47E-03
1289	4.13E+00	-8.66E-01	4.40E-04	8.10E-04		-2.35E+02	1.42E+02	-2.67E+01	2.24E-03
1290	4.23E+00	-6.56E-01	7.78E-04	6.78E-04		-8.39E+02	2.12E+02	2.33E+02	6.58E-03

1291	4.32E+00	-5.95E-01	1.85E-04	8.41E-04		-4.55E+01	1.08E+03	-9.83E+02	1.36E-02
1292	4.42E+00	-3.88E-01	1.66E-04	1.64E-03		-1.16E+03	2.10E+03	-4.24E+02	4.98E-02
1293	4.43E+00	-3.41E-01	3.46E-04	1.80E-03		-1.37E+04	2.43E+03	-2.99E+03	4.95E-02
1294	4.44E+00	-1.95E-01	5.58E-04	1.91E-03		4.04E+03	-1.54E+03	1.98E+03	8.83E-02
1295	2.43E+00	-1.58E+00	7.61E-04	1.83E-04		1.02E+01	-1.10E+01	-2.41E+01	3.19E-04
1296	2.75E+00	-1.51E+00	7.40E-04	3.05E-04		1.72E+01	-1.87E+01	-2.06E+01	3.41E-04
1297	3.05E+00	-1.41E+00	7.09E-04	4.25E-04		2.49E+01	-2.71E+01	-1.50E+01	3.88E-04
1298	3.35E+00	-1.27E+00	6.71E-04	5.48E-04		2.62E+01	-3.10E+01	-6.20E+00	4.30E-04
1299	3.63E+00	-1.11E+00	6.23E-04	6.59E-04		4.75E+01	-4.81E+01	9.11E+00	6.48E-04
1300	3.88E+00	-9.12E-01	5.85E-04	8.49E-04		-4.40E+01	9.28E+00	4.59E+01	8.74E-04
1301	4.12E+00	-6.92E-01	5.26E-04	7.95E-04		2.09E+02	-2.36E+02	7.20E+01	3.34E-03
1302	4.32E+00	-4.50E-01	1.50E-04	1.83E-03		-1.00E+03	1.64E+03	7.47E+01	1.37E-02
1303	4.43E+00	-2.43E-01	1.41E-03	2.04E-03		-4.82E+03	-3.20E+03	8.36E+03	9.73E-02
1304	6.18E-01	-1.70E+00	6.22E-04	-4.17E-04		1.02E+02	-1.06E+02	7.75E+01	1.37E-03
1305	7.62E-01	-1.92E+00	4.75E-04	-2.78E-04		1.36E+02	-1.31E+02	1.05E+02	1.88E-03
1306	1.03E+00	-1.91E+00	6.52E-04	-2.76E-04		8.08E+01	-8.22E+01	9.45E+01	1.36E-03
1307	1.22E+00	-2.11E+00	5.11E-04	-1.60E-04		8.04E+01	-8.01E+01	1.21E+02	1.65E-03
1308	1.48E+00	-2.04E+00	6.82E-04	-1.39E-04		3.83E+01	-3.86E+01	1.06E+02	1.24E-03
1309	7.64E-01	-1.49E+00	7.56E-04	-4.63E-04		5.75E+00	-1.33E+01	1.94E+01	3.95E-04
1310	8.88E-01	-1.69E+00	7.47E-04	-3.91E-04		5.23E+01	-5.02E+01	6.19E+01	8.87E-04
1311	1.14E+00	-1.65E+00	7.97E-04	-3.14E-04		1.19E+01	-1.36E+01	2.61E+01	3.73E-04
1312	1.30E+00	-1.83E+00	7.84E-04	-2.34E-04		3.40E+01	-3.23E+01	6.83E+01	8.42E-04
1313	1.54E+00	-1.74E+00	8.25E-04	-1.58E-04		5.88E+00	-6.57E+00	2.64E+01	3.34E-04
1314	1.01E+00	-1.45E+00	7.22E-04	-3.58E-04		-2.89E+01	3.34E+01	-2.55E+01	4.58E-04
1315	1.38E+00	-1.56E+00	7.55E-04	-2.17E-04		-1.50E+01	1.69E+01	-2.63E+01	3.60E-04
1316	-2.11E+00	2.52E+00	2.02E-04	2.82E-04		4.41E+02	-7.59E+03	-1.94E+03	5.00E-02
1317	-2.08E+00	2.51E+00	3.81E-04	5.15E-04		8.82E+01	-5.14E+02	8.59E+02	2.93E-02
1318	-2.04E+00	2.50E+00	5.64E-05	1.93E-04		-4.43E+02	5.85E+03	4.10E+03	4.69E-02
1319	-2.01E+00	2.49E+00	-3.77E-04	-8.09E-05		5.84E+02	-1.21E+03	4.37E+03	8.56E-02
1320	-2.43E+00	2.48E+00	-3.84E-05	-2.02E-04		-6.10E+01	3.89E+03	-5.07E+01	1.46E-02
1321	-2.34E+00	2.48E+00	1.66E-04	-3.62E-04		8.55E+02	9.21E+02	-7.99E+02	8.84E-03
1322	-2.24E+00	2.48E+00	8.68E-04	2.71E-04		1.95E+03	-7.10E+03	-3.46E+03	4.03E-02
1323	-2.14E+00	2.49E+00	9.56E-04	8.58E-04		-4.32E+02	-7.00E+04	-5.72E+04	4.46E-01
1324	-2.76E+00	2.37E+00	-1.01E-04	3.04E-05		-2.38E+02	-1.61E+02	3.70E+02	4.49E-03
1325	-2.61E+00	2.38E+00	-2.74E-04	7.48E-05		-1.80E+02	-3.38E+00	2.07E+02	3.15E-03
1326	-2.47E+00	2.38E+00	-3.00E-04	-1.30E-04		2.19E+01	1.20E+02	1.71E+02	4.05E-03
1327	-2.32E+00	2.38E+00	-2.78E-04	-1.22E-04		-4.37E+02	7.13E+02	1.48E+03	2.31E-02
1328	-3.07E+00	2.21E+00	-1.26E-04	-9.30E-05		-1.97E+02	2.62E+02	1.18E+02	2.86E-03
1329	-2.90E+00	2.20E+00	-3.31E-04	-2.02E-04		-1.82E+02	2.19E+02	1.24E+02	2.61E-03
1330	-2.73E+00	2.18E+00	-5.52E-04	-2.24E-04		-2.20E+02	2.43E+02	1.13E+02	2.74E-03
1331	-2.55E+00	2.16E+00	-7.21E-04	-1.94E-04		8.06E+01	1.72E+02	2.45E+01	3.04E-03
1332	-3.36E+00	2.01E+00	-1.40E-04	-9.23E-05		-1.99E+02	1.86E+02	5.70E+01	2.25E-03
1333	-3.16E+00	1.98E+00	-3.77E-04	-2.58E-04		-1.46E+02	1.46E+02	3.30E+01	1.69E-03
1334	-2.96E+00	1.95E+00	-5.17E-04	-3.41E-04		-6.30E+01	5.45E+01	3.23E+01	8.23E-04
1335	-2.76E+00	1.92E+00	-5.40E-04	-2.81E-04		1.35E+01	-7.53E+01	3.69E+01	8.23E-04
1336	-3.62E+00	1.77E+00	-1.34E-04	-1.34E-04		-1.70E+02	1.73E+02	-1.75E+00	1.92E-03
1337	-3.39E+00	1.74E+00	-3.55E-04	-3.31E-04		-1.31E+02	1.31E+02	-3.78E+00	1.49E-03
1338	-3.17E+00	1.70E+00	-4.97E-04	-4.27E-04		-6.48E+01	6.60E+01	-2.05E-01	7.43E-04

1339	-2.94E+00	1.66E+00	-5.14E-04	-3.65E-04		4.44E+01	-2.69E+01	3.05E+01	5.92E-04
1340	-3.85E+00	1.50E+00	-1.21E-04	-1.58E-04		-1.46E+02	1.45E+02	-4.49E+01	1.70E-03
1341	-3.60E+00	1.46E+00	-3.15E-04	-3.96E-04		-1.04E+02	1.05E+02	-3.59E+01	1.25E-03
1342	-3.34E+00	1.42E+00	-4.27E-04	-5.02E-04		-4.47E+01	4.44E+01	-1.39E+01	5.35E-04
1343	-3.09E+00	1.38E+00	-4.25E-04	-4.17E-04		3.61E+01	-4.15E+01	3.47E+01	5.93E-04
1344	-4.03E+00	1.20E+00	-1.00E-04	-1.81E-04		-1.16E+02	1.16E+02	-7.64E+01	1.55E-03
1345	-3.76E+00	1.16E+00	-2.59E-04	-4.47E-04		-8.17E+01	8.17E+01	-5.71E+01	1.13E-03
1346	-3.49E+00	1.13E+00	-3.46E-04	-5.60E-04		-3.27E+01	3.28E+01	-2.16E+01	4.47E-04
1347	-3.22E+00	1.09E+00	-3.39E-04	-4.62E-04		3.06E+01	-3.02E+01	4.03E+01	5.73E-04
1348	-4.18E+00	8.71E-01	-7.50E-05	-1.98E-04		-8.44E+01	8.44E+01	-9.92E+01	1.46E-03
1349	-3.89E+00	8.44E-01	-1.92E-04	-4.87E-04		-5.82E+01	5.83E+01	-7.15E+01	1.04E-03
1350	-3.60E+00	8.16E-01	-2.53E-04	-6.04E-04		-2.21E+01	2.20E+01	-2.62E+01	3.90E-04
1351	-3.31E+00	7.88E-01	-2.45E-04	-4.95E-04		2.24E+01	-2.32E+01	4.43E+01	5.66E-04
1352	-4.27E+00	5.30E-01	-4.62E-05	-2.09E-04		-5.12E+01	5.13E+01	-1.14E+02	1.40E-03
1353	-3.97E+00	5.12E-01	-1.18E-04	-5.13E-04		-3.49E+01	3.50E+01	-8.06E+01	9.92E-04
1354	-3.67E+00	4.94E-01	-1.55E-04	-6.34E-04		-1.29E+01	1.28E+01	-2.88E+01	3.58E-04
1355	-3.38E+00	4.76E-01	-1.49E-04	-5.17E-04		1.37E+01	-1.39E+01	4.71E+01	5.57E-04
1356	-4.32E+00	1.78E-01	-1.56E-05	-2.15E-04		-1.72E+01	1.72E+01	-1.21E+02	1.37E-03
1357	-4.02E+00	1.72E-01	-3.96E-05	-5.26E-04		-1.16E+01	1.17E+01	-8.50E+01	9.68E-04
1358	-3.71E+00	1.65E-01	-5.19E-05	-6.48E-04		-4.22E+00	4.21E+00	-3.00E+01	3.43E-04
1359	-3.41E+00	1.59E-01	-4.97E-05	-5.28E-04		4.58E+00	-4.71E+00	4.84E+01	5.53E-04
1360	-1.86E-01	1.66E+00	-2.27E-04	1.60E-04		1.14E+02	-9.00E+01	4.96E+01	1.53E-03
1361	-3.76E-01	1.86E+00	-1.42E-04	1.39E-04		1.68E+02	-1.88E+02	1.96E+01	2.01E-03
1362	-5.85E-01	2.04E+00	-1.63E-04	1.12E-04		1.89E+02	-1.83E+02	5.81E+01	2.19E-03
1363	-8.13E-01	2.20E+00	-1.58E-04	8.37E-05		2.05E+02	-2.07E+02	1.23E+02	2.68E-03
1364	-1.06E+00	2.33E+00	-1.26E-04	6.21E-05		1.92E+02	-2.06E+02	1.93E+02	3.14E-03
1365	-1.31E+00	2.44E+00	-9.58E-05	8.17E-06		2.13E+02	-2.07E+02	3.57E+02	4.63E-03
1366	-1.57E+00	2.50E+00	7.66E-05	7.69E-05		-4.46E+02	-4.72E+02	-8.06E+02	1.56E-02
1367	-1.82E+00	2.53E+00	7.04E-04	-2.36E-04		-1.02E+03	5.15E+03	-8.71E+03	8.33E-02
1368	-3.69E-01	1.51E+00	-4.29E-04	3.56E-04		2.83E+01	-2.52E+01	-2.89E+01	6.48E-04
1369	-5.38E-01	1.73E+00	-3.89E-04	3.57E-04		1.14E+02	-1.12E+02	4.87E+00	1.28E-03
1370	-7.28E-01	1.94E+00	-4.05E-04	2.94E-04		1.39E+02	-1.37E+02	2.65E+01	1.59E-03
1371	-9.37E-01	2.12E+00	-4.08E-04	2.26E-04		1.47E+02	-1.65E+02	7.58E+01	1.98E-03
1372	-1.16E+00	2.28E+00	-3.55E-04	1.33E-04		2.04E+02	-1.44E+02	1.80E+02	2.89E-03
1373	-1.41E+00	2.42E+00	-2.07E-04	9.84E-05		-4.87E+01	-5.20E+02	1.42E+02	4.11E-03
1374	-1.63E+00	2.50E+00	3.38E-04	-1.16E-04		-6.51E+02	5.52E+03	3.94E+02	3.27E-02
1375	-1.84E+00	2.52E+00	1.43E-03	-3.47E-04		-2.86E+02	-1.23E+03	-1.86E+03	3.30E-02
1376	-5.53E-01	1.35E+00	-4.49E-04	4.60E-04		-7.42E-01	8.77E+00	-4.28E+01	5.16E-04
1377	-7.00E-01	1.60E+00	-4.88E-04	4.56E-04		3.46E+01	-3.26E+01	-3.12E+00	4.00E-04
1378	-8.70E-01	1.83E+00	-5.33E-04	3.84E-04		6.15E+01	-5.89E+01	1.56E+01	7.13E-04
1379	-1.06E+00	2.04E+00	-5.44E-04	3.01E-04		6.40E+01	-6.79E+01	4.15E+01	9.43E-04
1380	-1.27E+00	2.24E+00	-5.68E-04	1.61E-04		1.77E+02	-1.47E+02	1.44E+02	2.45E-03
1381	-1.50E+00	2.41E+00	-1.27E-04	1.73E-04		-2.19E+02	-2.18E+02	4.34E+02	6.77E-03
1382	-1.70E+00	2.49E+00	3.79E-04	-4.64E-04		5.59E+02	4.98E+03	4.85E+03	6.93E-02
1383	-1.86E+00	2.51E+00	1.22E-03	-1.93E-04		2.32E+02	-2.59E+03	5.09E+03	7.11E-02
1384	-7.36E-01	1.20E+00	-3.67E-04	4.09E-04		-3.98E+01	3.74E+01	1.92E+01	5.51E-04
1385	-8.62E-01	1.47E+00	-4.48E-04	3.89E-04		-4.61E+01	5.23E+01	3.51E+01	6.85E-04
1386	-1.01E+00	1.72E+00	-5.23E-04	3.34E-04		-5.04E+01	4.36E+01	3.40E+01	6.78E-04

1387	-1.19E+00	1.97E+00	-5.60E-04	2.60E-04		-2.24E+01	5.36E+01	3.23E+01	6.78E-04
1388	-1.38E+00	2.19E+00	-6.57E-04	1.68E-04		-5.95E+01	-7.66E+01	2.46E+01	1.48E-03
1389	-1.60E+00	2.39E+00	-2.46E-04	-5.72E-05		7.60E+02	-4.77E+02	7.44E+02	1.41E-02
1390	-1.77E+00	2.49E+00	-4.51E-04	-3.65E-05		1.03E+03	-2.43E+03	1.04E+04	1.35E-01
1391	-1.89E+00	2.49E+00	1.49E-04	-5.28E-06		4.09E+02	-2.37E+03	1.19E+04	1.30E-01
1392	-3.41E+00	-1.59E-01	4.97E-05	-5.28E-04		-4.58E+00	4.71E+00	4.84E+01	5.53E-04
1393	-3.71E+00	-1.65E-01	5.19E-05	-6.48E-04		4.22E+00	-4.21E+00	-3.00E+01	3.43E-04
1394	-4.02E+00	-1.72E-01	3.96E-05	-5.26E-04		1.16E+01	-1.17E+01	-8.50E+01	9.68E-04
1395	-4.32E+00	-1.78E-01	1.56E-05	-2.15E-04		1.72E+01	-1.72E+01	-1.21E+02	1.37E-03
1396	-3.38E+00	-4.76E-01	1.49E-04	-5.17E-04		-1.37E+01	1.39E+01	4.71E+01	5.57E-04
1397	-3.67E+00	-4.94E-01	1.55E-04	-6.34E-04		1.29E+01	-1.28E+01	-2.88E+01	3.58E-04
1398	-3.97E+00	-5.12E-01	1.18E-04	-5.13E-04		3.49E+01	-3.50E+01	-8.06E+01	9.92E-04
1399	-4.27E+00	-5.30E-01	4.62E-05	-2.09E-04		5.12E+01	-5.13E+01	-1.14E+02	1.40E-03
1400	-3.31E+00	-7.88E-01	2.45E-04	-4.95E-04		-2.24E+01	2.32E+01	4.43E+01	5.66E-04
1401	-3.60E+00	-8.16E-01	2.53E-04	-6.04E-04		2.21E+01	-2.20E+01	-2.62E+01	3.90E-04
1402	-3.89E+00	-8.44E-01	1.92E-04	-4.87E-04		5.82E+01	-5.83E+01	-7.15E+01	1.04E-03
1403	-4.18E+00	-8.71E-01	7.50E-05	-1.98E-04		8.44E+01	-8.44E+01	-9.92E+01	1.46E-03
1404	-3.22E+00	-1.09E+00	3.39E-04	-4.62E-04		-3.06E+01	3.02E+01	4.03E+01	5.73E-04
1405	-3.49E+00	-1.13E+00	3.46E-04	-5.60E-04		3.27E+01	-3.28E+01	-2.16E+01	4.47E-04
1406	-3.76E+00	-1.16E+00	2.59E-04	-4.47E-04		8.17E+01	-8.17E+01	-5.71E+01	1.13E-03
1407	-4.03E+00	-1.20E+00	1.00E-04	-1.81E-04		1.16E+02	-1.16E+02	-7.64E+01	1.55E-03
1408	-3.09E+00	-1.38E+00	4.25E-04	-4.17E-04		-3.62E+01	4.15E+01	3.47E+01	5.92E-04
1409	-3.34E+00	-1.42E+00	4.27E-04	-5.02E-04		4.47E+01	-4.44E+01	-1.39E+01	5.35E-04
1410	-3.60E+00	-1.46E+00	3.15E-04	-3.96E-04		1.04E+02	-1.05E+02	-3.59E+01	1.25E-03
1411	-3.85E+00	-1.50E+00	1.21E-04	-1.58E-04		1.46E+02	-1.45E+02	-4.49E+01	1.70E-03
1412	-2.94E+00	-1.66E+00	5.14E-04	-3.65E-04		-4.44E+01	2.70E+01	3.05E+01	5.92E-04
1413	-3.17E+00	-1.70E+00	4.97E-04	-4.27E-04		6.48E+01	-6.60E+01	-2.15E-01	7.43E-04
1414	-3.39E+00	-1.74E+00	3.55E-04	-3.31E-04		1.31E+02	-1.31E+02	-3.78E+00	1.49E-03
1415	-3.62E+00	-1.77E+00	1.34E-04	-1.34E-04		1.70E+02	-1.73E+02	-1.75E+00	1.92E-03
1416	-2.76E+00	-1.92E+00	5.40E-04	-2.81E-04		-1.36E+01	7.49E+01	3.67E+01	8.20E-04
1417	-2.96E+00	-1.95E+00	5.17E-04	-3.41E-04		6.31E+01	-5.45E+01	3.24E+01	8.24E-04
1418	-3.16E+00	-1.98E+00	3.77E-04	-2.58E-04		1.46E+02	-1.46E+02	3.30E+01	1.69E-03
1419	-3.36E+00	-2.01E+00	1.40E-04	-9.23E-05		1.99E+02	-1.86E+02	5.70E+01	2.25E-03
1420	-2.55E+00	-2.16E+00	7.21E-04	-1.94E-04		-8.07E+01	-1.71E+02	2.53E+01	3.03E-03
1421	-2.73E+00	-2.18E+00	5.52E-04	-2.23E-04		2.20E+02	-2.43E+02	1.13E+02	2.74E-03
1422	-2.90E+00	-2.20E+00	3.31E-04	-2.02E-04		1.82E+02	-2.18E+02	1.24E+02	2.61E-03
1423	-3.07E+00	-2.21E+00	1.26E-04	-9.29E-05		1.97E+02	-2.62E+02	1.18E+02	2.86E-03
1424	-2.32E+00	-2.38E+00	2.84E-04	-1.21E-04		4.31E+02	-7.21E+02	1.49E+03	2.32E-02
1425	-2.47E+00	-2.38E+00	3.01E-04	-1.29E-04		-1.50E+01	-1.16E+02	1.73E+02	4.06E-03
1426	-2.61E+00	-2.38E+00	2.73E-04	7.51E-05		1.80E+02	4.26E+00	2.07E+02	3.15E-03
1427	-2.76E+00	-2.37E+00	1.00E-04	3.03E-05		2.38E+02	1.61E+02	3.70E+02	4.48E-03
1428	-2.14E+00	-2.49E+00	-9.72E-04	8.60E-04		9.11E+01	7.25E+04	-6.00E+04	4.49E-01
1429	-2.24E+00	-2.48E+00	-8.74E-04	2.70E-04		-1.99E+03	7.12E+03	-3.54E+03	4.08E-02
1430	-2.34E+00	-2.48E+00	-1.65E-04	-3.63E-04		-8.58E+02	-9.43E+02	-8.02E+02	8.93E-03
1431	-2.43E+00	-2.48E+00	3.93E-05	-2.02E-04		6.49E+01	-3.89E+03	-4.20E+01	1.46E-02
1432	-2.01E+00	-2.49E+00	3.79E-04	-8.07E-05		-5.86E+02	1.22E+03	4.32E+03	8.55E-02
1433	-2.04E+00	-2.50E+00	-5.30E-05	1.93E-04		4.56E+02	-5.85E+03	4.11E+03	4.71E-02
1434	-2.08E+00	-2.51E+00	-3.79E-04	5.15E-04		-8.41E+01	5.25E+02	8.64E+02	2.96E-02

1435	-2.11E+00	-2.52E+00	-2.02E-04	2.82E-04		-4.40E+02	7.59E+03	-1.93E+03	4.99E-02
1436	-1.89E+00	-2.49E+00	-1.49E-04	-5.37E-06		-3.94E+02	2.37E+03	1.19E+04	1.30E-01
1437	-1.86E+00	-2.51E+00	-1.22E-03	-1.93E-04		-2.32E+02	2.59E+03	5.09E+03	7.11E-02
1438	-1.84E+00	-2.52E+00	-1.43E-03	-3.47E-04		2.84E+02	1.22E+03	-1.86E+03	3.30E-02
1439	-1.82E+00	-2.53E+00	-7.05E-04	-2.36E-04		1.03E+03	-5.15E+03	-8.71E+03	8.33E-02
1440	-1.77E+00	-2.49E+00	4.51E-04	-3.62E-05		-1.02E+03	2.42E+03	1.04E+04	1.35E-01
1441	-1.70E+00	-2.49E+00	-3.79E-04	-4.64E-04		-5.57E+02	-4.98E+03	4.85E+03	6.94E-02
1442	-1.63E+00	-2.50E+00	-3.38E-04	-1.16E-04		6.51E+02	-5.52E+03	3.96E+02	3.27E-02
1443	-1.57E+00	-2.50E+00	-7.67E-05	7.69E-05		4.46E+02	4.71E+02	-8.06E+02	1.56E-02
1444	-1.60E+00	-2.39E+00	2.46E-04	-5.73E-05		-7.61E+02	4.77E+02	7.43E+02	1.41E-02
1445	-1.50E+00	-2.41E+00	1.27E-04	1.73E-04		2.19E+02	2.18E+02	4.34E+02	6.77E-03
1446	-1.41E+00	-2.42E+00	2.07E-04	9.86E-05		4.88E+01	5.20E+02	1.42E+02	4.11E-03
1447	-1.31E+00	-2.44E+00	9.59E-05	8.22E-06		-2.13E+02	2.07E+02	3.57E+02	4.63E-03
1448	-1.38E+00	-2.19E+00	6.57E-04	1.68E-04		5.94E+01	7.66E+01	2.46E+01	1.48E-03
1449	-1.27E+00	-2.24E+00	5.68E-04	1.61E-04		-1.77E+02	1.46E+02	1.44E+02	2.45E-03
1450	-1.16E+00	-2.28E+00	3.55E-04	1.33E-04		-2.04E+02	1.44E+02	1.80E+02	2.89E-03
1451	-1.06E+00	-2.33E+00	1.26E-04	6.21E-05		-1.92E+02	2.06E+02	1.93E+02	3.14E-03
1452	-1.19E+00	-1.97E+00	5.60E-04	2.60E-04		2.24E+01	-5.36E+01	3.23E+01	6.78E-04
1453	-1.06E+00	-2.04E+00	5.44E-04	3.01E-04		-6.40E+01	6.79E+01	4.15E+01	9.43E-04
1454	-9.37E-01	-2.12E+00	4.08E-04	2.26E-04		-1.47E+02	1.65E+02	7.58E+01	1.98E-03
1455	-8.13E-01	-2.20E+00	1.58E-04	8.37E-05		-2.05E+02	2.07E+02	1.23E+02	2.68E-03
1456	-1.01E+00	-1.72E+00	5.23E-04	3.34E-04		5.04E+01	-4.36E+01	3.40E+01	6.78E-04
1457	-8.70E-01	-1.83E+00	5.33E-04	3.84E-04		-6.15E+01	5.89E+01	1.56E+01	7.13E-04
1458	-7.28E-01	-1.94E+00	4.05E-04	2.94E-04		-1.39E+02	1.37E+02	2.65E+01	1.59E-03
1459	-5.85E-01	-2.04E+00	1.63E-04	1.12E-04		-1.89E+02	1.83E+02	5.81E+01	2.19E-03
1460	-8.62E-01	-1.47E+00	4.48E-04	3.89E-04		4.61E+01	-5.23E+01	3.51E+01	6.85E-04
1461	-7.00E-01	-1.60E+00	4.88E-04	4.56E-04		-3.46E+01	3.26E+01	-3.12E+00	4.00E-04
1462	-5.38E-01	-1.73E+00	3.89E-04	3.57E-04		-1.14E+02	1.12E+02	4.87E+00	1.28E-03
1463	-3.76E-01	-1.86E+00	1.42E-04	1.39E-04		-1.68E+02	1.88E+02	1.96E+01	2.01E-03
1464	-7.36E-01	-1.20E+00	3.67E-04	4.09E-04		3.98E+01	-3.74E+01	1.92E+01	5.51E-04
1465	-5.53E-01	-1.35E+00	4.49E-04	4.60E-04		7.40E-01	-8.77E+00	-4.28E+01	5.16E-04
1466	-3.69E-01	-1.51E+00	4.29E-04	3.56E-04		-2.83E+01	2.52E+01	-2.89E+01	6.48E-04
1467	-1.86E-01	-1.66E+00	2.27E-04	1.60E-04		-1.14E+02	9.00E+01	4.96E+01	1.53E-03
1468	-6.70E-01	-9.89E-01	2.88E-04	4.25E-04		6.74E+00	4.43E+00	3.23E+01	5.44E-04
1469	-4.97E-01	-1.14E+00	3.58E-04	4.30E-04		-8.76E+00	1.01E+01	-9.26E+01	1.06E-03
1470	-3.24E-01	-1.29E+00	4.50E-04	3.05E-04		4.65E+01	-2.87E+01	-1.13E+02	1.35E-03
1471	-1.51E-01	-1.44E+00	5.11E-04	1.29E-04		6.12E+01	-5.50E+01	-5.96E+01	1.38E-03
1472	1.13E-02	-1.45E+00	5.54E-04	-1.16E-04		6.13E+01	-7.99E+01	-4.92E+01	1.46E-03
1473	1.62E-01	-1.32E+00	6.47E-04	-3.77E-04		4.85E+01	-5.97E+01	-1.02E+02	1.31E-03
1474	3.13E-01	-1.19E+00	6.27E-04	-5.11E-04		1.48E+01	-1.48E+01	-9.36E+01	1.09E-03
1475	4.64E-01	-1.07E+00	4.52E-04	-4.76E-04		-9.44E+01	8.79E+01	-1.06E+02	1.59E-03
1476	-6.54E-01	-8.40E-01	2.34E-04	4.66E-04		-3.25E+01	7.45E+01	1.18E+02	1.57E-03
1477	-5.21E-01	-9.69E-01	2.39E-04	4.75E-04		-8.16E+01	7.69E+01	-9.00E+01	1.44E-03
1478	-3.89E-01	-1.09E+00	3.20E-04	3.49E-04		-5.47E+00	-7.52E-01	-1.75E+02	2.01E-03
1479	-2.56E-01	-1.22E+00	4.34E-04	2.05E-04		4.52E+01	-5.06E+01	-1.73E+02	2.01E-03
1480	-1.32E-01	-1.23E+00	4.85E-04	2.04E-05		8.36E+01	-7.31E+01	-1.96E+02	2.38E-03
1481	-1.69E-02	-1.12E+00	4.56E-04	-2.18E-04		9.17E+01	-8.31E+01	-2.25E+02	2.70E-03
1482	9.85E-02	-1.01E+00	4.04E-04	-4.23E-04		7.76E+01	-6.63E+01	-1.88E+02	2.26E-03

1483	2.14E-01	-9.12E-01	3.19E-04	-5.06E-04		-1.23E+01	3.28E+01	-1.02E+02	1.31E-03
1484	-6.42E-01	-6.88E-01	1.84E-04	6.00E-04		-1.02E+02	1.62E+02	3.71E+02	4.75E-03
1485	-5.48E-01	-7.90E-01	1.01E-04	6.30E-04		-2.27E+02	2.99E+02	-1.74E+01	3.22E-03
1486	-4.53E-01	-8.89E-01	1.21E-04	4.72E-04		-9.36E+01	1.59E+02	-1.73E+02	2.56E-03
1487	-3.59E-01	-9.83E-01	1.99E-04	3.14E-04		-1.88E+00	3.68E+01	-2.18E+02	2.51E-03
1488	-2.70E-01	-9.86E-01	2.13E-04	1.70E-04		3.31E+01	-1.58E+01	-2.60E+02	3.05E-03
1489	-1.88E-01	-8.99E-01	1.26E-04	-1.51E-05		7.41E+01	-9.12E+01	-2.84E+02	3.41E-03
1490	-1.05E-01	-8.16E-01	9.11E-05	-2.39E-04		1.23E+02	-1.66E+02	-2.16E+02	3.03E-03
1491	-2.30E-02	-7.35E-01	1.34E-04	-4.48E-04		1.43E+02	-2.02E+02	-7.27E+01	2.25E-03
1492	-6.36E-01	-5.34E-01	1.77E-04	7.53E-04		-5.02E+01	7.50E+01	9.27E+02	1.07E-02
1493	-5.76E-01	-6.06E-01	5.03E-05	1.01E-03		-6.29E+02	4.21E+02	2.22E+02	6.64E-03
1494	-5.16E-01	-6.74E-01	-1.01E-04	8.89E-04		-5.91E+02	3.77E+02	-2.35E+02	6.68E-03
1495	-4.57E-01	-7.37E-01	-1.27E-04	6.53E-04		-1.49E+02	2.23E+02	-4.07E+02	6.94E-03
1496	-4.01E-01	-7.31E-01	-1.73E-04	4.83E-04		-5.11E+01	1.07E+02	-5.32E+02	6.35E-03
1497	-3.49E-01	-6.63E-01	-3.15E-04	2.55E-04		2.19E+02	-7.69E+01	-6.61E+02	7.88E-03
1498	-2.97E-01	-5.98E-01	-2.86E-04	-1.22E-04		5.83E+02	-2.97E+02	-5.74E+02	9.11E-03
1499	-2.45E-01	-5.38E-01	-3.59E-05	-5.15E-04		7.07E+02	-2.67E+02	-9.98E+01	8.91E-03
1500	-6.33E-01	-3.77E-01	1.14E-04	9.73E-04		-6.15E+01	4.69E+02	3.34E+03	4.60E-02
1501	-6.05E-01	-4.18E-01	4.81E-05	1.48E-03		-3.83E+02	1.43E+03	1.76E+03	2.97E-02
1502	-5.78E-01	-4.52E-01	-9.88E-06	1.59E-03		-2.30E+02	1.58E+03	9.76E+02	2.09E-02
1503	-5.50E-01	-4.80E-01	-5.75E-05	1.56E-03		-2.46E+02	1.50E+03	4.52E+02	1.54E-02
1504	-5.24E-01	-4.64E-01	-9.28E-05	1.74E-03		-2.63E+02	1.49E+03	-3.22E+02	1.82E-02
1505	-4.99E-01	-4.11E-01	-4.30E-04	1.98E-03		-6.01E+02	9.26E+02	-1.86E+03	2.44E-02
1506	-4.75E-01	-3.63E-01	-7.37E-04	1.49E-03		7.16E+02	-9.48E+02	-2.94E+03	3.56E-02
1507	-4.51E-01	-3.21E-01	-4.34E-04	1.52E-04		2.90E+03	-3.17E+03	-2.13E+03	5.96E-02
1508	-6.29E-01	-2.24E-01	4.16E-05	1.63E-03		-1.58E+03	-5.13E+02	1.56E+04	1.80E-01
1509	-6.17E-01	-2.42E-01	-1.85E-04	3.27E-03		-4.81E+03	2.09E+03	9.98E+03	1.19E-01
1510	-6.04E-01	-2.54E-01	-5.93E-04	4.13E-03		-6.84E+03	3.42E+03	5.72E+03	8.29E-02
1511	-5.92E-01	-2.62E-01	-1.10E-03	4.52E-03		-8.07E+03	3.79E+03	2.42E+03	6.25E-02
1512	-5.81E-01	-2.46E-01	-1.62E-03	4.95E-03		-8.95E+03	3.53E+03	-1.04E+03	6.39E-02
1513	-5.70E-01	-2.11E-01	-1.76E-03	5.09E-03		-4.66E+03	2.45E+03	-6.25E+03	9.01E-02
1514	-5.60E-01	-1.81E-01	-1.27E-03	3.93E-03		3.35E+03	4.42E+02	-1.52E+04	1.62E-01
1515	-5.49E-01	-1.55E-01	-3.14E-04	1.15E-03		6.89E+03	-1.46E+03	-2.51E+04	3.27E-01
1516	-6.23E-01	-7.46E-02	1.56E-04	2.54E-03		3.67E+03	-8.27E+02	3.11E+04	3.37E-01
1517	-6.12E-01	-8.06E-02	3.13E-04	5.86E-03		1.40E+03	4.55E+02	2.07E+04	2.23E-01
1518	-6.00E-01	-8.48E-02	3.39E-04	7.83E-03		-2.52E+02	1.42E+03	1.07E+04	1.19E-01
1519	-5.89E-01	-8.72E-02	2.86E-04	8.53E-03		-1.01E+03	1.92E+03	9.32E+02	4.03E-02
1520	-5.78E-01	-8.19E-02	2.34E-04	8.13E-03		-1.20E+03	1.75E+03	-7.95E+03	9.05E-02
1521	-5.68E-01	-7.03E-02	2.17E-04	6.85E-03		-9.54E+02	1.22E+03	-1.65E+04	1.86E-01
1522	-5.58E-01	-6.03E-02	1.58E-04	4.59E-03		-1.25E+03	7.26E+02	-2.53E+04	2.82E-01
1523	-5.49E-01	-5.18E-02	7.33E-05	1.32E-03		-1.51E+03	2.28E+02	-3.41E+04	3.77E-01
1524	-6.23E-01	7.46E-02	-1.56E-04	2.55E-03		-3.67E+03	9.42E+02	3.11E+04	3.37E-01
1525	-6.12E-01	8.06E-02	-3.13E-04	5.86E-03		-1.40E+03	-4.04E+02	2.07E+04	2.23E-01
1526	-6.00E-01	8.48E-02	-3.39E-04	7.83E-03		2.53E+02	-1.41E+03	1.07E+04	1.19E-01
1527	-5.89E-01	8.72E-02	-2.86E-04	8.53E-03		1.01E+03	-1.92E+03	9.29E+02	4.03E-02
1528	-5.78E-01	8.19E-02	-2.34E-04	8.13E-03		1.20E+03	-1.74E+03	-7.95E+03	9.05E-02
1529	-5.68E-01	7.03E-02	-2.17E-04	6.85E-03		9.55E+02	-1.18E+03	-1.65E+04	1.86E-01
1530	-5.58E-01	6.03E-02	-1.58E-04	4.59E-03		1.25E+03	-6.51E+02	-2.53E+04	2.82E-01

1531	-5.49E-01	5.18E-02	-7.34E-05	1.32E-03		1.51E+03	-9.29E+01	-3.41E+04	3.77E-01
1532	-6.29E-01	2.24E-01	-4.16E-05	1.63E-03		1.58E+03	5.42E+02	1.56E+04	1.80E-01
1533	-6.17E-01	2.42E-01	1.85E-04	3.27E-03		4.81E+03	-2.07E+03	9.99E+03	1.19E-01
1534	-6.04E-01	2.54E-01	5.93E-04	4.13E-03		6.85E+03	-3.41E+03	5.72E+03	8.29E-02
1535	-5.92E-01	2.62E-01	1.10E-03	4.52E-03		8.08E+03	-3.78E+03	2.42E+03	6.25E-02
1536	-5.81E-01	2.46E-01	1.62E-03	4.95E-03		8.96E+03	-3.53E+03	-1.04E+03	6.39E-02
1537	-5.70E-01	2.11E-01	1.76E-03	5.09E-03		4.67E+03	-2.45E+03	-6.24E+03	9.01E-02
1538	-5.60E-01	1.81E-01	1.27E-03	3.93E-03		-3.35E+03	-4.12E+02	-1.52E+04	1.62E-01
1539	-5.49E-01	1.55E-01	3.14E-04	1.15E-03		-6.90E+03	1.54E+03	-2.51E+04	3.27E-01
1540	-6.33E-01	3.77E-01	-1.14E-04	9.73E-04		6.11E+01	-4.68E+02	3.34E+03	4.60E-02
1541	-6.05E-01	4.18E-01	-4.82E-05	1.48E-03		3.82E+02	-1.43E+03	1.76E+03	2.97E-02
1542	-5.78E-01	4.52E-01	9.81E-06	1.59E-03		2.30E+02	-1.58E+03	9.76E+02	2.09E-02
1543	-5.50E-01	4.80E-01	5.75E-05	1.56E-03		2.47E+02	-1.50E+03	4.52E+02	1.54E-02
1544	-5.24E-01	4.64E-01	9.28E-05	1.74E-03		2.63E+02	-1.49E+03	-3.22E+02	1.82E-02
1545	-4.99E-01	4.11E-01	4.29E-04	1.98E-03		6.01E+02	-9.25E+02	-1.86E+03	2.44E-02
1546	-4.75E-01	3.63E-01	7.37E-04	1.49E-03		-7.16E+02	9.49E+02	-2.95E+03	3.56E-02
1547	-4.51E-01	3.21E-01	4.34E-04	1.52E-04		-2.90E+03	3.17E+03	-2.13E+03	5.96E-02
1548	-6.36E-01	5.34E-01	-1.77E-04	7.53E-04		5.02E+01	-7.49E+01	9.27E+02	1.07E-02
1549	-5.76E-01	6.06E-01	-5.03E-05	1.01E-03		6.29E+02	-4.21E+02	2.22E+02	6.64E-03
1550	-5.16E-01	6.74E-01	1.01E-04	8.89E-04		5.91E+02	-3.77E+02	-2.35E+02	6.68E-03
1551	-4.57E-01	7.37E-01	1.28E-04	6.53E-04		1.49E+02	-2.23E+02	-4.07E+02	6.94E-03
1552	-4.01E-01	7.31E-01	1.73E-04	4.83E-04		5.10E+01	-1.07E+02	-5.32E+02	6.35E-03
1553	-3.49E-01	6.63E-01	3.15E-04	2.55E-04		-2.20E+02	7.69E+01	-6.61E+02	7.88E-03
1554	-2.97E-01	5.98E-01	2.86E-04	-1.22E-04		-5.83E+02	2.97E+02	-5.74E+02	9.11E-03
1555	-2.45E-01	5.38E-01	3.59E-05	-5.15E-04		-7.07E+02	2.67E+02	-9.98E+01	8.91E-03
1556	-6.42E-01	6.88E-01	-1.84E-04	6.00E-04		1.02E+02	-1.62E+02	3.71E+02	4.75E-03
1557	-5.48E-01	7.90E-01	-1.01E-04	6.30E-04		2.27E+02	-2.99E+02	-1.75E+01	3.22E-03
1558	-4.53E-01	8.89E-01	-1.21E-04	4.72E-04		9.36E+01	-1.59E+02	-1.73E+02	2.56E-03
1559	-3.59E-01	9.83E-01	-1.99E-04	3.14E-04		1.87E+00	-3.68E+01	-2.18E+02	2.51E-03
1560	-2.70E-01	9.86E-01	-2.13E-04	1.70E-04		-3.31E+01	1.58E+01	-2.60E+02	3.05E-03
1561	-1.88E-01	8.99E-01	-1.26E-04	-1.51E-05		-7.41E+01	9.12E+01	-2.84E+02	3.41E-03
1562	-1.05E-01	8.16E-01	-9.11E-05	-2.39E-04		-1.23E+02	1.66E+02	-2.16E+02	3.03E-03
1563	-2.30E-02	7.35E-01	-1.34E-04	-4.48E-04		-1.43E+02	2.02E+02	-7.27E+01	2.25E-03
1564	-6.54E-01	8.40E-01	-2.34E-04	4.66E-04		3.25E+01	-7.45E+01	1.18E+02	1.57E-03
1565	-5.21E-01	9.69E-01	-2.39E-04	4.75E-04		8.16E+01	-7.69E+01	-9.00E+01	1.44E-03
1566	-3.89E-01	1.09E+00	-3.20E-04	3.49E-04		5.47E+00	7.54E-01	-1.75E+02	2.01E-03
1567	-2.56E-01	1.22E+00	-4.34E-04	2.05E-04		-4.52E+01	5.06E+01	-1.73E+02	2.01E-03
1568	-1.32E-01	1.23E+00	-4.85E-04	2.04E-05		-8.36E+01	7.31E+01	-1.96E+02	2.38E-03
1569	-1.69E-02	1.12E+00	-4.56E-04	-2.18E-04		-9.17E+01	8.31E+01	-2.25E+02	2.70E-03
1570	9.85E-02	1.01E+00	-4.04E-04	-4.23E-04		-7.76E+01	6.63E+01	-1.88E+02	2.26E-03
1571	2.14E-01	9.12E-01	-3.19E-04	-5.06E-04		1.23E+01	-3.28E+01	-1.02E+02	1.31E-03
1572	-6.70E-01	9.89E-01	-2.88E-04	4.25E-04		-6.74E+00	-4.43E+00	3.23E+01	5.44E-04
1573	-4.97E-01	1.14E+00	-3.58E-04	4.30E-04		8.76E+00	-1.01E+01	-9.26E+01	1.06E-03
1574	-3.24E-01	1.29E+00	-4.50E-04	3.05E-04		-4.65E+01	2.87E+01	-1.13E+02	1.35E-03
1575	-1.51E-01	1.44E+00	-5.11E-04	1.29E-04		-6.12E+01	5.50E+01	-5.96E+01	1.38E-03
1576	1.13E-02	1.45E+00	-5.54E-04	-1.16E-04		-6.13E+01	7.99E+01	-4.92E+01	1.46E-03
1577	1.62E-01	1.32E+00	-6.47E-04	-3.77E-04		-4.85E+01	5.97E+01	-1.02E+02	1.31E-03
1578	3.13E-01	1.19E+00	-6.27E-04	-5.11E-04		-1.48E+01	1.48E+01	-9.36E+01	1.09E-03

1579	4.64E-01	1.07E+00	-4.52E-04	-4.76E-04		9.44E+01	-8.79E+01	-1.06E+02	1.59E-03
1580	7.51E-01	1.21E+00	-5.30E-04	-4.07E-04		9.10E+01	-8.95E+01	-9.52E+01	1.49E-03
1581	1.08E+00	1.33E+00	-5.75E-04	-2.98E-04		6.31E+01	-6.00E+01	-8.90E+01	1.24E-03
1582	1.42E+00	1.42E+00	-6.03E-04	-1.81E-04		3.50E+01	-3.31E+01	-8.99E+01	1.09E-03
1583	1.77E+00	1.46E+00	-6.17E-04	-6.07E-05		1.17E+01	-1.11E+01	-9.04E+01	1.04E-03
1584	5.93E-01	1.38E+00	-7.30E-04	-5.12E-04		-3.96E+00	-1.31E+00	-1.06E+01	4.30E-04
1585	9.51E-01	1.57E+00	-7.76E-04	-3.91E-04		-8.74E+00	1.08E+01	2.14E+01	3.94E-04
1586	1.34E+00	1.70E+00	-8.12E-04	-2.35E-04		-7.58E+00	8.86E+00	2.35E+01	3.50E-04
1587	1.74E+00	1.76E+00	-8.30E-04	-8.00E-05		-1.90E+00	2.28E+00	2.44E+01	3.26E-04
1588	4.36E-01	1.56E+00	-6.40E-04	-4.58E-04		-9.32E+01	9.21E+01	3.64E+01	1.13E-03
1589	8.25E-01	1.80E+00	-6.43E-04	-3.53E-04		-9.12E+01	9.21E+01	8.50E+01	1.42E-03
1590	1.26E+00	1.97E+00	-6.80E-04	-2.09E-04		-5.72E+01	5.78E+01	9.74E+01	1.29E-03
1591	1.71E+00	2.06E+00	-6.99E-04	-7.25E-05		-1.82E+01	1.81E+01	1.06E+02	1.22E-03
1592	2.78E-01	1.74E+00	-2.88E-04	-2.11E-04		-2.09E+02	1.96E+02	6.56E+01	2.47E-03
1593	6.99E-01	2.04E+00	-2.54E-04	-1.61E-04		-1.62E+02	1.73E+02	1.02E+02	2.20E-03
1594	1.17E+00	2.25E+00	-2.86E-04	-9.07E-05		-1.02E+02	9.86E+01	1.42E+02	1.94E-03
1595	1.68E+00	2.36E+00	-2.93E-04	-3.34E-05		-3.42E+01	3.54E+01	1.62E+02	1.85E-03
1596	4.47E+00	1.64E-01	-5.64E-04	8.45E-04		1.36E+04	-1.62E+03	-1.02E+04	1.42E-01
1597	4.46E+00	1.31E-01	-8.72E-04	1.87E-03		-1.99E+03	-7.40E+02	-3.28E+03	6.19E-02
1598	4.45E+00	9.77E-02	-3.51E-04	1.91E-03		-6.11E+03	-2.34E+02	3.30E+03	7.41E-02
1599	4.44E+00	6.45E-02	-1.07E-04	1.33E-03		-2.25E+03	-5.80E+02	9.96E+03	1.33E-01
1600	4.42E+00	4.89E-01	3.30E-04	2.77E-04		-4.91E+03	-1.41E+03	-3.33E+03	3.79E-02
1601	4.43E+00	3.91E-01	1.84E-04	1.24E-03		5.44E+03	-2.27E+03	-2.99E+03	3.97E-02
1602	4.43E+00	2.92E-01	-1.01E-03	2.16E-03		1.34E+04	-4.13E+02	8.31E+02	7.85E-02
1603	4.43E+00	1.93E-01	-6.99E-04	1.17E-03		7.10E+04	4.31E+03	-1.59E+04	1.85E-01
1604	4.32E+00	8.13E-01	-1.97E-04	1.71E-04		1.09E+03	-4.19E+02	-3.54E+02	8.98E-03
1605	4.32E+00	6.67E-01	-3.51E-04	5.23E-04		3.44E+02	-6.41E+02	-7.44E+02	1.05E-02
1606	4.32E+00	5.22E-01	-1.03E-04	1.33E-03		3.72E+02	-1.23E+03	-4.87E+02	1.43E-02
1607	4.33E+00	3.77E-01	-4.96E-04	1.94E-03		-8.00E+02	1.50E+03	1.29E+03	2.42E-02
1608	4.16E+00	1.13E+00	-7.10E-05	2.40E-04		2.98E+02	-4.19E+02	-2.68E+02	4.99E-03
1609	4.14E+00	9.53E-01	-3.00E-04	6.77E-04		2.88E+02	-2.94E+02	-1.15E+02	3.68E-03
1610	4.13E+00	7.79E-01	-5.30E-04	8.45E-04		-2.38E+01	3.61E+01	3.16E+00	1.89E-03
1611	4.11E+00	6.05E-01	-4.24E-04	6.74E-04		-5.88E+02	1.73E+02	-1.51E+01	5.83E-03
1612	3.96E+00	1.42E+00	-1.75E-04	2.13E-04		3.15E+02	-2.96E+02	-7.56E+01	3.50E-03
1613	3.93E+00	1.22E+00	-4.24E-04	5.75E-04		2.37E+02	-2.51E+02	-3.58E+01	2.82E-03
1614	3.90E+00	1.01E+00	-5.78E-04	8.26E-04		1.17E+02	-1.15E+02	3.47E+01	1.40E-03
1615	3.87E+00	8.11E-01	-4.81E-04	7.70E-04		-1.47E+02	2.43E+02	-1.52E+01	2.38E-03
1616	3.72E+00	1.68E+00	-1.93E-04	2.00E-04		2.51E+02	-2.55E+02	1.06E+01	2.83E-03
1617	3.68E+00	1.45E+00	-5.09E-04	5.14E-04		1.77E+02	-1.71E+02	3.17E+01	2.01E-03
1618	3.64E+00	1.22E+00	-6.53E-04	6.66E-04		4.00E+01	-4.14E+01	2.53E+01	6.49E-04
1619	3.61E+00	9.92E-01	-4.93E-04	5.83E-04		-1.72E+02	1.34E+02	-5.29E+01	1.87E-03
1620	3.44E+00	1.90E+00	-2.27E-04	1.70E-04		2.04E+02	-2.02E+02	6.71E+01	2.39E-03
1621	3.41E+00	1.65E+00	-5.66E-04	4.32E-04		1.35E+02	-1.36E+02	6.14E+01	1.69E-03
1622	3.37E+00	1.40E+00	-7.09E-04	5.56E-04		3.09E+01	-3.18E+01	2.66E+01	5.06E-04
1623	3.33E+00	1.15E+00	-5.36E-04	4.89E-04		-1.01E+02	1.04E+02	-7.07E+01	1.41E-03
1624	3.14E+00	2.09E+00	-2.50E-04	1.38E-04		1.57E+02	-1.57E+02	1.08E+02	2.13E-03
1625	3.11E+00	1.82E+00	-6.17E-04	3.44E-04		1.01E+02	-1.00E+02	8.17E+01	1.47E-03
1626	3.07E+00	1.54E+00	-7.56E-04	4.34E-04		1.99E+01	-2.06E+01	2.61E+01	4.18E-04

1627	3.04E+00	1.27E+00	-5.65E-04	3.78E-04		-7.74E+01	7.30E+01	-7.89E+01	1.24E-03
1628	2.82E+00	2.23E+00	-2.69E-04	1.01E-04		1.12E+02	-1.12E+02	1.35E+02	1.97E-03
1629	2.79E+00	1.94E+00	-6.55E-04	2.50E-04		7.00E+01	-7.00E+01	9.52E+01	1.34E-03
1630	2.76E+00	1.65E+00	-7.92E-04	3.12E-04		1.32E+01	-1.36E+01	2.58E+01	3.64E-04
1631	2.73E+00	1.37E+00	-5.91E-04	2.71E-04		-5.08E+01	4.96E+01	-8.44E+01	1.11E-03
1632	2.48E+00	2.33E+00	-2.81E-04	6.15E-05		6.69E+01	-6.70E+01	1.52E+02	1.86E-03
1633	2.46E+00	2.03E+00	-6.80E-04	1.51E-04		4.13E+01	-4.12E+01	1.04E+02	1.26E-03
1634	2.44E+00	1.73E+00	-8.17E-04	1.88E-04		7.70E+00	-7.93E+00	2.58E+01	3.36E-04
1635	2.42E+00	1.43E+00	-6.09E-04	1.63E-04		-2.95E+01	2.86E+01	-8.77E+01	1.05E-03
1636	2.12E+00	2.38E+00	-2.85E-04	1.93E-05		2.11E+01	-2.10E+01	1.61E+02	1.82E-03
1637	2.12E+00	2.07E+00	-6.93E-04	4.83E-05		1.40E+01	-1.38E+01	1.09E+02	1.23E-03
1638	2.11E+00	1.77E+00	-8.30E-04	6.14E-05		3.22E+00	-3.27E+00	2.60E+01	3.25E-04
1639	2.10E+00	1.46E+00	-6.18E-04	5.42E-05		-9.12E+00	8.95E+00	-8.95E+01	1.02E-03
1640	2.12E+00	-2.38E+00	2.85E-04	1.93E-05		-2.11E+01	2.10E+01	1.61E+02	1.82E-03
1641	2.12E+00	-2.07E+00	6.93E-04	4.83E-05		-1.40E+01	1.38E+01	1.09E+02	1.23E-03
1642	2.11E+00	-1.77E+00	8.30E-04	6.14E-05		-3.22E+00	3.27E+00	2.60E+01	3.25E-04
1643	2.10E+00	-1.46E+00	6.18E-04	5.42E-05		9.12E+00	-8.95E+00	-8.95E+01	1.02E-03
1644	2.48E+00	-2.33E+00	2.81E-04	6.15E-05		-6.69E+01	6.70E+01	1.52E+02	1.86E-03
1645	2.46E+00	-2.03E+00	6.80E-04	1.51E-04		-4.13E+01	4.12E+01	1.04E+02	1.26E-03
1646	2.44E+00	-1.73E+00	8.17E-04	1.88E-04		-7.70E+00	7.93E+00	2.58E+01	3.36E-04
1647	2.42E+00	-1.43E+00	6.09E-04	1.63E-04		2.95E+01	-2.86E+01	-8.77E+01	1.05E-03
1648	2.82E+00	-2.23E+00	2.69E-04	1.01E-04		-1.12E+02	1.12E+02	1.35E+02	1.97E-03
1649	2.79E+00	-1.94E+00	6.55E-04	2.50E-04		-7.00E+01	7.00E+01	9.52E+01	1.34E-03
1650	2.76E+00	-1.65E+00	7.92E-04	3.12E-04		-1.32E+01	1.36E+01	2.58E+01	3.64E-04
1651	2.73E+00	-1.37E+00	5.91E-04	2.71E-04		5.08E+01	-4.96E+01	-8.44E+01	1.11E-03
1652	3.14E+00	-2.09E+00	2.50E-04	1.38E-04		-1.57E+02	1.57E+02	1.08E+02	2.13E-03
1653	3.11E+00	-1.82E+00	6.17E-04	3.44E-04		-1.01E+02	1.00E+02	8.17E+01	1.47E-03
1654	3.07E+00	-1.54E+00	7.56E-04	4.34E-04		-1.99E+01	2.06E+01	2.61E+01	4.18E-04
1655	3.04E+00	-1.27E+00	5.65E-04	3.78E-04		7.74E+01	-7.30E+01	-7.89E+01	1.24E-03
1656	3.44E+00	-1.90E+00	2.27E-04	1.70E-04		-2.04E+02	2.02E+02	6.71E+01	2.39E-03
1657	3.41E+00	-1.65E+00	5.66E-04	4.32E-04		-1.35E+02	1.36E+02	6.14E+01	1.69E-03
1658	3.37E+00	-1.40E+00	7.09E-04	5.56E-04		-3.09E+01	3.18E+01	2.66E+01	5.06E-04
1659	3.33E+00	-1.15E+00	5.36E-04	4.89E-04		1.01E+02	-1.04E+02	-7.07E+01	1.41E-03
1660	3.72E+00	-1.68E+00	1.93E-04	2.00E-04		-2.51E+02	2.55E+02	1.06E+01	2.83E-03
1661	3.68E+00	-1.45E+00	5.09E-04	5.14E-04		-1.77E+02	1.71E+02	3.17E+01	2.01E-03
1662	3.64E+00	-1.22E+00	6.53E-04	6.66E-04		-4.00E+01	4.14E+01	2.53E+01	6.49E-04
1663	3.61E+00	-9.92E-01	4.93E-04	5.83E-04		1.72E+02	-1.34E+02	-5.29E+01	1.87E-03
1664	3.96E+00	-1.42E+00	1.75E-04	2.13E-04		-3.15E+02	2.96E+02	-7.56E+01	3.50E-03
1665	3.93E+00	-1.22E+00	4.24E-04	5.75E-04		-2.37E+02	2.51E+02	-3.58E+01	2.82E-03
1666	3.90E+00	-1.01E+00	5.78E-04	8.26E-04		-1.17E+02	1.15E+02	3.47E+01	1.40E-03
1667	3.87E+00	-8.11E-01	4.81E-04	7.70E-04		1.47E+02	-2.43E+02	-1.52E+01	2.38E-03
1668	4.16E+00	-1.13E+00	7.10E-05	2.40E-04		-2.98E+02	4.19E+02	-2.68E+02	4.99E-03
1669	4.14E+00	-9.53E-01	3.00E-04	6.77E-04		-2.88E+02	2.94E+02	-1.15E+02	3.68E-03
1670	4.13E+00	-7.79E-01	5.30E-04	8.45E-04		2.35E+01	-3.61E+01	3.10E+00	1.89E-03
1671	4.11E+00	-6.05E-01	4.24E-04	6.74E-04		5.88E+02	-1.73E+02	-1.52E+01	5.83E-03
1672	4.32E+00	-8.13E-01	1.97E-04	1.71E-04		-1.09E+03	4.19E+02	-3.54E+02	8.98E-03
1673	4.32E+00	-6.67E-01	3.51E-04	5.23E-04		-3.43E+02	6.41E+02	-7.44E+02	1.05E-02
1674	4.32E+00	-5.22E-01	1.03E-04	1.33E-03		-3.72E+02	1.23E+03	-4.87E+02	1.43E-02

1675	4.33E+00	-3.77E-01	4.97E-04	1.94E-03		8.00E+02	-1.51E+03	1.29E+03	2.42E-02
1676	4.42E+00	-4.89E-01	-3.30E-04	2.77E-04		4.91E+03	1.41E+03	-3.33E+03	3.79E-02
1677	4.43E+00	-3.91E-01	-1.83E-04	1.24E-03		-5.45E+03	2.27E+03	-2.98E+03	3.97E-02
1678	4.43E+00	-2.92E-01	1.01E-03	2.16E-03		-1.33E+04	4.08E+02	8.48E+02	7.87E-02
1679	4.43E+00	-1.93E-01	6.98E-04	1.17E-03		-6.99E+04	-4.89E+03	-1.55E+04	1.85E-01
1680	4.47E+00	-1.64E-01	5.64E-04	8.46E-04		-1.36E+04	1.63E+03	-1.02E+04	1.42E-01
1681	4.46E+00	-1.31E-01	8.72E-04	1.87E-03		2.00E+03	7.40E+02	-3.27E+03	6.18E-02
1682	4.45E+00	-9.77E-02	3.51E-04	1.91E-03		6.10E+03	2.36E+02	3.30E+03	7.42E-02
1683	4.44E+00	-6.45E-02	1.08E-04	1.33E-03		2.26E+03	5.89E+02	9.97E+03	1.33E-01
1684	2.78E-01	-1.74E+00	2.88E-04	-2.11E-04		2.09E+02	-1.96E+02	6.56E+01	2.47E-03
1685	4.36E-01	-1.56E+00	6.40E-04	-4.58E-04		9.32E+01	-9.21E+01	3.64E+01	1.13E-03
1686	5.93E-01	-1.38E+00	7.30E-04	-5.12E-04		3.96E+00	1.31E+00	-1.06E+01	4.30E-04
1687	7.51E-01	-1.21E+00	5.30E-04	-4.07E-04		-9.10E+01	8.95E+01	-9.52E+01	1.49E-03
1688	6.99E-01	-2.04E+00	2.54E-04	-1.61E-04		1.62E+02	-1.73E+02	1.02E+02	2.20E-03
1689	8.25E-01	-1.80E+00	6.43E-04	-3.53E-04		9.12E+01	-9.21E+01	8.50E+01	1.42E-03
1690	9.51E-01	-1.57E+00	7.76E-04	-3.91E-04		8.74E+00	-1.08E+01	2.14E+01	3.94E-04
1691	1.08E+00	-1.33E+00	5.75E-04	-2.98E-04		-6.31E+01	6.00E+01	-8.90E+01	1.24E-03
1692	1.17E+00	-2.25E+00	2.86E-04	-9.07E-05		1.02E+02	-9.86E+01	1.42E+02	1.94E-03
1693	1.26E+00	-1.97E+00	6.80E-04	-2.09E-04		5.72E+01	-5.78E+01	9.74E+01	1.29E-03
1694	1.34E+00	-1.70E+00	8.12E-04	-2.35E-04		7.58E+00	-8.86E+00	2.35E+01	3.50E-04
1695	1.42E+00	-1.42E+00	6.03E-04	-1.81E-04		-3.50E+01	3.31E+01	-8.99E+01	1.09E-03
1696	1.68E+00	-2.36E+00	2.93E-04	-3.34E-05		3.42E+01	-3.54E+01	1.62E+02	1.85E-03
1697	1.71E+00	-2.06E+00	6.99E-04	-7.25E-05		1.82E+01	-1.81E+01	1.06E+02	1.22E-03
1698	1.74E+00	-1.76E+00	8.30E-04	-8.00E-05		1.90E+00	-2.28E+00	2.44E+01	3.26E-04
1699	1.77E+00	-1.46E+00	6.17E-04	-6.07E-05		-1.17E+01	1.11E+01	-9.04E+01	1.04E-03

CURRICULUM VITA

BHARANI KUMAR ASHOKAN

EDUCATION

- 06/95 – 05/99 Osmania University, Hyderabad, India.
Food Technology, Bachelor of Technology (B.Tech).
- 09/99 – 10/08 Rutgers University, New Brunswick, NJ, USA.
Food Science, Ph.D.

EXPERIENCE

- 09/99 – 12/06 Graduate Research Assistant, Department of Food Science,
Rutgers University, New Brunswick, NJ, USA.
- 02/07 – 05/08 Senior Associate Product Development Scientist, Cadbury Schweppes
Americas Confectionery. Whippany, NJ, USA.
- 05/08 – present Associate Functional Ingredients Scientist, Dr Pepper Snapple Group,
Plano, TX, USA.

PUBLICATIONS

Determination of the WLF constants of cooked soy flour and their dependence on the extent of cooking, Ashokan, B.K. and Kokini, J.L., *Rheologica Acta*, 45(2):192-201.

Use of CFD for optimization, design and scale-up of food extrusion, Ashokan, B.K., Dhanasekharan, M. and Kokini, J.L. in *Computational Fluid Dynamics in Food Processing*, ed. Sun, D, CRC press, 2007.

Determination of the flow and mixing in a continuous mixer using LDA and 3D simulation, Ashokan, B.K., Fanning, L., Connelly, R.K. and Kokini, J.L. , *Proceedings of the Eighth Conference of Food Engineering, A topical conference held in conjunction with the 2003 AIChE Annual Meeting, San Francisco, CA, 16-21, 2003.*

The Fragility of glassy foods, Ashokan, B.K. and Kokini, J.L., *Proceedings of the Ninth Conference of Food Engineering, A topical conference held in conjunction with the 2005 AIChE Annual Meeting, Cincinnati, OH, 2005.*